TESNAT 2018

20-22 April 2018 Akdeniz University, Antalya, Turkey

4th International Conference on Theoretical and Experimental Studies in Nuclear Applications and Technology

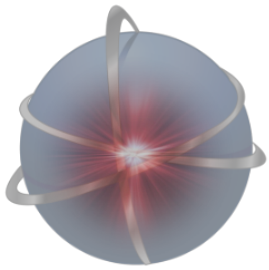

Proceedings

Editors
Eyyup TEL, Abdullah AYDIN, İsmail Hakkı SARPÜN

isbn: 978-605-83680-1-9

TESNAT 2018

4th International Conference on Theoretical and Experimental Studies in Nuclear Applications and Technology

20-22 April 2018
Akdeniz University
Antalya, Turkey

Proceedings

Editors

Eyyup TEL
Abdullah AYDIN
İsmail Hakkı SARPÜN

2018
tesnat.org

isbn: 978-605-83680-1-9

Dear Colleagues,

Welcome to the 4th International Conference on Theoretical and Experimental Studies in Nuclear Applications and Technology (TESNAT 2018). This conference is the fourth step of the TESNAT Conference series. TESNAT 2015 was held in Osmaniye Korkut Ata University, Osmaniye, TESNAT 2016 was held in Mustafa Kemal University, Hatay and TESNAT 2017 was held in Çukurova University, Adana. The world of nuclear physics is an exciting area in which to work, and we'll continue to meet and bring inspired people together in conference like this, to ensure TESNAT remains at the cutting edge.

We intend in this conference to discuss and compare all applicable methods as are being applied at present in nuclear physics. The problems faced in these fields at present are focused in the development of new methods and in the improving of existing techniques to achieve an understanding of existing experimental data and in predicting with high reliability new properties and processes. We propose this conference as a mean to bring together all these related communities with the goal of creating an enriching dialog across the disciplines. The conference will give an overview on the theoretical and experimental challenges in nuclear physics and applications.

We'd like to thank each of you for attending our conference and bringing your expertise to our gathering. You are truly our greatest asset today and tomorrow, and we could not accomplish what we do without your support and leadership.

TESNAT 2018 Organization Committe

Contents

Contents iv
Committees vii
Scientific Program ix
Invited Talks 1
Nuclear energy; Historical developments and future perspectives 2
Green Nuclear Energy: Thorium 5
LHC Experiments and Future Circular Collider (FCC) Project 6
How Innovation Is Related to STEM Education? Where are we at? What can be Done? 7
Nuclear imaging of paintings 8
Türkiye neden nükleer enerji teknolojisine girmeli? 9
Oral Presentations 10
Spectral statisitcs of transition probablities in regular nuclei 11
A new Aziz potential parameter set for nucleon-nucleon interaction: First results 12
VMC calculations for nuclear matter by using Aziz potential with a new parameter set 13
Investigation of fusion-fission target systems with Monte Carlo method by using accelerated deuterons 14
Excitation of heliumlike Kr34+(1s2) ions by neutrals at intermediate impact energies: Projectile nuclear charge dependence 15
Exploring the magicity for the ^{78}Ni nucleus 16
Radon (Rn-222) activity in some deep well water in Uşak and its surrounding 17
Double beta decay and its potential to investigate BSM physics 18
How effective are the PN-QRPA calculation of weak rates of odd-a nuclei in stellar environment 19
Reaction mechanism of ^{8}Li(a,n)^{11}B at low energies 20
Calculation of Astrophysical S-Factors for ^{13}C(α,n)^{16}O Reaction by Means of Low Energy Permeability 21
Investigation of the geometric shapes of $^{80-88}$Zr isotopes within the interacting boson model-1 23
Light charged particle emission of VC composites 24
An assessment of therapy dosimeter calibrations performed in SSDL 26
Nuclear level densities of ^{143,147}Nd isotopes 27
Comparison of different embolization materials on gamma knife arteriovenous malformation dose distributions 28
Material selection for gamma knife phantoms 29
Physical properties of TiN reactor structural material 30
Structural properties of the candidate reactor material VC composites 32
Investigation of the potential use of 3D graphene networks and composites for high-performance electromagnetic interference shielding 34
Radiation shielding properties of concrete containing ferro-boron and barite-colemanite using Monte Carlo method 35
The effect of the linear-quadratic anisotropic scattering and the slab thickness over the albedo problem 36
The criticality problem with the quadratically anisotropic scattering 37
Indoor radon in Isparta 38
Determination of the full energy peak efficiency of HPGe detector using Monte Carlo simulation 39
Use of boron and boron compounds as shielding material in reactors 40
Investigation of the use of samarium and gadolinium materials in nuclear technology 41
Relation of spectral statisitcs and medical applications 42
A study of excitation functions calculations for some A<20 target nuclei 43
Cytogenetic biodosimetery for the assessment of radiation doses in cases of radiological accidents 45
One trap one recombination model under the first order kinetic parameters 46
Comparison of radon concentration results measured by two different methods in well waters 47
Gamma exposure and annual effective dose due to terrestrial and cosmic radiation in Ortaköy granitic zone of Aksaray province (Turkey) 51
Development of an algorithm for the spectrum deconvolution of uranium samples measured by CdZnTe detector 52
MDM spectrometer and Oxford detector (mdm-focal plane) at tamu cyclotron institute 53
Implementation of two-window and three-window peak area methods to determine the ^{235}U abundance in uranium samples measured by a $LaBr_3$(Ce) scintillation detector 54
Use of boron in reactors as shielding and moderator material 55
Effects of gamma ray strenght function on reaction cross section calculations in some osmium isotopes 56
Stopping Power and Range of Protons between 10-1000 MeV Energies in Water Using the Monte Carlo Technique 60
Investigation of lateral spread of 80-250 MeV energy protons in water and cortal bone 64
Excitation functions systematics studies of (n,a) nuclear reactions with neutron energy range from threshold to 20 MeV 65
Effects of biomaterials on lateral spreading dose in proton therapy 66
A novel approach to electromagnetic interference shielding: Conductive polymer/graphene nanocomposites 67
Evaluation of the perlite as a new radiation shielding material 68
X-ray shielding performance of sodium metasilicate/barium oxide glassy composites 69
As a shielding glassy structures against gamma rays: epoxy/PbO and epoxy/BaO composites 70
Investigation of gamma-ray shielding parameters of $Na_2Si_3O_7/Bi_2O_3$ glassy composites 71
Genetic programming modelling of radon measurements of some touristic places in Hatay, Turkey 72
The radiochemical purity test of ^{99m}Tc-sestamibi 73

Quality control tests of cardiac spect camera ... 74
Measurements of generated proton energy spectra by high power lasers ... 75
Dosimetric comparison of two different VMAT techniques in lung cancer radiotherapy ... 76
Design of a 352.21 MHz RF power coupler for the Sanaem RFQ ... 77
Electromagnetic simulations for 800 MHz pillbox cavity and power coupler ... 78
On the determination of binding energy of hypernuclei ... 79
Effects of radiation pressure acceleration on heavy ion generation for ultra intense laser solid interaction ... 80
Acceleration of carbon ions by high power lasers ... 81
Investigation of the excitation-autoionization states of helium ... 82
Investigation of the effects of the level density models and g-strength function models on the ^{92,94,98,100}Mo(p,g) reaction cross sections ... 85
Comparison of gamma-ray sources which used to measure of material density especially -metals and alloys via using transmission technique ... 86
Outdoor gamma dose in air and investigation cancer risk for Hatay province, Turkey ... 87
Bohr hamiltonian for γ=30◦ with Kratzer potential ... 88
A solution of bohr hamiltonian for γ=0° with Kratzer potential ... 89
Comparison of radiation shielding properties of fir with other wooden materials at 6 MeV x-rays energy ... 90
Mean Free Path Calculations for (n,p) Reactions of Ba Target Nuclei ... 93
Radiologic risk assessment of outdoor radioactivity in capital city Ankara, Turkey ... 95
Investigation of the use of boron and clay materials in radioactive waste storage systems ... 96
Excitation function of (g,xn) reaction in some lanthanides ... 97
Preparation of organic nano thin film sensor for harmful gas detections ... 98
Prediction of breast cancer pattern using artificial neural network algorithms ... 99
Classification of breast cancer patients' blood samples using machine learning algorithms ... 100
Investigation of the possibility of producing ^{225}Ac radioisotope in a proton cyclotron ... 101
An application of the dead time correction program at gamma-rays detectors ... 102
A program for dead time correction at gamma-rays detectors ... 103
Can Fluka determine light yields of the scintillators used in medical imaging? ... 104
Investigation of gamma ray percent absorption efficiencies of the crystals used in medical imaging by means of Fluka Monte Carlo program ... 108
Determination of secondary neutrons produced by 100 MeV energy protons in water ... 113
A theoretical study on the production cross–section calculations for ^{86}Y medical isotope ... 114
Investigation of p, d and α emission spectra for neutron and proton induced reactions on ^{63}Cu ... 117
Temporal evolution of lead isotope ratios and metal concentrations in sediments of the North Aegean Sea, in Turkish coast ... 120
Determination of count intensity and elemental weight percentages of sediments in the Altinova shipyard region (Yalova-İzmit gulf) by SEM-EDX ... 121
Luminescence dating of Harran ruins bricks ... 122
Study on shape structure of even-even cerium isotopes within the interacting boson model-1 and the Cranking Nilsson Strutinsky model ... 123
The comparison of the effect of the different sets of the deformation parameters on the cross sections calculations of $^{96-104}$Ru targets ... 124
The calculation of (n,x) reaction cross sections for ^{209}Bi, ^{232}Th and ^{238}U nuclei between 0 and 30 MeV ... 125
Investigation of level density parameter dependence for some even-odd and odd-even nuclei in fission cross sections induced by neutrons with the incident energy up to 20 MeV ... 126
Experimental study of double excitation-ionization resonance profiles of helium by electrons ... 127
A solution of Bohr hamiltonian for γ≈30° with Kratzer potential ... 130
Bohr hamiltonian for γ≈0° with Kratzer potential ... 131
Thermoluminescence properties of calcite mineral conducted by bacterial calcium carbonate (CaCO3) precipitation in organic soil ... 132
Excitation functions of nuclear reactions induced by alpha particles up to 50 MeV on ^{46}Ti, ^{45}Sc and ^{51}V ... 135
Theoretically proton emission DDX calculation on Ge isotopes of neutron induced reactions ... 137
Investigation of 131-Cs medical radioisotope production by TALYS ... 139
Outdoor gamma dose rates in air and assessment of cancer risk for Kocaeli province, Turkey ... 140
Sediment chronology and historical evolution of heavy metal contamination in terms of pollution index in Turkish coast, North Aegean Sea ... 141
Study of gross alpha and gross beta activity concentration in sediments in the Büyükçekmece lake basin (Istanbul, Turkey) ... 142
Cross-section calculations of gallium and arsenic nuclei for (n,2n) and (n,p) reactions up to 20 MeV ... 143
(n,p) reaction cross–section calculations of fission reactor control rod materials ^{107}Ag, ^{111,112,113}Cd, ^{115}In ... 144
(n,2n) reaction cross–section calculations of some Cd isotopes ... 146
Calculation of the in-air output factors of 6mv photon beam of a medical linear accelerator by means of photon phase spaces attained by the GEANT4/GATE simulation ... 149
The radiation dose measurements on linear accelarator (linac) unit, produces high energy x-rays ... 150
Medical imaging from analog to digital systems: A review ... 155
Recent developments in medical imaging ... 156
Calculation of radiological properties of iodine compounds contrast agents (iodixanol, iohexol, iopamidol, iopromide, ioxagalete) ... 157
Node locator: An intraoperative gamma camera ... 158
Application of active-OSL approximation to experimental decay curves from nacl sample exposed to different doses ... 159
Calculation specific heat capacity of uranium nitride nuclear fuel ... 160
A survey distribution of terrestrial radionuclides in surface soil samples in and around Erzin province, Turkey. ... 161
Measurements of gross alpha and gross beta activities in Erzin water ... 162
Tritium activity levels in drinking water of Adana, Turkey ... 163
Investigation of the glow curves of the Ermenek-Sariveliler-Başyayla region soil samples ... 164
Calculation of diffusion length with Anli-Güngör phase function using un method ... 165
The γ-ray strength functions of ^{143,147}Nd isotopes ... 166

Investigation of radiation effects on polymer concretes designed with different aggregates 167
Proton and alpha radiation effects on hematite aggregated polymer concretes by using GEANT4 170
Comparison of penetrating distance calculations for magnetite and ordinary concrete 173
Comparison of stopping power calculations for magnetite and ordinary concrete 175
Deuteron induced reaction cross–section calculations for ^{107,109}Ag, ^{151,153}Eu and ^{160}Gd isotopes 178
Neutron production cross–section calculations of ^{111}Cd for (p,xn) reactions 180
ESR investigation of radiation effect on CoQ10 drug 182
Thermoluminescence heating rate behaviour of $Zn(BO_2)2:0.05Dy3+$ 184
Variation of the kinetic parameters of traps found in the fluorapatite mineral ($Ca_5F(PO_4)_3$) in tooth enamel under the different annealing temperatures 185
Investigation of the lambda hypernuclei in nuclear reactions 188
Excitation function of (p,xn) reactions for ^{113}Cd nucleous 189
Evaluation of the dosimetric results of 3 mm geometric error in linear accelerator (linac) beam data measurements 190
Calculation of mass attenuation coefficients of hormirad and galena materials for radiation shielding by Monte Carlo method 191
Dosimetric comparison of three different VMAT techniques in head and neck cancer radiotherapy 193
Triple differential cross sections for the single ionization of water molecule (H_2O) by electron impact 194
Theoretical calculation of neutron induced fission cross section on some actinides 195
Theoretical calculation of gamma induced fission cross section on some actinides 197
High performance graphene-based photodetectors 199
Photo-neutron cross section calculations of ^{84,86,87,88}Sr 200
Proton, deuteron and alpha emission of TiN composites 202
Calculation of linear attenuation coefficient of amethyst material for radiation shielding by Monte Carlo method 204
Leukemia incidence in the Russian cohort of Chernobyl emergency workers: estimates of radiation risks in the follow-up period 1986–2014 206
Influence of backscattering on fission rate of excited nuclei 207
Measurement of natural radioactivity in quartz stone 208
Determination of radioactivity levels in feldspar samples in Turkey 209
The effects on radiation damage of some nuclear libraries in a hybrid reactor 210
The calculation of neutron flux for some nuclear libraries using Monte Carlo method 213
Three-dimensional Monte Carlo calculation of the nuclear parameters for some nuclear libraries 216
The investigation of convert ^{232}Th(n,γ)^{233}U for some nuclear libraries in a hybrid reactor 219
The effect of varying constant source over albedo problem for quadratically anisotropic scattering 221
Tritium activity levels in bottled water and mineral water sold in Azerbaijan 222
Investigation of using neutron generator source in thorium fuel efficiency at new generation nuclear reactor types 223
Determination of the dead layer thickness for hpge detector: Measurements vs Monte Carlo methods 224
Validation of a NaI(Tl) and $LaBr_3$(Ce) detector's models: Experiment and Monte Carlo simulations 226
Determination of direct capture reaction rate for ^{26}Si(p,γ)^{27}P 227
Optimization of the electrophoretic deposition parameters (hydroxyapatite concentration, collagen concentration, and deposition temperature speed) for biocomposite hydroxyapatite/chitosan/collagen/h-BN coatings via response surface methodology 228
The effect of chitosan concentration on the corrosion characteristics of the biomedical grade Ti_6Al_4V implants electrophretically coated with hydroxyapatite/chitosan biocomposites 229
A study of mean free path on the radiation shielding properties of normal concrete 230
Necessity of nuclear energy in Turkey 233
The role of nuclear energy for generating electric in Turkey 237
Hydrogen recombination in REKO-4 facility and analysis of recombination 238
Determination of morphological characteristics and mineralogical structure of the Kulakcayiri sediments by SEM and XRD 241
Evaluation outdoor gamma dose rates in air and cancer risk determination for nevsehir, turkey 242
Estimate of individualized radiation risk coefficients under internal exposure for the cohort of Russian emergency workers 243
A Monte Carlo calculation of the x-ray attenuation of tungsten functional papers (TFP) 244

Participant list 245

Index 247

Committees

Honorary Committee

Prof.Dr. Mustafa ÜNAL	Rector, Akdeniz Uni.
Dr. Zafer DEMİRCAN	Director, TAEK

Organising Committee

Prof.Dr. Eyyup TEL (Chair)	Osmaniye Korkut Ata University, Turkey
Assoc.Prof.Dr. Ismail H. Sarpün (Sci.Sec.)	Akdeniz University, Turkey
Prof. Dr. Arjan KONING	International Atomic Energy Agency (IAEA), Austria
Prof.Dr. Abdullah AYDIN	Kırıkkale University, Turkey
Prof. Dr. Mohamed BELGAID	University of Sciences and Technology Houari Boumediene, Algeria
Prof.Dr. Abdullah KAPLAN	Süleyman Demirel University, Turkey
Prof. Dr. Jameel-Un NABI	GIK, Pakistan
Prof.Dr. Ahmet BOZKURT	Akdeniz University, Turkey
Prof.Dr. Bayram DEMİR	Istanbul University, Turkey
Assoc.Prof.Dr. Muhittin ŞAHAN	Osmaniye Korkut Ata University, Turkey
Assoc.Prof.Dr. Nina TUNCEL	Akdeniz University, Turkey

Local Organizing Committee

Assoc.Prof.Dr. Ahmet BÜLBÜL	Osmaniye Korkut Ata University
Dr. Ercan YILDIZ	Kırıkkale University
Dr. Yusuf KAVUN	Osmaniye Korkut Ata University
Res. Asst. Dr. Hasan ÖZDOĞAN	Akdeniz University
Res. Asst. Nuri YORULMAZ	Harran University
Res. Asst. Mehmet Murat YAŞAR	Harran University
Gözde DEMİRELLİ	Doğa Private Schools
Tuğba ÇEPNİ	İstanbul University

Scientific Committee

Prof. Dr. Yousry ABUSHADY	Alexandria University, Egypt
Prof. Dr. Emel ALĞIN	Eskisehir Osmangazi University, Turkey
Prof. Dr. Hüseyin AYTEKİN	Bulent Ecevit University, Turkey
Dr. Ahmed AZBOUCHE	Nuclear Research Center of Algeria, Algeria
Prof. Dr. Mohamed BELGAID	University of Sciences and Technology Houari Boumediene, Algeria
Assoc.Prof.Dr. Mahmut BÖYÜKATA	Kırıkkale University, Turkey
Dr. Thomas CALLIGARO	Louvre Museum, France
Prof. Dr. Üner ÇOLAK	Istanbul Technical University, Turkey
Prof. Dr. Mitra DJAMAL	ITB, Indonesia
Prof.Dr. Stéphane GORIELY	Université libre de Bruxelles, Belgium

Prof.Dr. Nalan ÖZKAN GÜRAY	Kocaeli University, Turkey
Prof. Dr. Orhan GÜRLER	Uludağ University, Turkey
Dr. Lama HADID-BEURRIER	PSRPM, France
Assoc.Prof.Dr. Erol KAM	Yıldız Technical University, Turkey
Prof. Dr. Salem KESSAL	University of Sciences and Technology Houari Boumediene, Algeria
Dr. Ali İhsan KILIÇ	TRIUMF, Canada
Prof. Dr. Arjan KONING	International Atomic Energy Agency (IAEA), Austria
Prof. Dr. Jameel-Un NABI	GIK, Pakistan
Prof. Dr. Dimitri A. ROCHMAN	Paul Scherrer Institute, Switzerland
Prof. Dr. Mahdi SADEGHI	University of Medical Sciences, Iran
Prof. Dr. Cevad SELAM	Mus Alparslan University, Turkey
Prof. Dr. Saleh SULTANSOY	TOBB University of Economics & Technology, Turkey
Prof. Dr. Güneş TANIR	Gazi University, Turkey
Prof. Dr. Mustafa TOPAKSU	Cukurova University, Turkey
Prof. Dr. Osman YILMAZ	Middle East Technical University (METU), Turkey

Scientific Program

20 April 2018 Friday

09:00	REGISTRATION			
10:30	OPENING CEREMONY			
11:00	Inv. Talk: Prof. Dr. Yousry ABUSHADY Current and future nuclear reactors option in the World			
11:30	Inv. Talk: Prof. Dr. Nazmi Turan OKUMUŞOĞLU Türkiye neden nükleer enerji teknolojisine girmeli?			
	FERMI HALL Chair: Prof.Dr. Saleh SULTANSOY	BECQUEREL HALL Chair: Prof.Dr. İlkay TÜRK ÇAKIR	HESS HALL Chair: Prof.Dr. Hüseyin Ali YALIM	LAWRENCE HALL Chair: Prof.Dr. Mohamed BELGAID
13:00 – 13:15	Aidin GHALEHASADI Spectral statistics of transition probabilities in regular nuclei	Sabin STOICA Double beta decay and its potential to investigate BSM physics	Doğan YAŞAR An assessment of therapy dosimeter calibrations performed in SSDL	Muhammad Syahir SARKAWI Radiation shielding properties of concrete containing ferro-boron and barite-colemanite using Monte Carlo method
13:15 – 13:30	Hasan BİRCAN A new Aziz potential parameter set for nucleon-nucleon interaction: first results		Kürşad Osman AY Nuclear level densities of ^{143,147}Nd isotopes	R. Gökhan TÜRECİ The effect of the linear-quadratic anisotropic scattering and the slab thickness over the albedo problem
13:30 – 13:45	Kaan MANİSA VMC calculations for nuclear matter by using Aziz potential with a new parameter set	Jameel-Un NABI How effective are the pn-QRPA calculation of weak rates of odd-A nuclei in stellar environment	Özlem DAĞLI Comparison of different embolization materials on gamma knife arteriovenous malformation dose distributions	Pınar KAAN The criticality problem with the quadratically anisotropic scattering
13:45 – 14:00	Mehmet Emin KORKMAZ Investigation of fusion-fission target systems with Monte Carlo method by using accelerated deuterons	Ali İhsan KILIÇ Reaction mechanism of ^{8}Li(a,n)^{11}B at low energies	Özlem DAĞLI Material selection for gamma knife phantoms	Mehmet Ertan KÜRKÇÜOĞLU Indoor Radon in Isparta
14:00 – 14:05	Boumediene LASRI Excitation of heliumlike Kr34+(1s2) ions by neutrals at intermediate impact energies: projectile nuclear charge dependence	Ercan YILDIZ Calculations of cross-sections and astrophysical S-factors for the ^{13}C(a,n)^{16}O reaction	Vildan ÖZKAN BİLİCİ Physical properties of TiN reactor structural material	Esra UYAR Determination of the full energy peak efficiency of HPGe detector using Monte Carlo simulation
14:05 – 14:10	Furkan OK Exploring the magicity for the ^{78}Ni nucleus	Merve AYDOĞAN Investigation of the geometric shapes of $^{80-88}$Zr isotopes within the interacting boson model-1	Vildan ÖZKAN BİLİCİ Structural properties of the candidate reactor material VC composites	Fatma YAKUT Use of Boron and Boron compounds as shielding material in reactors
14:10 – 14:15	Rıdvan ÜNAL Radon (Rn-222) activity in some deep well water in Uşak and its surrounding	İsmail Hakkı SARPÜN Light charged particle emission of VC composites	Ceren KARAMAN Investigation of the potential use of 3D graphene networks and composites for high-performance electromagnetic interference shielding	Fatma YAKUT Investigation of the use of Samarium and Gadolinium materials in nuclear technology
14:15	BREAK			
	FERMI HALL Chair: Prof. Dr. Yousry ABUSHADY			
14:30	Inv. Talk: Prof. Dr. Saleh SULTANSOY Green Nuclear Energy: Thorium			
15:00	Inv. Talk: Prof. Dr. İlkay TÜRK ÇAKIR LHC Experiments and Future Circular Collider (FCC) Project			
15:30	BREAK			
	FERMI HALL Chair: Prof.Dr. Jameel-Un NABI	BECQUEREL HALL Chair: Prof.Dr. Abdullah AYDIN	HESS HALL Chair: Prof.Dr. Ahmet BOZKURT	LAWRENCE HALL Chair: Prof.Dr. Rıdvan ÜNAL
15:45 – 16:00	Seyed Khalil MOBAREKH Relation of spectral statisitcs and medical applications	Sefer BALCI Development of an algorithm for the spectrum deconvolution of uranium samples measured by CdZnTe detector	Ahmet BOZKURT Stopping power and range of protons between 10-1000 MeV energies in water using the Monte Carlo technique	Hande KAYACIK X-ray shielding performance of Sodium metasilicate/Barium oxide glassy composites
16:00 – 16:15	Yusuf KAVUN A study of excitation functions calculations for some A<20 target nuclei	Murat DAĞ MDM spectrometer and Oxford detector (MDM-focal plane) at TAMU cyclotron institute	Fatih EKİNCİ Investigation of lateral spread of 80-250 MeV energy protons in water and cortal bone	Yaren ERGİN As a shielding glassy structures against gamma rays: epoxy/PbO and epoxy/BaO composites

16:15 – 16:30	Ghazi ALSBEIH Cytogenetic biodosimetery for the assessment of radiation doses in cases of radiological accidents	Sefer BALCI Implementation of two-window and three-window peak area methods to determine the ^{235}U abundance in Uranium samples measured by a $LaBr_3(Ce)$ scintillation detector	Mohamed BELGAID Excitation functions systematics studies of (n,a) nuclear reactions with neutron energy range from threshold to 20 MeV	Tuğba DEMİRBAY Investigation of gamma-ray shielding parameters of $Na_2Si_3O_7/Bi_2O_3$ glassy composites
16:30 – 16:45	Erdem UZUN One trap one recombination model under the first order kinetic parameters	M. Cüneyt KAHRAMAN Hydrogen recombination in REKO-4 facility and analysis of recombination	Fatih EKİNCİ Effects of Biomaterials on Lateral Spreading Dose in Proton Therapy	İsmail Hakkı KARAHAN Genetic programming modelling of Radon measurements of some touristic places in Hatay, Turkey
16:45 – 16:50	Ayla GÜMÜŞ Comparison of Radon Concentration Results Measured by Two Different Methods in Well Waters	Fatma Aysun UĞUR Use of Boron in reactors as shielding and moderator material	Ceren KARAMAN A novel approach to electromagnetic interference shielding: conductive polymer/graphene nanocomposites	Tuğba ÇEPNİ The radiochemical purity test of ^{99m}Tc-sestamibi
16:60 – 16:55	Mehmet ERDOĞAN Gamma exposure and annual effective dose due to terrestrial radioactivity in Ortaköy granitic zone of Aksaray province (Turkey)	Kemal TAŞDÖVEN Gamma ray strength function calculations in some Osmium isotopes	Mehmet Emin KORKMAZ Evaluation of the perlite as a new radiation shielding material	Tuğba ÇEPNİ Quality control tests of cardiac SPECT camera

21 April 2018 SATURDAY

	FERMI HALL Chair: Prof.Dr. Eyyup TEL	BECQUEREL HALL Chair: Prof.Dr. Muhittin ŞAHAN	HESS HALL Chair: Prof.Dr. Sabin STOICA	LAWRENCE HALL Chair: Assoc.Prof.Dr. Doğan YAŞAR
09:00 – 09.15	Özgür CULFA Measurements of generated proton energy spectra by high power lasers	Abdullah AYDIN Investigation of the effects of the level density models and g-strength function models on the $^{92,94,98,100}Mo(p,g)$ reaction cross sections	İlker SERT Temporal evolution of lead isotope ratios and metal concentrations in sediments of the North Aegean sea, in Turkish coast	Hatice Kübra BELEN Investigation of the possibility of producing ^{225}Ac radioisotope in a proton cyclotron
09:15 – 09:30	Duygu BOLAT Dosimetric comparison of two different VMAT techniques in lung cancer radiotherapy	Erol KAM Comparison of gamma-ray sources which used to measure of material density especially -metals and alloys via using transmission technique	Kübra BAYRAK Determination of count intensity and elemental weight percentages of sediments in the Altınova shipyard region (Yalova-Izmit gulf) by SEM-EDX	Salih Mustafa KARABIDAK An application of the dead time correction program at gamma-rays detectors
09:30 – 09.45	Ersin ÇİÇEK Design of a 352.21 MHz RF power coupler for the SANAEM RFQ	Erol KAM Outdoor gamma dose in air and investigation cancer risk for Hatay province, Turkey	Mehmet KOŞAL Luminescence dating of Harran ruins bricks	Salih Mustafa KARABIDAK A program for dead time correction at gamma-rays detectors
09:45	BREAK			
	FERMI HALL Chair: Assoc.Prof.Dr. Kaan MANİSA	BECQUEREL HALL Chair: Assoc.Prof.Dr. R. Gökhan TÜRECİ	HESS HALL Chair: Assoc.Prof.Dr. Mahmut BÖYÜKATA	LAWRENCE HALL Chair: Dr. Zafer SAĞEL
10:00 – 10:15	Aslıhan ÇAĞLAR Electromagnetic Simulations for 800 MHz Pillbox Cavity and Power Coupler	Burcu UÇAR Bohr Hamiltonian for $\gamma=30^\circ$ with Kratzer potential	Fatma Aysun UĞUR Investigation of the use of Boron and clay materials in radioactive waste storage systems	Elif Ebru ERMİŞ Can FLUKA determine light yields of the scintillators used in medical imaging?
10:15 – 10:30	Nihal BÜYÜKÇİZMECİ On the determination of binding energy of hypernuclei	Tuğba TURAN A Solution of Bohr Hamiltonian for $\gamma=0°$ with Kratzer Potential	Yunus Emre DOĞAN Excitation function of (g,xn) reaction in some lanthanides	Elif Ebru ERMİŞ Investigation of gamma ray percent absorption efficiencies of the crystals used in medical imaging by means of FLUKA Monte Carlo program
10:30 – 10:35	Özgür CULFA Effects of Radiation Pressure Acceleration on Heavy Ion Generation for Ultra Intense Laser Solid Interaction	Yusuf KAVUN Comparison of Radiation Shielding Properties of Fir with other Wooden Materials at 6 MeV X-rays Energy	Rıdvan ÜNAL Preparation of Organic Nano Thin Film Sensor for Harmful Gas Detections	Adem PEHLİVANLI Determination of secondary neutrons produced by 100 MeV energy protons in water
10:35 – 10:40	Volkan SERT Acceleration of Carbon ions by high power lasers	R. Ömer TURHAN Mean Free Path Calculations for (n,p) Reactions of Ba Target Nuclei	Ozan TOKER Prediction of breast cancer pattern using artificial neural network algorithms	Tuğçe GÜLÜMSER Investigation of p, d and α emission spectra for neutron and proton induced reactions on ^{63}Cu

10:40 – 10:45	Hüseyin Ali YALIM Investigation of the Excitation-Autoionization States of Helium	Enis KAPDAN Radiologic risk assessment of outdoor radioactivity in capital city Ankara, Turkey	Ozan TOKER Classification of breast cancer patients' blood samples using machine learning algorithms	Tuğçe GÜLÜMSER A theoretical study on the production cross–section calculations for ^{86}Y medical isotope
10:45	BREAK			
11:00	FERMI HALL Chair: Prof.Dr. Nazmi Turan OKUMUŞOĞLU			
11:30	Inv. Talk: Prof.Dr. Üner ÇOLAK Nuclear Energy: Historical Developments and Future Perspectives Inv. Talk: Dr. Zafer SAĞEL Nuclear Applications in Agriculture			
	FERMI HALL Chair: Prof.Dr. Nihal BÜYÜKÇİZMECİ	BECQUEREL HALL Chair: Assoc.Prof.Dr. M.Hicabi BÖLÜKDEMİR	HESS HALL Chair: Prof. Dr. Abdellatif Elanique	LAWRENCE HALL Chair: Assoc.Prof.Dr. İsmail Hakkı SARPÜN
13:00 – 13:15	Yousry ABUSHADY Reactor design calculations	Burcu UÇAR A solution of Bohr hamiltonian for γ≈30° with Kratzer potential	Erol KAM Outdoor gamma dose rates in air and assessment of cancer risk for Kocaeli province, Turkey	Nina TUNÇEL Medical imaging from analog to digital systems: A review
13:15 – 13:30	Mahmut BÖYÜKATA Study on shape structure of even-even cerium isotopes within the interacting boson model-1 and the cranking Nilsson Strutinsky model	A. Güneş TANIR Application of active-OSL approximation to experimental decay curves from NaCl sample exposed to different doses	İlker SERT Sediment chronology and historical evolution of heavy metal contamination in terms of pollution index in Turkish coast, North Aegean Sea	Önder SÖNMEZ Investigation of level density parameter dependence for some even-odd and odd-even nuclei in fission cross sections induced by neutrons with the incident energy up to 20 MeV
13:30 – 13:45	Abdullah AYDIN The comparison of the effect of the different sets of the deformation parameters on the cross sections calculations of $^{96\text{-}104}$Ru targets	Hüseyin TOKTAMIŞ Investigation of thermoluminescence properties of calcite mineral conducted by bacterial calcium carbonate ($CaCO_3$) precipitation in organic soil	Kübra BAYRAK Study of gross alpha and gross beta activity concentration in sediments in the Büyükçekmece lake basin (İstanbul, Turkey)	Hediye ACUN BUCHT Calculation of the in-air output factors of 6MV photon beam of a medical linear accelerator by means of photon phase spaces attained by the Geant4/GATE Simulation
13:45 – 13:50	Rıdvan ÜNAL The calculation of (n,x) reaction cross sections for ^{209}Bi, ^{232}Th and ^{238}U nuclei between 0 and 30 MeV	Hatice BİLGİN Excitation functions of nuclear reactions induced by alpha particles up to 50 MeV on ^{46}Ti, ^{45}Sc and ^{51}V	Muhittin ŞAHAN Cross-section calculations of Gallium and Arsenic nuclei for (n,2n) and (n,p) Reactions up to 20 MeV	Oğuz AYDIN Dosimetric comparison of three different VMAT techniques in head and neck cancer radiotherapy
13:50 – 13:55	Aysun İNAL The radiation dose measurements on linear accelerator (Linac) unit, produces high energy x-rays	Gözde DEMİRELLİ Theoretically proton emission DDX calculation on Ge isotopes of neutron induced reactions	Mert ŞEKERCİ (n,p) reaction cross–section calculations of fission reactor control rod materials ^{107}Ag, ^{111,112,113}Cd, ^{115}In	Tahir ÇAKIR Calculation of radiological properties of iodine compounds contrast agents (iodixanol, iohexol, iopamidol, iopromide, ioxagalete)
13:55 – 14:00	Hüseyin Ali YALIM Experimental study of double excitation-ionization resonance profiles of helium by electrons	Mehmet BÜYÜKTÜRKMEN Investigation of ^{131}Cs medical radioisotope production by TALYS	Mert ŞEKERCİ (n,2n) reaction cross–section calculations of some Cd isotopes	Asuman KOLBAŞI Node locator: An intraoperative gamma camera
14:00	BREAK			
14:15	FERMI HALL Chair: Prof.Dr. A. Güneş TANIR Inv. Talk: Dr. Thomas CALLIGARO Nuclear Imaging of Paintings			
	FERMI HALL Chair: Asst.Prof.Dr. Tahir ÇAKIR	BECQUEREL HALL Chair: Prof.Dr. Abdullah KAPLAN	HESS HALL Chair: Assoc.Prof.Dr. Erol KAM	LAWRENCE HALL Chair: Assoc.Prof.Dr. Nina TUNÇEL
14:45 – 15:00	Tuğba TURAN Bohr hamiltonian for γ≈0° with Kratzer potential	Mustafa ÖZGÜR The γ-ray strength functions of ^{143,147}Nd isotopes	M. Özgür SEZER ESR investigation of radiation effect on CoQ10 drug	Hülya ÖZDEMİR Recent developments in medical imaging
15:15 – 15:20	Erhan ESER Calculation specific heat capacity of Uranium Nitride nuclear fuel	Ali Nadi KAPLAN Investigation of radiation effects on polymer concretes designed with different aggregates	Sümeyra BALCI YEĞEN Thermoluminescence heating rate behaviour of Zn(BO2)2:0.05Dy3+	Boumediene LASRI Triple differential cross sections for the single ionization of water molecule (H_2O) by electron impact
15:20 – 15:25	Uğur BÜYÜKER A survey distribution of terrestrial radionuclides in surface soil samples in and around Erzin province, Turkey	Ali Nadi KAPLAN Proton and alpha radiation effects on hematite aggregated polymer concretes by using Geant4	Dilek TOKTAMIŞ Variation of the kinetic parameters of traps found in the fluorapatite mineral ($Ca_5F(PO_4)_3$) in tooth enamel under the different annealing temperatures	Mehmet Murat YAŞAR Calculation of mass attenuation coefficients of hormirad and galena materials for radiation shielding by Monte Carlo method
15:25 – 15:30	Uğur BÜYÜKER Measurements of gross alpha and gross beta activities in Erzin Water	Hasan ÖZDOĞAN Comparison of penetrating distance calculations for magnetite and ordinary concrete	Nihal BÜYÜKÇİZMECİ Investigation of the Lambda hypernuclei in nuclear reactions	Asiye GÜROL Theoretical calculation of gamma induced fission cross section on some actinides

15:30 – 15:35	Elif GÖREN Tritium activity levels in drinking water of Adana, Turkey	Hasan ÖZDOĞAN Comparison of stopping power calculations for magnetite and ordinary concrete	Bekir ORUNCAK Excitation Function of (p,xn) reactions for ^{113}Cd Nucleus	Ceren KARAMAN High performance graphene-based photodetectors
15:35 – 15:40	Erdem UZUN Investigation of the glow curves of the Ermenek-Sarıveliler-Başyayla region soil samples	Abdullah KAPLAN Deuteron induced reaction cross–section calculations for ^{107,109}Ag, ^{151,153}Eu and ^{160}Gd isotopes	Aysun İNAL Evaluation of the dosimetric results of 3 mm geometric error in linear accelerator (LINAC) beam data measurements	İsmail Hakkı SARPÜN Photo-neutron cross section calculations of ^{84,86,87,88}Sr
15:40 – 15:45	Ahmet BÜLBÜL Calculation of diffusion length with Anli-Güngör phase function using UN method	Abdullah KAPLAN Neutron production cross–section calculations of ^{111}Cd for (p,xn) reactions	Asiye GÜROL Theoretical calculation of neutron induced fission cross section on some actinides	İsmail Hakkı SARPÜN Proton, deuteron and alpha emission of TiN composites

22 April 2018 SUNDAY

	FERMI HALL Chair: Assoc.Prof.Dr. Ahmet BÜLBÜL	BECQUEREL HALL Chair: Assoc.Prof.Dr. Hüseyin TOKTAMIŞ	HESS HALL Chair: Dr. Ercan YILDIZ	LAWRENCE HALL Chair: Prof.Dr. İbrahim Halil MUTLU
09:00 – 09.15	Mehmet Murat YAŞAR Calculation of linear attenuation coefficient of amethyst material for radiation shielding by Monte Carlo method	Gökmen ŞEKER The effects on radiation damage of some nuclear libraries in a hybrid reactor	Orkhan MUKHTARLI Tritium activity levels in bottled water and mineral water sold in Azerbaijan	İsmail Hakkı KARAHAN Optimization of the electrophoretic deposition parameters for Biocomposite hydroxyapatite /chitosan/ collagen/h-BN
09:15 – 09:30	Sergey KARPENKO Leukemia Incidence in the Russian Cohort of Chernobyl Emergency Workers: Estimates of Radiation Risks in the Follow-up Period 1986–2014	Erol KAM Determination of morphological characteristics and mineralogical structure of the Kulakcayiri sediments by SEM and XRD	Sergey LOVACHEV Estimate of individualized radiation risk coefficients under internal exposure for the cohort of Russian emergency workers	İsmail Hakkı KARAHAN The effect of chitosan concentration on the corrosion characteristics of the biomedical grade Ti_6Al_4V implants electrophretically coated with hydroxyapatite/chitosan biocomposites
09:30 – 09.45	Maria CHUSHNYAKOVA Influence of backscattering on fission rate of excited nuclei	Hilal BARDAKÇI Three-dimensional Monte Carlo calculation of the nuclear parameters for some nuclear libraries	Abdellatif ELANIQUE Determination of the dead layer thickness for HPGe detector: measurements vs. Monte Carlo methods	Ali Armağan GÖK A study of mean free path on the radiation shielding properties of normal concrete
09:45	BREAK			
	FERMI HALL Chair: Assoc.Prof.Dr. Mehmet ERDOĞAN	BECQUEREL HALL Chair: Assoc.Prof.Dr. Fatma Aysun UĞUR	HESS HALL Chair: Dr. Yusuf KAVUN	LAWRENCE HALL Chair:Dr. Hasan ÖZDOĞAN
10:00 – 10:15	Aydan ALTIKULAÇ Measurement of natural radioactivity in quartz stone	Gökmen ŞEKER The investigation of convert ^{232}Th(n,γ)^{233}U for some nuclear libraries in a hybrid reactor	Abdellatif ELANIQUE validation of a NaI(Tl) and $LaBr_3$(Ce) detector's models: experiment and Monte Carlo simulations	Yusuf Alper KAPLAN Necessity of nuclear energy in Turkey
10:15 – 10:30	Aydan ALTIKULAÇ Determination of radioactivity levels in feldspar samples in Turkey	Erol KAM Evaluation outdoor gamma dose rates in air and cancer risk determination for Nevsehir, Turkey	Murat DAĞ Determination of direct capture reaction rate for ^{26}Si(p,γ)^{27}P	Yusuf Alper KAPLAN The role of nuclear energy for generating electric in Turkey
10:30 – 10:45	Eyyup TEL Investigation of using neutron generator source in Thorium fuel efficiency at new generation nuclear reactor types	Hilal BARDAKÇI The calculation of neutron flux for some nuclear libraries using Monte Carlo method	Ali Zafer BOZKIR The effect of varying constant source over albedo problem for quadratically anisotropic scattering	Asuman KOLBAŞI A Monte Carlo calculation of the x-ray attenuation of tungsten functional papers (TFP)
10:45	BREAK			
	FERMI HALL Chair: Prof.Dr. Üner ÇOLAK			
11:00	Inv. Talk: Prof.Dr. İbrahim Halil MUTLU How Innovation is Related to STEM Education? Where are we at? What can be Done?			
11:30	Inv. Talk: Prof. Dr. Yousry ABUSHADY 3NS [Nuclear Safety, Nuclear Security and Nuclear Safeguards] and World Nuclear Crises			

Invited Talks

Nuclear energy; Historical developments and future perspectives

ÜNER ÇOLAK

Istanbul Technical University, Energy Institute, İstanbul, Turkey

Abstract

Nuclear energy has been utilized commercially since the late 1950's. Currently, there are 450 reactors worldwide producing 10% of the world's electricity. It is expected to preserve this share for the next 40 years. The development of civilian use of nuclear energy was initiated in the US, The UK, France, Canada, and the Soviet Union. Each country decided to follow a different path to develop different technology. Later on, these technologies converged into only a number of alternatives with water cooled reactors. In addition to these countrıes, Japan, South Korea, and China developed their own reactor designs. Countries like, Czech Republic, Italy, and Spain developed industrial infrastructure to manufacture almost all the heavy equipment in their countries and capacity to export them. Currently, nuclear industry focused on safety improvements and better fuel utilization with improved economy. Meanwhile, major nuclear accidents, Three Mile Island, Chernobyl, and Fukushima, influenced the fate on the nuclear industry. Public perception of nuclear energy was also affected by these accidents. Nuclear is still considered to be an important way of generating electricity without greenhouse gas emission and base load capability. The historical developments in nuclear energy and future perspectives are discussed in this study.

Keywords: Nuclear technology

Introduction

Energy is an important commodity with the highest trade volume in the World. The resources as well as consumption are not well distributed around the World. Out of the primary energy resources more than 80% of the resources are based on fossil such as coal, oil, and natural gas. Remaining 20% is covered by hydro, nuclear, and renewables. This partition has not changed since 1973. However, the contribution of oil decreased to 31% from 46%, and in case of natural gas, it increased from 16% to 21%. Similarly, the share of coal increased by 3.5 %.

History And Future Prspective

Commercial utilization of nuclear energy for electricity production was started in late 1950's. The share of nuclear electricity reached to 3.3% in 1973 and 10.6% in 2015. On the other hand, electricity generation is dominated by fossil fuel with a share of 66.3% (39.3% coal, 4.1% oil, and 22.9% natural gas). Recently, a special attention has been given to renewable resources in order to cope with climate change and global warming problems. Nuclear energy has also positive contribution from this respect.

Nuclear energy has been widely utilized especially in developed countries. Currently, there are 454 nuclear power reactor being operated with a 400 285 MWe total net installed capacity. So far, accumulated experience is 17 813 reactor years of operation. Moreover, there are 54 new reactors under construction and they will provide an extra 55 013 MWe new generation capacity.

Currently, there are 30 countries commercially operating 450 nuclear reactors. The United States of America is the leading country with 98 nuclear reactors currently in operation. There are also a

number of countries with one or few reactors. It is also interesting to see each country's nuclear share in electricity. In this respect, France is the leading country with 71% with 58 reactors. It is followed by Ukraine and Slovakia with 55 and 54% shares using 15 and 4 reactors, respectively. It is also note to worth that there are 54 new reactors under construction as shown in Fig. 3 including the one in Akkuyu Nuclear Power Plant in Turkey.

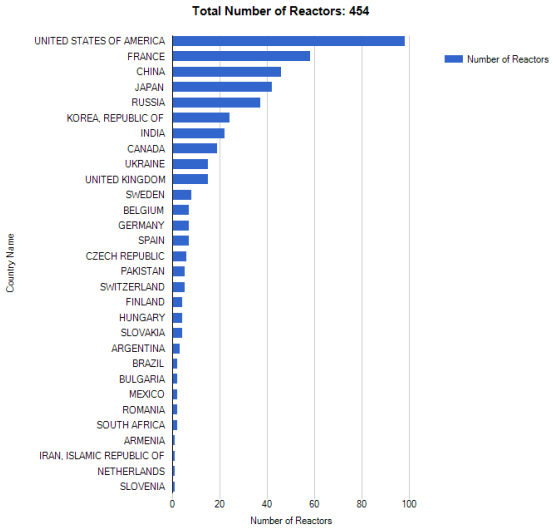

Figure 1. Operating nuclear reactors in different countries (1)

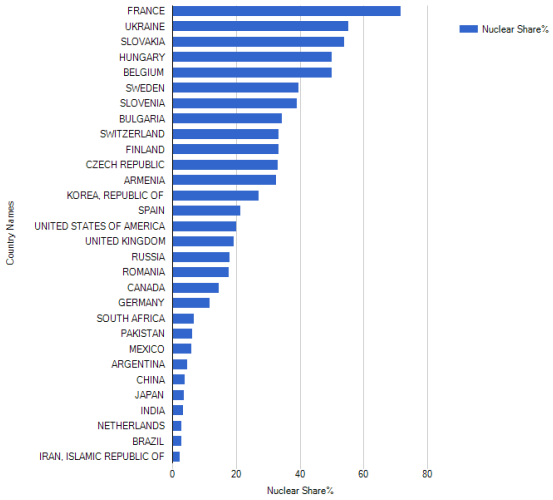

Figure 2. Share of nuclear energy in electricity production in different countries (1)

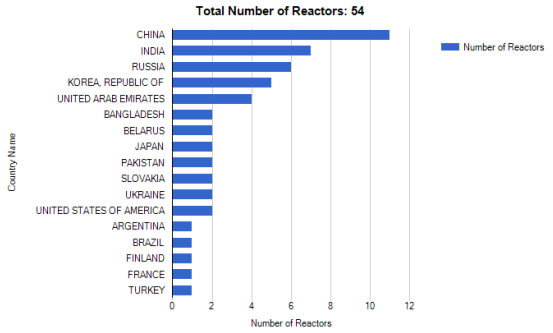

Figure 3. Nuclear reactors under construction in different countries (1)

Extended work on nuclear technology was first considered after the end of World War II. Initially, Canada was focused on the development of heavy water moderated reactors. France and the United Kingdom considered gas cooled reactors as an option for the future. Meanwhile, the light water technology was taken by the USA especially for the development of nuclear propulsion of submarines. The USSR at that time developed water cooled and graphite moderated reactors. Later, the first commercial nuclear reactor was introduced for operation in 1957 in Shippingport Atomic Power Station. It was one of the first prototype reactors of Pressurized Power Reactors (PWRs).

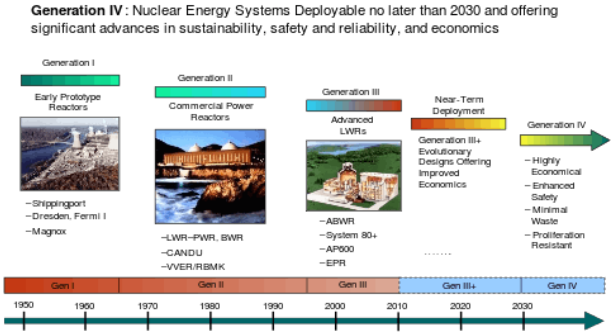

Figure 4. Progress in the development of new reactor technologies (2).

As shown in Fig. 4, development and commercialization of early prototype reactors, Shippingport (PWR), Dresden (BWR), Fermi I (FBR), and Magnox (GCR), have taken place till the end of 1960s. 1979's are the years of widespread construction of new reactors. During these years, the US, Canada, France, and Germany became important technology provider countries in nuclear industry. AECL from Canada, KWU from Germany, Framatome from France, Hithachi, Toshiba, and Mitsubishi from Japan, ASEA-ATOM

and ABB from Sweden, Babcok Wilcox, Combustion Engineering, General Electric and, Westinghouse from the US, and KEPCO from South Korea, Rosatom from Russian Federation have been important vendor and technology developer companies in the World.

Nuclear energy provides certain advantages for electricity production. Some of these may be highlighted as

- Carbon free base load electricity generation
- Stable uranium prices
- High capacity factor
- Competitive price of electricity generation
- Small footprint

Meanwhile the following disadvantages may be mentioned

- High capital cost
- Long construction period
- Need supporting infrastructure and human resources
- Large units
- Waste issues
- Public perception

During the development of nuclear technology, there were ups and downs. Oil crisis in 1970's caused significant concern for energy security in the US and nuclear energy considered to be a viable solution. Later on Three Mile Island accident took place in 1979 in the US as the first severe accident in the World. Then, there was a downtrend for nuclear. There have been no new build orders for a long time. Later on, Chernobyl accident in Ukraine in 1986 resulted in similar consequences in the world. During the turn of the century, there was significant increase in nuclear capacity due to life extensions and power uprates. It was considered as "Nuclear Renaissance" and many new orders have been expected. As these developments happened, technology developer companies came up with new reactor designs providing better safety features. Large units were preferred for the economy of scale. The interest to nuclear power was really significant.

Then, Fukushima Daiichi accident took place in 2011. It was another undesired event to halt the industry again. Currently, recovery process is going on. These ups and downs are well reflected in the Fig. 5.

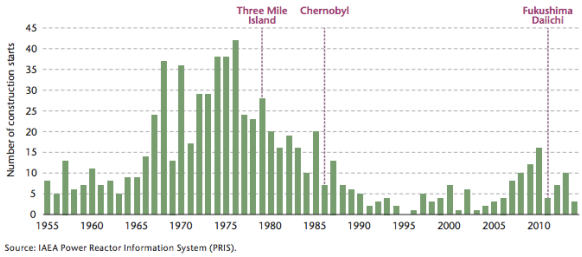

Figure 5. The number of new constructions initiated each year (1).

Nowadays, Rosatom is busy to make agreements with especially developing countries to promote nuclear energy and their technology. Their difficulty is to provide finance and respective workforce to all prospective projects. They have on-going projects in Belarus, Finland, Bangladesh, and Turkey in addition to their own domestic projects. Meanwhile, China has been busy with their domestic projects and is getting ready for international projects as the main competitor to Russian Federation. Western countries are mainly focused on duties for existing fleet. Development work is focused on new generation reactors (Generation IV) and Small and Medium Sized Reactors (SMR's)

Conclusions

Nuclear energy has been an important source for producing electricity. It is expected to remain with the same share for the next 50 years. In the near future, developing countries in the World will be the main market. Russian Federation and Chine will be two important role players. The main target of vendor companies will be reducing the capital cost without compromising from safety. SMR's may appear in the market as early as 10 years from now. They may affect the market significantly. On the other hand, in order for nuclear to survive against renewables, cost competitiveness, waste and decommissioning issues should be taken care of and improved.

Reference

1. International Atomic Energy Agency (IAEA), Power Reactor Information System. https://pris.iaea.org
2. The Generation IV International Forum, https://www.gen-4.org/gif/jcms/c_9260/public

Green Nuclear Energy: Thorium

SALEH SULTANSOY
TOBB ETÜ Engineering Faculty
Azerbaycan Elmler Akademiyası Fizika İnstitutu
ATLAS, CLIC and LHeC Collaborations, CERN
European Committee for Future Accelerators

Energy production and consumption are among the most important indicators of the level of development of the countries. In particular, electricity consumption is directly related to the level of prosperity. In this respect, the diversity of energy sources and optimization are very important. Today, the lion's share of energy production is obtained from fossil resources; but the rate of fossil resources must be reduced rapidly in terms of reducing global warming. In terms of meeting the energy supply at the required level, we have two options: renewable energy sources and nuclear energy. Actually, these two sources are not alternatives to each other; they should be considered as complementary.

Electricity generation from renewable sources has two major disadvantages: it is expensive and non-persistent (the problem of continuity can be overcome in the coming years thanks to new energy storage technologies). Even the developed countries are still forced with the cost problem. In fact, renewable energy sources are not as ecological as one might think. For example, space required for 100 GW plants: nuclear – 100 km^2, solar – 50.000 km^2, wind – 60.000 km^2, hydraulic – 240.000 km^2, biomass – 600.000 km^2 (for comparison: Turkey's area is 780.000 km^2). Concerning developing and underdeveloped countries, there is no serious alternative to nuclear energy. We meet here with two major problems: the risk of accidents and nuclear waste. The 3rd and especially the 4th generation technologies solve the reliability problem (Chernobyl and Fukushima were based on 2nd generation technology). Concerning GNP per capita: if > 30.000 $ renewable, if < 10.000 $ nuclear.
Thorium-fueled nuclear systems, especially ADS, which are much safer than uranium-fueled reactors, will also be able to solve the waste problem. While the amount of waste generated in these systems is much lower, they can also be used to burn waste from uranium-fueled reactors, as well as military plutonium.
Forecasts:

- commercialization of thorium-fueled conventional type nuclear reactors within next 5-10 years,
- commercialization of thorium-fueled molten salt reactors within next 10-15 years,
- commercialization of 100% thorium-fueled (real "green" nuclear energy) accelerator driven (ADS) nuclear reactors within next 15-20 years.

Finally, in the 21st century, this scenario is much more realistic than ITER's choice to solve the energy problem of mankind and requires an order less investments.

LHC Experiments and Future Circular Collider (FCC) Project

İLKAY TÜRK ÇAKIR

Giresun University

This presentation includes information about the world's largest particle-physics laboratory, European Organization for Nuclear Research (CERN). In addition, the Large Hadron Collider (LHC) and its dedectors called ATLAS, CMS, ALICE and LHCb are introduced. Moreover, current status of Turkey and CERN relationship has been given in this presentation. Furthermore, a nuclear experiment namely the Isotope mass Separator On-Line facility (ISOLDE) is explained. Finally, the next generation collider as Future Circular Collider (FCC) and its options (FCC-hh, FCC-ee, and FCC-he) are mentioned for comparision, which is supported by EuroCirCol project.

How Innovation Is Related to STEM Education? Where are we at? What can be Done?

İBRAHİM HALİL MUTLU
Akdeniz University

In this study, we will briefly discuss the applications of physics as a basic science in our daily lives and provide important scientific contributions to physics by the scientists along with the training they received. In addition, the requirements for admission on basic science and engineering programs in developed countries will be presented and compared the current system in Turkey and the relationship between education and development will be addressed. It is important that the STEM education or the basic science education programs should be updated in accordance with the developing techniques and technologies of educational sciences. Taking the best practices in the world as an example, the efforts that can be practiced to correct the situation in our country should be put forward on such platforms where all stakeholders can contribute. The proposal for a solution that will increase the competitiveness of our future generations on the world scale that will also conform to our culture should be urgently addressed and put into practice.

Nuclear imaging of paintings

THOMAS CALLIGARO

Centre de Recherche et de Restauration des Musées de France, C2RMF, Palais du Louvre - Porte des Lions, 14 Quai François Mitterrand, 75001 Paris, France

Beams of X-rays ions and neutrons have been successfully applied to record elemental maps of historical paintings. Such probes can notably reveal without contact and in a non-destructive way pigment distribution within entire paintworks through their elemental fingerprints. The comparison of the images recorded using such nuclear techniques with pictures taken with routine imaging techniques (e.g. visible, UV, IR photography and X-ray radiography) provide curators, art historians and restorers information concerning the painter techniques and choices, and can help in the preparation and the monitoring of restorations.
The presentation will focus on three nuclear imaging techniques employed in the study of paintworks. First is the scanning X-ray fluorescence technique that was initially developed at the synchrotron, and then transposed to the laboratory under the name MA-XRF [1]. The second approach is the PIXE scanning using an external microbeam of protons of a few MeV [2]. The last is the Neutron-Activation Auto-Radiography technique (NAAR), which exploits the flux of cold neurons from a nuclear reactor. The merits and limitations of the three approaches will be discussed. For example, excitation with protons confers to PIXE a probing depth that can be adapted with incident ion energy, an improved yield for light elements compared to heavier ones, and an easy beam scanning. On the other hand, the scanning X-ray beam is probing deeper and exhibits unique features such as Compton scattering and is less susceptible to induce modifications in paint materials than ion beams. Finally, the deep penetration of neutrons and gamma-rays permits to image isotopes independently of the paint layer thickness and stratigraphy.
The capabilities and limitations of the nuclear imaging of paintings will be illustrated by the results obtained on Leonardo da Vinci masterpieces from the Louvre museum (MA-XRF), 19th c paintings (scanning-PIXE) and a portrait by Rembrandt (NAAR).

[1] E. Ravaud, L. Pichon, E. Laval, V. Gonzalez, M. Eveno, T. Calligaro, Development of a versatile XRF scanner for the elemental imaging of paintworks, Appl. Phys. A122 (2016) 17
[2] T. Calligaro, V. Gonzalez, L. Pichon, PIXE analysis of historical paintings: Is the gain worth the risk?, Nucl. Instr. And Meth. B363 (2015) 135

Türkiye neden nükleer enerji teknolojisine girmeli?

NAZMİ TURAN OKUMUŞOĞLU
Ondokuz Mayıs University

Türkiye'nin enerji durumu ve nükleer enerji teknolojisine girmesi için gerekçeler. Nükleer enerjinin tarihçesi, gelişimi. Dünya'da nükleer enerjinin bugünkü durumu. Türkiey'de nükleer enerji santralleri kurma çalışmaları. Akkuyu nükleer santrali ile ilgili ana başlıklar.

Oral Presentations

Spectral statisitcs of transition probablities in regular nuclei

[1] HADI SABRI University of Tabriz
[2] AIDIN GHALEHASADI University of Tabriz
[3] ASGAR HOSSEINNEZHAD University of Tabriz

In this study, we have analyzed the fluctuation properteis of electromagnetic transition intensities in the regular nuclei. All the available experimental data are used to construct different sequences and consider the effect of mass and deformation on statistical properties. Results show a Poisson-like behavior for quadrupole transitions. Also, we have observed GOE like statitics for the transition probabilities of deformed regular nuclei.

Keywords: transition probablities, Spectral statisitcs, quadrupole t, quadrupole transitions, nuclear deformation

A new Aziz potential parameter set for nucleon-nucleon interaction: First results

[1] HASAN BİRCAN Dumlupınar University
[2] KAAN MANİSA Dumlupınar University
[3] MEHMET ERDOĞAN Selçuk University
[4] AHMET BİÇER Dumlupınar University

Atomic theory based on the shell model has provided remarkable clarification of the complicated details of atomic structure. Therefore, nuclear physicists attempted to use a similar theory to attack the problem of nuclear structure in the hope of similar success in clarifying the properties of nuclei. We keep it in our mind, we have tried to obtain a new parameter set for Aziz potential, which used in atomic interaction for Helium, for nucleon-nucleon interactions.

Keywords: Aziz potential, nucleon-nucleon interaction, nuclear matter

VMC calculations for nuclear matter by using Aziz potential with a new parameter set

[1] HASAN BİRCAN Dumlupınar University
[2] KAAN MANİSA Dumlupınar University
[3] MEHMET ERDOĞAN Selçuk University
[4] AHMET BİÇER Dumlupınar University

We have obtained ground state properties of Symmetric nuclear matter (SNM) by using a Variational Monte Carlo method (VMC) in our previous studies. Accepting these studies as the results of a computer experiment, a new parameter set for Aziz potential is found to consistently reproduce the saturation properties of the nuclear matter obtained VMC calculations. The saturation properties of SNM are calculated by the Aziz potential with the new parameter set.

Keywords: Aziz potential, nuclear matter, Variational Monte Carlo

Investigation of fusion-fission target systems with Monte Carlo method by using accelerated deuterons

[1] MEHMET EMİN KORKMAZ Karamanoğlu Mehmetbey University
[2] ÖZGÜR CULFA Karamanoğlu Mehmetbey University

Fusion-fission reactions can be performed on a fine pitch of micron thickness by using high power lasers. The basic concept of this scenario is based on the density and energy of accelerated particles or ion beams by high intense lasers. In this study, we have used accelerated deuteron energy spectra by high power laser-solid interactions obtained computationally using 2D EPOCH PIC simulations. These accelerated deuterons bombarded the solid Fusion-Fission targets. The Monte Carlo code MCNPX2.7.0 was used for reactions occurring in the fusion-fission target system. As a result; fusion-fission reactions have been achieved with accelerated deuteron by high-intense table-top terawatt laser and the deuterons can reach up to 10 MeV of energy.

Keywords: High intensity lasers, Deuteron, Monte Carlo Method, PIC code, Fusion-Fission

Excitation of heliumlike Kr34+(1s2) ions by neutrals at intermediate impact energies: Projectile nuclear charge dependence

[1] BOUMEDIENE LASRI University tahar Moulay of Saïda, Algeria Theoretical Physics laboratory, University of tlemcen, Algeria
[2] FATIMA BOUASRIA University tahar Moulay of Saïda, Algeria
[3] MOHAMMED SAHLAOUI Theoretical Physics laboratory, University of tlemcen, Algeria
[4] MAMMAR BOUAMOUD Theoretical Physics laboratory, University of tlemcen, Algeria

Schwinger variational approach to the process of direct electronic excitation of atoms by impact of ions at intermediate impact energies was shown to be very successful in predicting the saturation of excitation cross sections when the projectile charge is increased. In this study, our new approach is based on the fractional form of the Schwinger variational principle and applied to study the excitation of Kr34+ (1s2) ions impinging at 34 MeV/u (v=35 a.u) by various atoms of nuclear charges Zp (2<ZT<54) which include neutral gaseous (He, N_2, Ne, Ar, Kr, Xe). Our theoretical calculations of the excitation cross sections stay in good agreement with experimental data of Chabot et al.

Keywords: Schwinger variational principle, excitation cross section, saturation effect.

Exploring the magicity for the ^{78}Ni nucleus

[1] FURKAN OK Yıldız Teknik University Physics Department
[2] HAŞİM ZAHİD GÜVEN Yıldız Teknik University Physics Department
[3] KUTSAL BOZKURT Yıldız Teknik University Physics Department
[4] ESRA YÜKSEL Yıldız Teknik University Physics Department

Exploration of nuclei with extreme number of protons and neutrons has become a very active area of research with the advances in the experimental facilities and theoretical models. In recent years, it has been shown that exotic nuclei display some special properties like weakening or disappearance of some well-known magic numbers (2, 8, 20, 28, 50 and 82), and formation of the new ones [1]. Therefore, exploration of these nuclei is quite important in order to understand the changes in the nucleon-nucleon interaction and shell structure of nuclei through the nuclear drip lines. Presently the Hartree-Fock Bogoliubov (HFB) approach with Skyrme type energy density functionals provide the most complete and reliable results in the calculation of the properties of nuclei over the nuclide chart [2].

In this work, we explore the magic nature of the ^{78}Ni nucleus using the Hartree-Fock-Bogoliubov approach with Skyrme type energy density functionals. The effect of the tensor interaction on the Z=28 and N=50 magic numbers is investigated using SLy5 (without tensor) and SLy5+T, T44 and T66 (with tensor) interactions in Nickel isotopic chain and N=50 isotones, respectively. The single-particle energies and two-nucleon gaps are analyzed and compared with the available experimental data. It is shown that the tensor force strengthens the magicity of the ^{78}Ni nucleus by increasing the single-particle gap of protons and neutrons, which also supports the results of the recent experimental data in Refs. [3,4].

[1] O. Sorlin and M.-G. Porquet, Prog. Part. Nucl. Phys. 61, 602 (2008).
[2] K. Bennaceur and J. Dobaczewski, Comput. Phys. Commun. 168 (2005) 96.
[3] L. Olivier et al., Phys. Rev. Lett. 119 (2017) 192501.
[4] A. Welker et al., Phys. Rev. Lett. 119 (2017) 192502.

This work is supported by the Scientific and Technological Research Council of Turkey (TÜBİTAK) under project number MFAG-114F335.

Keywords: magicity, skyrme, hfb, tensor interaction, nickel

Radon (Rn-222) activity in some deep well water in Uşak and its surrounding

[1] RIDVAN ÜNAL Uşak University Vocational School of Health Services, ,
[2] TUNCAY ERDOĞAN Alpay Günbayram Anadolu Lisesi

Radon gas and other decay products constitute half of natural radiation exposition. One of the main sources of radioactive elements is underground water that includes radioactive elements from ^{238}U and ^{232}Th group because of radioactive materials which it passes through and contacts. Moreover, there are studies trying to predict eartquakes by focusing on the relation between changing radon gas activities and seismic activities. This study aims on determining radon and radium activities contained in deep well water in Uşak and its surroundings. The water samples taken from 10 different wells by weekly periods between August and September are examined in the Nuclear Physics Laboratory of Physics Department at Afyon Kocatepe University. According to analysis, maximum and minimum radon activities are 21.56 Bq/L and 0.05 Bq/L, respectively. Regarding radium activity in the deep well water, its maximum and minimum activities are found as 5.84 Bq/L and 0.02 Bq/L, respectively.

Keywords: Radon, Radium, Earthquake, Activity, Deep Well Water

Double beta decay and its potential to investigate BSM physics

[1] SABIN STOICA International Centre for Advanced Training and Research in Physics (CIFRA), Romania

International Centre for Advanced Training and Research in Physics, Bucharest-Magurele, Romania Double beta decay (DBD) is a rare nuclear process of great interest due to its potential to provide information about physics beyond the Standard Model (BSM). Indeed, the discovery of the so called neutrinoless DBD mode would give answers to fundamental issues about possible violation of the Lorentz and CP symmetries in the weak sector, lepton number conservation, or neutrino properties such as i) are neutrinos Dirac or Majorana particles? ii) what are the neutrino absolute masses; iii) what is the correct hierarchy of the neutrino masses? iv) are there sterile neutrinos? In my talk, I will give a short review on the actual DBD investigations, especially the theoretical ones. I will present the theoretical challenges related to the DBD study, namely the calculation of the nuclear matrix elements, phase space factors, predictions of half-lives and constrains on BSM parameters. Finally, I will present results obtained by our group in the study of this process.

Keywords: nuclear physics, double beta decay, nuclear matrix elements, beyond SM physics

How effective are the PN-QRPA calculation of weak rates of odd-a nuclei in stellar environment

[1] JAMEEL-UN NABI [2] MUHAMMAD MAJID [3] MUHAMMAD RIAZ GIK

GIK Institute of Engineering Sciences & Technology

In a recent study by Cole et al. [Phys. Rev. C 86 (2012) 015809], it was concluded that quasi-particle random phase approximation (QRPA) calculations show larger deviations and overestimate the total experimental Gamow–Teller (GT) strength. It was also concluded that QRPA calculated electron capture rates exhibit larger deviation than those derived from the measured GT strength distributions. The main purpose of this study is to probe the findings of the Cole et al. paper. This study gives useful information on the performance of QRPA-based nuclear models. As per simulation results, the capturing of electrons that occur on medium heavy isotopes have a significant role in decreasing the ratio of electron-to-baryon content of the stellar interior during the late stages of core evolution. We report the calculation of allowed charge-changing transitions strength for odd-A fp-shell nuclei (^{45}Sc and ^{55}Mn) by employing the deformed pn-QRPA approach. The computed GT transition strength is compared with previous theoretical calculations and measured data. For stellar applications, the corresponding electron capture rates are computed and compared with rates using previously calculated and measured GT values. Our finding shows that our calculated results are in decent accordance with measured data. At higher stellar temperature, our calculated electron capture rates are larger than those calculated by independent particle model (IPM) and shell model. It was further concluded that at low temperature and high density regions, the positron emission weak-rates from ^{45}Sc and ^{55}Mn may be neglected in simulation codes.

Keywords: Gamow–Teller transitions; electron capture rates; pn-QRPA theory; stellar evolution; core-collapse

Reaction mechanism of $^{8}Li(a,n)^{11}B$ at low energies

[1] ALİ İHSAN KILIÇ Czech Academy of Science, Czech Rep.
[2] BARRY DAVIDS TRIUMF, Canada
[3] FADİME KILIÇ Gazi University
[4] İSMAİL HAKKI SARPÜN Akdeniz University
[5] ALEX BROWN Michigan State University, USA

The investigation of cross sections for the $^{8}Li(a,n)^{11}B$ reaction has important impact for both primordial nucleosynthesis in the inhomogeneous models as well as constraining the physical conditions characterizing the r-process. However, there are large discrepancies existing between inclusive and exclusive measurements of the $^{8}Li(a,n)^{11}B$ reaction cross section below 3 MeV. In the present work, in order to undertand reaction mechnanism of $^{8}Li(a,n)^{11}B$, we have applied WKB, DWBA and R matrix theory. Spectroscopic factor has been calculated for 12B compound structures. The cross section for the $^{8}Li+^{4}He$ reaction comes from not only direct reaction but also compound nucleus ^{12}B. Inclusive measurements are close to calculated the theoretical calculations which including direct reaction contribution with DWBA below 3 MeV. However, there are dramatic discrepancy between theory and experimental cross section data below the 3 MeV. Furthermore, channel dependence of WKB approximation for penetration factor dependency of cross-section and S-factor calculation have been applied to illustrate the cross section measurements below the Coulomb barrier. The new R-matrix calculations have been carried out to achieve both reaction rates and partial S factor, R-matrix calculation shows that there could be a new resonance structure in the astrophysical site. Moreover, nobody has mentioned up to now that it is important to remark that the tail of sub-threshold resonance effect might be effect of the total cross section below the 0.6 MeV.

Keywords: inhomogeneous models, exclusive measurements, Spectroscopic factor, compound structures

Calculation of Astrophysical S-Factors for $^{13}C(\alpha,n)^{16}O$ Reaction by Means of Low Energy Permeability

ERCAN YILDIZ

Kırıkkale University, Kirikkale, Turkey

Abstract

This study cross sections of the $^{13}C(\alpha,n)^{16}O$ reaction have been calculated at low energy ranges. In these theoretical calculations, the TALYS 1.8 codes were used. Also, the astrophysical S-factors which describe the possibility of reaction in low energies were calculated. Results of our calculations were checked to the experimental data obtained from EXFOR database.

Keywords: cross section s-factor, TALYS

Introduction

The root of the chemical elements has been subject of numerical studies since contemporary physics was born. For the decades, its examination has drawn the curiosity of cosmologists, astrophysicists, and astronomers, besides experimental, theoretical particle, and nuclear physicists. The $^{13}C(\alpha,n)^{16}O$ reaction is the neutron source for the major collateral of the p-process, managing for the producing of the best part of the nuclei in the mass range 90 <A <208 [1].

A joint question in nuclear astrophysics is that the cross sections at the Gamow energy area are very little be measured in the laboratory [2].

The $^{13}C(\alpha,n)^{16}O$ reaction detect the predominant neutron root of the s-process in thermally pulsing, low-mass, asymptotic gigantean branch (TP-AGB) stars. The temperature in the course of the s-process in the ^{13}C pocket of 90×10^6 K comply with a Gamow window of 140-230 keV. Since this energy is far under the Coulomb barrier, the cross section of this reaction is highly little and its ratio may solely be calculated from the measurements at higher energies [1].

Astrophysical s-factor the major typical of a reaction is the cross section σ(E), which has the size of a superficial and related on energy also the cross section at stellar energies is governed by Coulomb effects. The astrophysical s-factor is defined as [2]

$$S(E) = \sigma(E).E.\exp(2\pi\eta) \quad (1)$$

where, η is the Sommerfeld parameter, $(Z_1Z_2e^2)/\hbar v$. S(E) is function of energy with leisurely changing than $\exp(-2\pi\eta)$ and cross-sections σ(E). The astrophysical S-factors characterize the probability of reaction in low energies. In astrophysical implementation, S(E) should be known for numerous reactions at low energies, E≤a few MeV. Empirical measurements of σ(E) at lower energy are mainly not existing (because of the Coulomb barrier exponentially depress low-energy cross sections) [3].

Results

In this study, the reaction cross-sections and astrophysical S-factors of the $^{13}C(\alpha,n)^{16}O$ reactions were calculated. The (α,n) reaction cross sections were calculated in the occurance energy range of 0 to 8 MeV. In these calculations, the TALYS 1.8 [4] codes used. Results of our calculations were checked to the experimental data obtained from EXFOR [5] database.

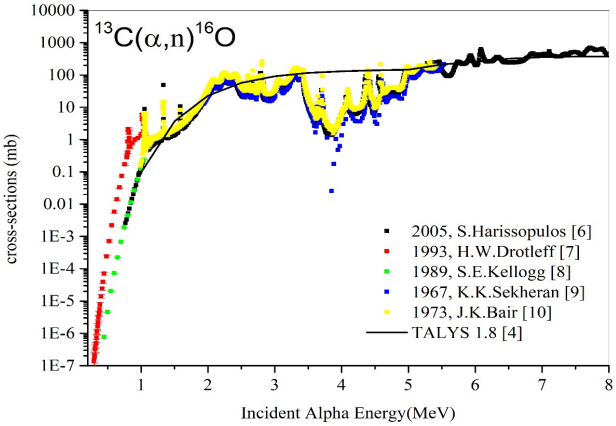

Fig.1. Empirical of experimental and evaluated cross-sections of $^{13}C(\alpha,n)^{16}O$ as a function α energy.

As already said, the S(E) factor is beneficial for an extrapolation from experimental data measured at higher energies because of its small energy addiction. The standard procedure consists in fitting the high energy data using a proper theoretical function (in the simplest

approximation, polynomial). Then this is extrapolated to the astrophysical energies.

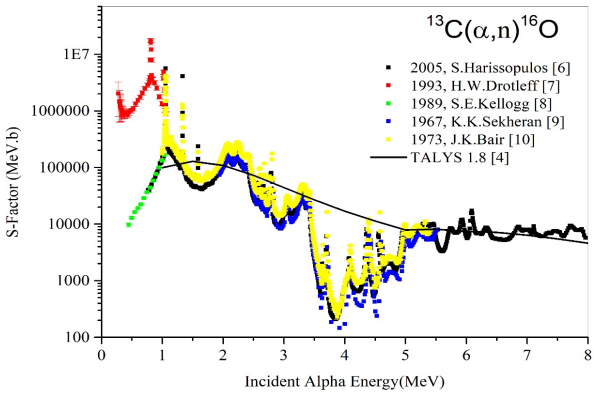

Fig.2. Empirical of experimental and evaluated astrophysical s-factors of $^{13}C(\alpha,n)^{16}O$ as a function α energy.

In Figure 1, empirical and theoretical cross sections for the $^{13}C(\alpha,n)^{16}O$ reaction demonstrate that TALYS 1.8 [4] and values greater than 1 MeV are compatible with [6,9,10]. However, it can be said that the similar harmony has decreased in values below 1 MeV.

In Figure 2, when the experimental and theoretical astrophysical s-factor values for the $^{13}C(\alpha,n)^{16}O$ reaction are examined, it can be said that TALYS 1.8 [4] values are consistent with the values of [6,9,10].

As we said before, $^{13}C(\alpha,n)^{16}O$ reaction is determine the main neutron source for the s-process ,but as can be seen in Figure 1, especially in the low energy ($E \leq 1$ MeV) region and in the Gamow energy region, the lack of data attracts attention. Recent working continuation to energies especially below 1 MeV are necessary for this astrophysical important system for a better theoretical treatment

Reference

[1] L.S. Alinka and P. Descouvermont, International Journal of Astrobiology, 11, (2012).

[2] I. Kochanek, A. Boeltzig and G.F. Ciani, G.F., EPJ Web of Conferences 136 ,01010 (2017).

[3] E. Yildiz and A. Aydin, Journal Of Fusion Energy 35, (2016).

[4] http://www.talys.eu, Date of access 09.11.2017

[5] EXFOR/CSISRS, Brookhaven National Laboratory, National Nuclear Data Center, Database Version of September 2017.

[6] S. Harissopulos et al., Physical Review Part C 72, (2005).

[7] H.W. Drotleff et al., Astrophysical Journal 414, (1993).

[8] S.E. Kellogg, R.B. Vogelaar and R.W. Kavanagh Bulletin of the American Physical Society 34, (1989).

[9] K. K. Sekheran et al., Physical Review 156-4, (1967).

[10] J.K. Bair, F. X. Haas, Physical Review, Part C 7, (1973).

Investigation of the geometric shapes of $^{80-88}$Zr isotopes within the interacting boson model-1

[1] MERVE AYDOĞAN Kırıkkale University
[2] MAHMUT BÖYÜKATA Kırıkkale University

In this recent work, we focus on the prediction of the geometric shapes of the even-even ^{80,82,84,86,88}Zr isotopes. For this purpose, the potential energy surfaces (PES) obtained from the interacting boson model-1 (IBM-1) were plotted as a function of the deformation parameters (β,γ) by using common Hamiltonian parameters of IBM-1. For this process, the energy levels of given nuclei were calculated by fitting the parameters of the constructed IBM-1 Hamiltonian. Later, the B(E2) transition values were calculated to obtain other set of the deformation parameters. We compared all calculated β deformations within the experimental ones.

Keywords: energy levels, B(E2) values, deformation parameters, IBM-1 model

Light charged particle emission of VC composites

[1]İSMAİL HAKKI SARPÜN, [2]AHMET BOZKURT, [3]ABDULLAH AYDIN, [4]SUAT PAT, [5]MOHAMED BELGAID

[1]Akdeniz University, Physics Dept., Antalya, Turkey
[2]Akdeniz University, Biomedical Engineering Dept., Antalya, Turkey
[3]Kırıkkale University, Physics Dept., Kırıkkale, Turkey
[4]Eskişehir Osmangazi University, Physics Dept., Eskişehir, Turkey
[5]USTHB, Physics Faculty, Algiers, Algeria

Abstracts

Composite materials that are made of ceramics are considered to be suitable as structural materials for the first-wall or blanket material in fusion research. Vanadium carbide (VC) composites that are known to be radiation-resistant have been developed to serve as candidate structural materials for future fusion reactors that will operate at extremely high temperatures. In this study, VC composites, which were produced in Eskisehir Osmangazi University by plasma RF sputtering method, have been investigated as a target material using Monte Carlo simulations to obtain light charged particle (proton, deuteron and alpha) emission spectra.

Keywords: MCNP, VC, Composite

Introduction

The candidate reactor structural materials can be classified according to their activation characteristics: C, Si, Ti, Fe, Cr and V are considered as low activation elements and Al, Ni, Ag, Co and Nb elements are some of the high activation materials [1 –4]. The choice of the structural materials for reactor components depends not only on mechanical properties, compatibility with other materials and irradiation performance, but also on their radiological properties [5 –7].

The neutron radioactivity is related with the irradiated material. First-wall and blanket materials have high radioactivity concentration due to being the most neutron flux exposed components. Therefore, structural material selection will has been delimitated the radioactivity in a fusion reactor [8]. The development of fusion reactor structural materials with good thermo-mechanical and physical properties coupled with low activation characteristics is the aim of the fusion structural material research studies. Ni and its alloys have been irradiated with 14–15 MeV neutrons in several studies to determine H trapping and He bubbles effects and also displacement per atom (DPA) of the material [9 –13].

Vanadium carbide (VC) is the inorganic compound and an extremely hard refractory ceramic - composite material, which hardness is of 9-9.5 Mohs [14].

In this study, one of the candidate materials, VC composites, which were produced in Eskişehir Osmangazi University by plasma RF sputtering method, have been investigated as a target material under the bombardment of neutrons using MCNP code to obtain light charged particle (proton, deuteron and alpha) emission spectra.

Calculation Methods

MCNP (Monte Carlo N - Particle Transport) is a simulation code developed in LANL (Los Alamos National Laboratory) to simulate radiation interactions using the Monte Carlo method. Each card in the input file, which should be introduced to the MCNP code, describes the information on geometrical properties of the problem, information describing the materials in the problem, the properties of the source, and the type of results desired by using three basic sets of cards: cell, surface and data cards. The MCNP code obtains the physical rules of interactions in the form of evaluated cross section data files to transport each particle through target materials located between the source and the detectors [15]. Electron microscopy image is shown in Fig. 1.

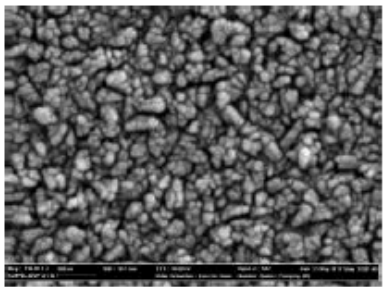

Fig. 1. Electron microscope image of VC composite

In this work, a neutron beam of 14 MeV was directed toward VC composite samples which is used as a target material in MCNP simulation. In simulations, energy and flux values of protons, deuterons and alpha particles were tracked as a result neutron interaction with the target using special types of tallies that serve as detectors. The spectrum of these secondary particles produced from neutron interactions is shown in Fig. 2.

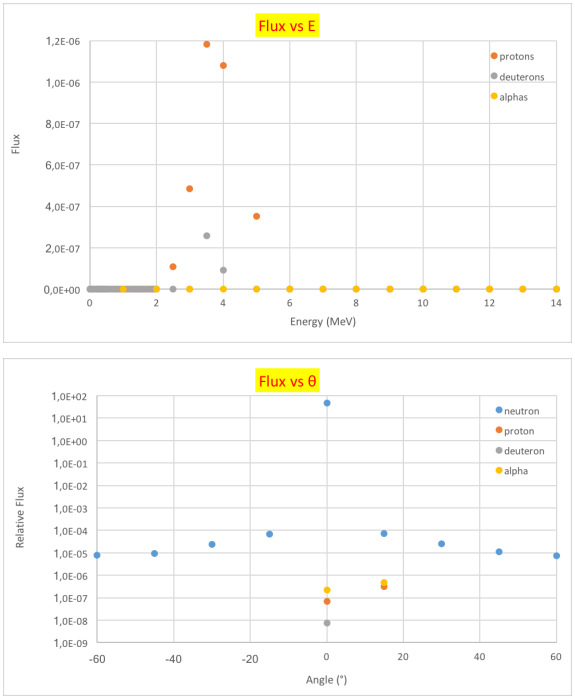

Fig. 2. The spectrum of charged particles

Different sample thickness have used in calculations and Table 1 shows the effect of thickness to charged particle emission.

Table 1. The effect of sample thickness to charged particle emission

Thickness	neutron	proton	deuteron	alpha
mm	ptcl/cm^2	ptcl/cm^2	ptcl/cm^2	ptcl/cm^2
1	47.1209	6.7159E-08	7.3067E-09	2.2607E-07
10	47.1208	6.71628E-08	7.30674E-09	2.26077E-07
100	47.12	6.7200E-08	7.30673E-09	2.26152E-07
1000	47.1122	6.75595E-08	7.30669E-09	2.2691E-07

Conclusion

The major outcome of the investigation was establishing the fact that the VC composites are potential candidate structural materials for reactor applications. The next step of the project will be held in Algeria, via USTHB. The samples will be bombarded with neutrons.

References

1. E.E. Bloom et al., J. Nucl. Mater. 122–123, 17 (1984)
2. M. Victoria et al., Nucl. Fusion 41(8), 1047 (2001)
3. P.M. Raole et al., Trans. IIM 62, 2–105 (2009)
4. R.J. Kurtz et al., J. Nucl. Mater. 386–388, 411 (2009)
5. D.R. Harries et al., J. Nucl. Mater. 191–194, 92 (1992)
6. A. Möslang et al., Int. J. Mater. Res. 99, 1045 (2008)
7. S.J. Zinkle, J.T. Busby, Mater. Today 12, 12 (2009)
8. M. Zucchetti, M. Merola, J. Nucl. Mater. 233–237, 1486 (1996)
9. B. Constantinescu et al., Radiat. Phys. Chem. 49(4), 411 (1997)
10. V.N. Chernikov et al., J. Nucl. Mater. 250, 103 (1997)
11. B. Constantinescu et al., Fusion Eng. Des. 41, 79 (1998)
12. B. Lommel et al., Nucl. Instrum. Methods A 655, 44 (2011)
13. B. Constantinescu et al., Int. J. Hydrog Energy 26, 507 (2011)
14. D.R. *Lide, Handbook of Chemistry and Physics (87 ed.), CRC Press, pp. 4–93 (1998)*
15. Briesmeister, J.F., Editor. MCNP- A General Monte Carlo N-Particle Transport Code System. LA-12625-M, Version C (2000)

An assessment of therapy dosimeter calibrations performed in SSDL

[1] DOĞAN YAŞAR TAEK
[2] ENİS KAPDAN TAEK
[3] MUHARREM KORKMAZ TAEK

Purpose: In this study, it was aimed to evaluate the calibration performance and stabilities of user ionization chambers and the reference standards between 2006 and 2016. Methods: The user dosimeters were calibrated according to the international dose protocols, air kerma, NK and absorbed dose to water, ND, W methods. The extended uncertainties for NK and ND, W calibration coefficients were calculated to be 1.0% and 0.9%, for a coverage factor k=2, with a confidence probability of 95%, respectively. The stability was obtained by repeated calibrations and intercomparison of IAEA/WHO transfer chamber calibrations. Results: Relative response of reference dosimeter was in the range of 0.993-1.005 and 0.999-1.013 for NK and ND, W, respectively. The results are within the acceptable limit (±1.5%) determined by the IAEA. The stability of user ionization chambers is determined by evaluating repeated calibrations and is calculated to be in the range 0.9946±0.0034 to 1.0104±0.0014 for NK and 0.9968±0.0096 to 1.0024±0.0009 for ND, W. Conclusions: User chambers'stability was observed to be within 0.3% limit as recommended by TG-51 addendum. This study confirms the opinion that the calibration of therapy dosimeters does not need to be performed every year, taking into account long-term stability of the chambers and except for breakdown and maintenance.

Keywords: Calibration, SSDL, Standardization, Ionization chambers, Radiotherapy

Nuclear level densities of ^{143,147}Nd isotopes

[1]KÜRŞAD OSMAN AY, [1]MUSTAFA ÖZGÜR, [2]MAGNE GUTTORMSEN, [3]EMEL ALĞIN, [2]FRANK LEONEL BELLO GARROTE, [2]LUCIA CRESPO CAMPO, [2]ANDREAS GORGEN, [2]TRINE WIBORG HAGEN, [2]ANN CECILIE LARSEN, [2]VICTOR MODAMIO, [2]FABIO ZEISER, [2]SUNNIVA SIEM, [2]VETLE WEGNER INGEBERG, [2]SUNNIVA ROSE, [2]EDA ŞAHİN, [2]GRY MERETE TVETEN, [2]JORGEN ERIKSSON MIDTBO, [2]BONGINKOSI VINCENT KHESWA, [2]MALIN KLINTEFJORD, [2]THERESE RENSTROM

[1]Eskişehir Osmangazi University,
[2]University of Oslo
[3]Adana Bilim ve Teknoloji University

Nuclear level densities, which are described as number of accessible quantum levels per unit energy at a certain excitation energy, have been very important quantities since first described by Hans Bethe [1]. They are used in various areas, including neutron-capture cross section calculations in astrophysics, designing and testing nuclear reactors, transmutation of nuclear waste. The Nuclear Physics Group at the University of Oslo has established a method to determine simultaneously the nuclear level densities and γ-ray strength functions from particle-γ coincidences [2,3]. For nearly three decades, the so-called Oslo method has been a robust way to obtain level densities and γ-ray strength functions. ^{142,146}Nd metallic isotopes were bombarded by deuteron beam at the Oslo Cyclotron Laboratory and ^{142}Nd(d,p) and ^{146}Nd(d,p) reactions were studied. The level densities of ^{143,147}Nd isotopes will be presented.

[1] H.A. Bethe, Phys. Rev. 50, 332 (1936) .
[2] A. Schiller et al., Nucl. Instrum. Methods Phys. Res. A 447 (2000).
[3] A.C. Larsen et al., Phys. Rev. C 83, 034315 (2011).

This study is supported by the Scientific and Technological Research Council of Turkey (TUBITAK) under the Project No: 115F196. kursadosmanay@gmail.com

Keywords: Nuclear, level, Density,^{143}Nd,^{147}Nd

Comparison of different embolization materials on gamma knife arteriovenous malformation dose distributions

[1] ÖZLEM DAĞLI Gazi University
[2] ERKAN BOSTANCI Ankara University
[3] HAKAN EMMEZ Gazi University
[4] FATİH EKİNCİ Gazi University

Embolization materials are employed in AVM (Arteriovenous malformation) treatment. Gamma Knife treatment is generally applied in AVM and AVM residue situations. This study analyses the doses accumulated by three different embolization materials, namely: onyx, cyanoacrylate and polyvinyl alcohol (PVA). A collimator helmet size of 8mm was used in a Monte-Carlo simulation implemented in Geant4. Obtained dose accumulations are analysed and results show differences in the dosimetries computed.

Keywords: Embolization, onyx, cyanoacrylate, polyvinyl alcohol, Gamma Knife, Geant4, dosimetry

Material selection for gamma knife phantoms

[1] ÖZLEM DAĞLI Gazi University
[2] ERKAN BOSTANCI Ankara University
[3] GÖKHAN KURT Gazi University
[4] FATİH EKİNCİ Gazi University

This study analyses the dose difference for a variety of phantom materials that can be used for Leksell Gamma Knife. These materials have properties that are very similar to the human tissue not including the skull bone. Geant4 was employed in the analysis for collimator helmet sizes of 4mm and 8mm. The phantom had a radius of 80mm. Water, brain, PMMA (Poly-methyl methacrylate) and polystyrene were used as the material types. Results show different radiation dosimetries depending on the material types.

Keywords: Gamma Knife, Geant4, material types, dosimetry

Physical properties of TiN reactor structural material

[1]VİLDAN ÖZKAN BİLİCİ, [2]ZEYNEP ŞİLAN TURHAN IRAK, [3]CEREN KARAMAN, [4]AHMET BOZKURT, [5]SUAT PAT, [6]İSMAİL HAKKI SARPÜN

[1]Afyon Kocatepe University, Physics Dept., Afyonkarahisar, Turkey.
[2]Iğdır University, Engineering Faculty, Iğdır, Turkey.
[3]Pamukkale University, Chemical Engineering Dept., Denizli, Turkey.
[4]Akdeniz University, Engineering Faculty, Antalya, Turkey.
[5]Eskisehir Osmangazi University, Physics Dept., Eskişehir, Turkey.
[6]Akdeniz University, Physics Dept., Antalya, Turkey.

Abstract

The composites were accepted as suitable structural materials for both fission and fusion reactors. The physical properties of nitrites and its coatings are very high temperature stability, excellent corrosion resistance, superior mechanical properties and good thermal conductivity applications. Titanium nitride has found numerous applications due to its excellent corrosion and erosion resistance, excellent adhesion on various steel substrates, high inertness, high melting temperature, high hardness and optimum optical and electronic properties. For this study, TiN composite samples were produced at Eskişehir Osmangazi University to investigate some physical properties.

Introduction

Development of nuclear power shows increased requirements to used structural materials, technologies of their manufacture and the control of serviceability [1]. In the nuclear energy research, materials with enhanced performance play a central role. Based on material development advances, composites, and in particular ceramic composites, seem to inherently possess properties suitable for key functions within the operating envelope of reactors. One of the main goals of materials research for fusion is the development and selection of alloys for those components with good thermomechanical and physical properties, coupled with low-activation characteristics [2]. Depending on its stoichiometry, creating titanium nitride (TiN) provides high temperature oxidation resistance, advanced wear/abrasion resistance and improved toughness under extreme environments. TiN has successfully been used for coating the heads of steel cutting and forming tools to improve their wear lifetime [3] and the advantages of TiN coating include high hardness and adhesion, good ductility, excellent lubricity, high chemical stability and tough resistance to wear, corrosion and temperature [4]. The original composition of the electrical, mechanical and thermal properties of TiN has become attractive in industrial applications in recent years.

Samples

TiN nanocomposite sample is one of the candidate composites, have been produced in Eskisehir Osmangazi University by using Plasma RF method. The nanocomposites were thoroughly characterized by Field emission scanning electron microscopy (FESEM).

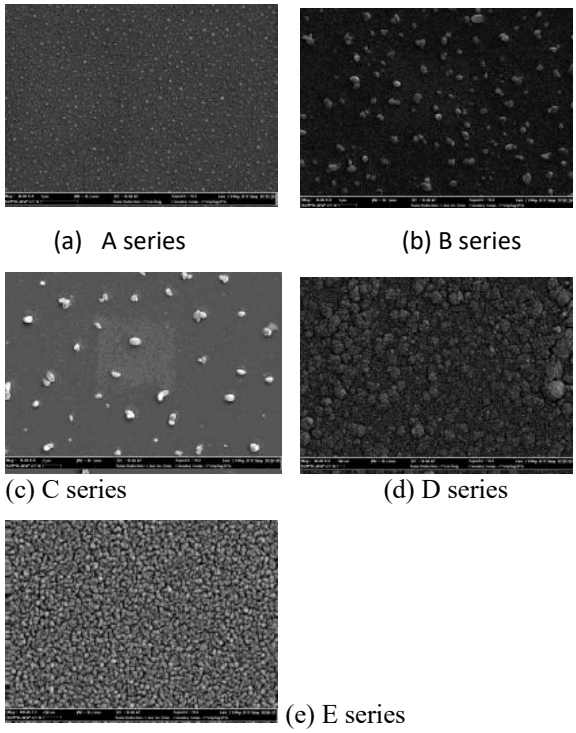

Fig.1. FESEM images

Table 1. Production parameters for TiN nanocomposite samples

Samples	Ar (%)	N_2 (%)	Pressure (Torr)	Power (W)	Time (Min.)
A Series	10	90	4.6×10^{-1}	300	70
B Series	30	70	3.41×10^{-1}	300	70
C Series	50	50	3×10^{-1}	300	70
D Series	70	30	2.8×10^{-1}	300	70
E Series	90	10	1.46×10^{-1}	300	70

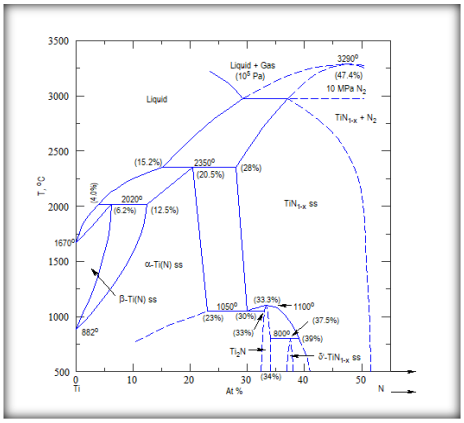

Fig. 2. Phase Diagram

Results and Discussion

The production parameters of the TiN nanocomposite samples are given Table 1. In this study, the samples were the result of bombardment with neutrons. The compositions that have been specified FESEM images of the TiN nanocomposite samples A, B, C, D and E are illustrated in Fig. 1. The particles are homogeneously dispersed, with no alignment or orientation in the first sample. Any impurity is observed in the patterns. Additionally, Phase diagram of TiN nanocomposite samples is given Fig. 2.The diagrams are the product of an optimization procedure to evaluate available data on the phases and phase equilibria of the system for the derivation of the compound thermodynamic constants. Five condensed phases were considered as existing in the system: the liquid, the hcp a-Ti(N) ss, the bcc b-Ti(N) ss, the broad TiN_{1-x} ss (NaCl structure), and tetragonal Ti_2N. Field emission scanning electron microscopy (FESEM) of samples provided topographical and elemental information in different magnifications. The results of FESEM studies of the coating surface structure confirm the results of studies carried out. FESEM images were taken from the cross section perpendicular to the press direction. The particles are homogeneously dispersed, with no alignment or orientation in the first sample. The necessary information about the method is given by Sarpun et.al in their works. They will also be tested using Hybrid Monte Carlo Simulation Model simulations. The results show an acceptable agreement.

References

[1] S. Kislitsini I. Gorlachevi V. Uglovi, SMINS-3, 2015, pp 266-279.

[2] M. Zucchetti, M. Merolai, J Nucl Mater 233-237, pp 1486-1490.

[3] I. Kim, F. Khatkhatay, L. Jiao, G.Swadener, J. I. Cole, J. Gan, H. Wang, , J Nucl Mater 429, 2012, pp 143-148.

[4] S. Zhangi W. Zhu, J Mater Process Tech 39, 1993, pp 165-177.

Structural properties of the candidate reactor material VC composites

[1]VİLDAN ÖZKAN BİLİCİ, [2]ZEYNEP ŞİLAN TURHAN IRAK, [3]CEREN KARAMAN, [4]AHMET BOZKURT, [5]SUAT PAT, [6]İSMAİL HAKKI SARPÜN

[1]Afyon Kocatepe University, Physics Dept., Afyonkarahisar, Turkey.
[2]Iğdır University, Engineering Faculty, Iğdır, Turkey.
[3]Pamukkale University, Chemical Engineering Dept., Denizli, Turkey.
[4]Akdeniz University, Engineering Faculty, Antalya, Turkey.
[5]Eskisehir Osmangazi University, Physics Dept., Eskişehir, Turkey.
[6]Akdeniz University, Physics Dept., Antalya, Turkey.

Abstract:

In the nuclear energy renaissance, performance-enhanced materials, driven by fission reactor concepts using very high temperatures and fast neutron spectra, play a central role. The development of advanced materials to be used in next-generation reactors is due to the need for extreme environmental resistance due to long-term, high-damage radiation flows, extreme temperatures and high stress conditions combined with well understood and widely used materials. In fusion and fission reactor applications, materials that play an important role have some important characteristics that must be maintained. These include low activation, structural integrity, dimensional stability, thermal conductivity, and thermal odor absorption. In this study, some features of VC composites produced as candidate materials (diameter, refraction index, wsd analysis, electron imaging with GOF and FESEM) were investigated.

Introduction

Carbon based materials due to their wide range of structures and several desirable neutronic properties are used in nuclear reactors and in the recent past there has been growing interest to develop speciality carbon for high temperature nuclear and fusion reactors [1-2]. For this reason, new material has been searched for. One of them is vanadium. Vanadium is never found unbound in nature. Vanadium occurs in about 65 different minerals among which are patronite, vanadinite, carnotite and bauxite. Vanadium occurs in carbon containing deposits such as crude oil, coal, oil shale and tar sands. Vanadium alloys are also used in nuclear reactors because vanadium has low neutron-adsorption abilities and it doesn't deform in creeping under high temperatures.

Methods&Analysis

VC composite sample is one of the candidate composites, have been produced in Eskisehir Osmangazi University by using Plasma RF method. The composites were thoroughly characterized by Field emission scanning electron microscopy (FESEM).

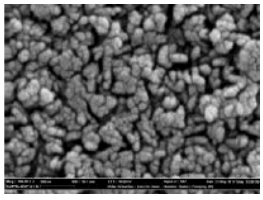

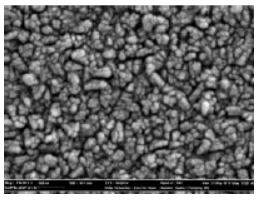

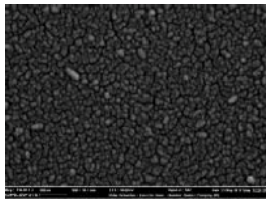

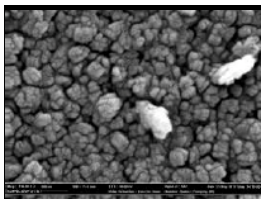

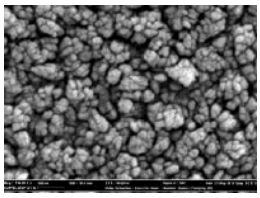

Fig. 1. FESEM images of (a) M series (150.000 magnification), (b) N series (150.000 magnification), (c) P series (150.000 magnification), (d) O series (200.000 magnification), (e) R series (150.000 magnification), respectively.

Samples	Thickness, nm	Refractive Index, n	GOF
M1	62	1.4628	0.1187
M2	62	1.4895	0.0539
M3	63	1.49	0.0246
M4	121	1.501	0
N1	149	1.5451	0.0844
N2	136	1.5561	0
N3	147	1.5653	0.0294
N4	181	1.5885	0.1757
O1	145	1.6056	0.2003
O2	164	1.6021	0.1464
O3	140	1.6384	0.0617
O4	111	1.63	0.2328
P1	152	1.5474	0.1624
P2	132	1.6142	0.0532
P3	115	1.4718	0.3086
P4	166	1.5755	0.0309
R1	194	1.4767	0.0102
R2	64	1.4892	0.0103
R3	105	1.5306	0.0715
R4	128	1.5749	0.1165

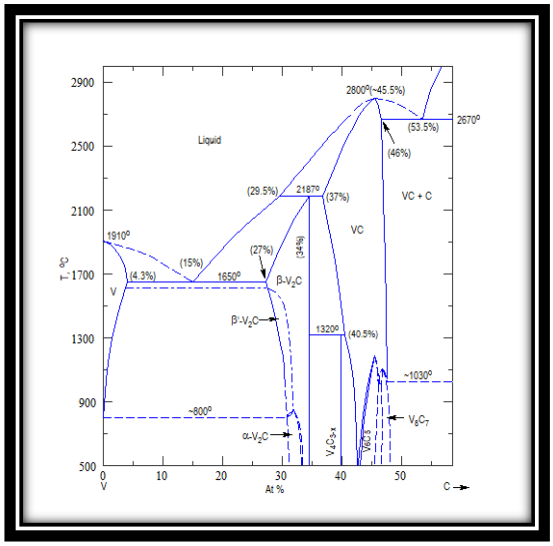

Fig.2. Phase Diagram

Results and *Discussion*

Some features of VC composites produced as candidate materials are investigated. Values of thickness, refractive index and GOF parameters of VC composite samples are given Table 1. We can say that in this study, the samples are the result of bombardment with neutrons. Photomicrographs of vanadium carbon samples are shown in Figure 1. The compositions that have been specified FESEM images of the VC composite samples. The particles are homogeneously dispersed. Any impurity is observed in the samples. Additionally, Phase diagram of VC composite samples is given Fig. 2. T crystallographic and thermochemical data for the phases and end-members are tabulated. The phases V_6C_5 and V_8C_7 arise from ordering of C atoms. The transition b ® b¢-V_2C is probably second or higher order, involving a statistical variation in the ordering scheme of C occupancy of sublattice sites, and is indicated by a dashed line. Field emission scanning electron microscopy (FESEM) of samples provided topographical and elemental information in different magnifications. The results of FESEM studies of the coating surface structure confirm the results of this study. The necessary information about the method is given by İsmail Hakkı et.al in their works. They will also be tested using Hybrid Monte Carlo Simulation Model simulations. The results show an acceptable agreement.

References

[1] S Nikolaos, INTECH Open Access Publisher (2011).

[2] R Venugopalan, D. Sathiyamoorthy, A. K. Tyagi, Barc Newsletter, 325 (2012).

Investigation of the potential use of 3D graphene networks and composites for high-performance electromagnetic interference shielding

[1] CEREN KARAMAN Pamukkale University, Department of Chemical Engineering
[2] EDİP BAYRAM Akdeniz University, Department of Chemistry
[3] ONUR KARAMAN Akdeniz University Vocational School of Health Services,
[4] İSMAİL HAKKI SARPÜN Akdeniz University, Department of Physics

Electromagnetic radiation is one of the serious problems that threaten human health, affect the nervous system and endocrine system. Shielding protection is the most effective way of preventing electromagnetic radiation. Hence, development of high-performance electromagnetic interference (EMI) shielding materials has gained importance. Materials which have high electrical conductivity such as metals are the most common EMI shielding materials with high shielding effectiveness (SE). For example, Cu-Ni composite and silver nanowires exhibited a SE of 25.0 dB at a thickness of 15.0 mm, and 35.0 dB at a thickness of 5.0 mm, respectively. However, metals suffer from high cost, poor resistance to corrosion, and high weight. Carbon nanomaterials with a high specific surface area and electrical conductivity can be used as lightweight and high-performance EMI shielding materials. With excellent optical and electrical properties, graphene networks are one of the prominent structures among these carbon materials. Considering the requirement of being lightweight and flexible, assembling two dimensional (2D) graphene sheets into three dimensional (3D) graphene structures (e.g., graphene foams, graphene aerogels or graphene sponge) emerged as an effective approach. In this work, with the light of detailed literature survey, it is concluded that 3D graphene networks have been considered as one of the most promising candidates for providing EMI shielding performance. It is provided that they can be directly used as high-performance EMI shielding films in areas such as flexible electronics, aerospace, packaging, and communication.

Keywords: 3D graphene, Electromagnetic interference shielding, Electrical conductivity

Radiation shielding properties of concrete containing ferro-boron and barite-colemanite using Monte Carlo method

[1] MUHAMMAD SYAHIR SARKAWI Universiti Teknologi Malaysia
[2] MUHAMMAD RAWI MOHAMED ZAIN Malaysian Nuclear Agency
[3] JASMAN ZAINAL Universiti Teknologi Malaysia
[4] FARIDAH MOHAMAD IDRIS Malaysian Nuclear Agency
[5] MOHAMAD HAIRIE RABIR Malaysian Nuclear Agency

Radiation shielding is very important component in nuclear facility since unwanted radiation can cause contamination and health problems. The problem of shielding against neutron and gamma radiation have always captivate by the important of this issue. Normally, the best known materials for shielding both neutron and gamma radiation are concrete. Concrete is made up form three basic components which are water, aggregate (rock, sand, gravel) and porland cement. However, normal concrete has low neutron absorption cross section. Hence, additional compound is needed to increase the neutron absorption cross section of the concrete. In this work, ferro-boron and barite-colemanite compound is used to enhance the radiation shielding properties of the concrete. Ferro-boron is an alloy, which is formed by combining iron with boron compound content between 10% to 17%. In this paper, Monte Carlo simulation code of MCNPX is used to simulate the radiation shielding properties of ferro-boron and barite-colemanite concrete. There are limited studies related to these concrete. According to the simulation results, it is clearly shows that adding ferro-boron compound into concrete mixture can significantly enhance the radiation shielding properties of the concrete.

Keywords: Radiation shielding, Ferro-Boron, Monte Carlo simulation code, Concrete mixture

The effect of the linear-quadratic anisotropic scattering and the slab thickness over the albedo problem

R. GÖKHAN TÜRECİ Kırıkkale University

Case's eigenfunctions and the orthogonality properties between these eigenfunctions is expanded to both linearly and quadratically anisotropic scattering for one-speed neutron transport theory. The slab albedo problem is investigated with the proper boundary conditions and with the suggested neutron fluxes over the surfaces by using Modified FN method. The calculated numerical results are tabulated according to the varying slab thicknesses and with varying scattering coefficients.

Keywords: Linear-Quadratic anisotropy, slab albeo, Modified FN method, Case's eigenfunctions

The criticality problem with the quadratically anisotropic scattering

[1] PINAR KAAN Kırıkkale University
[2] R. GÖKHAN TÜRECİ Kırıkkale University

One speed, time independent neutron transport equation is solved for a slab reactor. The general solution is written according to the quadratically anisotropic scattering. The criticality equation, which defines a relation between the secondary neutron number and the thickness of slab, is written with proper boundary conditions. The thickness of slab is calculated for varying secondary neutron numbers and varying scattering coefficients. The tabulated values represent the calculated critical thickness.

Keywords: Neutron transport theory, General solution of transport equation, Quadratically Anisotropic scattering, Criticality equation, Modified FN method

Indoor radon in Isparta

MEHMET ERTAN KÜRKÇÜOĞLU Süleyman Demirel University

Radon, a naturally occurring noble gas, is the most significant contributor to the natural indoor radioactivity. At the end of its half-life (3.82 days), radon-222 emits an α-particle (5.48 MeV) and then, decays into the first short-lived radon product (radioactive polonium-218). ^{222}Rn is much heavier than air therefore it can accumulate in enclosed spaces by time. When this is the case for dwellings or work places, radon may become a serious health concern for the habitants. Since radon is a class-A carcinogen and inhalation of radon and radon products is related to aetiology of lung cancer, it is quite important to determine the indoor radon levels from the point view of public health. In worldwide, up to 15% of the lung cancer cases are connected to radon (world's indoor radon average is 39 Bq/m^3). The average value for atmospheric radon concentration of the dwellings in Turkey is ~83 Bq/m^3. In addition, our previous surveys performed for Isparta city centre showed that, all of the atmospheric indoor radon concentration averages are higher than the national level (up to by a factor of 4). In the present study, the results of the atmospheric radon level measurements, which were performed for different dwellings and work places in the city centre by using passive measurement techniques (by using either long-term CR-39 nuclear etched track detectors, or long-term E-PERM electret ion chambers) at different time periods during the last ten years, have been summarized. Then, the annual effective doses taken by people in the city centre have been estimated. Within the limitations of this study it is revealed that, although all the averages obtained for both dwellings and work places are lower than the national limits, local people can receive annual doses close to 10 mSv due to radon inhalation.

Keywords: Isparta, indoor radon, annual effective dose equivalent

Determination of the full energy peak efficiency of HPGe detector using Monte Carlo simulation

[1] ESRA UYAR Gazi University
[2] MUSTAFA HİCABİ BÖLÜKDEMİR Gazi University
[3] ERHAN ESER Gazi University

High purity germanium (HPGe) detectors are widely used in γ-ray spectrometry to identify radionuclides and to determine their activity. To determine the activity, one of the most important characteristics of an HPGe detector is its full energy peak (photopeak) efficiency. In this study, the Monte Carlo method was used in calculating full energy peak efficiency for the HPGe detector within the 46.5-1836 keV energy range. The detector considered for the Monte Carlo simulation was a coaxial HPGe detector with an active volume of ~207 cm^3. Monte Carlo simulations were performed using the PHITS (Particle and Heavy Ion Transport code System) software, version 2.88. At least three separate simulations were done, with 108 particles for each energy and in modeling the pulse height mode detector, T-Deposit tally was chosen. Energy bin width in the tally was set low to 0.2 keV. As a result, the coaxial HPGe detector was modeled with PHITS software and it has been that the efficiency results obtained are in good agreement with the literature.

Keywords: PHITS, HPGe detector, efficiency, Monte Carlo simulations

Use of boron and boron compounds as shielding material in reactors

[1] FATMA AYSUN UĞUR Osmaniye Korkut Ata University
[2] FATMA YAKUT Osmaniye Korkut Ata University

Boron and boron compounds can be used as a moderator material around the control rods in reactors. The data obtained from the Xcom photon cross section data program have been observed to be a good material when fast neutrons are slowed down to the level of thermal neutrons. From the results obtained, the neutron flux cross sections are graphically investigated for neutron energies ranging from 0.001 MeV to 10000 MeV.

Investigation of the use of samarium and gadolinium materials in nuclear technology

[1] FATMA AYSUN UĞUR Osmani ye Korkut Ata University
[2] FATMA YAKUT Osmaniye Korkut Ata University

In this study, the applications of samarium and gadolinium materials in nuclear technology were investigated. Using the Xcom data program, the linear absorption coefficients of the samarium and the gadolinium are obtained at the energy range of 0.001 MeV and 100 GeV, and the graphs are discussed.

Relation of spectral statisitcs and medical applications

[1] HADI SABRI University of Tabriz
[2] SEYED KHALIL MOUSAVI MOBARAKEH University of Tabriz

In this paper, the spectral statistic of radionuclides which are used in therapeutic and imaging applications have been investigated by Random Matrix Theory. The Maximum Likelihood Estimation technique is used for estimating the chaotic parameter of each category. The results suggest that radionuclides which are being used for treatment and therapeutic are more regular in comparison with nuclei that are used for imaging. These results can be considered in choosing the appropriate radionuclides for different critical organs an application.

Keywords: spectral statisitcs, Random Matrix Theory, therapy, imaging

A study of excitation functions calculations for some A<20 target nuclei

[1] YUSUF KAVUN, [2]EYYUP TEL

[1]Kahramanmaras Sutcu Imam University, Vocational School of Health Services, Department of Medical Imaging Techniques, Kahramanmaras, Turkey
[2]Osmaniye Korkut Ata University, Physics Department, Osmaniye 80000, Turkey

Abstract

Many research activities to produce new energy sources are available due to the ever-increasing energy consumption on the world. One of the clean reliable and abundant energy sources on the nature is fusion energy. It may be used as a continuously alternative energy source for humankind when compared to other sources. Many researches have therefore done for designing and development of fusion reactor technology. In this study, the excitation functions for some reactions have been calculated by using PCROSS nuclear reaction calculation code. Charged particles induced nuclear reactions of some target nuclei (A<20) have been investigated in the incident proton and alpha at energy range from threshold to 50 MeV. Also, the semi-empirical calculations for (p,a) reactions have been done by developed new coefficient cross section formula that is in the literature. The results were compared with the experimental data for different energy levels that is taken from the EXFOR.

Keywords: Cross-section, Excitation function, PCROSS, EXFOR

Introduction

Nuclear power plants have an important place in today's world in energy production since the early 1970s in order to respond to the increasing demand for energy. Countries that do not have oil and other hydrocarbon resources have turned to nuclear power stations in order to counter the crises that took place in the energy sector. This is why nuclear power plant technology and energy production studies from nuclear fuel have been developed day by day and has an important place in the world economy. it has also led to the foreground of separating nuclear power plants from other production methods because of the need for a more reliable, economical, continuous and accessible energy source than other production methods. The 450 nuclear power plants that have been established to date provide 11% of the world's energy production. Moreover, the process of establishing 56 nuclear power plants in 17 countries continues. So, on a country basis, France accounts for 72% of electricity demand, 55% for Ukraine, 50% for Belgium, 40% for Sweden, 27% for South Korea, 30% of the total supply.

In a nuclear reactor, energy is produced by the decomposition of atoms, and thus electricity is generated by steam power generated by evaporating water through the energy released. A series of chain reactions for the production of this atomic energy take place in the core of the nuclear reactor. As a result of the interaction of energy generated during these reactions with materials located at the core of the reactor, a number of changes in the structure of the material may occur.

In this study, for some A<20 target nuclei, excitation functions of the charge particle induced nuclear reactions have been investigated in the incident proton that energies ranging from 1 to 50 MeV. For theoretical cross section calculations of this targets, PCROSS code [1] was used. For these calculations, some nuclear theories were used such as; Weisskopf-Ewing model for equilibrium [2]. According to the obtained results, possible effects of A<20 Target Nuclei were investigated on structural materials of the fusion reactor. In Figs. 1-3, calculated PCROSS code [1] and also the experimental data is taken from (EXFOR) [3].

Cross Section Calculation Methods

When the exciton energy shared between p (particles) and (h) holes that shows Fermi energy and below at the excited particles above, exciton number can found as $n=p+h$. For calculations $n_0=1$ is initial exciton number is used and so the gamma emission should be taken into account directly;

$$n_{eq} = \sqrt{1.4gE} \qquad (1)$$

By Cline [4] and Ribansky [5] a unified model proposed and the PCROSS code used that is based on the solution of the master equation. Also, Akkermans et al. [6] proposed an algorithm to solve of algebraic equations. So, it gives an accurate result for any initial condition of the problem.

There are many semi-empirical cross section formulae to charged and uncharged particles at the different energies [4-12]. The new semi-empirical cross section formulae

developed by Tel et al that is induced by proton as follows [7] for the (p,α) reaction at 17.9 MeV energy,

$$\sigma_{(p,\alpha)} = C\sigma_{p-ne}e^{as} \quad (2)$$

$$\sigma_{p-ne} = \pi r_0^2\left(A^{1/3}+1\right)^2 \quad (3)$$

σ_{p-ne} is the proton non-elastic cross section and the C and a coefficients are given in Tel et al. (2010) [8]. r_0 is the radius of the nucleus and given as r_0=1.2 fm. Coulomb effects for proton induced reactions;

$$V_{Coul} \approx \frac{Z^2}{R} \approx \frac{Z^2}{(A^{1/3}+1)} \quad (4)$$

$$\sigma_{Coul} = \frac{Z^2}{(A^{1/3}+1)} \quad (5)$$

where σ_{Coul} is the proton Coulomb effect cross section.

Results and Discussion

The new evaluated semi-empirical formulas were used at 17.6 MeV energy that was developed by Tel et al. [9] for (p,a) reaction cross-sections of ^{25}Mg calculated in this study.In figüre 1, for 25Mg(p,α) reaction are investigated and according to the obtained results, experimental data that is studied by Cohen [10] close to theoretical calculations. To investigate theoretical calculations, PCROSS code used and equilibrium and pre-equilibrium reaction models were used in figüre 1. Equilibrium and pre-equilibrium reaction model calculations shows same tendency after 15 MeV. Additionally, Tel et al. semi-empirical formulae are compatible with experimental data at 17.6 MeV energy.

In Fig.2, for 25Mg(p,n) reaction are close to experimental data with equilibrium and preequilibrium. Theoretical calculations are compatible at 6-7 MeV energy with experimental data.

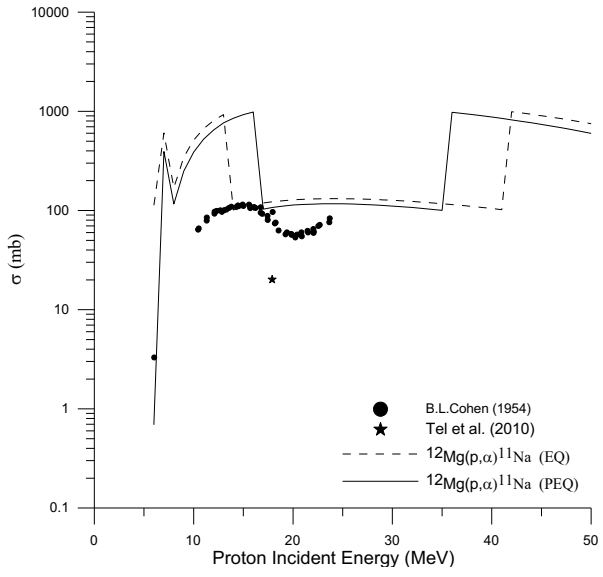

Fig. 1. Theoretical (PCROSS) and experimental (EXFOR) data of ^{12}Mg(p,α) reactions.

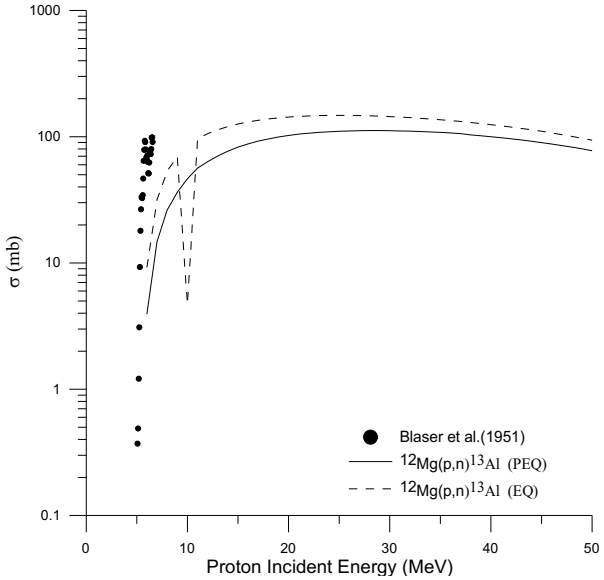

Fig. 2. Theoretical (PCROSS) and experimental (EXFOR) data of ^{12}Mg(p,n) reactions.

Reference

[1] *R. Capote et al., Final Report on Research Contract 5472/RB, INDC(CUB)-004 (Higher Institute of Nuclear Science and Technology, Cuba). Translated by the IAEA on March 1991 (PCROSS program code) (1991).*

[2] *V.F. Weisskopf, D.H. Ewing, Phys. Rev. 57, 472, (1940).*

[3] *EXFOR/CSISRS (Experimental Nuclear Reaction Data File). Database Version of December 19, 2007, Brookhaven National Laboratory, National Nuclear Data Center, http://www.nndc.bnl.gov/exfor/exfor00.htm (2007).*

[4] *C.K. Cline, M. Blann: Nucl. Phys. A 172, 225, (1971).*

[5] *Ribansky et al.: Nucl. Phys. A 205, (1973), 545.*

[6] *J.M. Akkermans et al.: Phys. Rev. C 22 (1980) 73.*

[7] *E. Tel, S. Akca, M. Sahan, M. Depedelen, I.H. Sarpun, J Fusion Energ 35 (2016) 709.*

[8] *E. Tel, A. Aydın, E.G. Aydın, A. Kaplan, O. Yavas, I.A. Reyhancan, PRAMANA Indian Academy of Sciences 74, 6, 931, (2010).*

[9] *M. Sahan, E. Tel, H. Sahan, A. Kara, A. Aydin, A. Kaplan, I.H. Sarpun, B. Demir, S. Akca, E. Yildiz, J Fusion Energ 34 (2015) 493.*

[10] *Cohen B.L. et al., Phys. Rev. 96, 1617 (1954).*

[11] *M. Belgaid, M. Asghar, Appl. Radiat. Isot. 49 (1998) 1497.*

[12] *E. Tel, A. A. Gok, M. Sahan, I˙. H. Sarpun, Y. Kavun, A. Aydin, J. Fusion Energ, 36 (4-5), (2017).*

Cytogenetic biodosimetery for the assessment of radiation doses in cases of radiological accidents

GHAZI ALSBEIH King Faisal Specialist Hospital and Research Centre Biomedical Physics Dept.

The continuous expansions in the applications of nuclear technologies in various aspects of life increase the probability of overexposure due to involuntary or premeditated nuclear accidents. National radiation-protection preparedness response plan requires adequate estimate of dose received for efficient medical assistance of victims. Cytogenetic biodosimetry is a proven, ISO/IAEA standardized biotechnology technique for calculating medically relevant radiation doses. In addition to diagnosis of overexposure, it provides triage capability for rapid stratification of patients who need more specialized medical care. It can also detect false positives and false negatives exposure particularly in cases of legal allegations. This study aimed to build biological dosimetry capabilities in and construct the dose-response calibration curve for dicentric chromosomes pre-required to estimate doses received. These were accomplished and a fully-fledged biodosimetry laboratory was established, a standard dose-response calibration curve was determined. Networking was established with international biodosimetry network in cooperation with IAEA/WHO. Being the first in the region, the formation of this laboratory in biodosimetry may have an impact on the ability to respond to nuclear events. It enhances the nation's casualty management capabilities by providing a platform for diagnostic technique for triage and medical management purposes as part of a national emergency response plan. The various activities of this reference biodosimetry laboratory can also provide officials with tools to distinguish affected from the worried individuals, and alleviate public concerns about the health effects of possible radiological exposures. It also adds depth to information for decision-makers and public health officials who assess the magnitude of public, medical, occupational and accidental radiation exposures in addition to providing a platform for advanced education, research and development.

Supported by Operational Transformation Initiatives #31, titled “Integrated Biomedical Physics Center: Delivery of Precision Radiation Medicine” (RAC# 2170 005).

Keywords: biodosimetry, radiation accident

One trap one recombination model under the first order kinetic parameters

ERDEM UZUN Karamanoğlu Mehmetbey University

Lots of models were proposed to explain complex emission mechanisms of the thermoluminescence event and one of the models is one trap one recombination center model. According to the model, one trap and one recombination centers are available for electrons and holes, respectively. Charge carrier transitions and thermoluminescence emissions are determined by a simple set of differential equations but the equations are not linear and analytical solutions are not possible. In this work, the model was applied to a first ordered glow curve. Firstly, numerical solutions of the model were performed for different initial irradiation conditions and different heating rates. Numerical solutions were performed iteratively by using ninth order Explicit Runge–Kutta method for Fehlberg coefficients. Results were compared thermoluminescence glow curve of the Seydişehir alumina.

Keywords: otor model, numerical solutions, Runge–Kutta method, Fehlberg coefficients, Şeydişehir alumina

Comparison of radon concentration results measured by two different methods in well waters

AYLA GÜMÜŞ, HÜSEYİN ALİ YALIM

Afyon Kocatepe University, Physics Department., Afyonkarahisar, Turkey

Abstract

Radon occurs as a result of radioactive decay of natural uranium in rock, soil, and water. The radon with atomic number 86 is the only radioactive gas in nature, with no reaction and a half-life of 3.82 days. Since radon is a colorless, tasteless, odorless radioactive gas, it cannot be detected and recognized by the human senses. Today, many radon measurement techniques have been developed to measure radon and decay products and they can be categorized into two groups; namely active and passive. Instant radon measurements are made by the active radon measurement technique. In the passive measurement technique, long-term radon measurements are made using nuclear trace detectors. In this study, radon concentrations in water were actively measured by using two different model devices. One of the devices is the WG-1001 Gas Separation Unit and AB-5R detector manufactured by Pylon Electronics; the other is the AlphaGUARD PQ2000 PRO Radon Imaging System. Measurements were made at 15 different deep-water sources determined in and around Afyonkarahisar's Sultandağı and Çay districts. The measurements in water samples were fortnightly repeated for 54 weeks using the two devices separately and the obtained results were compared.

Keywords: radon in well water, Afyonkarahisar

Introduction

Radon is a colorless, odorless, tasteless and heaviest radioactive noble gas which is produced by uranium decay series. It occurs as a result of radioactive decay of natural uranium in rock, soil, and water. The radon with atomic number 86 is the only radioactive gas in nature, with no reaction and a half-life of 3.82 days. It is produced continuously in rocks and minerals through α decay of ^{226}Ra [1]. It can diffuse directly or as solution in water to the earth's surface. The reason for the high concentration of radon in intracutaneous groundwater is that six-valence uranium is relatively easily soluble and is leached out of the rock by the groundwater [2]. Due to the fact that it is a moving gas, it can easily leave the soil and rocks by escaping from the pores between the soil granules, through the openings in the rock, cracks, and fractures. Radon is found in soil, rocks, building materials, water and natural gas. Since radon is a colorless, tasteless, odorless radioactive gas, it cannot be detected and recognized by the human senses. Today, many radon measurement techniques have been developed to measure radon and decay products and they can be categorized into two groups; namely active and passive. Instant radon measurements are made by the active radon measurement technique. In the passive measurement technique, long-term radon measurements are made using nuclear trace detectors.

While simple methods are used for short time measurements in radon investigations, more complex and detailed tools are used for long time measurements [3]. Instant radon measurements are made by the active radon measurement technique. In the passive measurement technique, long-term radon measurements are made using nuclear trace detectors. Radon gas measurement with nuclear track detectors is performed using film layers made of various plastic materials. The most widely used plastic materials are cellulose acetate, polycarbonate and allyl diglycol carbonates [4,5].

Materials and Methods

Location and working area of the city of Afyonkarahisar in Turkey is shown in Fig. 1. Water samples were taken from 15 different deep wells, whose details are given in Table 1, located on the Afyonkarahisar's Sultandağı and Çay districts as shown in Fig. 2. The measurements in water samples were fortnightly repeated for 54 weeks using the two devices separately and the obtained results were compared.

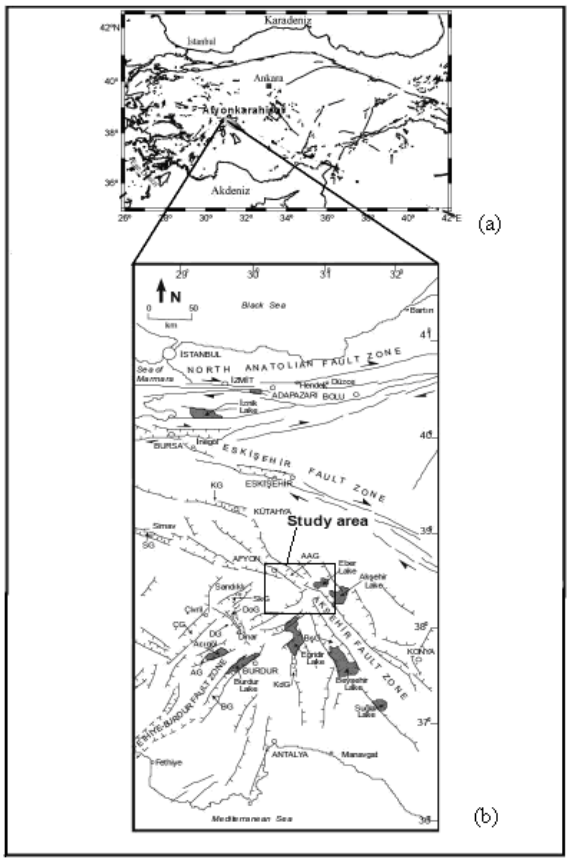

Fig. 1. (a) The study area and faults shown on the map of Turkey, (b) Study area (compiled from [6] and [7]).

Table 1. Details of the wells.

Well no	Latitude	Longitude	Altitude (m)	Depth (m)
1	38.7110°	30.6055°	1008	117
2	38.7141°	30.6258°	1008	100
3	38.6759°	30.7372°	1000	45
4	38.6458°	30.8342°	1001	280
5	38.6070°	30.9098°	1005	---
6	38.6373°	30.9185°	988	50
7	38.6402°	30.8687°	976	600
8	38.6412°	30.8686°	982	700
9	38.6020°	30.9386°	998	85
10	38.5979°	30.9882°	988	120
11	385.971	31.0415°	1023	160
12	38.5900°	31.0951°	996	100
13	38.6093°	31.1623°	983	80
14	38.5799°	31.2251°	991	200
15	38.5012°	31.2680°	1015	10

In this study, radon concentrations in water were actively measured by using two different model devices. One of the devices is the WG-1001 Gas Separation Unit and AB-5R detector manufactured by Pylon Electronics; the other is the AlphaGUARD PQ2000 PRO Radon Imaging System.



Fig. 2 Locations of the wells (1-15).

Radon concentrations in water were measured using an AlphaGUARD PQ2000PRO detector equipped with a special unit of AquaKIT following the protocols proposed by the manufacturer [8-10]. Fig. 3 shows AlphaGUARD PQ2000 PRO Radon Imaging System and special unit of AquaKIT.

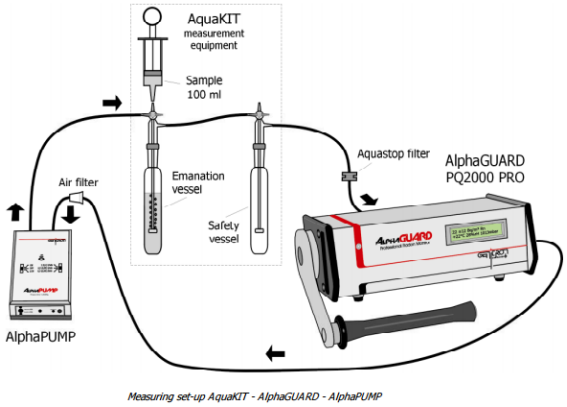

Fig. 3. AlphaGUARD PQ2000 PRO Radon Imaging System.

AlphaGUARD is an ionizing chamber which measures radon via alpha spectrometric techniques. Experimental set-up was based on the professional AlphaGUARD PQ2000PRO detector connected to specific kit of glass vessels AquaKIT through the air pump. The measurement cycle time was 10 min in the diffusion mode and the equipment was adjusted with air flow of 0.5 L/min. Radon concentration levels were detected and analyzed by the computer every 10 min (for two cycles) using the software DataEXPERT. For each sampling date, radon concentrations in water samples were obtained using the following equation provided by the manufacturer. For each sampling date, radon concentrations in water samples have been obtained using the following equation provided by the manufacturer [8,10];

$$C_w = \frac{C_{air} x \left(\frac{V_{system} - V_{sample}}{V_{sample}} + k \right) - C_0}{1000} \quad (1)$$

where C_w is radon concentration in water sample, Bq/L; C_{air} is radon concentration in the measuring set-up after expelling the radon, Bq/m^3; C_0 is radon concentration in the measuring set-up before sampling, Bq/m^3; V_{system} is the interior volume of the measurement set-up, 1102 mL; V_{sample} is the volume of the water sample, 100 mL; and k is radon distribution coefficient, k= 0.26.

The radon concentrations were measured using the commercially available WG-1001 Vacuum Water Degassing System and AB-5R Radiation Monitor produced by Pylon Electronics [11]. Background radiation of the scintillation cell was measured for 15min and the outcome was converted to a cpm (count per minute) basis; B. For counting, the scintillation cell was placed in the radiation monitor for approximately 3.5 h after sampling (i.e. when the radon activity in the cell had come to equilibrium). After the decay of fluorescence, the cell is counted for three 5-min intervals. Figure 3 shows the WG-1001 Vacuum Water Degassing System and AB-5R Radiation Monitor.



Fig. 3. WG-1001 Vacuum Water Degassing System and AB-5R Radiation Monitor.

Radon concentrations were determined in water using the following relationship described in detail by the manufacturer (Pylon 1991):

$$A = \frac{(C-B)}{Fx6.66xDxSxV} x0.037 \quad (2)$$

where A is the radon concentration in Bq/L; C is the gross count rate (cpm); B is the background rate (cpm); F is the cell counting efficiency which normally is 0.745 in the present case; D is the degassing efficiency of 300 A Lucas cell and its value is 0.9; S is the correction for decay of radon from sample time Ts to the count time Tc; V is the sample volume in litres (0.19 L) and 0.037 is the conversion factor between pCi and Bq.

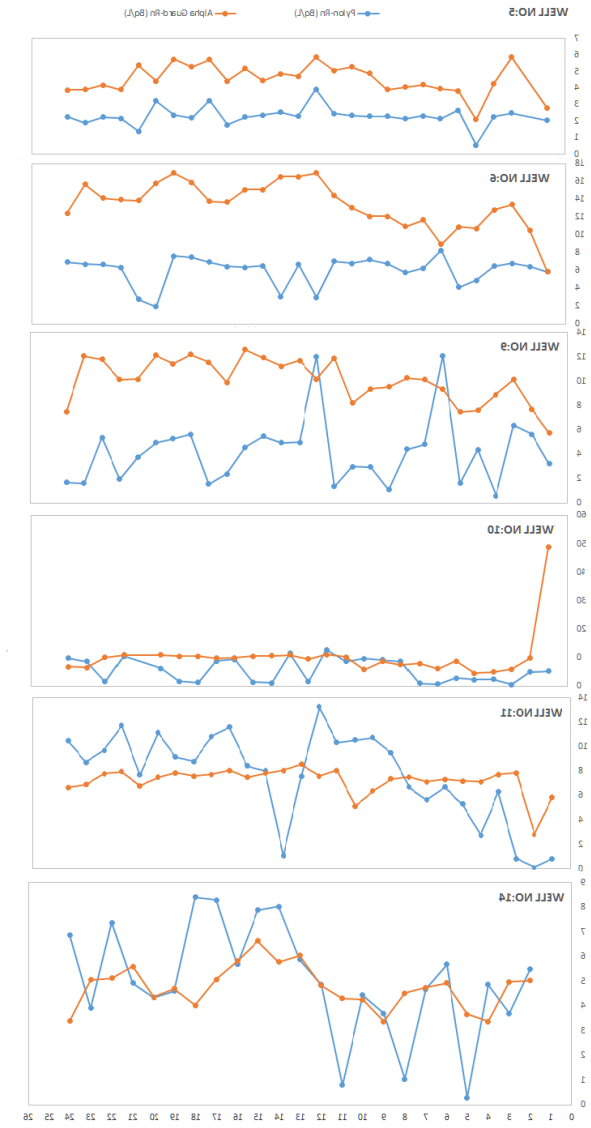

Fig. 4. Radon concentrations in well water.

Results

Average radon concentrations in water determined for the sampled wells by using two devices are given in Fig. 4. The ratio of the average radon concentration results obtained from AlphaGUARD PQ2000PRO detector to the Pylon AB-5R Radiation Monitor is given in Table 2 for the well numbers of 5,6,9,10,11 and 14.

Table 2. The ratio of the average radon concentrations.

Well No	Alpha Guard/Pylon [Average Rn(Bq/L)]
5	2.07
6	2.58
9	3.73
10	3.81
11	2.67
14	1.74

From the present results following conclusions can be done:

- The results obtained using AlphaGUARD PQ2000PRO detector are generally higher than the results of the Pylon AB-5R Radiation Monitor.
- The results of AlphaGUARD have less flactuations than the results of the Pylon AB-5R Radiation Monitor.
- The reason of these flactuations can be the parameters used in concentration calculations of Pylon AB-5R Radiation Monitor.

Reference

[1] O. Baykara, M. Doğru, *Radiat. Meas.* **41**, 362–367, (2006).

[2] *O.* Landstrom, E. L. Tullborg, *Swedish Nuclear Fuel and Waste Management Company,* Report AR **44-93-005**, (1990).

[3] C. R. Cothern, and J. E. Smith,., *Plenum Press*, New York, A.B.D, (1987).

[4] P. Korhonen, H. Kokotti, and P. Kalliokoski, *Atmospheric Environment*, **34**, 2373-2378, (2000).

[5] P. T. Wasiolek, A. C. James, *Journal of Environmental Radioactivity,* **51**, 137-151, (2000).

[6] A. Koçyiğit., E. Ünay, G.Saraç, *Geological Society*, London, Special Publication, **173**, 405-421, (2000).

[7] E. Bozkurt, *Geodinamica Acta,* **14**, 3-30 (2001).

[8] Saphymo GmbH, *AlphaGUARD User Manual Portable Radon Monitor*, Heerstrasse 149 D-60488 Frankfurt, Germany, (1998).

[9] Saphymo GmbH, *AlphaPUMP Technical Description*, Heerstrasse 149 D–60488 Frankfurt, Germany, (2001).

[10] Genitron Instruments, *AquaKIT User Manual*, Heerstrasse 149 D-60488 Frankfurt, Germany, (2008).

[11] Pylon Electronic Development Company Ltd, *Vacuum Water-Degassing System Manual* A900037 Rev. 2 147 Colonnade Road, Ottawa, Canada K2 E7 C9, 1991.

Gamma exposure and annual effective dose due to terrestrial and cosmic radiation in Ortaköy granitic zone of Aksaray province (Turkey)

[1] MEHMET ERDOĞAN Selçuk University Science Faculty, Physics Department
[2] KAAN MANİSA Dumlupınar University Art and Science Faculty, Physics Department
[3] HASAN BİRCAN Dumlupınar University Art and Science Faculty, Physics Department
[4] EMRE VATAN Selçuk University Science Faculty, Physics Department
[5] NESLİ BİNGÖLDAĞ TAEK, Çekmece Nuclear Research and Training Center,
[6] RECEP BIYIK TAEK Çekmece Nuclear Research and Training Center

The radiation exposure for people and all living things is inevitable. The 80 % of these exposures is natural, while the 20 % is artificial. The terrestrial and cosmic radiation sources are the most important contribution to these exposures which originated from the fractionation of U-238, Th-232, gamma radiation of K-40 and high-energy cosmic particles incident on the earth's atmosphere. These radionuclides are found various concentrations in the crust of earth depending on geological conditions of the region. This study assesses environmental outdoor gamma dose rates (terrestrial and cosmic radiation) from the naturally occurring radionuclides and cosmic ray particles in Ortaköy Granitic Zone of Aksaray province of Turkey since this area has plenty of acidic magmatic, granitic, intrusive rocks. The measurements were performed on surface soil using NaI(Tl) scintillation type gamma-ray detector. The average external annual effective doses are also calculated from such terrestrial and cosmic gamma radiation dose rates for each individual.

Keywords: Natural Radiation, Terrestrial and Cosmic Radiation, Annual Effective Dose, Ortaköy Granitic Zone, Aksaray Province

Development of an algorithm for the spectrum deconvolution of uranium samples measured by CdZnTe detector

[1] HALUK YÜCEL Ankara University Institute of Nuclear Science
[2] SEFER BALCI Ankara University Institute of Nuclear Science
[3] RECEP BORA NARTTÜRK Ankara University Institute of Nuclear Science
[4] EMİN YELTEPE Ankara University Institute of Nuclear Science

The determination of ^{235}U enrichment value in uranium samples has great importance in nuclear technology. Especially, there is a need to determine the abundances of uranium isotopes for obtaining basic sample information to compare with facility records, and for reporting or comparison purposes for data validation and evaluation in safeguards and illicit trafficiking activities. On the other hand, gamma-ray spectrometry is used to identify special nuclear materials such as enriched uranium or plutonium. The current semiconductor detector technology such as CdZnTe presents new opportunities to measure uranium samples in room temperature and/or onsite conditions. This type of detector has better resolution than the scintillation detectors such as NaI:Tl and all plastic scintillators. However, the problem is that the measured gamma-ray spectra of uranium between 80-130 keV is quite complex and it requires a careful de-convolution process to obtain accurate peak information to estimate ^{235}U enrichment value. In this study, an algorithm was developed to determine the net peak areas of analytical peaks in the spectra of low enriched uranium taken by a 1000 mm^3 coplanar grid CdZnTe detector. The algorithm is implemented in MATLAB software to get automatic results. In this deconvolution algorithm, the Gaussian function is applied to 92.4 keV double peak and the pseudo Voight functions to 94.6keV and 98.4 keV UKX-rays (Yücel, 2009). The developed algorithm was applied to de-convolute the gamma-ray spectra of certified reference uranium standards having 0.31%,0.71%,1.94%, 2.95% and 4.46% ^{235}U enrichment values in U_3O_8 powder. The developed methodology and the results obtained from the study will presented in detail.

This work was supported by IAEA coordinated research project(CRP), J02012 coded and titled “Advancing Radiation Detection Equipment for Detecting Nuclear and Other Radioactive out of Material Out of Regulatory Control”

Keywords: CdZnTe, de-convolution, Gamma ray spectrum, ^{235}U enrichment

MDM spectrometer and Oxford detector (mdm-focal plane) at tamu cyclotron institute

MURAT DAĞ Ahi Evran University

One of spectrometers hosted at The Texas A&M University Cyclotron Institute is MDM (Multipole-Dipole-Multipole) spectrometer primarily used to conduct experiments involving proton and neutron transfer reactions along with Oxford detector. MDM spectrometer was designed based on a single dipole magnet to achieve large dispersion, low magnification and a high-energy product. One of the focal plane detection systems coupled with the MDM spectrometer is the Oxford detector sitting at the back of the spectrometer, which is used to identify particles, measure their energy and trajectory. This gridded ionization chamber is made of stainless steel, with entrance and exit windows covered by Aramica foil. The inside of the chamber is filled with isobutane gas. In order to minimize any further impurities of the gas during the experiment, this gas is continuously refreshed at a constant rate by a low flow regulation system. The inside structure of the detector consisted of a cathode plate, three anode plates to measure particle energy loss in isobutane gas, four resistive avalanche counters to determine the position of the particles in the focal plane as well as their deviation angles, a thick scintillator (type BC-400) placed behind the exit window where the particles stop, and two photomultiplier tubes positioned at each end to determine their residual energy.The Oxford detector had been used with this setup to study scattering and transfer reactions involving beams up to Ne. However, we encountered significant difficulties such as the energy resolutions obtained from the anode plates and the scintillator for the particle identification (PID), especially at larger scattering angles where cross sections of interest drop. Hence, in order to improve the particle identification resolution for the heavier particles, and increase the detection of both of these signals, the Oxford detector was upgraded by replacing the aluminum anode plate with a Micromegas array.

Keywords: MDM spectrometer, Oxford Detector

Implementation of two-window and three-window peak area methods to determine the ^{235}U abundance in uranium samples measured by a $LaBr_3(Ce)$ scintillation detector

[1] HALUK YÜCEL Ankara University
[2] RECEP BORA NARTTÜRK Ankara University Institute of Nuclear Science
[3] EMİN YELTEPE Ankara University Institute of Nuclear Science
[4] SEFER BALCI Ankara University Institute of Nuclear Science
[5] AYŞEN BARUT Ankara University Institute of Nuclear Science
[6] NESLİHAN CEREN KAPLAN Ankara University Institute of Nuclear Science
[7] SELİN SAATCI Ankara University Institute of Nuclear Science

In recent years, new types of scintillation detectors such as Lanthanum Bromide $LaBr_3(Ce)$ and Lanthanum Chloride $LaCl_3(Ce)$ are commercially available for the measurement of ^{235}U abundance in uranium samples. Historically, NaI(Tl) detectors are commonly used to determine ^{235}U abundance from 185.7 keV peak using enrichment meter principle if the sample thickness and the detector are met the required conditions. However, the measurement accuracy is generally affected the used detector resolution. Depending on its crystal size, NaI(Tl) detectors have relatively worse resolution (7-11% at 662keV) than those of especially new technology LaBr detectors, and thus they cannot separate the185.7 keV analytical peak from the close peaks in the measured spectrum. This might lead to erroneous results for ^{235}U isotopic abundance. In this study, a relatively high resolution (2.7% at 662 keV) LaBr(Ce) (its crystal size: 38mmx38mm, BrilLanCe 380 purchased from Saint Gobain Inc.) detector was used to obtain more accurate results for ^{235}U isotopic abundance in certified uranium samples (NRM 171-031,071, 195, 295 and 446). In this work, two-window peak area and three-window peak area calculation methods were employed in the enrichment meter principle to estimate the 185.7 keV peak counts. To do this, the first region-of-interest(ROI1) for 185.7 keV peak, the second window (ROI2) and third window for linear background continuum at right side is chosen to be about 10 keV. For the measured uranium samples, the results obtained from both two-window and three window peak area methods are compared, the results will be presented in detail.

This work was supported by the IAEA coordinated research project(CRP), coded J02012 and titled “Advancing Radiation Detection Equipment for Detecting Nuclear and Other Radioactive out of Material Out of Regulatory Control”.

Keywords: ^{235}U, uranium, LanthanBromide detector, Enrichment meter principle, Two-window, Three window, Peak area calculation, Gamma-ray spectroscopy

Use of boron in reactors as shielding and moderator material

[1] FATMA AYSUN UĞUR Osmaniye Korkut Ata University
[2] ELİF GÖREN Çukurova University

In this study, the use of boron and boron compounds as a moderator and shielding material in reactor control rods has been investigated. The data was taken from the Xcom photon cross section program. At different energies, the attenuation coefficient for the gamma and the mean free path were calculated while the reaction cross sections were calculated for the neutrons. It has been observed that boron and boron compounds are good shielding and moderator materials in the reactors.

Keywords: Boron, Shielding, Gamma, Neutron

Effects of gamma ray strenght function on reaction cross section calculations in some osmium isotopes

[1]KEMAL TAŞDÖVEN, [2] İSMAİL HAKKI SARPÜN, [1]HÜSEYİN ALİ YALIM

[1]Afyon Kocatepe University, Physics Dept., Afyonkarahisar, Turkey.
[2]Akdeniz University, Physics Dept., Antalya, Turkey.

Abstract

Gamma-ray strength functions are important for description of the gamma emission channel in nuclear reactions. This is an almost universal reaction channel since gamma rays, in general, may accompany emission of any other emitted particle. In this study, theoretical evaluation of gamma ray strength function for some Osmium isotopes (Os-186, Os-188, Os-189, Os-190, Os-192) have been investigated in the different incident photon energy range. TALYS 1.8 was used to show the effects of gamma ray strength function models to cross-section calculations. The present results were compared with the experimental values in EXFOR Library.

Keywords: Talys 1.8, EXFOR, Gamma-ray, radiative function

Introductıon

Photonuclear reactions are shown to be of potential interest for nuclear transmutation. The photonuclear cross-sections are rather uniform as a function of the mass number, and thus quite insensitive to nuclear species in contrast to (n,γ) reactions. Photonuclear reactions of (γ,2n) and (γ,n) have several unique features in view of their application for nuclear transmutation. They have been overlooked so far.In fact (n,γ) reactions have been considered to be realistic reactions to be used for nuclear transmutation. The neutron-induced reaction is caused by the strong interaction, while the photonuclear reaction by the electromagnetic one. [1]

Nuclear data of photonuclear reactions are important for a variety of present or emerging applications. Among them are radiation transport simulation and radiation shielding design of innovative reactors, diagnostics and shielding of plasma in fusion reactors, activation analysis, safeguards and inspection technologies, nuclear waste transmutation. Most of these applications need evaluated cross sections and emission spectra [2].

The interaction of high energy photons with target material can cause ejection of the nucleon/s, depending upon the energy of the incident photon. This reaction is considered as a photonuclear reaction. Photons should have sufficient energy above the binding energy of the nucleus for nucleon emission. As the nuclear binding energies are above 6 MeV for most of the isotopes, photons should have such threshold energy. There are three basic mechanisms for the photonuclear reactions: (a) Giant dipole resonance (GDR), (b) Quasi-deuteron (QD) and (c) Intranuclear cascade. A photon with energy below 30 MeV follows GDR mechanism. In this process, the photon energy is transferred to the nucleus by the oscillating electrical field of the photon, which induces oscillations among nucleons inside nucleus. The photo neutron production is more probable since proton ejection needs to overcome a large Coulomb barrier. For different isotopes at a particular energy, there is a peak of photo neutron production for (γ,n) reaction. This is called GDR peak energy. For isotopes above Z = 60, the peak energies are between 10-18 MeV. Above 30 MeV, the photo neutron production is mainly due to the QD effect. In this mechanism, a photon interacts with the dipole moment of a pair of proton-neutron in place of nucleus as a whole . Above 140 MeV, photo neutron production results from photo-pion production. Further the study of thermal fluctuation on GDR parameters are also of interest and studies are ongoing[3].

Nuclear reactions with different projectiles provide an information on properties of the excited nuclear states and nuclear reaction mechanisms. They are also required to different applications. Specifically, data of (n,xγ) reactions with any outgoing particle (x) and gamma-rays for atomic nuclei of the reactor materials and photofission reactions are needed for estimations of energy release, γ-ray shielding and radiation swelling of the reactor pressure vessel internals. Photo- fission reactions are also essential to an explanation of nuclear fission dynamics. Here, we consider reliability of description of gamma-transitions in (n,xγ) reactions and photofission by the use of simple closed-form expressions for photon strength function (PSF).

Giant Dipole Resonance

In the energy range of 10 to 30 MeV, the photon has the frequency comparable to the natural frequency of nucleus oscillations and it comes into a resonance with the nucleus. The so-called giant dipole resonance is

characterized by a collective vibrational motion of all protons against all neutrons within the nucleus. The most important contribution comes from the dipole mode, hence the name giant dipole resonance.

The giant dipole resonance peak cross section for photonuclear reaction can be ex-plained in semi-classical theory .

$$\sigma(E_\gamma) = \sigma_0 \frac{E_\gamma^2 (\Gamma/2)^2}{(E_\gamma^2 - E_0^2)^2 + E_\gamma^2 (\Gamma/2)^2} \quad (1)$$

Here σ_0 is the peak cross section, E_0 is the peak resonance energy, and Γ is the full width half maximum (FWHM) for the GDR peak. The width varies between 4 MeV and 8 MeV for medium and heavy nuclei. The peak cross section strongly increases with increasing mass number.

Semi-classical theory of electromagnetic radiation also reveals the empirical expression for the total photo-absorption cross section as [5]:

$$\int \sigma(E_\gamma) dE = 60 \left(\frac{NZ}{A}\right) [MeV.Milibarn] \quad (2)$$

where N is the number of neutrons in the nucleus, Z is the number of protons, and A is the mass number.

The giant dipole resonance is the primary contributor to the total photon absorption cross section; all other vibrational-mode contributions are generally negligible.

Gama Strenght Function

The γSF; $f_{XL}(E_\gamma)$ is a measure of the average electromagnetic propert of excited nuclei. The $f_{XL}(E_\gamma)$ is described as the average transitition strenght for a γ ray decay with γ-ray energy E_γ, electromagnetic character X and multipolarity L, decaying from an initial state E_i to a final state E_f. The $f_{XL}(E_\gamma)$ can be discriminated as the "downward" γSF, $f_{XL}(E_\gamma)$"upward" γSF olarak ayrılabilir. Şekilde görülmektedir.

Only the "downward" γSF, $f^j_{ifXL}(E_\gamma)$, which is of interest in this thesis, will be discussed. Hence, the notation $f_{XL}(E_\gamma)$ will be used instead of $f^j_{ifXL}(E_\gamma)$, to denote the γ-ray decay strength function. The γSF for a transition between an excited state E_i, with spin and parity J^π, and a lower energy state E_f, is given by

$$f_{XL}(E_\gamma) = \frac{\rho(Ef)\langle\overline{\Gamma_{\gamma XL}}\rangle}{E_\gamma^{(2l+1)}} \quad (3)$$

where $\langle\overline{\Gamma_{\gamma XL}}\rangle$ is the average radiative width, which is usually determined from the s- or p-wave resonances obtained from neutron capture experiments and $\rho(Ef)$ is the level density of the final states E_f. However, there are different theoretical models that are widely used to interpret the γSF for different modes of excitations and multipole types. A summary of these theoretical models, referred to as resonance models will be given below, together with their respective resonances that are observed as part of the total γSF and are relevant to this

Calculation Methods

Talys simulation program; Is a Unix-based computer program used to describe monte carlo simulation method.

The Talys program is a simulation program that allows us to simulate long-running or difficult nuclear reactions and make comparisons scientifically. The values obtained agree with the experimental results.

The calculated photonuclear reaction cross sections were obtained using the Talys 1.8 code program. Photonuclear reaction cross sections for Os-186, Os-188, Os-190, Os-192; (g, n) were calculated at specific energy intervals for the reaction. The results obtained with Talys were compared with the experimental results obtained from Exfor.

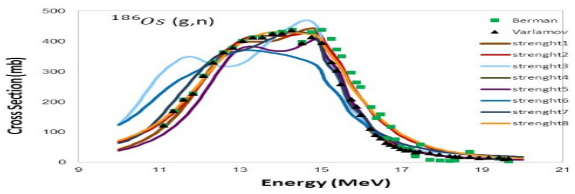

		Gstrnght1	Gstrnght2	Gstrnght3	Gstrnght4	Gstrnght5	Gstrnght6	Gstrnght7	Gstrnght8
((186)Os	Berman	30.893	**19.807**	51.874	57.169	38.562	57.161	35.145	21.867
	Varlamov	**8.891**	24.100	29.828	34.370	18.652	34.396	16.496	24.195

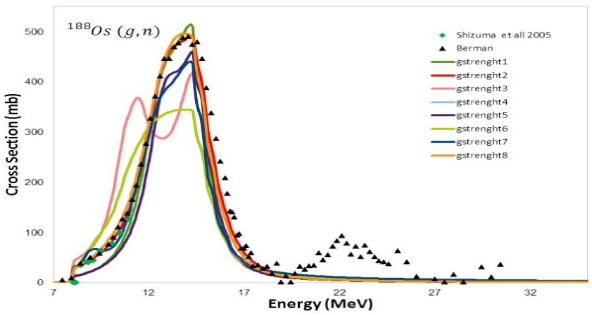

		Gstrnght1	Gstrnght2	Gstrnght3	Gstrnght4	Gstrnght5	Gstrnght6	Gstrnght7	Gstrnght8
(188)Os	Berman	38.791	**25.057**	63.504	55.930	44.224	55.900	40.085	29.876
	Varlamov	26.595	**12.783**	50.581	42.974	32.081	42.941	27.690	17.733

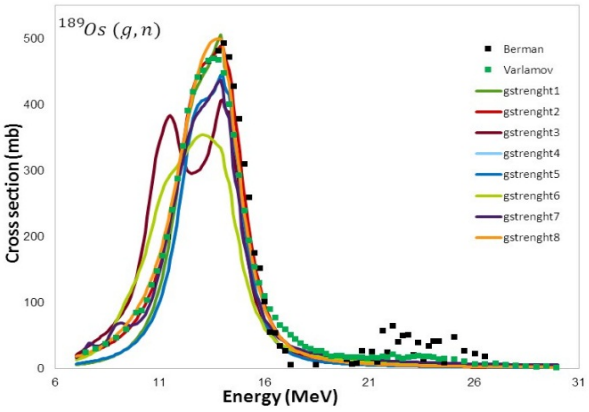

		Gstrnght1	Gstrnght2	Gstrnght3	Gstrnght4	Gstrnght5	Gstrnght6	Gstrnght7	Gstrnght8
(^189)Os	Berman	27.727	**16.888**	57.948	54.439	36.062	54.418	31.004	21.913
	Varlamov	17.616	**11.235**	39.564	35.969	23.385	35.934	15.273	11.420

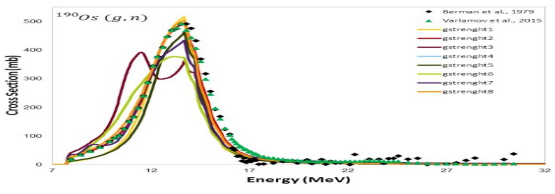

		Gstrnght1	Gstrnght2	Gstrnght3	Gstrnght4	Gstrnght5	Gstrnght6	Gstrnght7	Gstrnght8

(190)Os	Berman	24.811	**15.670**	51.553	38.823	30.408	38.819	27.165	18.624
	Varlamov	22.142	**11.884**	44.832	32.021	27.674	32.000	20.768	14.880

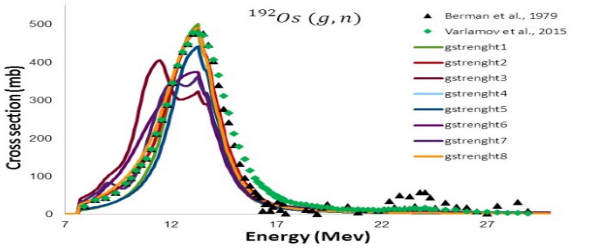

		Gstrnght1	Gstrnght2	Gstrnght3	Gstrnght4	Gstrnght5	Gstrnght6	Gstrnght7	Gstrnght8
(192)Os	Berman	26.916	**17.323**	56.115	40.039	33.126	40.030	35.933	22.291
	Varlam	27.829	**18.352**	52.659	37.565	33.538	37.549	33.220	22.800

Discussion

The photoneutron cross section were calculated for Os-186,Os-188,Os-190,Os-192 isotops in some energy values. In this sudy Talys 1.8 simulation program were used for these calculating cross section.İsotop of osmium was used for target in this calculated.

The calculated values of the emitted n particles in the energy values given are compared with the experimental data of berman and varlamov. It was taken from the EXFOR library in the figures.

An impact of the characteristics of nuclear excited states on the calculation results is studied using different energy levels for gama strength function.

References

1. Mariani et al., 2000
2. I. Raˇskinyt˙e, E. Dupont and D. Ridikas DSM/DAPNIA/SPhN, CEA-Saclay, F-91191 Gif-sur-Yvette Cedex, France
3. M. Mamtimin, 2014, Phd thesis, Idaho State University, “A Study of electron accelerator based

photon-neutron production and application to nuclear transmutation technology"
4. B.S. Iskhanov, V.N. Orlin, K.A. Stopani and V.V. Varlamov, March 7 2014, *Physics of Atomic Nuclei, Vol.* **77***, Number* **12***,* Russian Federation, "Photonuclear Reactions and Astrophysics"
5. Kgashane L. M., 2016, Master degree, University of The Westwern Cape, "Nuclear Level Density and Gamma-Ray Strenght Functions Ta isotopes and Nucleo-synthesis of ^{180}Ta "

Stopping Power and Range of Protons between 10-1000 MeV Energies in Water Using the Monte Carlo Technique

Ahmet BOZKURT [1] and Ismail Hakki SARPUN [2]

[1] *Akdeniz University, Faculty of Engineering, Department of Biomedical Engineering, Antalya, Turkiye*
[2] *Akdeniz University, Faculty of Sciences, Department of Physics, Antalya, Turkey*

Abstract

Monte Carlo simulations were carried out to obtain stopping power and range of protons in the energy range 10-1000 MeV in water medium. A point source emitting mono-energetic pencil beam of protons was employed. A water cylinder placed in vacuum represented the phantom, a cylinder of 30 cm radius and 100 cm height. Thin disk-shaped detectors (r=2 cm) were created in this phantom to compute average values of absorbed dose and flux. The position and thickness of each detector cell varied from simulation to simulation depending on the energy of the primary protons. The Monte Carlo simulations provided average flux and absorbed dose from proton interactions computed in each detector cell to later evaluate, for water, the value of the stopping power and the range of protons at that specific energy. In addition, the simulations yielded the location of the Bragg peak for the proton energies investigated in this study. The simulation results were later compared with the data available in the NIST compilation.

Introduction

When charged particles get absorbed in a material, they go through certain types of interactions with its orbital electrons and the nuclei. The parameter of choice to describe these interactions and thus the energy loss mechanism is usually the stopping power, which is a measure of the rate of energy lost in the absorbing medium and is denoted as $-dE/\rho dx$. This quantity is a function of the energy of the incoming charged particle and the density ρ and atomic number Z of the absorber and offers help in deriving the range of the charged particles as well as the amount of absorber thickness to shield against them.

The track that a charged particle beam follows upon penetrating an absorbing material is heavily affected by the type of interaction it experiences. The transfer of kinetic energy to atomic electrons or nuclei is carried out through elastic and inelastic scatterings of the particles in the beam. Consequently, there are two components that determine the total stopping power $\left(-\frac{dE}{dx}\right)_{tot}$ of charged particles in a medium: [1]

$$\left(-\frac{dE}{dx}\right)_{total} = \left(-\frac{dE}{dx}\right)_{col} + \left(-\frac{dE}{dx}\right)_{rad} \qquad (1)$$

In this equation, $\left(-\frac{dE}{dx}\right)_{col}$ is the collisional stopping power and is related to Coulomb interactions that take place between the charged particle beam and the atomic electrons of the absorber. $\left(-\frac{dE}{dx}\right)_{rad}$ is known as the radiative stopping power that leads to bremsstrahlung emission. Compared to the collisional stopping power, the latter is usually ignored especially for heavy charged particles such as protons and alpha particles, and therefore most of the particle's energy is transferred to atomic electrons through Coulomb collisions.

The traditional unit of stopping power for any type of charged particles is $\frac{MeV\ cm^2}{g}$ (for mass stopping power) and is obtained theoretically from the Bethe formula which involves derivations based on quantum mechanics and relativistic treatment. Additionally, there are data tables (from NIST) or computer codes (such as SRIM) existing for obtaining the stopping powers and ranges of vaious types of charged particles. [2, 3] Figure 1 describes for water how the electronic stopping power changes as a function of energy of the incoming charged particle. Figure 2 emphasizes on different behaviors that heavy charged particles and electrons exhibit in relation to the charge of the particle for most of the energy range.

The above mentioned Bethe's equation is very beneficial in determining collisional stopping power and is generally regarded as a complicated approach especially in applications involving materials composed of mixtures and compunds. Its alternatives, on the other hand, are limited to a certain number of materials and are based on either tabular data or computer codes. This study offers a different approach to compute stopping powers and ranges of charged particles based on the Monte Carlo technique. Here, we use the Monte Carlo software package MCNPX to obtain the total mass stopping power of protons in water over a wide energy range of 10-1000 MeV.

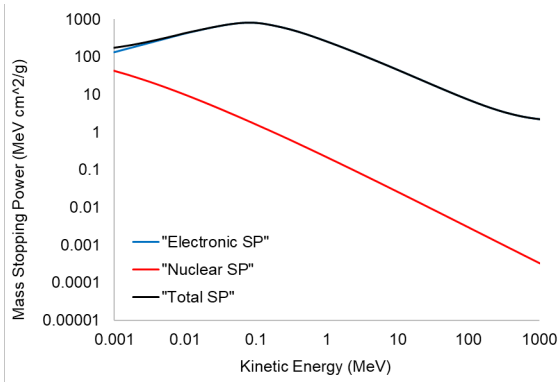

Fig. 1. Different components of mass stopping power of water as a function of proton energy.

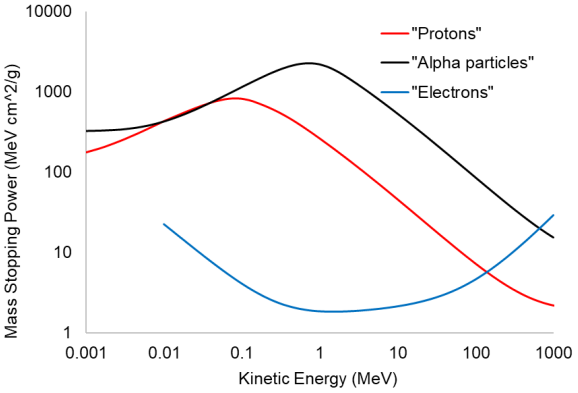

Fig. 2. Mass stopping power versus particle energy for electrons, protons, and alpha particles in water.

Materials and Methods

Monte Carlo method offers a numerical approach in solving problems which have no practical or analytical solutions and therefore it is considered an alternative way for simulating radiation transport through any material media. Using certain probability distributions, the technique starts with generating random numbers to find estimates for quantities such as energy, position, direction and path-length of individual radiation particles. It extensively uses the validated libraries of interaction cross sections to estimate probabilities of particle reactions that emerge when particles traverse materials. When these steps are followed for a finite number of particle histories, the simulation returns an average value for the quantity being searched. Hence, the Monte Carlo technique provides a stochastic approach that is considered as an alternative to analytical or deterministic methods and has many advantages in charged particle transport. For this reason, Monte Carlo simulations are viewed as a substitute for the Bethe-Bloche equation. [4]

Among the many Monte Carlo packages that are available for handling radiation transport, MCNP6 (version 2.7.0) is a well benchmarked code developed at the Los Alamos National Laboratory (LANL, USA) and is distributed by the Oak Ridge National Laboratory (ORNL). [5] The code can treat the transport of charged or uncharged particles in wide energy ranges and can model complex geometries arbitrarily in three dimensions. The particle interactions are taken from either continuous or discrete energies based on ENDF/B cross-section libraries (Evaluated Nuclear Data Files, version B). Various source distributions and detectors can be modeled in the code.

Figure 3 presents a plot of the problem geometry where a water phantom (cylinder; r=30 cm, h=50 cm) placed in a vacuum sphere (r=100 cm) is tracked with 1000 detector disks (r=0.1 cm) positioned consecutively from the surface. The thickness of each disk varies depending on the source particle's energy, basically taken as a fraction of the range of charged particle at that energy. Protons emitted from the source were mono-energetic and mono-directional created from a point source at one end of the water phantom. Tally types F4 and +F6 were employed in each of 1000 detector cells (r=1 cm; positioned consecutively from the surface) to record the average cell flux (in units of $\#/cm^2/source\ particle$) and the absorbed dose (in units of $MeV/g/source\ particle$) by all primary and secondary particles, respectively. Secondary particles created after the proton interactions were included in the simulations. Each run was carried out for one million particle histories which usually yields better than 1% statistical errors. A total of 23 cases were studied, each at a different source energy from 10 MeV to 1000 MeV.

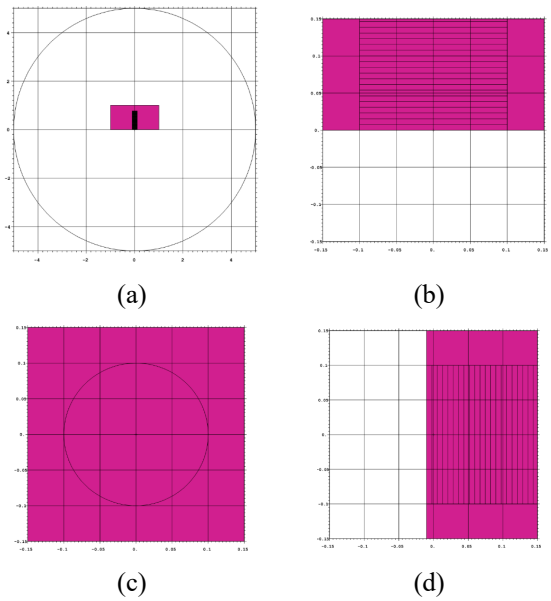

Fig. 3. A view of the problem geometry as seen by MCNP6. (a) Whole geometry, y-z slice at EXT 5. (b) Detector array, y-z slice at EXT 0.1. (c) Detector array, x-y slice at EXT 0.1. (d) Detector array, z-x slice at EXT 0.1.

Results

MCNPX was used to compute the absorbed dose and flux at each detector with varying material depths from proton interactions in the energy range of 10-1000 MeV.

Total mass stopping power (in $MeV\ cm^2/g$) for each proton energy was computed at the first detector of the array from the ratio of the absorbed dose recorded by +F6 tally (in $MeV/g/source\ particle$) and the flux from F4 tally (in $\#/cm^2\ /source\ particle$). Table 1 presents the total mass stopping power of water for protons along with the corresponding NIST data. The data from the Monte Carlo simulations and the NIST database agree reasonably well, the discrepancy being at most 9% as depicted by Figure 4.

Later, for each source energy (for each simulation), the depth of the detector cell at which the absorbed dose falls below 1% of the Bragg peak was determined and chosen as the range of the incoming protons at that particular energy. The proton ranges obtained by this approach for water are given in Table 2 along with the NIST data for comparison purposes. As shown, the Monte Carlo approach provides data that are in good agreement with those of the NIST database. Again, the data follow the same trend and deviate at no more than 4%. A similar trend is observed in proton ranges as seen in Table 2 and Figure 5.

Table 1. Monte Carlo calculated total mass stopping power (in $MeV\ cm^2/g$) of protons in water and comparison with NIST values.

E (MeV)	MCNPX	NIST	% Diff
10	44.91	45.67	-1.7%
20	25.72	26.07	-1.3%
30	19.48	18.76	3.8%
40	14.78	14.88	-0.7%
50	12.90	12.45	3.6%
60	11.29	10.78	4.7%
70	9.884	9.559	3.4%
80	8.681	8.625	0.7%
90	8.158	7.888	3.4%
100	7.668	7.289	5.2%
150	5.751	5.445	5.6%
200	4.651	4.492	3.5%
250	3.969	3.911	1.5%
300	3.606	3.520	2.4%
350	3.290	3.241	1.5%
400	3.160	3.032	4.2%
450	2.935	2.871	2.2%
500	2.847	2.743	3.8%
600	2.693	2.556	5.3%
700	2.569	2.426	5.9%
800	2.522	2.333	8.1%
900	2.440	2.264	7.8%
1000	2.414	2.211	9.2%

Conclusions

In this study, Monte Carlo approach was applied to determine stopping power and range data for protons of 10-1000 MeV energy. MCNPX simulations provide results that confirm to tabular data. This methodlogy is promising for other charged particles, different materials, and wider energy range.

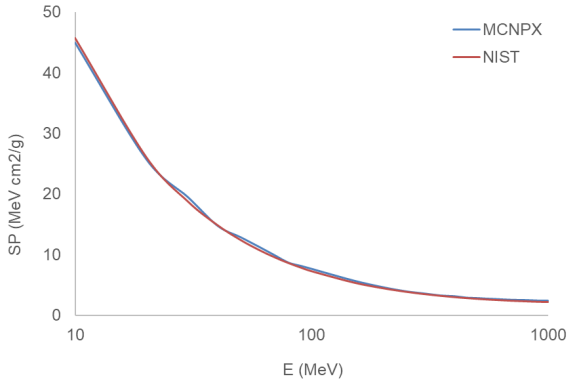

Fig. 4. Comparison of stopping powers from MCNP and NIST for water.

Table 2. Monte Carlo calculated range (in cm) of protons in water and comparison with NIST values.

E (MeV)	MCNPX	NIST	% Diff
10	0.1225	0.1228	-0.3%
20	0.4267	0.4252	0.3%
30	0.8865	0.8839	0.3%
40	1.492	1.486	0.4%
50	2.231	2.224	0.3%
60	3.096	3.089	0.2%
70	4.090	4.075	0.4%
80	5.197	5.176	0.4%
90	6.408	6.389	0.3%
100	7.728	7.707	0.3%
150	15.81	15.76	0.3%
200	26.00	25.93	0.3%
250	38.00	37.90	0.3%
300	51.53	51.39	0.3%
350	66.39	66.21	0.3%
400	82.29	82.17	0.1%
450	99.26	99.12	0.1%
500	117.2	116.9	0.3%
600	155.1	154.7	0.3%
700	195.2	194.9	0.1%
800	237.3	237.0	0.1%
900	280.6	280.5	0.0%
1000	325.7	325.2	0.1%

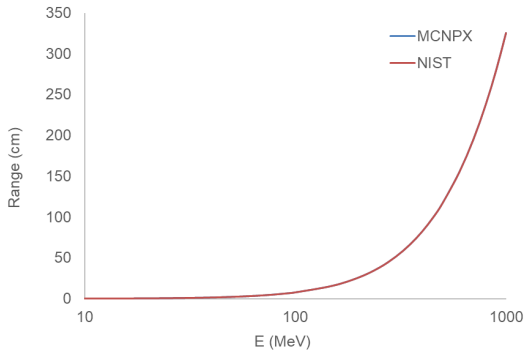

Fig. 5. Comparison of ranges from MCNP and NIST for water.

References

[1] James E. Turner, Atoms, Radiation, and Radiation Protection, 3rd Ed., ISBN: 978-3-527-40606-7, Wiley (2007).

[2] NIST, https://physics.nist.gov/PhysRefData/Star/Text/ASTAR.html, Last accessed: 09.07.2018.

[3] SRIM – The stopping and range of ions in matter., Nuclear Instruments and Methods in Physics Research Section B: Beam Interactions with Materials and Atoms, **268**(11-12):1818-1823 (2010).

[4] Andreo, P., Monte Carlo techniques in medical radiation physics. Phys. Med. Biol.; **36**(7):861-920 (1991).

[5] C.J. Werner (editor), "MCNP Users Manual - Code Version 6.2", LA-UR-17-29981 (2017).

Investigation of lateral spread of 80-250 MeV energy protons in water and cortal bone

[1] FATİH EKİNCİ Gazi University Türkiye
[2] MUSTAFA HİCABİ BÖLÜKDEMİR Gazi University Türkiye

The most important advantage of interacting protons with the target is maximum energy transfer at a certain depth. In other words, the maximum energy is stored at Bragg Peak point. But Coulomb collisions of protons are caused by numerous small angular deviations. These deviations also cause multiple scattering and lateral expansion in the dose profile, so the range of the proton beam is not a straight line. Lateral deviations are important in determining the closeness of irradiation to critical tissues, particularly in the treatment of tumors closed to critical tissues. In this study, Bragg peak and lateral scattering of the 80-250 MeV proton beam were calculated and evaluated by Monte Carlo simulation using the TRIM code in the case in water and 1 cm thick cortical bone.

Keywords: Lateral spreading, Bragg peak, Proton therapy, Monte Carlo

Excitation functions systematics studies of (n,a) nuclear reactions with neutron energy range from threshold to 20 MeV

MOHAMED BELGAID USTHB, Physics Faculty, Algeria

As not charged particle, the neutron is projectile who interacts only with atomic nucleus and consequently it can be the most penetrating projectile in the matter. The fast neutrons brings more understanding about the nuclear interaction and it can be used in inspections of transported goods as neutron interrogation system. To describe neutron-nucleus interaction, a several models have been developed, and used to quantify the neutron interaction by means of the nuclear cross sections determination. In the incident energy range from threshold to 30 MeV, the statistical equilibrium and pre-equilibrium models are the most models used to carried out several codes (TALYS, EMPIRE, GNASH, STAPRE-H etc..) and several systematics studies for nuclear reaction cross sections calculations. In this study, the formalism of these models is developed in order to obtain excitation functions formulae of (n, charged particles) reactions in the incident energy range from threshold to 20 MeV. The new formulae derived from the evaporation model and the pre-equilibrium exciton model contains an adjustable free parameter. The Droplet model of Myers and Swiatecki was used to express the reaction energy Q and the Dostrovsky model was introduced to formulate the expression of the inverse cross section channel. The systematics behavior of the different terms of the Droplet model involved in the reaction energy Q was verified individually before choosing the relevant terms and setting up the formulae. By fitting these formulae to the existing cross-section data, the adjustable parameters have been determined and the systematics of the (n,α) reaction have been studied. New semi-empirical formula for the predictions excitation functions has been obtained for the first time and it was compared with the experimental data and EMPIRE code calculations. A good agreement between excitation functions systematics and EXFOR data was observed for great number of (n, α) reactions.

Keywords: Fast Neutrons, systematics cross sections, pre-equilibrium exciton model, statistical evaporation model, neutrons interrogation

Effects of biomaterials on lateral spreading dose in proton therapy

[1] FATİH EKİNCİ Gazi University Türkiye
[2] MUSTAFA HİCABİ BÖLÜKDEMİR Gazi University Türkiye

Hard tissues in human body are generally damaged due to aging, accidents, birth defects, genetic defects and cancer. The displacement of hard tissue damaged with biomaterials by surgery is a widely practiced method in practice. In proton therapy, the thickness, density and electronic properties of the biomaterial used affect the range of the protons, the Bragg peak point and lateral spreading. As the protons interact with the biomaterials, a second peak near or below the Bragg peak occurs. In this study, Bragg peak and lateral spreading were calculated and evaluated for five different (1.2, 1, 0.8, 0.6 and 0.4 cm) thicknesses of seven different biomaterials (Nital (TiNi), Ti_6Al_4V, Co-Ni-Cr-Mo, Vitallium, Al_2O_3, Teflon and Stainless Steel) at the 100, 120, 140, 160 and 200 MeV energetic proton beams using TRIM Monte Carlo code.

Keywords: Lateral spreading, Biomaterial, Proton therapy, Monte Carlo

A novel approach to electromagnetic interference shielding: Conductive polymer/graphene nanocomposites

[1] CEREN KARAMAN Pamukkale University, Chemical Engineering Department
[2] EDİP BAYRAM Akdeniz University, Department of Chemistry
[3] İSMAİL HAKKI SARPÜN Akdeniz University, Department of Physics
[4] ONUR KARAMAN Akdeniz University Vocational School of Health Services

Nowadays, in information and signal processing, and telecommunication technologies, electronic devices are widely used. Electromagnetic (EM) pollution not also increases the degradation of the electronic devices performance but also threats the human health. Therefore, it is important to develop advanced electromagnetic interference (EMI) shielding materials for the prevention of damages caused by unwanted interference. Traditionally, thin sheets or sheathing forms of metals are used as EMI shielding materials. However, generally, metals are heavy, prone to corrosion, expensive and difficult to process. Hence, it need to develop alternative materials which are light, cheap and resistant to corrosion. In the last four decades, owing to their physicochemical properties, carbon materials and conductive polymers have gained prominence as EMI shielding materials. The EMI shielding and microwave absorption properties of these materials can be explained in terms of electrical conductivity and presence of polarons/bipolarons. The properties of these materials can be tunned by controlling of production conditions and precursors. However, in some cases, it may require using a high concentration of conductive polymers in the matrix to obtain acceptable electrical properties which often affect adversely the mechanical properties of resultant composites. This problem can be solved by combining the good properties of carbon materials and conductive polymers. Graphene is one of the promising carbon materials due to its multi-faceted superiority in electrical and thermal conductivity, flame retardancy, mechanical stability, and biocompatibility. In this study, a survey of the literature on the potential use of conductive polymers and graphene to improve EMI shielding efficiency is presented. The structure-performance of different nanocomposites are reviewed in detail. As a result, it is suggested that conductive polymer/graphene nanocomposites (such as PEDOT/graphene or PPy/graphene) can be a promising EMI shielding materials thanks to combining their superior features.

Keywords: Conductive polymers, Nanocomposites, Graphene, EMI shielding

Evaluation of the perlite as a new radiation shielding material

[1] OSMAN AĞAR Karamanoğlu Mehmetbey University
[2] GENCEBAY KARAKAYA Karamanoğlu Mehmetbey University
[3] CAN ERTUGAY Akdeniz University
[4] HÜSEYİN OZAN TEKİN Üsküdar University
[5] MEHMET EMİN KORKMAZ Karamanoğlu Mehmetbey University
[6] ÖZGÜR CULFA Karamanoğlu Mehmetbey University

In this study, the photon interaction parameters of concretes containing the natural perlite mineral and boron carbide (B_4C) in different ratios have been investigated experimentally by using ^{133}Ba (81, 276, 303, 356 and 384 keV), ^{137}Cs (662 keV), ^{60}Co (1173 and 1333 keV) and ^{22}Na (1275 keV) radioactive point sources. The experimental results of the mass attenuation coefficient, the mean free path (MFP), the half (HVL) and tenth value layers (TVL) will be presented and also compared to the other materials such as lead, granite and concrete.

Keywords: Shielding, Attenuation coefficients, Radiation, Perlite

X-ray shielding performance of sodium metasilicate/barium oxide glassy composites

[1] HANDE KAYACIK Yildiz Technical University
[2] YAŞAR KARABUL Yıldız Teknik University
[3] MEHMET KILIÇ Yıldız Teknik University
[4] ZEYNEP GÜVEN ÖZDEMİR Yıldız Teknik University
[5] ORHAN İÇELLİ Yıldız Teknik University

Radiation shielding panels, which are used in hospitals and nuclear plants, are usually made of lead and concrete. In recent years, as an alternative to lead and concrete, the search for non-toxic, low cost and light-weight materials with high radiation shielding ability has gained momentum. In the search of new radiation shielding materials, glassy structures are at the forefront due to their remarkable properties such as high light transmittance, easy preparation and low cost. In this work, Sodium silicate/Barium oxide ($Na_2Si_3O_7$/BaO) glassy composites were prepared with different concentrations of BaO (10%, 20% and 40%). During the preparation process of the composites, $Na_2Si_3O_7$ and BaO were mixed in appropriate ratios and each mixtures was allowed to dry at room temperature for 96 hours to ensure hardening. Finally, the mixtures were grinded to obtain a homogenous dispersion and the mixtures were brought into a tablet form by applying a pressure of five tons. The related glassy samples were irradiated by Ba-133 gamma-ray source for the photon energies of 81 and 356 keV. The mass attenuation coefficients (μ/ρ) of the samples were measured at 81 and 356 keV energies by using NaI(Tl) scintillation detector. The effective atomic number (Z_{eff}), half value layer (HVL), tenth-value layer (TVL) and mean free path (λ) were calculated. The experimental values of gamma-ray shielding parameters were also determined by WinXCom. A good agreement was achieved between the experimental and simulation results of the radiation shielding parameters. The details of the results will be presented in the conference.

Keywords: Glassy structure, Radiation Shielding, Monte Carlo Simulation, Gamma spectroscopy

As a shielding glassy structures against gamma rays: epoxy/PbO and epoxy/BaO composites

[1] YAREN ERGİN Yildiz technical university
[2] YAŞAR KARABUL Yıldız Teknik University
[3] MEHMET KILIÇ Yıldız Teknik University
[4] ZEYNEP GÜVEN ÖZDEMİR Yıldız Teknik University
[5] ORHAN İÇELLİ Yıldız Teknik University

With the increasing usage of nuclear radiation sources in medicine, nuclear plants and mobile devices, scientists have focused on producing new polymer based radiation shielding glassy structures. In recent years, the radiation shielding ability of filler-reinforced polymer composites have been extensively investigated due to their light weights and high workability properties. In this study, the low cost commercial epoxy polymers were reinforced by lead oxide and barium oxide with different weight percentages (10%, 20% and 40%) to enhance the gamma ray shielding property of the epoxy resins. The ratio of the resin to the hardener (isophorone diamine) was 65/25 in the epoxy polymer. All samples including pure epoxy were irradiated by gamma ray point source of Ba-133 at the 81 keV and 356 keV energies. The mass attenuation coefficients (μ/ρ) of the samples were measured for the related photon energies by using NaI(Tl) scintillation detector. The experimental half value layer (HVL), tenth-value layer (TVL) and mean free path were calculated to determine the radiation shielding performance of the samples. In the context of gamma ray shielding parameters, the influence of adding PbO and BaO to the epoxy polymer was discussed. The details of the results will be presented in the conference.

Keywords: Glassy structure, Radiation shielding, Gamma spectroscopy, Epoxy resin

Investigation of gamma-ray shielding parameters of $Na_2Si_3O_7/Bi_2O_3$ glassy composites

[1] TUĞBA DEMİRBAY Yıldız Teknik University
[2] YAŞAR KARABUL Yıldız Teknik University
[3] MEHMET KILIÇ Yıldız Teknik University
[4] ZEYNEP GÜVEN ÖZDEMİR Yıldız Teknik University
[5] ORHAN İÇELLİ Yıldız Teknik University

Due to increasing gamma ray sources in nuclear medicine and various industrial applications, the production of new lead free gamma ray shielding materials has become inevitable. Among various gamma ray shielding materials, glassy composites have promising properties such as having high transparency to visible light, 100% recyclability, low cost and considerable easy preparation methods. In the present study, Sodium silicate/Bismuth (III) oxide glassy composite structures have been produced with different Bi_2O_3 wt. concentrations which is varying from 10 wt.% to 35wt. %. The samples were irradiated by Ba-133 gamma ray point source with the photon energies of 81 and 356 keV. The mass attenuation coefficients (μ/ρ) of the samples were measured 81 and 356 keV energies by using NaI(Tl) scintillation detector. The experimental half value layer (HVL), tenth-value layer (TVL) and mean free path were calculated. The experimental values of gamma ray shielding parameters such as μ/ρ, HVL, TVL and mean free path were also determined by WINXCOM software. A good agreement was achieved between the experimental and theoretical results of the radiation shielding parameters. The details of the results will be presented in the conference.

Keywords: Glassy structure, Radiation shielding, WINXCOM, Gamma spectroscopy

Genetic programming modelling of radon measurements of some touristic places in Hatay, Turkey

[1] İSMAİL HAKKI KARAHAN Mustafa Kemal University
[2] ALİ TOZAR Mustafa Kemal University

^{222}Radon is a colorless, odorless, tasteless, radioactive gas that occurs naturally in soil, rocks, underground water, and air. It is produced by the natural breakdown of ^{226}Radium in soil and rocks. In outdoor air, radon is usually presents at such low levels that there is very little risk. However, when radon enters a building, it and its decay products can accumulate to high concentrations. Radon, itself, naturally breaks down and forms radioactive decay products. As one breathes, the radon decay products can become trapped in lungs. As these decay products break down further, they release small bursts of energy which can damage lung tissue and lead to lung cancer. This paper proposes a Genetic Programming approach to learn how to effect trace numbers, density of traces and number of measurement to radon measurement of touristic places in Hatay. Input parameters were selected as trace numbers, density of traces and number of measurement. Radon values (Bq/m^3) values was the output parameter. Training and testing sets in total of 45 samples were selected. The comparative results prove the superior performance for predicting Radon values of the touristic places. The produced model proposed close relationship for all the input parameters with the Radon values of the outdoor touristic places.

Keywords: Radon measuruments; Genetic Programming; Touristic places

The radiochemical purity test of ^{99m}Tc-sestamibi

[1] TUĞBA ÇEPNİ İstanbul University Science Faculty
[2] HATİCE KOVAN Okmeydani Training and Research Hospital
[3] BURCU DİRLİK SEVİM İstanbul University Cardiology Institute
[4] BAYRAM DEMİR İstanbul University Science Faculty
[5] VEDAT SANSOY İstanbul University Cardiology Institute
[6] ZERRİN YİĞİT İstanbul University Cardiology Institute

A radiopharmaceutial consists of two components. The first component is an isotope emitting gamma rays and the second component is a type of drug which is engaged to the organ chosen to be screening. In cardiac scanning, ^{99m}Tc-sestamibi radiopharmaceutical is used. The quality of scanning will be negatively affected if the patient has free ^{99m}Tc during the scanning. For this reason, the radiochemical purity of ^{99m}Tc-sestamibi should be higher than %90. In this research, our objective has been to determine the radiochemical purity rate of ^{99m}Tc-sestamibi right after the process and after 7 hours from process. In the tests results, we found out the radiochemical purity rate to be 95% right after the process. We also found out the radiochemical purity rate to be 52% after 7 hours. In order for the quality of imaging to be higher, it is determined that two ^{99m}Tc-sestamibi procedures in the morning and afternoon are found out better.

Quality control tests of cardiac spect camera

[1] TUĞBA ÇEPNİ İstanbul University Science Faculty
[2] BURCU DİRLİK SEVİM İstanbul University Cardiology Institute
[3] BİLAL KOVAN İstanbul University Istanbul Medicine Faculty, Department of Nuclear Medicine
[4] BAYRAM DEMİR İstanbul University Science Faculty
[5] VEDAT SANSOY İstanbul University Cardiology Institute
[6] ZERRİN YİĞİT İstanbul University Cardiology Institute

Nuclear medicine is a medical field specialized in imaging various diseases with the help of radio-isotopes giving out gamma rays. There are cameras designed specifically for imaging functions of the heart. This camera system is a SPECT system consisting of two gamma cameras stabilized to each other in a 90° angle. In this research, the quality control tests of cardiac SPECT camera has been evaluated. In COR (Center of Rotation) tests, the value of Mean X – error is found to be as -0.86 (with a maximum error rate of 4.6 mm), the value of maximum X-Error is found to be as 0.24 (maximum 0±2 mm), the value of maximum X-Error -1.4 (maximum 0±2 mm) and Range X-Error 1.63 (maximum 0±2 mm). Furthermore, maximum Y-error value is found to be as 0.51 (maximum 0±2 mm), maximum Y-error is -0.59 (maximum 0±2 mm) and Range Y-error is 1.10 (maximum 0±2 mm). As a result of quality control test, the Cardiac SPECT camera test values have been determined within the acceptable limits.

Measurements of generated proton energy spectra by high power lasers

ÖZGÜR CULFA Karamanoglu Mehmetbey University

In this research, the energy spectra of protons generated by ultra-intense (10^{20} W cm^{-2}) laser with a preformed plasma of scale length are presented. The effects of the preformed plasma with a controlled pre-pulse and the varied target thickness on the proton beam temperature, the number of protons and maximum energy of protons are evaluated. Simulations and experimental parameters show that preformed plasma scale length and target thickness have a significant importance on proton acceleration by high power lasers. Two-dimensional EPOCH particle-in-cell code simulations of the proton spectra are in a good agreement with measurements over a range of experimental parameters.

Keywords: High Power Lasers, Laser-Plasma Interactions, Proton Acceleration

Dosimetric comparison of two different VMAT techniques in lung cancer radiotherapy

[1] DUYGU BOLAT Uludağ University
[2] OĞUZ AYDIN Uludağ University
[3] SEMA GÖZCÜ TUNÇ Uludağ University
[4] ZENCİYE KIRAY Uludağ University
[5] SÜREYYA SARIHAN Uludağ University

Volumetric modulated arc therapy (VMAT) was introduced as a new treatment modality for lung tumors. In this study we aimed to compare angled table non-coplanar VMAT(n-VMAT) and coplanar VMAT (c-VMAT) techniques dosimetrically in lung cancer radiotherapy. For this study: A patient with NSCLC (non-small cell lung cancer) treated with 50 curative radiotherapy was randomly selected. For each patient, two VMAT plans were generated to meet the same objectives with 60 Gy covering 95% of the PTV. Dynamic arcs were used in each VMAT plan. The couch was set at ± 15° to the 0° straight position for the two non-coplanar arcs. Monaco treatment planning system with VMAT was used. We analyzed the conformity index (CI), the homogeneity index (HI); as well as the V5, V10, V20 and mean lung dose (Dmean). Paired non-parametric analysis of variance tests with post-tests were performed to examine the statistical significance of the differences of the dosimetric indices. There was no significant difference in the D2% ($p = 0.692$), D95% ($p = 0.989$) and Dmean ($p = 0.504$) in the two treatment techniques could be given the desired dose PTV. And no difference between the two techniques in terms of HI .CI and MU were found to be statistically better then the c-VMAT technique. c-VMAT was lower than the MU value of the n-VMAT. Dmean lung ($p = 0.191$) were no differences between the two techniques is examined. However, the n-VMAT technique is statistically better in patients with V5% ($p = 0.001$) and V10% ($p = 0.001$) in the whole lung. V20 was also lower in n-VMAT plans than c-VMAT. The results show that the n-VMAT is superior to the c-VMAT in terms of protection of critical organ doses. n-VMAT is preferable because of was superior in dosimetric outcomes for treating locally-advanced NSCLC compared to c-VMAT.

Keywords: Lung cancer, Volumetric Modulated Arc Therapy, Lung R, Lung Radiotherapy

Design of a 352.21 MHz RF power coupler for the Sanaem RFQ

[1] ERSİN ÇİÇEK Gazi University, Department of Physics
[2] YEŞİM OLGAÇ TAEK, Saraykoy Nuclear Research and Training Center
[3] ARİFE SEDA BÖLÜKDEMİR TAEK, Saraykoy Nuclear Research and Training Center
[4] BETÜL YASATEKİN TAEK, Saraykoy Nuclear Research and Training Center
[5] MUSTAFA HİCABİ BÖLÜKDEMİR Gazi University, Department of Physics
[6] İHSAN KILIÇ TAEK, Saraykoy Nuclear Research and Training Center
[7] ALİ ALAÇAKIR TAEK, Saraykoy Nuclear Research and Training Center

In all accelerator systems in which Radio Frequency (RF) Electromagnetic (EM) waves are used, one of the most critical component designed to feed RF power to a particle accelerating cavity is the power coupler. The Radio Frequency Quadrupole (RFQ) accelerators, designed for a given natural oscillation frequency, performing complicated tasks such as bunching, accelerating and focusing are the most popular method to accelerate the low energy beams. The RF power must be transferred to the cavity under the right conditions to provide the power needed for operation. In this study, we will discuss the EM design of the new coupler structures with grooved plexiglass vacuum windows for the RFQ with 352.21 MHz frequency, developed under a project at the Turkish Atomic Energy Authority (TAEK), Sarayköy Nuclear Research and Training Center (SANAEM). The coupler is required to operate in the pulsed mode with up to 120 kW of the forward power. Its important parameters such as scattering parameters, quality factor and resonant frequency, the determination of RF window, the power feeding scheme are optimized with the CST Microwave Studio.

Keywords: Power Coupler, Radio Frequency, Accelerator, Radio Frequency Quadrupole, Turkish Atomic Energy Authority, Computer Simulation Technology

Electromagnetic simulations for 800 MHz pillbox cavity and power coupler

[1] ASLIHAN ÇAĞLAR İzmir Yüksek Teknoloji Enstitüsü
[2] HAKAN ÇETİNKAYA Boğaziçi University
[3] CİHAN ÇİÇEK Boğaziçi University
[4] AYDIN ÖZBEY İstanbul University
[5] EZGİ SUNAR Boğaziçi University
[6] GÖRKEM TÜREMEN Ankara University
[7] HÜSEYİN YILDIZ İstanbul University
[8] ALPEREN YÜNCÜ Boğaziçi University
[9] VEYSİ ERKCAN ÖZCAN Boğaziçi University
[10] GÖKHAN ÜNEL University of California
[11] FATİH YAMAN İzmir Yüksek Teknoloji Enstitüsü

RF800 project aims to build a high power radio frequency transmission line operating at 800 MHz. The RF source is a Valvo YK 1198 klystron generating 60 kW continuous power; and the goal is to channel this power into an accelerator cavity. The transmission line consists of coaxial to waveguide converter, rectangular waveguides, E and H bends, 3-port waveguide circulator, waveguide to coaxial converter and an RF cavity with input power coupler. As a part educational project, all components are to be designed and produced locally. In the first phase of the project, a simple pillbox cavity is selected due to its convenient design and manufacture. In order to obtain high power transmission from RF power generator to cavity efficiently, power coupler with a loop antenna is designed to achieve critical coupling condition. The electromagnetic wave reflections due to possible impedance mismatch between the cavity and the coupler are minimized for 800 MHz. Effective coupling is observed in the S11 vs. frequency variation of the coupler-cavity structure. Design and error studies for both the cavity and the coupler, completed using CST-MWS, along with the current status of the RF transmission line will be presented.

On the determination of binding energy of hypernuclei

[1] NİHAL BÜYÜKÇİZMECİ Selçuk University
[2] RIZA OĞUL Selçuk University

In nuclear reactions of high energy one can simultaneously produce a lot of hypernuclei after the capture of hyperons by nuclear residues. We consider statistical disintegration of such hypernuclear systems and the connection of fragment production with the binding energies of hyperons. It is demonstrated that the hyperon binding energies can be effectively evaluated from the yields of different isotopes of hypernuclei. The double ratio method is suggested for this purpose. The advantage of this procedure is its universality and the possibility to involve many different isotopes. This method can also be applied for multi-strange nuclei, which binding energies were very difficult to measure in previous hypernuclear experiments. We believe that our calculations would be the pioneering for the extraction and analysis of future hyperon experiments such as GSI/FAIR or other similar facilities.

*The work has been performed in the framework of TUBITAK 114F328 and COST Action THOR-CA15213.

Keywords: nuclear reactions, hypernuclei, evaporation

Effects of radiation pressure acceleration on heavy ion generation for ultra intense laser solid interaction

[1] ÖZGÜR CULFA Karamanoglu Mehmetbey University
[2] MEHMET EMİN KORKMAZ Karamanoglu Mehmetbey University
[3] OSMAN AĞAR Karamanoglu Mehmetbey University
[4] VOLKAN SERT Karamanoglu Mehmetbey University

Particle acceleration with high power lasers has been studied for last two decades. It is well known that laser acceleration mechanisms have a dependence on target thicknesses. Radiation pressure acceleration (RPA) is on the process for such thin targets (nm levels). High power laser solid target interactions for the irradiances of up to the ~10^{20} W/cm^2 have been studied experimentally and theoretically for such thin targets. ELI-NP project gives an opportunity to us to study laser solid interactions with the irradiances of up to the ~ 10^{23} W/cm^2 with fs level short pulse durations experimentally. In this research, we investigated the laser solid interactions theoretically with such high power lasers (irradiances of 5x10^{22} W/cm^2) with such thin targets (few nanometers). We used 2D EPOCH PIC code simulations to investigate heavy ion acceleration in ultra thin targets and studied effects of the target thicknesses on heavy ion angular and energy distributions.

Keywords: Particle Acceleration, Laser-Plasma Interactions, High Power Lasers

Acceleration of carbon ions by high power lasers

[1] VOLKAN SERT Karamanoglu Mehmetbey University
[2] ÖZGÜR CULFA Karamanoglu Mehmetbey University
[3] MEHMET EMİN KORKMAZ Karamanoglu Mehmetbey University

Nowadays, with the rapidly advancing technology lasers can reach up to 10PW. With the right focusing, the intensity of the lasers at this level can easily go up to $>10^{22}W/cm^2$. Extremely high intense lasers have an important role especially in particle accelerator technology. In this study, we have investigated the effects of the future laser technology on particle acceleration. With this aim, we have investigated the maximum energy and heat exchange between fully ionized C^{+6} ions and electrons, and preformed plasma produced before the main laser interaction by using 10PW lasers with the irradiances of $5x10^{22}W/cm^2$. In this study, we have employed two-dimensional EPOCH PIC (particle in cell) simulation codes.

Keywords: High Power Lasers, Carbon Ions

Investigation of the excitation-autoionization states of helium

ZEHRA NUR ÖZER, NURÇİN KARADENİZ, HÜSEYİN ALİ YALIM

Afyon Kocatepe University, Physics Dept., Afyonkarahisar, Turkey

Abstract

In this study, the autoionization energy levels of Helium were experimentally investigated by measuring the intermediate angular distributions of ejected electrons. The experimental setup is located in the Electron Collision Laboratory at Afyon Kocatepe University. The main purpose of these type studies is to examine the structure of atomic systems, to see how the electron correlations occur in such processes, to produce experimental data for solving the multiparticle problem and to test the correctness of theoretical models. Further studies on autoinizing states of Helium in combination with theoretical calculation is needed to interpretation of the results and correlation dynamics.

Keywords: Electron spectrometry, Autoionization, Angular spectrum, Resonance levels, Helium atom

Introduction

The physical and practical significance of the autoionization phenomenona has been attracted the attention of many researchers for many years. Autoionization and resonance profiles, interactions between electrons and differences observed in the energy and angle dependent cross sections are important in atomic collision studies. The first experimental work with sufficient resolution to resolve and identify the autoionization levels with ions was carried out by Rudd (1964). Since then autoionization of helium atom has been the focus of attention for many years both experimentally and theoretically. The following references on autoionization and resonance profiles have an important role in understanding the interactions between electrons, shapes of the electron clouds and energy/angle dependent cross sections (Pochat et al. 1982, Lower and Wiegold 1990, Crowe et al. 1996, Brunger et al. 1997, Samardzic et al. 1997, Jureta 2014).

Optically absorptive spectra are used to study the resonance profiles of permissive transitions, but optically forbidden transitions have been observed in the results of the collision of charged particles (such as electrons, protons, and ions) with these targets. The resonance levels in the most basic two-electronic atom, helium are above the first ionization threshold. In the electron collision experiments, when two electrons in the ground state are excited to these levels, an electron spontaneously ionizes and the incoming and breaking electrons are scattered at all angles. Measurements of the autoionization region of an atom depend on the electron collision energy and ejected electron angle. For this reason, it is necessary to make measurements at different electron impact energies and at different ejected angles to correctly interpret the results.

In this study, differential cross section (DCS) measurements were made to determine the intermediate angular distributions of the double excitation-ionization energy levels of the helium atom and the autoionization energy levels of helium were experimentally investigated. Experiments are carried out in electron spectrometer that is located in the Electron Collision (e-COL) Laboratory in the Physics Department of Afyon Kocatepe University and it is essentially a combination of an electron gun, two turntable hemispherical electrostatic energy analyzers and a Faraday cup. An incident electron beam intersects at the right angle of the gas jet formed at the collision center. A coplanar geometry is used, where all electrons are observed in the collision plane defined by the incident and scattered momentum vectors respectively. The main purpose of the studies using this set up is to examine the structure of atomic and molecular systems, to investigate how the electron correlations occur in the ionization process, to produce experimental data for solving the multiparticle problem and to test the correctness of theoretical models.

The electron impact excitation of doubly excited states is usually investigated by the electron energy loss measurements of scattered electrons or the energy spectra measurements of ejected electrons. These states are degenerate in energy with continuum states

from the direct ionization process, resulting in their non-radioactive decay, autoionization. Since the final states for both processes are indistinguishable, an interference can occur between the two processes depending on both the magnitudes and relative phases of the competing direct and resonant amplitudes.

Results

The angular distributions of the auto ionization energy levels of the helium atom were determined by detecting electrons after the excitation of it by 200 eV energetic electrons. Differential cross section measurements (DCS) were taken in the 20º-45º angular range for 32,5-35 eV resonance energy levels. In the spectra, peaks consisting of the addition of ionization and direct ionization have been observed.

Strong interaction between two electrons, autoionization and sharp lines in excitation processes. These lines embedded in the ionization zone are determined by the shape called Fano. The first theoretical work on autoionization was reported by Fano in 1961.

Depending on the resolution of the analyzers, ^{1}D and ^{1}P levels which are very close to each other for n= 2 can not be distinguished. In the spectra, resonance profiles with symmetric and asymmetric structures are formed above the direct ionization cross sections in the vicinity of their resonance levels.

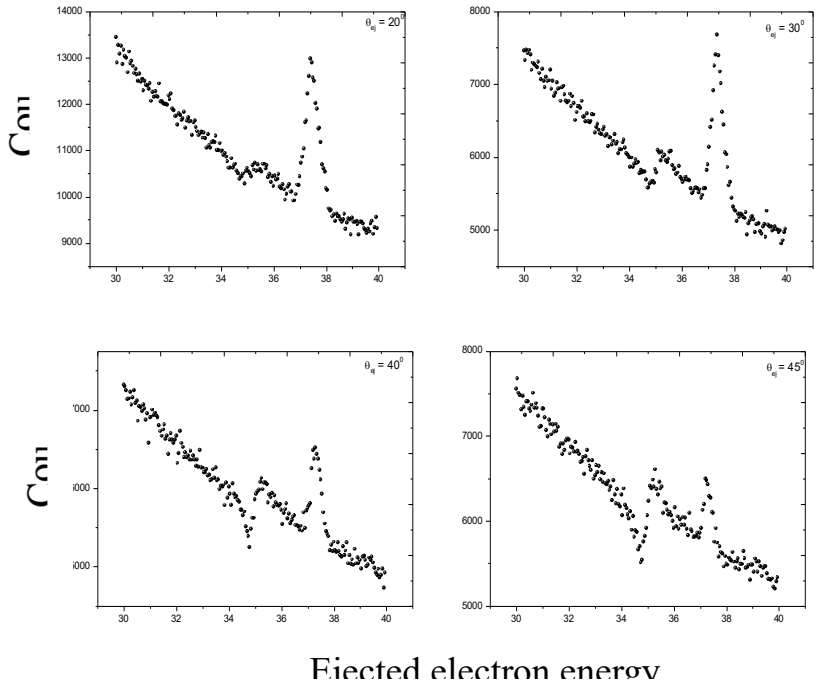

Fig. 1. Differential cross sections for 200 eV at 20º-40º ejected electron angles.

The present results is a step forward in the direction of better understanding the autoionization region in atoms accessed by electron impact. Further studies on autoinizing states in He in combination with theoretical calculations are needed to interpret the results and the correlation dynamics.

This work was supported by AKU-BAPK through Grants 15.FEN.BİL.14 and 15.HIZ.DES.131-132.

References

[1] A. Pochat, R.J. Tweed, M. Doritch, and J. Peresse, *Journal of Physics B: Atomic and Molecular Physics*, 15: 2269-2283 (1982).

[2] U. Fano, *Physical Review*, 124: 1866-1878 (1961).

[3] M.E. Rudd, *Physical Review Letters*, 13(16): 503-505 (1964).

[4] J.Lower and E. Weigold, *Journal of Physics B: Atomic, Moleclar and Optical Physics*, 23: 2819-2845 (1990).

[5] A. Crowe, D.G., Mcdonald, S.E. Martin, and V.V. Balashov, *Canadian Journal Physics*, 74(11): 736-742 (1996).

[6] M.J., Brunger, O., Samardzic, A.S. Kheifets, and E. Weigold, *Journal of Physics B: Atomic, Molecular and Optical Physics*, 30: 3267-3285(1997).

[7] O. Samardzic, L. Campbell, M.J. Brunger, A.S. Kheifets, E. Weigold, *Journal of Physics B: Atomic, Molecular and Optical Physics*, 30: 4383-

4394 (1997).
[8] J. Jureta, A.R. Milosavljevic, and B.P. Marinkovic, *International Journal of Mass Spectrometry*, 365: 114-120 (2014).

Investigation of the effects of the level density models and g-strength function models on the ^{92,94,98,100}Mo(p,g) reaction cross sections

[1] ABDULLAH AYDIN Kırıkkale University
[2] HANDE BOYDAŞ Kırıkkale University

The nuclear reaction studies and the cross section calculations related the astrophysical processes are very important to the nucleosynthesis. We have studied the cross sections of (p,g) reactions for ^{92,94,98,100}Mo isotopes in the energy range of the Gamow window. The cross sections have been calculated by using TALYS 1.8 code. In the calculations, different level density models and g-strength function models have been used and the effects of these models have been investigated on the cross sections. The calculated cross sections have been compared with the experimental data from EXFOR database. Results obtained in the present work show that the cross section calculations have a strong dependence on the level density models and g-strength function models, which used as an input for TALYS 1.8 code.

Keywords: level density model, g-strength function, cross section, astrophysical processes

Comparison of gamma-ray sources which used to measure of material density especially -metals and alloys via using transmission technique

[1] M. ERGÜN TURGAY Yalova University
[2] EROL KAM Yıldız Teknik University

One of solutions for density measurement is to use the gamma-ray transmission technique. Its outstanding specification is to applicable without any connection to material. Herewith we studied this technique by two gamma-ray sources as Co-60 and Cs-137. At first, each source, without materials in the geometry, was counted and noted intensities as (I_0) Then, all materials were counted and noted intensities as (I). By using these initial radiation intensity (I_0) and radiation intensity (I); [I/I_0] rates were calculated and then density of materials could be determined by using Beer-Lambert Equation. Experimental application was performed on widespread industrial metals or metal alloys e.g. lead, copper and steel, brass. Minimum difference was obtained as 0.26% and 1.11% up for steel and copper, near by 5.07% and 5.73% down for brass and lead (source: Co-60). Minimum difference was obtained as 0.22% down for copper, near by 1.07%, 2.34% and 3.08% up for lead, brass and steel respectively (source: Cs-137). Another point, these difference ratios would be references for next studies about another material density measurement, too. Besides, it will be also useful to select the gamma ray source for future different studies. With this study, it is shown that gamma transmission technique, can be used for density measurements. There were acceptable differences obtained between the measured densities and given densities of them.

Keywords: Co-60, Cs-137, Density Measurement, Gamma-Transmission Technique

Outdoor gamma dose in air and investigation cancer risk for Hatay province, Turkey

[1] M. ERGÜN TURGAY Yalova University
[2] EROL KAM Yıldız Teknik University

The radioactivity analysis was performed for air measurements around Hatay province which is in the Southeast region of Turkey. By measuring of the outdoor gamma dose rates on 215 different stations, it was calculated to annual dose in air. On the other hand, cancer risk was evaluated for Hatay. These values were compared with the World's references (UNSCEAR) and assumed. It was measured the average dose rate as 52.13 $nGyhr^{-1}$ and annual dose was calculated to 63.93 μSv. This dose is required to excess lifetime cancer risk as $2.24x10^{-4}$. These values could be compared with the similar studies which existed around the world. Finally, the average annual effective dose equivalent and excess lifetime cancer risk for Hatay, are less than the world average. This study would be also reference for future researches, besides it will be useful to compare with different studies for Hatay which, will be evaluated in the future, for example after a nuclear pollution, such as based on a reactor leakage, nuclear attacks, etc., too.

Keywords: Radioactivity, ADRA, AEDE, Air, Outdoor Gamma, Cancer Risk, RESA, Hatay

Bohr hamiltonian for γ=30◦ with Kratzer potential

[1] İBRAHİM YİĞİTOĞLU Gaziosmanpaşa University Physics Department
[2] BURCU UÇAR Gaziosmanpaşa University Physics Department

A γ-rigid solution of the Bohr Hamiltonian is derived for γ=30° using the Kratzer potential in the β variable. The model is conventionally called Z(4)-Kratzer. The energy eigenvalues and wave functions are obtained by using an analytic method developed by Nikiforov and Uvarov. The obtained energy spectra and the calculated B(E2) transition rates are presented and compared with existing experimental data.

Keywords: Critical Point Symmetries, Kratzer potential, Nikiforov-Uvarov Method, Bohr Hamiltonian

A solution of bohr hamiltonian for γ=0° with Kratzer potential

[1] İBRAHİM YİĞİTOĞLU Gaziosmanpaşa University Physics Department
[2] TUĞBA TURAN Gaziosmanpaşa University Physics Department

A γ-rigid solution of Bohr Hamiltonian for γ=0° is derived with Kratzer Potential. This solution will be called X(3)-Kratzer. The energy eigenvalues and wave functions are obtained by using an analytic method which has been developed by Nikiforov and Uvarov. The B (E2) transition rates are also calculated. The obtained results are compared to the previous studies. The agreement with the experiment is achieved.

Keywords: Bohr Hamiltonian, Critical Point Symmetries, Kratzer Potential, X(3) Model

Comparison of radiation shielding properties of fir with other wooden materials at 6 MeV x-rays energy

[1]YUSUF KAVUN, [2]MUHİTTİN ŞAHAN, [2]MAHMUT ÖZGEN, [2]EYYUP TEL

[1]Kahramanmaras Sutcu Imam University, Vocational School of Health Services
Department of Medical Imaging Techniques, Kahramanmaras, Turkey
[2]Osmaniye Korkut Ata University, Department of Physics, Osmaniye, Turkey

Abstract

With the development of technology, radiation shielding is essential for the protection of human and environment. Various materials can affect the amount of radiation transmitted from the source to the receptor when placed between a source and a receptor. In this study, to reveal efficiency of wooden materials, we aim to compare usability of fir wooden material with other woodens as a shielding material in the radiation treatment centers that in use Medical Linac. We analysed dose-thickness relations of fir and some of other wooden materials at 6 MeV X-rays energy for different surface areas and thicknesses and these results compared with literature.

Keywords: fir, x-ray, dose measurement, radiation shielding, wooden material

Introduction

The radiation safety is a safety culture that must be in radiation health centers due to workers engaged in radiation work, cured patients and other exposed persons in health care. Because, Ionizing radiation has sufficient energy to cause chemical changes in body cells and damage them. Therefore, some cells may die or become abnormal, by damaging the genetic material (DNA) contained in the body's cells [1]. For such reasons, it is very important to comply with radiation protection rules and to raise public awareness about radiation.

Time, distance, and shielding are the three basic concepts of radiation protection that apply to all types of ionizing radiation. Radiation shielding is based on the principle of attenuation [2], which is the gradual loss in intensity of any energy through a medium. Also the nature of the material that is the ability to reduce a wave's or ray's effect by blocking or bouncing particles through a barrier material to be chosen to stop and absorb of the radiation in the shielding is very important.

The choice of shield material depends on attenuated radiation levels, resistance to radiation damage, required thickness and weight, permanence of shielding and availability. Due to the regardless of its form or shape, the purity of the selected material is related to the nature of the radiation source. Therefore, lead is usually used for radiation shielding. In some cases, some contamination in lead shielding material may cause secondary radiation. But, some Tropical wood species have been found to provide shielding against ionising radiation and these wooden material can usable instead of lead shielding material [3].

Within the scope of this study, fir and other wood materials (mulberry and walnut) in various sizes and thicknesses (5x5 cm^2, 8x8 cm^2, 10x10 cm^2, 12x12 cm^2 thicknesses ranging from 0.5 cm to 9.0 cm) produced in the inner Anatolia region were investigated by using 6 MeV X-rays energy and it is compared in order to investigate the efficiency and efficiency of shielding in treatment centers with radiation. Thus, the efficiency of radiation protection of the fir and other tree species will be examined by comparing radiation absorption characteristics.

Material and Method

In order to investigate the efficacy and efficiency of shielding in treatment centers with radiation, fir wooden materials in various sizes and thicknesses produced in the inner Anatolian region have been examined by comparing with other tree species. The dose absorption efficiency was measured by the experiments performed in Radiation oncology unit of Ankara Atatürk Chest Diseases and Chest Surgery Training and Research Hospital and the efficiency of these materials in shielding was examined. By using medical linac, 6 MeV energized x-rays were applied to these wooden materials and solid phantoms placed at various angles. Siemens Oncor Model [4] linear accelerator was used for irradiation and parallel ion chamber detectors of PTW model were used for experimental dose measurements. Each of the solid phantoms and wood materials were exposed to x-rays of 6 MeV for 15 seconds. The amount of radiation dose given to each item during this period is 10 Gy. Absorption data for wood materials for each thickness were obtained in mGy units. The calibration of the PTW model [5] parallel ion chamber detectors used in the measurement was measured by photon beams sent at a distance of 100 cm from the target in the 10 x 10 cm^2 area to the target surface and 10 cm water depth in the central axis. The amount of radiation dose in the phantom was

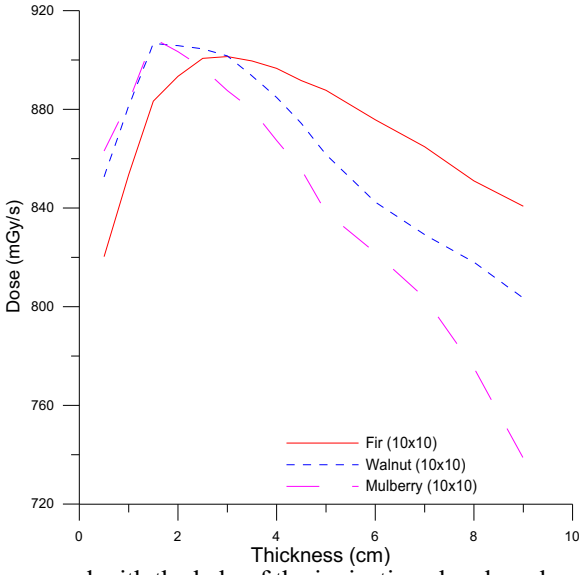

measured with the help of the ionization chamber placed at this depth. The Ion collection time of the detector is 0.03 ms and the error ratio (± 10 °) is % ≤ 5 [5].

Results

A wide variety of shielding materials are being developed every day for the purpose of radiation protection. In addition to the effectiveness and efficiency of the shielding material being protected, it is also necessary that the cost is low for widespread applicability. Thus, radiation shielding, which will be made using low cost, high-shielding materials, will be important in reducing the effects of many accidents that can occur as a result of significantly reducing the exposure of workers in radiation centers. According to the figure 1-4 obtained from 6 MeV energy, the measured dose increased up to 2 cm thickness and then decreased slowly. It is understood that it would not be very efficient to use the mulberry and walnut wooden as a shielding material in this energy but on the other hand fir wooden material provides much better protection than walnut and mulberry wooden material. For this reason it is obvious that fir, walnut and mulberry wooden material can be used in radiation shielding technology in patient treatment centers in used Medical Linac at low energies due to the lower cost of shielding.

Fig. 1. Dose measurement for 5×5 cm2 area versus thickness

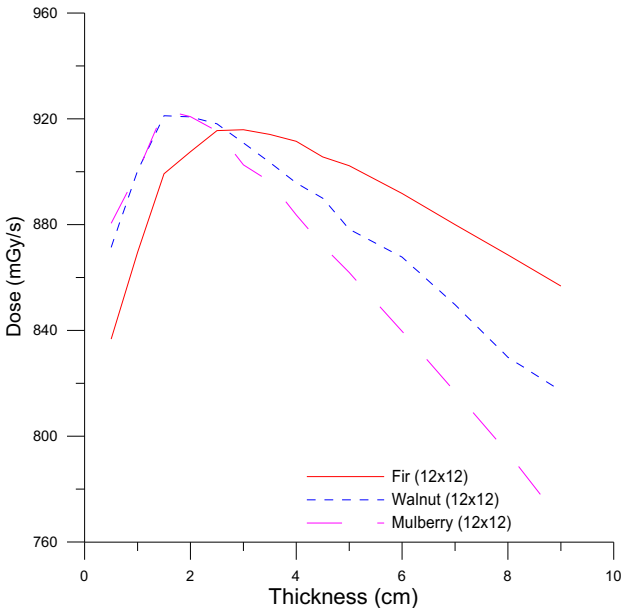

Fig. 2. Dose measurement for 8x8 cm2 area versus thickness

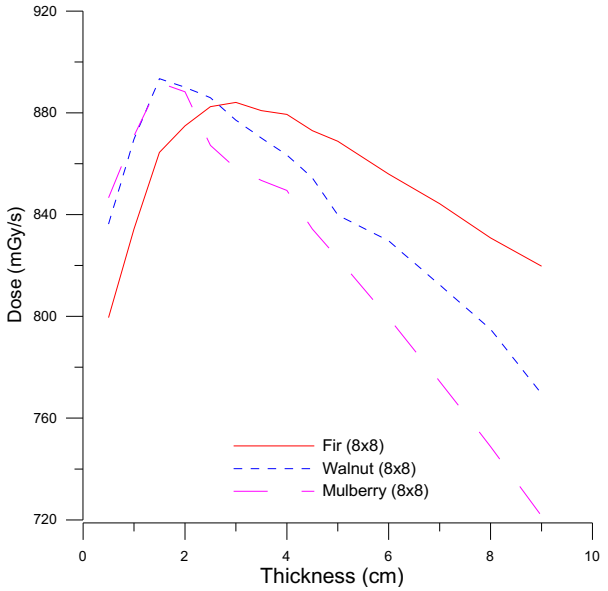

Fig. 3. Dose measurement for 10x10 cm2 area versus thickness

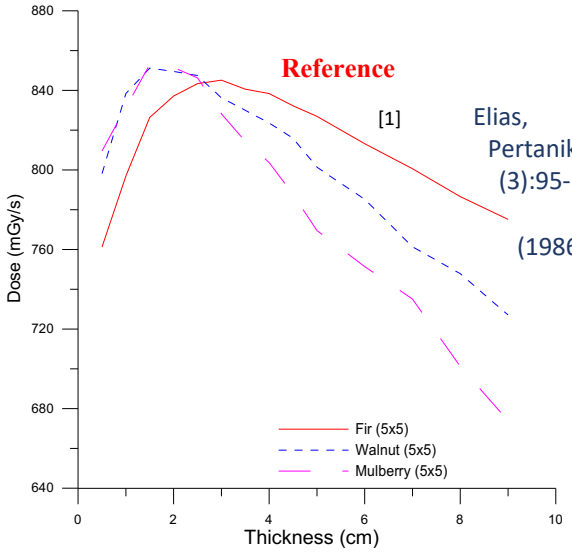

Reference

[1] Elias, S. Pertanika6 (3):95- 98 (1986).

[2] Martin, J.E. "Physics for Radiation Protection: A Handbook. 2nd Edition.WILEYVCH Verlag GmbH & Co. KGaA, Weinheim, (2006).
[3] Aggrey-Smith, S. et al., The Open Access Journal of Science and Technology Vol. 4 (2016).
[4] ONCOR Impression Operator Manual, Siemens Medical Solutions USA, Inc., Malvern, PA.(2015).
[5] PTW-Freiburg and PTW-New York: Advanced Markus, Bragg Peak, CURIEMENTOR, DIAMENTOR, FARMER, Markus, NOMEX, OCTAVIUS, Pin Point, ROOS, TRUFIX, (2017).

Fig. 4. Dose measurement for 12x12 cm2 area versus thickness

Mean Free Path Calculations for (n,p) Reactions of Ba Target Nuclei

EYYUP TEL[1], AHMET BÜLBÜL[2], R. ÖMER TURHAN[1], MUHİTTİN ŞAHAN[1]

[1]Osmaniye Korkut Ata University, Department of Physics, Osmaniye, Turkey
[2]Osmaniye Korkut Ata University, Department of Electricity and Energy, Osmaniye, Turkey

Abstracts

Calculations of macroscopic cross sections and mean free path have a great importance on shielding of the nuclear reactors. Unlike normal concrete, barite concrete is mostly used for shielding to reduce the negative effects of nuclear reactor to the environment. In this study, the macroscopic cross section and mean free path values obtained for (n,p) reactions with Ba element at the 14-15 MeV energy using Levkovski (1974) and Tel et al. (2003) formula. The obtained results are then compared with each other.

Keywords: barite concrete, Tel formula, mean free path

Introduction

Radiation is energy given off by matter in the form of rays or high-speed particles. This radiation includes electromagnetic spectrum (such as radio waves, micro-waves, visible light, x-rays, and gamma) and particle radiation (such as alpha and beta). As the radiation is hazardous for human health, it is important to keep radiation dose as low as possible. Protection for the radiation hazardous are required shielding. This is done mainly using shielding materials. The most important materials for this purpose is barite which is a mineral composed of barium sulfate ($BaSO_4$). Barite is generally white or colorless and is the main source of barium. As the barite is not used directly it can be used in some other materials such as fabric [1]. The concretes developed were tested under a variety of conditions to determine their physical, chemical, and structural characteristics. Barite behaves in concrete similarly to an ordinary crushed concrete materials such as limestone or basalt. No special problems were encountered in selecting and proportioning the constituents of the concretes [2]. In order to reduce the harm that the Nuclear Power Plants give to the environment, barite concretes are used very much as protective materials in Nuclear Power Plants.

Microscopic Cross Section Calculation

The formula of Levkovski for the (n,p) reaction cross-sections at the energy of 14 MeV can be given as follows:

$$\sigma_{n,p} = 45.2(A^{1/3}+1)^2 exp[-33.0(N-Z)/A] \qquad [1]$$

Tel and his colleagues have suggested a new empirical formula for the cross-sections of the (n,p) reactions which are dependent on the asymmetry parameter $s = (N-Z)/A$. The formula of Tel et al. for the (n,p) reaction cross-sections at the energy of 14 MeV can be given as follows:

$$\sigma_{n,p} = \begin{cases} 14.56(A^{1/3}+1)^2 exp[-26.58(N-Z)/A] \; 17 \le A \le 239 \\ 16.33(A^{1/3}+1)^2 exp[-26.17(N-Z)/A] \; even-Z, even-N \\ 9.71(A^{1/3}+1)^2 exp[-21.87(N-Z)/A] \; even-Z, odd-N \\ 7.31(A^{1/3}+1)^2 exp[-20.21(N-Z)/A] \; odd-Z, even-N \end{cases} \qquad [2]$$

Atomic density:

$$N_0 = \frac{\rho . N_A}{A}$$

N_0: Atomic Density $(molecule/cm^3)$, ρ: Density (g/cm^3), N_A: Avogadro Number (0.6022×10^{24}), A: Atomic Mass

Probability of being affected per path length taken in neutrons:

$$\Sigma_{(n,p)} = \sigma_{(n,p)} . N$$

Average free path;

$$\lambda = \frac{1}{\Sigma_{(n,p)}} \qquad [3]$$

Results and Conclusion

Table1. Using elements, atomic masses, neutron numbers, atomic numbers, densities

Elements	Atomic Mass (A)	Neutron Number (N)	Atomic Number (Z)	Density (ρ)
Ba	137	81	56	3.59

Calculation for Ba at 14-15 MeV energy range:

$$N_{Ba} = \frac{3.59 \times 0.6022 \times 10^{24}}{137} = 0.0158 \times 10^{24} \; molecule/cm^3$$

Tel formula implementation:

$$\sigma_{Tel(n,p)} = 9.71(A^{1/3}+1)^2 exp[-21.87(N-Z)/A]$$

$$\sigma_{Tel(n,p)} = 9.71(137^{1/3}+1)^2 exp[-21.87.(81-56)/137]$$

$$\sigma_{Tel(n,p)} = 0.0068\ barn$$

$$\sum_{Tel(n,p)} = \sigma_{Tel(n,p)}.N_{Ba}$$

$$\sum_{Tel(n,p)} = (0.0068\times10^{-24}).(0.0158\times10^{24})$$

$$\sum_{Tel(n,p)} = 0.0001074\ molecule/cm$$

$$\lambda = \frac{1}{\sum_{Tel(n,p)}.} = \frac{1}{0.0001074} = 9310.99\ cm^{-1}\lambda$$

Levkovski formula implementation:

$$\sigma_{Levkovski(n,p)} = 45.2(A^{1/3}+1)^2 exp[-33.0(N-Z)/A]$$

$$\sigma_{Levkovski(n,p)} = 45.2(137^{1/3}+1)^2 exp[-33.0(81-56)/137]$$

$$\sigma_{Levkovski(n,p)} = 0.0042\ barn$$

$$\sum_{Levkovski(n,p)} = \sigma_{Levkovski(n,p)}.N_{Ba}$$

$$\sum_{Levkovski(n,p)} = (0.0042.10^{-24})x(0.0158.10^{24})$$

$$\sum_{Levkovski(n,p)} = 0.0000656\ molecule/cm$$

$$\lambda = \frac{1}{\sum_{Levkovski(n,p)}.} = \frac{1}{0.0000656} = 15243.9\ cm^{-1}$$

Table 2. Cross-sections of the Tel and Levkovski formulas and mean free path calculations

	Tel Formula			Levkovski Formula		
	$\sigma_{n,p}(barn)$	$\sum_{(n,p)}(mole)$	$\lambda_{n,p}(cm^{-1})$	$\sigma_{n,p}(barn)$	$\sum_{(n,p)}(mole)$	$\lambda_{n,p}(cm^{-1})$
Ba	0.0068	0.00011	9310.99	0.0042	0.00007	15243.9

Since there is no experimental values for (n,p) reactions in literature, we cannot compare these results. The other reactions such as (n,2n), (n,d), (n,t), (n,gamma), (n,alpha), etc. have to added this obtained results. The obtained theoretical results are important for shielding at nuclear reactors and radiation and our purpose is to get new data to literature.

References

[1] Akarslan, F., Üncü, I., S., Kılınçarslan, S., Akkurt, I. and Molla, T., 1653, 020007 (2015). Radiation shielding properties of barite coated fabric by computer programme.

[2] Witte, L., P. and Backstrom, J., E., (1954). Properties of heavy concrete made with barite aggregates.

[3] V.N. Levkovskii, Sov. Phys. JETP 18, 213–217 (1964).

[4] Tel, E., Şarer, B., Okuducu, Ş, Aydın. A. and Tanır, G., (2003). A new empirical formula for 14-15 Mev neutron-induced (n,p) reaction cross sec-tions. Journal of Physics G: Nuclear and Par-ticle Physics29, 2169-2177

[5] Lamarsh, J., R., Baratta, A., J., Ankara, 2015.

Radiologic risk assessment of outdoor radioactivity in capital city Ankara, Turkey

[1] ENİS KAPDAN TAEK
[2] NESRİN ALTINSOY İTÜ

The aim of this study is to determine the outdoor radioactivity level and relevant health risks for Ankara, the capital city of Turkey. For this purpose, Absorbed Gamma Dose rate readings were taken at 379 stations around the province. The mean, minimum and maximum outdoor absorbed gamma dose rates were determined as 67.7, 14.3, 234.1 $nGyh^{-1}$ respectively for the region. The district of Etimesgut has minimum mean outdoor absorbed gamma dose rate with 42.8 $nGyh^{-1}$ and Evren district has maximum with 121.9 $nGyh^{-1}$. The annual effective cumulative dose equivalent was determined as 73μSv/y due to outdoor gamma exposure to the inhabitants. The mean estimated cancer risk value depending on irradiations was found to be $2.74x10^{-04}$ for the region using the risk factors of ICRP 103. Furthermore, maps for the demonstration of relative distribution of outdoor gamma dose rate and the relevant annual effective dose equivalent were plotted. Finally, it was found that the average outdoor gamma dose rate for Ankara were compatible to the most of the Turkish cities investigated depending radiological underground structure of the province.

Keywords: outdoor radioactivity; cancer risk; effective dose; drinking water; Ankara

Investigation of the use of boron and clay materials in radioactive waste storage systems

FATMA AYSUN UĞUR Osmaniye Korkut Ata University

In this study, the availability of boron and clay derived materials in radioactive waste storage systems has been investigated. Boron radiation is a slowing material while clay is a material that adsorbs radioactive materials. The new material obtained by mixing these two materials at different ratios has been evaluated and interpreted graphically by using the calculations in the systems formed for the storage of radioactive wastes.

Keywords: Boron, clay, adsorption, radioactive waste

Excitation function of (g,xn) reaction in some lanthanides

[1] YUNUS EMRE DOĞAN İstanbul University
[2] BAYRAM DEMİR İstanbul University
[3] İSMAİL HAKKI SARPÜN Akdeniz University

Several elements of the lanthanides are important in areas of nuclear medicine, radiation therapy, imaging and industrial applications as metals or compounds. Excitation function of (g,xn) reactions in some lanthanides elements have theoretically calculated using TALYS 1.8 nuclear reaction code different energy range. Theoretical calculations have compared with the available experimental data obtained from EXFOR Nuclear Data library.

Preparation of organic nano thin film sensor for harmful gas detections

[1] YASER AÇIKBAŞ Usak University Department of Materials Science and Nanotechnology Engineering
[2] SELAHATTİN BOZKURT Uşak University Vocational School of Health Services
[3] ERKAN HALAY Uşak University Scientific Analysis Technological Application and Research Center
[4] RIFAT ÇAPAN Balıkesir University Department of Physics,
[5] MATEM ERDOĞAN Balıkesir University Department of Physics
[6] ABDÜLKADİR SIRIT Necmettin Erbakan University Department of Chemistry,
[7] RIDVAN ÜNAL Uşak University Vocational School of Health Services

The harmful gas detection is a serious task due to their natural or nuclear toxicity with very serious irreversible effects for the environment and human beings. This study investigates the calix[4]arene(organic materials) nano thin film sensor element exposed to harmful vapors (dichloromethane, chloroform and toluene vapors). All measurements were carried out at room temperature. The gas kinetic measurement results show that, the photodetector response change, ΔIrf for saturated dichloromethane vapor is much larger than the other vapors with the ΔIrf value of 48 au and the diffusion coefficient value of 5.1 $x10^{-16}$ cm^2s^{-1}. Swelling process was analyzed by Fick's Equations. The diffusion coefficients for swelling were correlated with the volatile organic compounds. The present study indicated that calix[4]arene thin film is highly selective with a large response to dichloromethane. One may conclude that the calix[4]arene nanosensor has potential applications in the development of room temperature organic gas sensing devices.

Keywords: Nanosensors, calix[4]arene; gas detection.

Prediction of breast cancer pattern using artificial neural network algorithms.

[1] OZAN TOKER Yıldız Teknik University
[2] SELÇUK ALP Yıldız Teknik University
[3] ÖMER TOPDAĞI Atatürk University
[4] ÖNDER EYECİOĞLU Nişantaşı University
[5] MURAT BEKEN Nişantaşı University Statistics
[6] ERSOY ÖZ Yıldız Teknik University
[7] ORHAN İÇELLİ Yıldız Teknik University

Breast cancer is one of the most common types of cancer. In this type of cancer, effective and rapid diagnostic methods have great importance in increasing patients' quality of life. There are many studies in the literature about rapid and effective diagnostic methods. Some of these methods are prediction methods based on node biopsies or markers. Artificial neural network algorithms (ANN) are one of these prediction methods. In this study, we used Artificial Neural Network (ANN) prediction model as an effective and rapid model for breast cancer diagnosis. Firstly, Al, Cr, Fe, Cu, Zn, Se, Na, K, Ca and Mg element concentrations were determined in all blood samples. Determination of element concentrations were carried out with ICP-MS and ICP-OES systems. Same patients' CA 15.3 (biomarker) values were used as the "TARGET" data set. Blood samples from 40 breast cancer and 40 healthy individuals from living in Turkey were collected (Total 80 data sets). 60 randomly selected data sets were used for training and 20 randomly selected data sets were used for the testing. After that, pattern recognition with ANN model was applied. At this stage of the study, the "confusion matrix" of the samples was created. In this model, the predictive performance ratio was 96.4% in the training phase and 91.7% in the test phase.

This research is supported financially by TUBITAK (2210C) and Yildiz Technical University BAP (2015-01-01-YL04, 832)
Ethical Approval: Atatürk University Medical Faculty ethics committee; 10.24.2016, sesion 6, number: 22

Keywords: Artificial Neural Network Algoritm, Breast Cancer,

Classification of breast cancer patients' blood samples using machine learning algorithms

[1] OZAN TOKER Yıldız Teknik University
[2] SELÇUK ALP Yıldız Teknik University
[3] ÖMER TOPDAĞI Atatürk University
[4] ÖNDER EYECİOĞLU Nişantaşı University
[5] MURAT BEKEN Nişantaşı University
[6] ERSOY ÖZ Yıldız Teknik University
[7] ORHAN İÇELLİ Yıldız Teknik University

In this study, blood samples from 40 breast cancer and 40 healthy individuals from living in Turkey were collected. Firstly, Al, Cr, Fe, Cu, Zn, Se, Na, K, Ca and Mg element concentrations were determined in all blood samples. Determinations of element concentrations were carried out with ICP-MS and ICP-OES. In addition to this data, an outcome variable was defined which takes the value of 1 for cancer patients and 0 for healthy individuals. Since the classification using all the elements is time-consuming and performance-degrading, the ones that were effective among these data were identified. In order to identify the effective elements, Information Gain Ranking Filter, CFS Subset Evaluator, Correlation Ranking Filter, Gain Ratio feature evaluator, ReliefF Ranking Filter, OneR feature evaluator, Symmetrical Uncertainty Ranking Filter methods were used. So that Se, Cu, Cr, Al, Mg and Na elements were identified as the most effective elements. 80 samples were divided into 2 groups of 60 and 20 samples. The system was trained using data from 60 randomly selected samples (30 cancerous and 30 healthy) for Se, Cu, Cr, Al, Mg and Na elements. After, in order to test the validity of the generated models, 20 samples (other group) were accepted as test data. The trained system was tested with these 20 samples. As classification algorithms, logistic regression, decision tree, support vector machines and k-nearest neighbors methods were used. Classification successes of models obtained with data of 30 healthy 30 cancer patients were named with "Training". Also, models were tested with 20 samples (10 healthy, 10 Cancerous) and classification successes of models were given as "Testing". When the test phase is considered, Medium Gaussian SVM and Weighted KNN are the the most efficient algorithms with 90% correct classification rate.

Keywords: Breast Cancer, Classification, Blood Samples

Investigation of the possibility of producing ^{225}Ac radioisotope in a proton cyclotron

[1] HATİCE KÜBRA BELEN Kirikkale University, Physics Department
[2] ABDULLAH AYDIN Kirikkale UniveRSİTY, Physics Department

Today in nuclear medicine, diagnostic and therapeutic radioisotopes are used in numerous and will continue to be used. Radioisotopes are produced in cyclotron, reactor, neutron generator and linear accelerators. In recent years there has been a rapid increase in the use of therapeutic radioisotopes. Especially, Targeted Alpha Therapy (TAT) is an important cancer treatment. In this method, selected cancer cells are destroyed by alpha particle radiation. In this study, the potential of producing ^{225}Ac by proton irradiation of ^{226}Ra in a cyclotron through the reaction ^{226}Ra (p,2n) ^{225}Ac has been investigated. For this, the cross section of ^{226}Ra (p,2n) ^{225}Ac reaction have been calculated by using TALYS code and optimum proton energy range, maximum product activity and product yield have been determined. As a results it has been shown that 225Ac could be produce in a 30 MeV proton cyclotron.

Keywords: Medical radioisotope, radioisotope production, targeted alpha therapy, 225Ac

An application of the dead time correction program at gamma-rays detectors

[1] SALİH MUSTAFA KARABIDAK Gümüşhane University Physics Engineering
[2] ALİ KAYA Gümüşhane University Engineering Physics

For the dead time correction at gamma-rays detectors, a computer program was developed. This program has been applied to gamma ray measurements taken for the purpose of determining the radioactivity of the Bahçecik village network water and Bahçecik village highland water district of Gümüşhane province. According to the results obtained from gamma analysis without dead time correction from 10.8 ± 1.02 mBq/L to 13.7 ± 1.24 mBq/L for ^{226}Ra, from 2.1 ± 0.23 mBq/L to 3.6 ± 0.36 mBq/L for ^{232}Th, and from 91.3 ± 4.05 mBq/L to 118.0 ± 5.09 mBq/L for ^{40}K were determined to be in range. After correcting the dead time, these results ranged from 12.6 ± 1.07 mBq/L to 16.0 ± 1.31 mBq/L for ^{226}Ra, from 2.5 ± 0.24 mBq/L to 4.2 ± 0.38 mBq/L for ^{232}Th, and from 106.8 ± 4.56 mBq/L to 136.9 ± 5.34 mBq/L for ^{40}K. The average of these changes is around 17%. For this reason, the dead time correction must be performed in activity measurements and dose calculations.

Keywords: Gamma Rays, Dead Time Correcting, Activity Measurements, Dose Calculations

A program for dead time correction at gamma-rays detectors

[1] SALİH MUSTAFA KARABIDAK Gümüşhane University Physics Engineering
[2] ÖZKAN BİNGÖL Gümüşhane University Department of Software Engineering
[3] SELİM KAYA Gümüşhane University Physics Engineering

Determination of compensating for count losses for the correctness of analyses in spectrometric analysis of qualitative and quantitative use of x-gamma ray detectors are of importance. These counting losses in spectrometry are due to paralyzable and non-paralyzable system dead time. In this work, a new method is suggested for compensate for counting losses resulting from this factors. For this purpose, a computer program was developed. Experimental studies were performed to test of this program. As a result, it was seen to provide an effective correction. it is coded a computer program including original dead time correction, peak search, graphics module, program interface, a report module with the Delphi program compiler.

Keywords: Gamma Rays, Gamma Rays Detectors, Counting Loss, Dead Time, Computer Programs

Can Fluka determine light yields of the scintillators used in medical imaging?

ELİF EBRU ERMİŞ, CÜNEYT ÇELİKTAŞ

Ege University, Faculty of Science, Physics Dept., Izmir, Turkey

Abstract

BaF_2, BGO, GSO, LYSO, LSO, NaI(Tl), $CdWO_4$, CsI(Tl) and LFS scintillators that are often used in medical imaging systems were examined. Since the light yield value of a scintillation crystal is one of the most important parameter for these type systems, the above scintillators were handled from this point of view. These crystals were first formed, then their light yield values were determined using FLUKA Monte Carlo (MC) program in the present work. Comparisons between the calculated and the literature values were made in the final section of the study. Highly compatible results were found. Thus, we concluded that FLUKA MC program can be used to determine light yield values of different types of scintillators used in medical imaging.

Keywords: Light yield, scintillation crystals, FLUKA

Introduction

Scintillators are the materials that emit visible light or ultraviolet radiation after the interaction of ionizing radiation with the material. Scintillators are main components of radiation detectors. They are used in conventional film-screen radiography, many direct digital radiographic image receptors, fluoroscopy, scintillation cameras, computed tomography (CT) scanners, and positron emission tomography (PET) scanners [1-3].

Since the discovery of sodium iodide by Hofstadter in 1949, alkali-halide crystals have been the most widely-used scintillators in numerous applications, ranging from detectors for physics research, industrial and medical imaging devices. Sodium iodide (NaI) and more recently cesium iodide (CsI) have been for a long time the most common scintillators used in nuclear medical imaging devices, mostly because of their very high light yield and relatively easy and cheap production method. Bismuth germanate ($Bi_4Ge_3O_{12}$, BGO) crystals have introduced in the field of medical imaging, mostly because of its very high density. Most of the PET scanners produced in the last decade were built with BGO crystal [4]. Today lutetium oxyorthosilicate (Lu_2SiO_4O, LSO), lutetium yttrium oxyorthosilicate ($Lu_xY_{2-x}SiO_4O$, LYSO), and gadolinium oxyorthosilicate (Gd_2SiO_4O, GSO) are used in newer PET scanners [1]. The only crystalline material in use in CT is cadmium tungstate ($CdWO_4$). Its primary use is in low-end medical CT scanners, as well as, in a variety of security CT applications [5]. Early systems in PET has used barium fluoride (BaF_2) scintillators [6]. This scintillator has an emission component with subnanosecond decay time that yields very fast timing [BaF_2, 2018]. The Lutetium Fine Silicate (LFS) scintillation crystal is distinguished by its exceptional combination of high light yield, uniquely high radiation hardness, and ultra-fast decay time. In particular, it should be noted that the LFS technology provides the fastest decay constant, the highest light output and radiation hardness, which are taking many existing applications to a new level and enabling others. It has also proven to be superior to other scintillation materials. LFS scintillation crystal is essential for PET devices, and especially for high-resolution scanners [8].

Light yield is defined as an amount of photons produced by a scintillator per unit of absorbed energy [9, 10]. It is often expressed in photons/MeV (ph/MeV) [10]. A high light yield is also mandatory to improve the energy resolution [4]. The requirement of a scintillator to be a good candidate for PET is high light yield. High light yield improves the energy resolution of PET also [11, 12]. Additionally, high light yield from the scintillation process leads to reduce the exposure of the patients to the harmful radiation [2].

Some properties of used scintillators in medical imaging are listed in the following table.

Table 1. Some properties of the scintillation crystals.

Crystal Types		Decay Time (ns)	Density (g/cm^3)	Light yield (photons/MeV)
BaF_2 [7]	Fast	0.6-0.8	4.88	1,800
	Slow	630		10,000
BGO [13]		300	7.13	8,000-10,000
GSO [14]		50	6.70	13,000
CsI(Tl) [15]		1,000	4.51	54,000
$CdWO_4$ [16]		14,000	7.90	12,000-15,000
LYSO [14]		40	7.10	32,000
LSO [14]		40	7.40	26,000
NaI(Tl) [14]		230	3.70	38,000
LFS [17]		33-36	7.35	37,000-38,000

MC calculations are a standard tool in several areas of research, particularly in physics. This name is used to refer to any technique in which complex models are evaluated by generating successive random samples and interpreting statistically the global result after numerous iterations. In particle physics, the main application of MC calculation is to simulate particle transport and interactions in media. Main advantage of this approach is that it permits to study in various different configurations (for example geometries or primary particles) before (or even without) doing specific measurements [18]. FLUKA (FLUktuirende KAskade) is a general purpose tool for calculations of particle transport and interactions with matter in this manner [18-20]. The highest priority in the design and development of FLUKA has always been the implementation of modern physical models. FLUKA reads user input from an ASCII ''standard input'' file with extension .inp. The input consists of a variable number of ''commands'' (called also ''options''), each consisting of one or more ''lines'' [19]. In this file, a series of instructions (named cards) are written in each line. These are title, description of the geometry, definition of the materials, material assignment, definition of the particle, definition of requested cards that the user wants to calculate various physical quantities, initialization of the random number sequence and starting signal [18].

Nassalski et al. investigated the scintillator properties for PET/CT systems [21]. The response of the scintillation detector based on BaF_2 was examined by Batenkov et al. [22]. Lecoq studied the medical application by developing new scintillators [23]. Characteristics of scintillation crystals for PET were evaluated by Melcher [24]. Next generation PET system was studied with the multi-pixel photon counter and LFS scintillator by Yamazaki et al. [25].

Scintillation crystals have important roles because of their light yield values in medical imaging systems. Although their light yield values were given in catalogues, it has not been encountered any theoretical calculation for them in the literature. For this reason, the light yield values of BaF_2, BGO, GSO, LYSO, LSO, NaI(Tl), $CdWO_4$, CsI(Tl) and LFS crystals, which are often used in medical imaging systems, were first calculated using FLUKA MC method in this study. Then, the calculated results and the literature values were compared in order to check performance of FLUKA. It was concluded that FLUKA MC method was quite successful to determine the light yield values of various scintillation crystals.

Materials and Methods

The light yield values of BaF_2, BGO, GSO, LYSO, LSO, NaI(Tl), $CdWO_4$, CsI(Tl) and LFS crystals were determined in the present work. These crystals are commonly used in medical imaging systems [1, 3-8]. FLUKA MC program (ver. 2011.2c) was used for the proposed study. This program was installed on an Ubuntu operating system (ver. 13.10). Apart from FLUKA commands, the input file may also contain description of the geometry of the simulated set-up. Additionally, this description is provided by specific geometry ''command cards'' in a special format. All events are initiated by the primary particles which in the simplest case are monoenergetic, monodirectional and start from a single point in the space (special beam). The BEAM card defines the particle energy and the BEAMPOS card controls starting position and direction of the particle. The input for the Combinatorial Geometry (bodies, regions and optional region volumes) is preceded by a GEOBEGIN card and immediately followed by a GEOEND card. These two cards follow the normal FLUKA format. A compound is defined by a MATERIAL card, which is used to define a compound carriers only the compound name, density, etc., and COMPOUND card describes its composition. DCYSCORE associates selected scoring cards of giving estimator type with user-defined decay times. OPT-PROP defines optical properties of specified materials. It controls transition radiation photon production, and requests and controls production of transition and scintillation radiation in specified materials. OPT-PROD is also used to manage light generation. DEFAULTS sets and FLUKA defaults suitable for a specified kind of problems. Electromagnetic interactions are activated by using EM-CASCAde card [19].

The scintillation crystals were first formed in FLUKA MC program. The dimensions of the crystals were 3 inch x 3 inch. The shape of the formed scintillation crystal through the program is demonstrated in Fig.1.

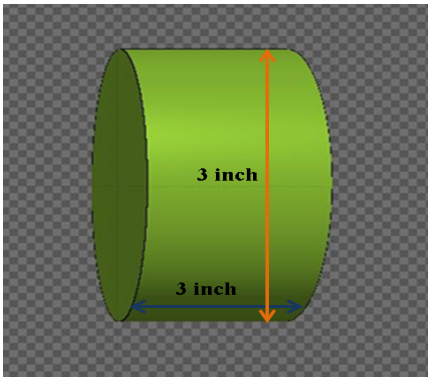

Fig. 1. Demonstration of the formed scintillation crystals in FLUKA MC program.

The light yield values of the used crystals were calculated at 1 MeV energy.

The comparison between the calculated light yield values and literature was given in the following section.

Results

Calculated light yield values of the handled scintillators using FLUKA MC program are given in the following table. The literature values are also written in the same table in order to check accuracy of the calculated ones.

Table 2. Calculated and literature light yield values of the handled scintillation crystals.

Crystal Types		Light yield value-FLUKA MC program (photons/MeV)	Light yield value-literature (photons/MeV)
BaF_2 [7]	fast	1,956	1,800

slow	10,423	10,000
GSO [14]	14,136	13,000
LSO [14]	26,274	26,000
LYSO [14]	33,690	32,000
NaI(Tl) [14]	39,096	38,000
BGO [13]	9,518	8,000-10,000
$CdWO_4$ [16]	14,006	12,000-15,000
CsI(Tl) [15]	59,165	54,000
LFS [17]	37,982	37,000-38,000

Conclusions and Discussion

The light yield values of BaF_2, BGO, GSO, LYSO, LSO, NaI(Tl), $CdWO_4$, CsI(Tl) and LFS crystals were calculated using FLUKA MC program. The reason for the selection of these crystals was the fact that they are mostly used in medical imaging devices in recent years [1, 3-8]. Since the light yield value of a crystal is one of the most important parameter for these type devices [2], calculated light yield values were compared to literature to check the accuracy of the obtained results.

In Table 2, calculated light yield values of the used crystals via FLUKA MC method were indicated. The literature values were given in the second column for easy comparison. Since gamma photons were sent to the crystals in vacuum medium in FLUKA (i.e. their energy losses and scatterings were omitted), calculated light yield values were slightly higher than the literature values. Therefore, it can be inferred from this result that calculated and literature values were in compatible with each other. A comprehensive literature research showed us that the light yield values of the handled crystals were mentioned only in the catalogues, and no MC calculation process about their light yields has been encountered in the literature so far. So, it is believed that the MC method and the results will contribute to the literature via the presented work.

All crystals mentioned above are often used in medical imaging devices as stated above whereas LFS has special importance for these devices in terms of its light yield [25-27]. Therefore, its light yield calculation was particularly made in this work. It was seen that obtained result through the MC method was consistent with the literature value as seen in Table 2.

The purpose in recent studies is to find best scintillation crystal for medical imaging systems. The most important parameter is light yield of a scintillation crystal used in these systems because it affects energy resolution of the devices and the radiation exposure of the patients [2, 4, 12]. Another reason for high light output request is to reduce electronic noise effect in the image for low signal level [23]. It is revealed from the presented work that, therefore, FLUKA MC program can help to choose the low noisy crystals by calculating their light yield values in this manner.

As a result of the calculation process, the light yield values of the scintillation crystals can be determined by means of FLUKA MC method. Thus, the light yield values of new generation scintillation crystals will be able to determine through FLUKA in the future studies.

Acknowledgements

This work was supported by Research Fund of Ege University under Project No. 14 FEN 026 and the Scientific and Technological Research Council of TURKEY (TUBITAK) under Project No. 116F324.

Reference

[1] *JT Bushberg et al, The Essential Physics of Medical Imaging William–Wilkins, USA (2001).*
[2] *C Ronda Luminescence Wiley-VCH Verlag GmbH & Co. KGa, Germany (2008).*
[3] *ME Phelps PET, Physics, Instrumentation, and Scanners Springer, USA (2006).*
[4] *P Lecoq, A Gektin, M Korzhik Inorganic Scintillators for Detector Systems, Physical Principles and Crystal Engineering Springer, Switzerland (2017).*
[5] *S Tavernier et al, Radiation Detectors for Medical Applications Springer, Netherlands (2006).*
[6] *JS Karp et al, J. Nucl. Med.* ***49****, 462 (2008).*
[7] *Barium Fluoride Scintillation Material, Saint-Gobain Crystals, http://www.crystals.saint-gobain.com/sites/imdf.crystals.com/files/documents/barium-fluoride-data-sheet_69762.pdf Accessed 2 July 2018.*
[8] *Zecotek Lutetium Fine Silicate (LFS) Scintillation Crystals, Enabling the Future of Imaging and Detection, http://zecotek.com/wp-content/uploads/2016/04/White-Paper-2016.pdf Accessed 2 July 2018.*
[9] *MS Alekhin New Halide Scintillators for γ-ray Detection Ph.D. Thesis, Delft University of Technology (2013).*
[10] *K Iniewski Radiation Detectors for Medical Imaging, Devices, Circuit, and Systems Taylor&Francis, New York (2016).*
[11] T Farncombe *and* K Iniewski *Medical Imaging Technology and Applications* Taylor&Francis, New York (2014).
[12] JE Moore *and* DJ Maitland *Biomedical Technology and Devices* Taylor&Francis, New York (2014).
[13] Bismuth Germanate Scintillation Material, *Saint-Gobain Crystals*, http://www.crystals.saint-gobain.com/sites/imdf.crystals.com/files/documents/bgo-material-data-sheet_69763.pdf Accessed 2 July 2018.
[14] International Atomic Energy Agency *Quality Assurance for PET and PET/CT Systems* IAEA Human Health Series No.1, Vienna (2009).
[15] Cesium Iodide Scintillation Material, *Saint-Gobain Crystals*, http://www.crystals.saint-gobain.com/sites/imdf.crystals.com/files/documents/csitl-and-na-material-data-sheet_69771.pdf Accessed 2 July 2018.
[16] Cadmium Tungstate Scintillation Material, *Saint-Gobain Crystals*, http://www.crystals.saint-gobain.com/sites /imdf.crystals.com/files/documents/cadmium-

tungstan-material-data-sheet_69766.pdf Accessed 2 July 2018.
[17] Zecotek, *Excellence in Imaging*, http://zecotek.com/wp-content/uploads /2016/02/zecotek-brochure.pdf Accessed 2 July 2018.
[18] F Collamati *An Intraoperative Beta-Probe for Cancer Surgery* Ph. D. Thesis, Sapienza University (2016).
[19] A Ferrari *et al, Fluka: A multi-particle transport code* CERN INFN/T_05/11 SLAC-R-773, Geneva (2005).
[20] G Battistoni *et al*, *AIP Conference Proceeding* **86**, 31 (2007).
[21] A Nassalski et al, *IEEE Trans. Nucl. Sci.* **54**, 3 (2007).
[22] OI Batenkov et al, *Phys. Part. Nucl. Lett.* **13**, 104 (2016).
[23] P Lecoq *Nucl. Intrum. Meth. A* **809**, 130 (2016).
[24] CL Melcher *J. Nucl. Med.* **41**, 1051 (2000).
[25] M Yamazaki *et al*, *IEEE NSS/MIC.* **15.S-56**, 3286 (2011).
[26] TK Lewellen *et al, IEEE NSS/MIC.* **9044480**, 2915 (2004).
[27] T Takeshita *et al, Phys. Procedia.* **37**, 1461 (2012).

Investigation of gamma ray percent absorption efficiencies of the crystals used in medical imaging by means of Fluka Monte Carlo program

ELİF EBRU ERMİŞ, CÜNEYT ÇELİKTAŞ

Ege University, Faculty of Science, Physics Dept., Izmir, Turkey

Abstract

This work has been focused on the calculating gamma ray percent absorption efficiency values of various scintillation crystals. BaF_2, BGO ($Bi_4Ge_3O_{12}$), CaF_2, CsI, $CdWO_4$, LYSO and polyvinyltoluene (PVT) scintillation crystals were chosen because they are often used in medical imaging systems. They were formed in various dimensions through Monte Carlo (MC) method. FLUKA MC program which is one of the MC method was used. It was evaluated how gamma rays in different numbers and energies affect these efficiency values using FLUKA MC program in the presented work. Extensive comparisons between calculated and literature values were also performed. Obtained results indicated that FLUKA MC program would be able to use as an alternative way to determine the gamma ray percent absorption efficiency of any scintillation crystal, which it is one of the important parameter of the sensitivity of medical imaging systems, believing this paper will be helpful in determining the most appropriate crystal type for an aimed application.

Keywords: Gamma ray percent absorption efficiency, scintillation crystals, FLUKA.

Introduction

In nuclear and particle physics research studies, scintillation detectors are currently used to detect the particles. When a nuclear particle or radiation struck the materials, they emit a small flash of light, i.e. scintillation [1]. They are also used in many different areas. These are industry, medicine, government research, and academic research. Medical imaging is one of the largest consumption areas of scintillation materials. In order to provide better diagnostic care for the patient, development and test of the new detector designs are non-stop being developed [2].

Many types of the scintillator material have been proposed and implemented to improve the detection performance of Positron emission tomography (PET) scanners [3]. PET is a medical imaging modality that measures the three dimensional distribution of a molecule labelled with a positron emitter. The acquisition is carried out by a set of detectors arranged around the patient. The detectors consist of a scintillator which is selected according to many properties [4]. For example, BaF_2 scintillation crystal was one of the best scintillators available in early 1980s for PET. These systems were capable of brain and heart studies [5-7]. BGO has been widely used in clinical positron emission tomography (PET) scanners since 1990s [3, 7-11]. LYSO scintillators are used in most state-of-art commercial whole-body PET scanners [12]. Also, it has high stopping power (increased system sensitivity) and short decay time. These characteristics of LYSO provide an advantage for PET scanners [13-15]. And also, these systems which were composed of LYSO crystals are used to take image different regions of human body and diagnose of various cancer type. These are cervical cancer, lung cancer, colorectal cancer, myocardial imaging, brain imaging, breast imaging [12, 16, 17]. LYSO crystals are used in animal PET as well [18, 19]. $CdWO_4$ is used in computed tomography system which is one of the medical imaging system [20].

Plastic scintillator crystals are recently used in current research studies about medical imaging systems. The reason of its use in these systems is short decay time. It is thought that promising results will be obtained in new generation PET systems which are consisted of plastic scintillation crystals [21-23]. Consequently, it can be deduced that no single scintillator has ideal properties [2].

The number of gamma photons absorbed by a certain thickness of the scintillator is the difference I_0-I where I_0 is the number of gamma ray of a certain energy incident or entering the sheet of material, and I is the number of gamma ray that have passed through a layer of thickness.

However, instead of calculating for different I0's, the ratio of

$$G.R.P.A.E = \left(\frac{I_0 - I}{I_0}\right) x100 \qquad (1)$$

is more preferred, where G.R.P.A.E is 'gamma ray percent absorption efficiency' [24].

The sensitivity of PET, like that of all imaging devices, is determined primarily by the absorption efficiency of the detector system [17]. The high density of a crystal (high linear attenuation coefficient) increases the detector sensitivity [2]. That is, one of the required attributes is maximum absorption. This situation is positively affected the image quality of medical imaging system, and is also associated with gamma-ray percent absorption efficiency values. In that case, one of the important properties in medical imaging system is photon absorption efficiency value of the scintillator. In this work, for this reason, photon absorption efficiency values of BaF_2, BGO ($Bi_4Ge_3O_{12}$), CaF_2, CsI, $CdWO_4$, LYSO and polyvinyltoluene (PVT) scintillators were investigated. Some properties of the used scintillators were listed in the following table.

Table 1. Some properties of used scintillation crystals.

Crystal Names	Decay Time (ns)	Density (g/cm^3)
BaF_2 [13]	0.6 (25%) 620 (75%)	4.890
BGO [3]	300	7.130
CaF_2 [2]	900	3.190
CsI [2]	680	4.510
$CdWO_4$ [2]	5000	7.900
LYSO [8]	40	7.100
PVT [25]	2.4	1.032

In many research areas in physics, Monte Carlo (MC) calculations are a standard tool for any simulation. In this technique, sequential random examples are generated to evaluate complex models. After various iterations, the results are interpreted by statistically. The essential application area of this technique is simulation of the particle transport and interactions in particle physics. It has advantageous to make different configurations in this technique [26]. One of the general purpose tools for calculations of particle transport and interactions is (FLUktuirende KAskade) [27, 28]. FLUKA obtains a simple input file rather than other MC particle codes. FLUKA presents many options to score quantities and to apply mumerous variance reduction techniques; thus, the users do not write a single line of code [27]. FLUKA input files consist in ASCII file with extension .inp. Instructions (named cards) are given in each line of this file. Title, geometry description, material, particle and requested card definitions, material assignments together with the random number sequence are given in these cards [27].

Qin et al. evaluated the gamma ray response and efficiency values of BC507 and BC501A type liquid scintillators [29]. Gamma ray timing responses of NaI and plastic scintillation crystals were experimentally examined by Ermis et al. [30]. Nikolopoulos et al. determined the radiation detection efficiency values of different scintillators ($LuSiO_5$ (LSO), $LuAlO_3$ (LuAP), Gd_2SiO_5 (GSO) and $YAlO_3$ (YAP)) using Monte Carlo code [31]. Gamma ray response function of EJ301 type organic liquid scintillator was calculated by FLUKA and GEANT4 Monte Carlo programs by Zhang et al. [32]. Gamma ray detection efficiency values of EJ-309 type liquid scintillator were examined through an experimental method by Pino et al. [33]. Krishnamoothy et al. investigated performance of PET system consisted of LYSO scintillation crystal [34].

Gamma ray percent absorption efficiency values of BaF_2, BGO ($Bi_4Ge_3O_{12}$), CaF_2, CsI, $CdWO_4$, LYSO and polyvinyltoluene type scintillation crystals were determined by means of FLUKA MC method in the present work. Comparisons between the calculated results and the literature values were also performed. It was found that, finally, FLUKA MC method can alternatively be used to determine the gamma ray percent absorption efficiency values of different scintillation crystals with high precision, leading to reveal the most appropriate type of detector material for better application.

Although the information about the scintillation crystals is well documented, we noticed that lack of comprehensive records between the calculated and the literature values about percent absorption efficiency were given. So, we thought that this study can be a reference work for the researchers who are studying on the detector development and radiation detection instrumentation.

Materials and Methods

BaF_2, BGO ($Bi_4Ge_3O_{12}$), CaF_2, CsI, $CdWO_4$, LYSO and polyvinyltoluene (PVT) type scintillation crystals were handled to determine the gamma ray percent absorption efficiency values. Because of the fact that these crystals are often used in gamma ray spectroscopy measurements and medical imaging systems [2, 3, 5, 6, 8, 9, 13-15, 35-38] they were selected in the introduced study. FLUKA MC program (ver. 2011.2c), which was installed on an Ubuntu operating system (ver. 13.10), was used for this aim. The transport of gamma photons in FLUKA (EMF, for Electro Magnetic FLUKA) handles all interactions and scattering process. DEFAULTS card sets FLUKA defaults suitable for a specified kind of problems [27]. In this study, PRECISIOn was selected. PRECISIOn defaults for precision simulations. In this selection, EMF is on, that is, gamma photons are transported. And also, FLUKA provides a BEAM card by which it is possible to choose the particle kind, its energy. BEAMPOS card defines the starting point of beam particles and the beam direction. Materials can be defined by the option; MATERIAL, by assigning a density, a name, a code number, in the case of single elements, an atomic number and atomic weight [27].

Each crystal was formed in different dimensions in the program. In the supplier's catalogue of the used crystals

[24], the dimensions of some crystals were given in terms of cm, and some of them are in inch. For this reason, the dimensions of BaF_2, BGO ($Bi_4Ge_3O_{12}$), CaF_2 and CsI crystals were chosen as 1´´x 1´´, 2´´x 2´´ and 3´´x 3´´. $CdWO_4$, LYSO and polyvinytoluene crystals were taken in the dimension of 1 cm x 1cm, 3 cm x 3 cm and 5 cm x 5 cm respectively according to the supplier's catalogue for better consistency. A simple demonstration of the formed scintillation crystals in FLUKA MC program is shown in Fig. 1.

Gamma ray absorption efficiency values of BaF_2, BGO ($Bi_4Ge_3O_{12}$), CaF_2, CsI, $CdWO_4$ and LYSO crystals were calculated at 500; 1,000; 2,000; 4,000 and 10,000 keV energies. 10; 50; 100; 500 and 1,000 keV-energy gamma rays were used for polyvinyltoluene crystal for the calculation. These energies were chosen according to the supplier's catalogue again.

In the first part of the study, 100; 1,000; 10,000 and 100,000 gamma photons were sent to each formed scintillation crystal, respectively. Secondly, the number of transmitted gamma photons through each crystal was determined. Finally, gamma ray percent absorption efficiency values were calculated by the program, and the calculation process was repeated in ten cycles for each scintillation crystal.

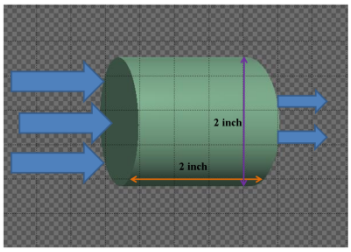

Fig. 1. A schematic of the formed scintillation crystals (e.g. 2 inch x 2 inch) in FLUKA MC program.

Calculated gamma ray percent absorption efficiency values were finally compared with the literature values given in the supplier's catalogue of the used scintillation crystals. The error calculations were determined by first subtracting the calculated values from the literature ones then dividing the resultants to the literature ones.

Results

The percent absorption efficiency values of the formed scintillation crystals in the program for each dimension, gamma photon number and energy were calculated using Eq. (1). In the following figures, the graphs of gamma ray percent absorption efficiency values vs. energies for each scintillation crystal tabulated above were given in different dimensions and gamma photon numbers.

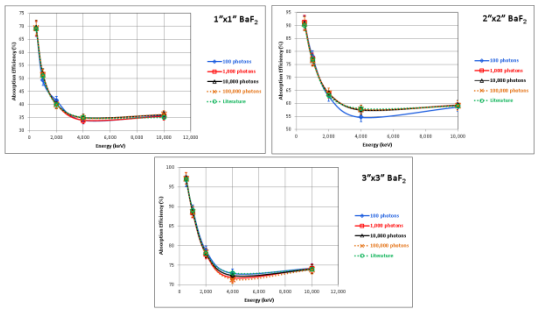

Fig. 2. Gamma ray percent absorption efficiency values of BaF_2 scintillator vs. gamma ray energies for different dimensions.

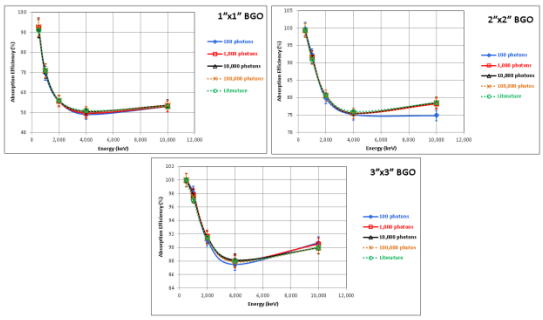

Fig. 3. Gamma ray percent absorption efficiency values of BGO scintillator vs. gamma ray energies for different dimensions.

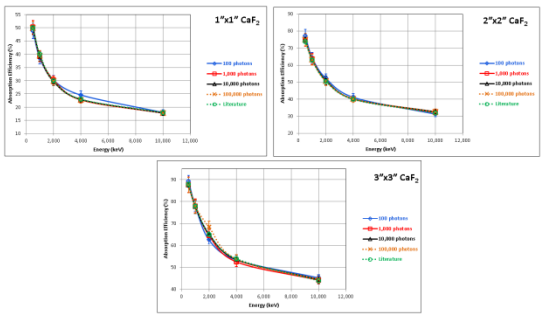

Fig. 4. Gamma ray percent absorption efficiency values of CaF_2 scintillator vs. gamma ray energies for different dimensions.

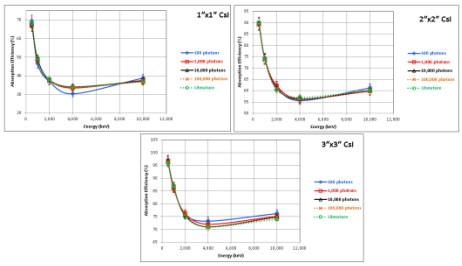

Fig. 5. Gamma ray percent absorption efficiency values of CsI scintillator vs. gamma ray energies for different dimensions.

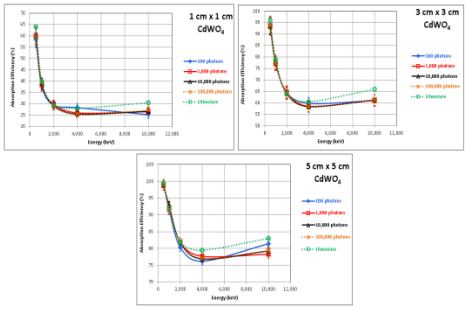

Fig. 6. Gamma ray percent absorption efficiency values of $CdWO_4$ scintillator vs. gamma ray energies for different dimensions.

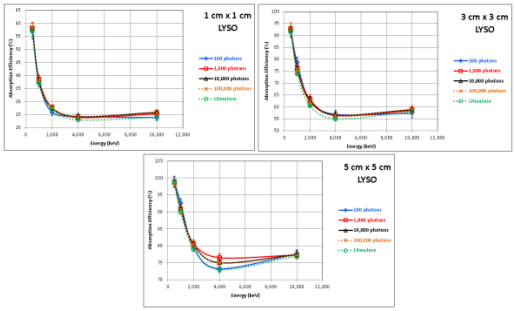

Fig. 7. Gamma ray percent absorption efficiency values of LYSO scintillator vs. gamma ray energies for different dimensions.

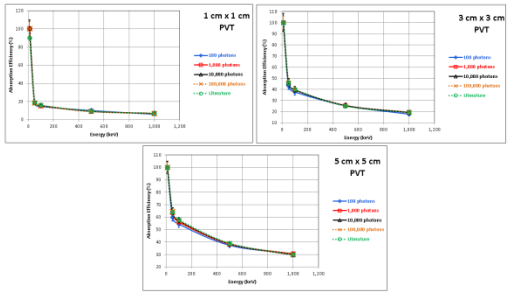

Fig. 8. Gamma ray percent absorption efficiency values of PVT scintillator vs. gamma ray energies for different dimensions.

Conclusions and Discussion

Gamma ray percent absorption efficiency values, which affect the sensitivity of imaging systems, of BaF_2, BGO, CaF_2, CsI, $CdWO_4$, LYSO and polyvinyltoluene type scintillation crystals, which are often used in medical imaging systems, were calculated by means of FLUKA MC method. The calculations were carried out at various gamma ray energies, gamma photon numbers and crystal dimensions for each crystal. Comparisons between the calculated values and the literature ones which were given in the supplier's catalogue [24] were performed in order to test whether the calculation results were compatible with the catalogue ones. That is, the effect of the incident gamma photons in different numbers and energies, and crystal thicknesses on absorption efficiency values of the crystals was investigated. How these quantities affect the absorption efficiency values of the crystals were examined, as well.

In order to find out the effect of the gamma photon number incident on the detector surface to the percent efficiency results, different photon numbers (100; 1,000; 10,000; 100,000) were used in the FLUKA MC simulation program. As the gamma photon numbers were increased, as seen in figures and tables, the calculated gamma ray percent absorption efficiency values were quite closed to the literature ones. It was concluded from this result that maximum number of gamma photons should be chosen in MC calculation process for better consistency.

The graphs of obtained gamma ray absorption efficiency values through FLUKA MC program and the literature values vs. gamma ray energies were shown in Figs. 2-8, respectively. As can be seen in all figures, calculated values were highly in accordance with the literature ones. This leads us to the conclusion that the study in this paper can be a reference work for the researchers who focus on the radiation detection instrumentation, medical imaging and the detector development since lack of papers comparing the calculated and the literature results as presented here are available in the literature.

Consequently, it was revealed that FLUKA MC program can easily be utilized for the calculation of the gamma ray percent absorption efficiency values of the scintillation crystals, which used in the fields such as medical imaging, space, nuclear and industrial researches, for the most appropriate type of detector material for better application. Since the program results are highly in compatible with the catalogue values, it is believed that the program can also be used for the gamma ray percent absorption efficiency value of any scintillation crystal that will be produced for a multidisciplinary investigation. In this respect, it is planned to make these calculations for the next generation scintillation crystals.

Acknowledgements

This work was supported by Research Fund of Ege University under Project No. 14 FEN 026 and the Scientific and Technological Research Council of TURKEY (TUBITAK) under Project No. 116F324.

Reference

[1] *RW Leo Techniques for nuclear and particle physics experiments Springer–Verlag, Germany (1987).*

[2] *MN Wernick and JN Aarsvold Emission tomography: The fundamentals of PET and SPECT Elseiver Academic Press, USA (2004).*

[3] *MM Khalil Basics sciences of nuclear medicine Springer–Verlag, Germany (2011).*

[4] *F Kharfi Imaging and radioanalytical techniques in interdisciplinary research-fundamentals and cutting edge applications, Intech, Croatia (2013).*

[5] *JS Karp Society of Nuclear Medicine and Molecular Imaging Newsletter: PET Center of Excellence* ***3,*** *1 (2006).*

[6] *JS Karp et al, J. Nucl. Med.* ***49****, 462 (2008).*

[7] WH Wong *J. Nucl. Med.* **29**, 338 (1988).

[8] International Atomic Energy Agency Quality Assurance for PET and PET/CT Systems IAEA Human Health Series No.1, Vienna (2009).
[9] J Torres *et al*, *Positron Emission Tomography-recent developments in instrumentation research and clinical oncological practice,* Intech, Croatia (2013).
[10] Manufacturer Specifications-Discovery ST 16 PET/CT, *GE Healthcare*, http://www.medwow.com/med/petct/ge-healthcare/discovery-st-16-petct/29220.model-spec Accessed 3 July 2018.
[11] Manufacturer Specifications-Discovery LS 16 PET CT, *GE Healthcare*, http://www.medwow.com/med/petct/ge-healthcare/discovery-ls-pet-ct/9697.model-spec Accessed 3 July 2018.
[12] AE Perkins *Technical overview of philips time-of-flight PET design and its clinical benefits* Philips Electronics, Netherlands (2011).
[13] S Surti *and* JS Karp *Physica Medica* **32**, 12 (2016).
[14] S Vandenberghe *et al*, *EJNMMI Phys.* **3**, 1 (2016).
[15] L Wang *et al, Phys. Med. Biol.* **60**, 137 (2015).
[16] L MacDonald *et al, J. Nucl. Med.* **50**, 1666 (2009).
[17] SR Cherry *et al, Physics in nuclear medicine* Elsevier Saunders, China (2012).
[18] H Alva-Sanchez *et al, IEEE Trans. Nucl. Sci.* **57**, 85 (2010).
[19] R Marcinkowski *et al*, *Phys. Med. Biol.* **61**, 2196 (2016).
[20] P Lecoq *Nucl. Intrum. Meth. A* **809**, 130 (2016).
[21] W Krzemien *et al, NSS/MIC IEEE* **16357168**, 1 (2015).
[22] P Moskal *et al, Nucl. Med. Rev.* **15**, C81 (2012).
[23] L Raczynski *et al, Nukleonika* **61**, 35 (2016).
[24] Saint-Gobain Crystals, *Efficiency Calculations for Selected Scintillators*, http://www.crystals. saint-gobain.com/sites/imdf.crystals.com/files/documents/efficiency_calculations_brochure_69670.pdf Accessed 3 July 2018.
[25] Saint-Gobain Premium Plastic Scintillators, http://www.phys.ufl.edu/courses/phy4803L/group_I/muon/bicron_bc400-416.pdf Accessed 3 July 2018.
[26] F Collamati *An Intraoperative Beta-Probe for Cancer Surgery* Ph. D. Thesis, Sapienza University (2016).
[27] A Ferrari *et al, Fluka: A multi-particle transport code* CERN INFN/T_05/11 SLAC-R-773, Geneva (2005).
[28] G Battistoni *et al*, *AIP Conference Proceeding* **86**, 31 (2007).
[29] J Qin *et al, Appl. Radiat. Isot.* **104**, 15 (2015).
[30] EE Ermis *et al, Rev. Sci. Instrum.* **87**, 053504 (2016).
[31] D Nikolopoulos *et al, Nucl. Instrum. Meth. A* **569**, 350 (2006).
[32] SYLT Zhang *et al, Chinese Phys. C* **37**, 126003 (2013).
[33] F Pino *et al, Appl. Radiat. Isot.* **89**, 79 (2014).
[34] S Krishnamoorthy *et al, IEEE Trans. Nucl. Sci.* **61**, 1092 (2014).
[35] I Holl *et al, IEEE Trans. Nucl. Sci*. **35**, 105 (1988).
[36] GM Onyshchenko *et al, Nucl. Instrum. Meth. A* **537**, 394 (2005).
[37] P Dorenbos *et al, IEEE Trans. Nucl. Sci.* **42**, 2190 (1995).
[38] U Ackermann *et al, Nucl. Instrum. Meth. A* **786**, 5 (2015).

Determination of secondary neutrons produced by 100 MeV energy protons in water

[1] ADEM PEHLİVANLI Gazi University
[2] MUSTAFA HİCABİ BÖLÜKDEMİR Gazi University

70-230 MeV energy protons are used to treat cancerous tumors in proton therapy and to protect healthy surrounding tissues as much as possible. Secondary neutrons can be produced by interaction with accelerator components or directly with the patient's body of protons. This leads to an undesirable dose contribution, which can be important for long-term health of cancer patients and healthy tissues outside the target volume concerned. Due to the high biological activity of secondary neutrons in terms of cancer induction, small neutron doses can be important. Published comparisons of neutron dose measurements and the corresponding estimates of cancer risk between different treatment modalities differ over orders of magnitude. The purpose of this study is to calculate neutrons produced in the water by the Monte Carlo simulation performed with the PHITS code. The calculations were performed for protons with 100 MeV energy. As a result, the distribution of neutron and other radiation doses was obtained at some depths in water.

Keywords: Proton therapy, Secondary neutrons, Monte Carlo, PHITS

A theoretical study on the production cross–section calculations for ^{86}Y medical isotope

TUĞÇE GÜLÜMSER, MERT ŞEKERCİ, ABDULLAH KAPLAN

Süleyman Demirel University, Physics Dept., Isparta, Turkey

Abstract

With the growth of technological and industrial developments, human beings daily life become more effected from their outcomes which may increase the carcinogenic effects. As a result, the importance of the cancer diagnostic becomes more crucial and the studies in this field have gain attention. Among the exist diagnostic methods for different cancer types, Positron Emission Tomography (PET) scanning is almost the most useful one in where different medical isotopes have been using for its operation. In this study ^{86}Y, which is one of these isotopes, has been studied in the manner of its production routes. In accordance with the aims of the study, ^{85}Rb(α,3n)^{86}Y, ^{88}Sr(p,3n)^{86}Y, ^{90}Zr(α,3n+p+ α)^{86}Y and ^{86}Sr(p,n)^{86}Y reactions have been selected and production cross–section values of ^{86}Y from these reactions have been calculated by using TALYS 1.8 computer code. The Two Component Exciton Model for pre-equilibrium and Hauser-Feshbach Model for equilibrium situations have been used for calculations. The results obtained from calculations have been compared with the experimental data from the literature.

Keywords: Yttrium, production cross-section, TALYS

Introduction

Technical developments in nuclear physics contribute the development in the fields of medical and industrial. Production of radioisotopes used in the industry, medical diagnosis and treatment are mostly based on the nuclear reactions. The data of the cross–section are important to understand the nuclear reaction models and also for the improvement of the radioisotope generation from the nuclear reactions. Experimental difficulties and lack of data may cause the theoretical calculations came forward in some cases. For these situations, scientists have developed different nuclear reaction codes to compute reaction cross–section, spectrum of out-going particles and dose calculations including many theoretical nuclear models [1].

Theoretical Calculations

PET is able to detect positron-emitter-labeled radiopharmaceuticals with it's high determination and developing quickly as an imaging innovation for the analysis of numerous illness states. An ideal PET radioisotope is required to have significant features such as effective half-life, suitable pharmaceutical affiliation and cross-section data knowledge which means optimum production energy range.

This work is related to one of the 'nonstandard' PET isotopes ^{86}Y (other than ^{15}O, ^{13}N, ^{11}C, or ^{18}F). ^{86}Y is a 14.7 hour half-life positron emitter (β+ (33%) and γ (77%) emission) and has maximum 3.14 MeV positron energy. ^{86}Y is mostly produced from enriched ^{86}Sr with (p,n) nuclear reaction on a cyclotron [2].

^{86}Y is a PET isotope in the experimental stage that is not widely used in the world. Even ^{90}Y is a perfect radiopharmaceutical which is commonly used in systemic therapy, gamma ray deficiency that occured during its usage in diagnostic make tissue imaging difficult. For this reason, usage of this radioisotope for diagnostic purposes is not appropriate. Therefore, researches on the use of ^{86}Y as an alternative of ^{90}Y for the diagnostic and therapeutic radioisotope usage have gained importance in recent years. The most important advantage of using ^{86}Y as a radioisotope is the gradual accumulation of dose at the tumor site slowly. Thus, healthy tissue dose remains at the minimum desired level [3].

The calculation of the cross-section of the radioisotope with computer based calculation codes gives us an advantage in both time and effort. TALYS is a computer code system, which is also used in this study, for the cross-section calculations of nuclear reactions. This code system involves neutrons, photons, protons, deuterons, tritons, helions and alpha particles, in the 1 keV - 1 GeV energy range and for target nuclides of mass 12 and heavier. The TALYS 1.8 code can be used to calculate

the energy spectra, elastic and inelastic angular distributions, partial and total cross-sectional data etc. of a parameterized reaction [4]. The pre-equilibrium calculation results have been obtained by using Two-Component Exciton Model [5] while the equilibrium calculation results have been obtained by using Hauser-Feshbach model of TALYS 1.8 code [6].

Results

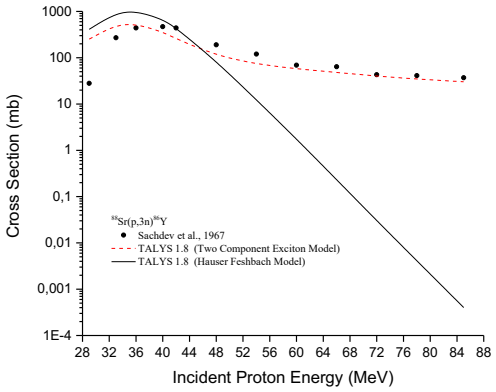

Fig. 1. Comparison of the calculated cross-sections of the $^{88}Sr(p,3n)^{86}Y$ reaction with experimental data.

In this study, cross-section calculations of $^{88}Sr(p,3n)^{86}Y$, $^{86}Sr(p,n)^{86}Y$, $^{90}Zr(\alpha,3n+p+\alpha)^{86}Y$ and $^{85}Rb(\alpha,3n)^{86}Y$ reactions have been completed. In these calculations, equilibrium and pre-equilibrium effects have been examined with Two-Component Exciton and Hauser-Feshbach models from TALYS 1.8. The calculated results are compared with the experimental data taken from the EXFOR library [7] and the figures obtained from this comparison have been listed. Also, the optimum energy ranges for the investigated radioisotope's production have been tabulated below.

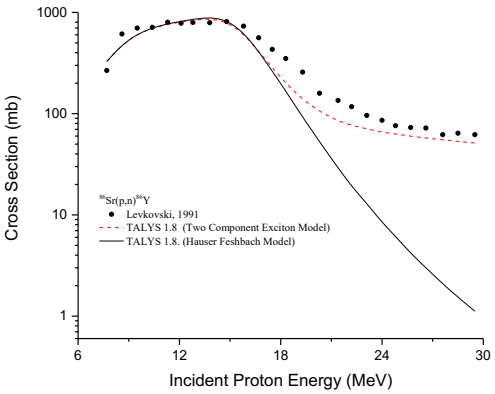

Fig. 2. Comparison of the calculated cross-sections of the $^{86}Sr(p,n)^{86}Y$ reaction with experimental data.

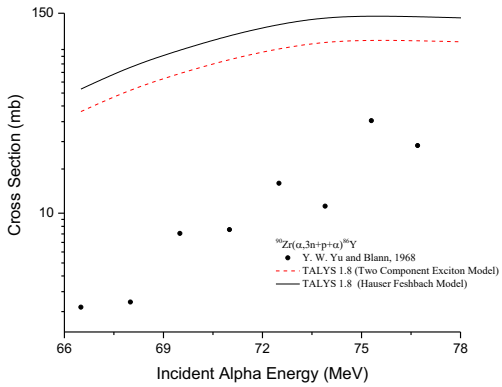

Fig. 3. Comparison of the calculated cross-sections of the $^{90}Zr(\alpha,3n+p+\alpha)^{86}Y$ reaction with experimental data.

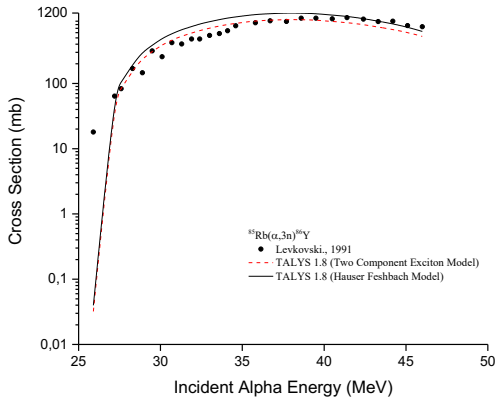

Fig. 4. Comparison of the calculated cross-sections of the $^{85}Rb(\alpha,3n)^{86}Y$ reaction with experimental data.

Table 1. Optimum Energy Range of ^{86}Y Production.

Radioisotope	Production Reaction	Optimum Energy Range
^{86}Y	$^{88}Sr(p,3n)^{86}Y$	50→36
^{86}Y	$^{86}Sr(p,n)^{86}Y$	18→8
^{86}Y	$^{90}Zr(\alpha,3n+p+\alpha)^{86}Y$	75→70
^{86}Y	$^{85}Rb(\alpha,3n)^{86}Y$	47→27

It can be concluded that, when the production cross-section calculations of ^{86}Y have been compared with the data taken from EXFOR library, the Two-Component Exciton model results are more compatible with the experimental data in general. If the figures are to be examined one by one, the two models are compatible with the experimental data up to 50 MeV but after this energy value, the Hauser-Feshbach model is not harmonious with the experimental data for the $^{88}Sr(p,3n)^{86}Y$ reaction. For other investigated proton induced reaction, which is $^{86}Sr(p,n)^{86}Y$, after 18 MeV energy value the Hauser-Feshbach model have not fit the experimental data similarly to the first examined reaction. For the α induced $^{90}Zr(\alpha,3n+p+\alpha)^{86}Y$ reaction,

experimental and calculated cross-section values are not in the same range despite the similar trends. For other α induced reaction, that is $^{85}Rb(\alpha,3n)^{86}Y$ both two models have been found in almost similar agreement with the exist cross-section data in literature that is also given in Fig. 4. All the graphs have been examined and the optimum energy regions for the radioisotope production have been given in Table 1 where the two models have been also compatible with the experimental data.

As a consequence, Two-Component Exciton model can be selected for the isotope production if the experimental data are not accesible or can not be produced because of experimental problems. Also, the optimum energy ranges that require less cost and effort for the radioisotope production can be obtained by using the results from computer code calculations.

Reference

[1] WD Webster *et al*, *Nucl. Med. Biol*. **41**, 7 (2014)

[2] OF Ikotun and SE Lapi, *Future Med. Chem*. **3**, 599 (2011)

[3] KS Pentlow et al, *Clinical Positron Imaging.* **3,** 85 (2000)

[4] A Koning, S Hilaire *and* S Goriely, TALYS–1.8 A Nuclear Reaction Program, User Manual, 1st edn. (NRG, The Netherlands, 2016).

[5] C Kalbach *Phys. Rev. C.* **33** 818 (1986).

[6] W Hauser *and* H Feshbach, H *Physical Review* **87** 366 (1952).

[7] Brookhaven National Laboratory, National Nuclear Data Center, EXFOR/CSISRS (Experimental Nuclear Reaction Data File). Database Version of 2018-04-11 (2018). (http://www.nndc.bnl.gov/exfor/)

Investigation of p, d and α emission spectra for neutron and proton induced reactions on ^{63}Cu

TUĞÇE GÜLÜMSER, MERT ŞEKERCİ, ABDULLAH KAPLAN

Süleyman Demirel University, Physics Dept., Isparta, Turkey

Abstract

Many studies in nuclear field require both theoretical and experimental data which could be helpful for the estimations before planning any particular study. One of the most important theoretical data is the cross–section value of a certain reaction in where it also indicates that particular reaction's occurrence probability. The importance of this data results the generation of many ways to obtain it in theoretical ways. The most improved theoretical calculation methods require advanced operations for calculations while developed computer codes give the opportunity for obtaining this data with less effort and more accuracy. Even there exists many computer codes developed for similar calculations, in this study one of the most well-known and used, TALYS 1.8 has been employed for calculations. The advantage of TALYS is the ability to select the desired method for calculations in where Two Component Exciton Model and Hauser- Feshbach Model have been selected for this study as pre-equilibrium and equilibrium reaction mechanism calculations, respectively. The p, d and α emission spectra calculations have been done for ^{63}Cu(n,xp), ^{63}Cu(n,xd), ^{63}Cu(p,xp) and ^{63}Cu(p,xα) reactions and the obtained results have been compared with the experimental data taken from the EXFOR database.

Keywords: emission spectra, copper, TALYS

Introduction

Computer based calculation and simulation codes have been getting attention and widen their usage area by time. The main reason of that could be pointed as the benefits they provide where faster calculations and higher accuracy could be given as the simplest examples. Like it happened in many industrial and scientific areas, nuclear physicist also use the benefits of computer based calculation codes. Most of the calculations to resolve the nature of a reaction contain very complicated and complex numeric operations that also differ according to the specifications of incident particle and target nuclei. As a benefit of computer based calculation codes, it is possible to overcome such situations by using the previously defined theoretical models exist in the codes. The theoretical models have been developing continuously yet their proved and accepted results may provide a good foresight and prediction to the researchers especially when it is not possible to perform an experiment due to some situations like the experimental difficulties or efficiency concerns.

Theoretical Calculations

Copper element is examined which is one of the most used isotope in the medical and industrial area. The emission spectrum of the p, d and α particles of ^{63}Cu was investigated at given energies. Cu isotopes widely used in the field of healthcare like; molecular imaging applications (^{60}Cu, ^{61}Cu, ^{62}Cu, and ^{64}Cu), in-vivo targeted radiation therapy (^{64}Cu and ^{67}Cu) [1] and as a medical linear accelerator (LINAC) source [2]. Cu radioisotopes can be produced by the use of the cyclotron or the nuclear reactors.

In this study, computer based calculation programs have been used to obtain the cross-section calculations, that is also known as the measurement of a reaction's occurrence, which provide useful information in many cases about a specific reaction's investigation. There exist many developed codes to obtain the cross-section calculations, where TALYS is one of them and the employed one in this study. Total cross-section calculations, elastic and inelastic scattering calculations, energy spectra and etc. could be given as the some of the abilities of TALYS code; where neutrons, photons, protons, deuterons, tritons, helions and alpha particles could be used as involved particles, where mass 12 and heavier nuclides could be used as targets. Also, TALYS is able to perform the calculations from 1 eV to 1 GeV energetic incident particle situations [3]. One of the other ability that the code have is the possibility of selecting the desired theoretical model involvement to the calculations. In this study, Two-Component Exciton and Hauser-Feshbach models have been selected for the calculations where Two-Component Exciton model has

been employed for pre-equilibrium calculations [4] and Hauser-Feshbach model has been chosen for equilibrium calculations [5].

Results

Emission spectra calculations have been done for ^{63}Cu(n,xp), ^{63}Cu(p,xp), ^{63}Cu(n,xd) and ^{63}Cu(p,xα) reactions. In these calculations, equilibrium and pre-equilibrium effects have been examined with TALYS 1.8 Two-Component Exciton and Hauser-Feshbach model. The calculated results are compared with the empirical data taken from the EXFOR library [6] and the figures obtained from this comparison are listed below.

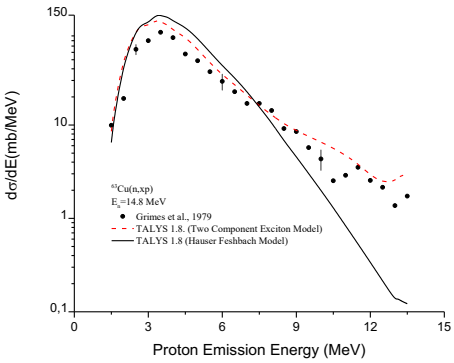

Fig. 1. Comparison of the calculated emission spectra of the ^{63}Cu(n,xp) reaction with experimental data.

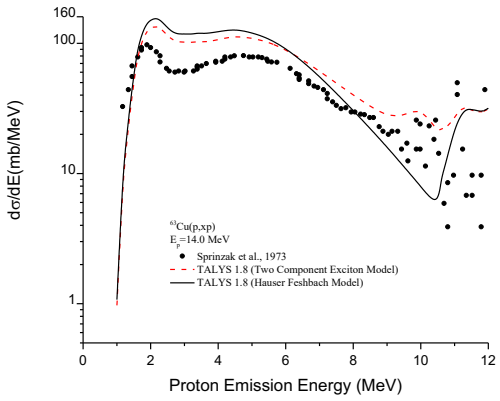

Fig. 2. Comparison of the calculated emission spectra of the ^{63}Cu(p,xp) reaction with experimental data.

In this study, TALYS 1.8 code calculations and EXFOR data library results have been compared for the previously given reactions. If the graphics are examined more closely, for the ^{63}Cu(n,xp) reaction, the two models are compatible with the experimental data up to 8 MeV but after this energy value, the Hauser-Feshbach model is not harmonious with the experimental data. For ^{63}Cu(p,xp) reaction, both two models were found in similar agreement with the existing cross-section data in Fig. 2. For another reaction, that is given in Fig. 3., which belongs to ^{63}Cu(n,xd) reaction, Two-Component Exciton model has a good harmony with the experimental data however Hauser-Feshbach model differs a lot. For ^{63}Cu(n,xα) reaction, it seems that both models have achieved a good fit with the experimental data.

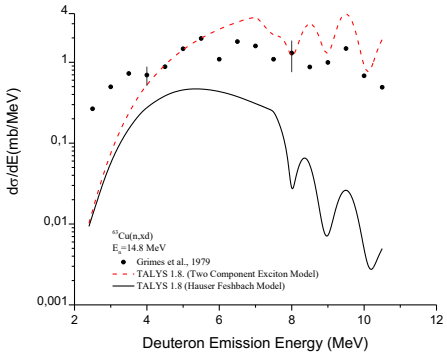

Fig. 3. Comparison of the calculated emission spectra of the ^{63}Cu(n,xd) reaction with experimental data.

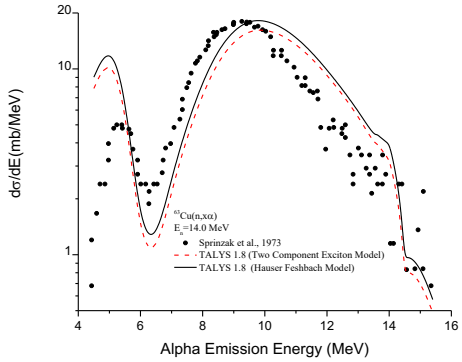

Fig. 4. Comparison of the calculated emission spectra of the ^{63}Cu(n,xα) reaction with experimental data.

As a consequence, Two-Component Exciton model can be selected for the isotope examination, if the experimental data are not accesible or can not be produced because of experimental problems. Also, the emission spectra studies of isotopes inform us about the structure of material and the reactions that can occur. Thus, the possible missing data can be completed by this type of studies.

Reference

[1] C Anderson and R Ferdani, *Cancer Biother Radiopharm*, **27** 379 (2009)

[2] T Shimozato et al, *J Med Phys,* **42** 61 (2017)

[3] A Koning, S Hilaire *and* S Goriely, TALYS–1.8 A Nuclear Reaction Program, User Manual, 1st edn. (NRG, The Netherlands, 2016).

[4] C Kalbach *Phys. Rev. C.* **33** 818 (1986).

[5] W Hauser *and* H Feshbach, H *Physical Review* **87** 366 (1952).

[6] Brookhaven National Laboratory, National Nuclear Data Center, EXFOR/CSISRS (Experimental Nuclear Reaction Data File). Database Version of 2018-04-11 (2018). (http://www.nndc.bnl.gov/exfor/)

Temporal evolution of lead isotope ratios and metal concentrations in sediments of the North Aegean Sea, in Turkish coast

İLKER SERT Ege University

In present research, fifteen surficial and two profile sediment samples were studied in terms of sediment chronology and pollution degree on the ground of pollution indexes (EF, CF, PLI) and lead isotope ratios ($^{206}Pb/^{207}Pb$, $^{208}Pb/^{206}Pb$). Lead-210 (Polonium-210) activity concentrations were measured by utilizing alpha spectrometry. Sediment chronology was determined via Modified CRS mathematical model. Average mass accumulation rates are 0.301 and 0.227 $gcm^{-2}y^{-1}$ in Bakırçay River mouth and Ayvalık offshore stations respectively. Mass accumulation rates do not display the systematic increases along the cores from bottom layers to top layers. In Bakırçay River mouth station ^{210}Pb flux is higher than the range of global atmospheric ^{210}Pb flux value. Due to the high CF and EF values of Sr both of stations have hydrothermal features. Ayvalık offshore station has displayed Na, Cd pollution since 1945, but Na, Cd, As, Mo, Ag pollutions have existed in Bakırçay River mouth station since 1983 in terms of CF and EF values. According to PLI index, Bakırçay River mouth station has "starting level pollution" degree and it displayed an "acute corruption" in 1981. $^{206}Pb/^{207}Pb$ ratios range from 1.17 to 1.25, $^{208}Pb/^{206}Pb$ ratios range from 1.99 to 2.16 in study area. When $^{206}Pb/^{207}Pb$ and $^{208}Pb/^{206}Pb$ ratios are evaluated with together, it is seen that both of the stations have had the natural (geologic) sediments since 2011.

Keywords: Mass accumulation rates, EF, CF, PLI, Lead-isotope ratios ($^{206}Pb/^{207}Pb$, $^{208}Pb/^{206}Pb$).

Determination of count intensity and elemental weight percentages of sediments in the Altinova shipyard region (Yalova-İzmit gulf) by SEM-EDX

[1] KÜBRA BAYRAK Yıldız Teknik University
[2] EROL KAM Yıldız Teknik University
[3] ZEKİ ÜNAL YÜMÜN Namık Kemal University

In this study, the count intensity and elemental weight percentages of sediment samples taken from Altınova region was evaluated using scanning electron microscopy (SEM) and energy dispersive X-ray (EDX). Within the scope of the study, six sea sediment samples were obtained from different depths along the shoreline of the Altinova shipyard area. The samples were subjected to a series of classical laboratory procedures to make the samples suitable for analysis. Then, SEM images of sediment samples were taken with JEOL JSM-6390, which has high resolution power. At the same time, from the EDX analysis, count intensity and elemental weight percentages are calculated by EDX spectra. According to the count intensity of ALT-2 are calculated as N-33.46 c/s, O-30.35 c/s, Na-1.66 c/s, Mg-0.03 c/s, Al-3.31 c/s, Si-11.09 c/s, Ca-2.71 c/s and Fe-1.61 c/s. Besides, elemental weight percentages of ALT-2 are calculated as N-34.269%, O-58.138%, Na-1.108%, Mg-0.013%, Al-1.180%, Si-3.388%, Ca-0.874% and Fe-1.029%. The count intensity and elemental weight percentages of six sediment samples were calculated and evaluated, respectively. The results were similar because all the samples were taken from the same region. In conclusion, this study provides preliminary information about the elemental composition of the sedimentology of the region. For being one of the few studies in the study area, it will be the source for future work.

Keywords: Count Intensity, Elemental Weight Percentages, SEM, EDX, Altınova, Yalova, Izmit Gulf

Luminescence dating of Harran ruins bricks

MEHMET KOŞAL Harran University

Luminescence dating of different brick samples taken from archaeological excavations in a tumulus at Harran Ruins was done. At the end of the scraping and crushing process (<20 mm), the polymineral samples were prepared using HCl (10%) and H_2O_2 acids. Luminescence counts were performed with a Lexsyg OSL reader. The equivalent doses were determined from the infrared-stimulated optical luminescence (IRSL) counts according to a single aliquot (SAR) protocol. The annual dose values were calculated by counting of K-40, uranium and thorium activities in the samples in a NaI scintillation detector. It was finally determined that the bricks were produced in the 12th century, dividing the equivalent doses by the annual doses.

Keywords: Luminescence Dating, annual dose, Harran, archaeology

Study on shape structure of even-even cerium isotopes within the interacting boson model-1 and the Cranking Nilsson Strutinsky model

[1] MAHMUT BÖYÜKATA Kırıkkale University
[2] SAMRA KAİM Université des Frères Mentouri Constantine1

In this study, the Interacting Boson Model-1 (IBM-1) and the Cranking Nilsson Strutinsky (CNS) model were applied to investigate the geometric shape of even-even $^{122-138}$Ce isotopes. For the process of IBM-1 calculations, the parametrizations of the constructed Hamiltonian were firstly performed to calculate the energy levels of the given isotopes. Then same set of parameters were used to plot the energy surface as a function of deformation parameters. The β parameters were obtained by minimizing the potential energy surface. According to the patential energy surfaces of IBM-1 calculations, $^{122-132}$Ce isotopes have prolate shape and $^{134-138}$Ce isotopes show spherical behavior when moving to the shell. Later the potential energy surfaces of these isotopes obtained by the CNS code were presented to compare with the energy surfaces of IBM-1 to see differences of shape changing along to isotopic chain of Cerium isotopes.

Keywords: Cerium, Interacting Boson Model-1, Cranked Nilsson Strutinsky, deformation, energy surface.

The comparison of the effect of the different sets of the deformation parameters on the cross sections calculations of $^{96\text{-}104}$Ru targets

[1] MAHMUT BÖYÜKATA Kırıkkale University
[2] HANDE BOYDAŞ Kırıkkale University
[3] ABDULLAH AYDIN Kırıkkale University

The quadrupole collectivities of even-even $^{96\text{-}104}$Ru isotopes were studied on in the framework of interacting boson model-1 (IBM-1) in this work. Their energy levels and B(E2) values were calculated within the established IBM-1 Hamiltonian. The Hamiltonian parameters were fitting from the experimental data obtained from the National Nuclear Data Center (NNDC). The potential energy surfaces (PES) of the given isotopes were plotted as a function of deformation parameters to predict their shapes and to get β deformation parameters of target nuclei. Also same deformation parameters were calculated from the experimental B(E2)↑ values and the theoretical ones of IBM-1. By this way, three sets of deformation parameters were used as input in the TALYS 1.8 code to calculate the cross sections of the stable $^{96\text{-}104}$Ru target nuclei for photo-nuclear reactions to compare the effect of each deformation sets on the cross sections.

Keywords: deformation parameter, cross section

The calculation of (n,x) reaction cross sections for ^{209}Bi, ^{232}Th and ^{238}U nuclei between 0 and 30 MeV

[1] RIDVAN ÜNAL Uşak University
[2] GÜLNUR ERASLAN İskenderun Doğru Cevap Okulları

In this study, (n,2n) and (n,3n) total reaction cross sections were calculated between 0 and 30 MeV neutron incident energy on ^{209}Bi, ^{232}Th and ^{238}U nucleiby using pre-equilibrium models. The model calculations were performed by using TALYS 1.2 and ALICE-ASH nuclear reaction computer codes. The results are compared with experimental results available in literature and found to be in good agreement.

Keywords: Direct Reactions, Reaction Cross Sections, TALYS 1.2, ALICE-ASH

Investigation of level density parameter dependence for some even-odd and odd-even nuclei in fission cross sections induced by neutrons with the incident energy up to 20 MeV

[1] ÖNDER SÖNMEZ Gazi University
[2] AYNUR ÖZCAN Gazi University

This study aims to show the dependence on of the level density parameters regarding the cases of even-odd odd-even neutron, proton numbers of four selected subactinite targets. These cases are analyzed for the neutron induced fission cross sections of ^{227}Ac, ^{251}Cf, ^{231}Pa, ^{235}Pu subactinide targets. The method was implemented using different level density parameters for each fission cross-section calculation in TALYS computer code. The TALYS code calculations were compared with the available experimental data. It is found that the fission cross sections are highly dependent on level density parameters in the neutron fission channels for these four subactinide nuclei. Besides, the even-odd odd-even number of neutron proton cases are investigated and it is found that the fission cross sections are also dependant to these even-odd odd-even cases.

Keywords: Fission cross-section, Level density parameter, Even-Odd Odd-Even neutron proton numbers, TALYS 1.8

Experimental study of double excitation-ionization resonance profiles of helium by electrons

ZEHRA NUR ÖZER, NURÇİN KARADENİZ KAYAR, HÜSEYİN ALİ YALIM

Afyon Kocatepe University, Physics Dept., Afyonkarahisar, Turkey

Abstract

Excitation to any energy level in the atom can be examined by looking at the energy loss spectra of the emitted electrons. For excitation to the resonance levels, incoming electrons loose energy as the excitation energy and the remaining energy is shared between the scattered and ejected electrons. Resonance levels can be examined by detecting electrons scattered or ejected from the atom after the collision event.

From the resonance energy levels, the ionization and the direct ionization event overlap in the energy spectrum. This situation effects the symmetry of the resonance profiles. Resonance profiles are formed in an asymmetric structure above the direct ionization cross sections around the resonance levels. In this study, cross sections were measured at a determined low and high angle to better see the resonance levels. Since the resolution of the system is independent of the electron gun, only the energy resolution of the analyzer is determined. Depending on energy resoluitio of the analyzer, levels close to each other can be distinguished. The measurements taken at low and high angles will be evaluated in terms of resonance profiles in this work.

Keywords: Electron spectrometry, Autoionization, Angular spectrum of resonance levels, Helium atom

Introduction

An autoionizing atomic state is the one in which the atomic excitation energy is in excess of the first ionization limit of the atom, but the atom is not in an ionized state. The study of electrons ejected through autoionization to the excited states is expected to provide important information on their properties.

Resonances and the autoionization phenomenona present interesting challenges to the quantum theory of the dynamics of multi electronic systems. The autoionization of atoms (excited by electron impact) involves interference between the direct ionization and the resonance or autoionization amplitude.

If any atom has two electrons excited from its base state, this atom is in the doubly excited energy state and the energy level is above the first ionization threshold. Since these electrons in the excited state have more energy than the excitation energy, one of these two electrons gives its energy to the other one causing it to leave the system automatically. The fact that one of the two electrons leave the system automatically without radiative. This event is called autoionization. The states that cause autoionization are called resonance states and their energies are called resonance energies.

In this event, the target atom is firstly autoionized or excited to resonance states by electron impact, and autoionizes after a certain lifetime. The autoionization levels have a lifetime between 10^{-16} s and 10^{-13} s. Both the autoionization and the direct ionization events are result as ionization of the atom.

Two electronic atoms are the simplest systems for autoionization. For this reason, their resonances above the first ionization threshold have been studied extensively both experimentally and theoretically. Considering now the case of helium, atomic excitation to an energy in excess of the ionization potentials will arise only through the simultaneous excitation of both atomic electrons.

The levels of autoionization by electron scattering were first investigated by Lassettre (1959). Fano (1961) later generalized the theory for photons to electron scattering. The doubly excitation energy levels in the helium atom are above the first ionization threshold and have series resonance levels up to the second ionization threshold (Fig 1). In electron collision experiments, the resonance levels was investigated by Wellenstein et al. (1973), Fon and Leung (2001), Liu et al. (2003) and Brotton et al. (1997) with the detection of scattering electrons. Experiments, in which electrons ejected from the resonance level are detected, are described by Gelebart et al. (1974), Hicks et al. (1974), Hicks and Comer (1975), Gelebart et al. (1976), Oda et al.), McDonald and Crowe (1992a), McDonald and Crowe (1992b) and DeHarak et

al. (2006).

The energy spectra of electrons that ejected from their resonance levels are critically depend on the energy and the angle of the incoming electron energy. Optically permissive transitions are observed at small angles and high energies while optically forbidden transitions are observed at large angles and at low energies. While optically permissive transitions are observed in photon collision experiments, forbidden transitions are seen in the electron collision experiments. Depending on the angular momentum of the resonance level and interference effect, some destructive levels make constructive interference.

Table 1. First four energy resonance levels of Helium. All values are in units of eV.

State	Excitation Energy	Ejected Electron Energy
$(2s^2)^1S$	57.83 (0.04)	33.24
$(2s2p)^3P$	58.31 (0.02)	33.72
$(2p^2)^1D$	59.91(0.02)	35.42
$(2s2p)^1P$	60.145	35.555

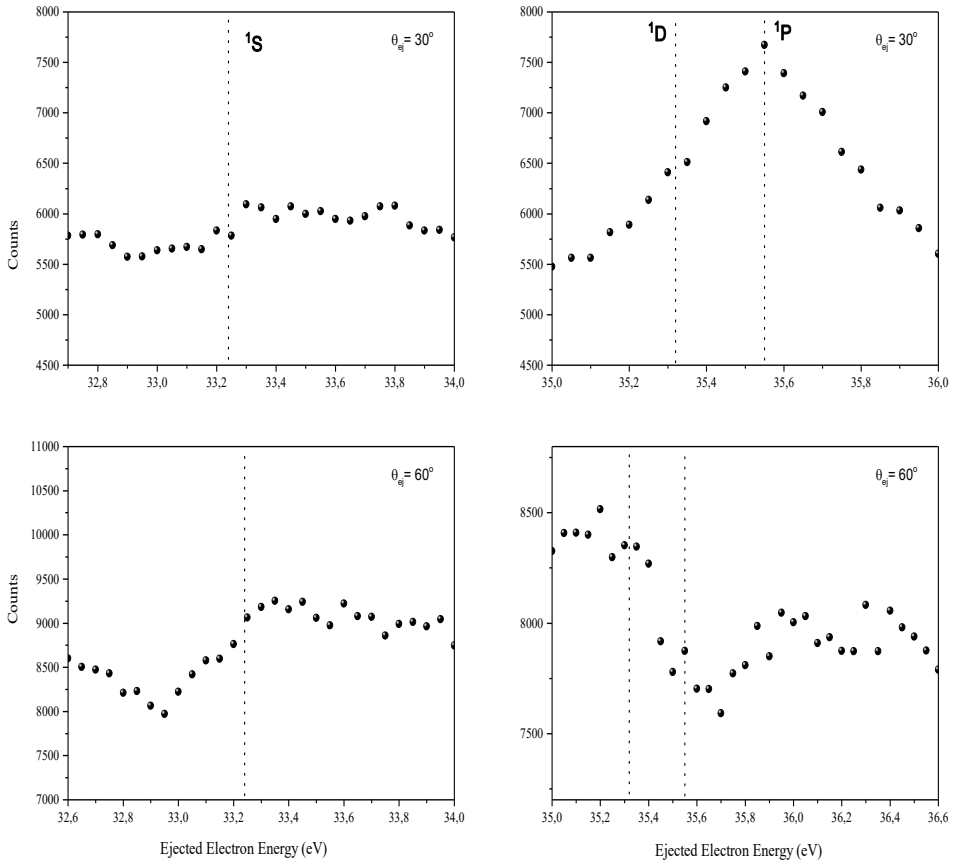

Fig. 1. Ejected electron energy spectra for 30° and 60°, the changes in the resonance profiles.

Results

In this work, the autoionization energy levels of the Helium atom were determined by detecting electrons after the excitation at 200 eV energetic electrons using the electron spectrometer in Electron Collision Laboratory at Afyon Kocatepe University. Differential cross section measurements (DCS) were taken at 30° and 60° angles for 32.5 - 35 eV resonance energy levels.

In order to see the $(2s^2)^1S$, $(2p^2)^1D$ and $(2s2p)^1P$ peaks clearly, the spectra is taken at three different angles for these resonance levels. As seen in the Fig. 2, the asymmetric structure is observed around 60°, while the symmetric structure is seen around 30°.

In the spectra, peaks consisting of the addition of ionization and direct ionization have been observed. While the symmetric and asymmetric structures are observed in the all cases, dominant structure changes depending on the angle.

Since the resolution of the analyzers is around 1 eV, ^1D and ^1P levels which are very close to each other for n = 2 can not be distinguished. In the spectra, resonance profiles with symmetric and asymmetric structures are formed above the direct ionization cross sections in the vicinity of their resonance levels. Further studies on this

work is in progress.

This work was supported by AKU-BAPK through Grants 15.FEN.BİL.14 and 15.HIZ.DES.131-132.

Reference

[1] E. N. Lassettre, *Radiat. Res. Suppl.* 1, 530-546, (1959).
[2] U. Fano, *Phys. Rev*. 124, 1866-1878, (1961).
[3] H. F. Wellenstein, R. A. Bonham, R. C. Ulsh, *Phys. Rev. A* 8, 304-314, (1973).
[4] W. Fon, C., K. A. Berrington, A. E. Kingston, *J. Phys. B: At. Mol. Phys.* 13, 2309-2320, (1980).
[5] X. J. Liu, L. F Zhu, Z. S. Yuan, W. B. Li, H. D. Cheng, Y. P. Huang, Z. P., Zhong, K. Z. Xu, J. M. Li, *Phys. Rev. Lett.* 91, 193203, (2003).
[6] S. J. Brotton, S. Cvejanovic, F. J. Currell, N. J. Bowring, F. H. Read, *Phys. Rev. A* 55, 318-328, (1997).
[7] G. Gelebart, R. J. Tweed, J. Peresse, *J. Phys. B: At. Mol. Phys.*, 9, 1739-1748, (1976).
[8] P. J. Hicks, J. Comer, , *J. Phys. B: At. Mol. Phys.* 8, 1866-1879, (1975).
[9] P. J. Hicks, S. Cvejanovic, J. Comer, F. H. Read, J. M. Sharp, *Vacuum,* 24, 573-580, (1974).
[10] G. Gelebart, R. J. Tweed, J. Peresse, *J. Phys. B: At. Mol. Phys*. 9, 1739-1748, (1976).
[11] N. Oda, S. Tahira, F. Nishimura, F. Koike, *Phys. Rev. A* 15, 574-587, (1977).
[12] D. G. Mcdonald, A. Crowe, *J. Phys. B: At. Mol. Opt. Phys.*25, 2129-2141, (1992a).
[13] D. G. Mcdonald, A. Crowe, *J. Phys. B: At. Mol. Opt. Phys*. 25, 4313-4324, (1992b).
[14] B. A. Deharak, J.G. Childers, N.L.S. MARTIN, *Phys. Rev. A* 74, 032714, (2006).

A solution of Bohr hamiltonian for γ≈30° with Kratzer potential

[1] İBRAHİM YİĞİTOĞLU Gaziosmanpaşa University Physics Departmen
[2] BURCU UÇAR Gaziosmanpaşa University Physics Department

A critical point symmetry for the prolate to oblate shape phase transition is introduced starting from the Bohr Hamiltonian and approximately separating variables for γ≈30°. The β part of Bohr Hamiltonian for γ≈30° is solved with Kratzer potential using the Nikiforov-Uvarov method. This solution is going to be called Z(5)-K. The calculated intraband and interband BE(2) transitions rates are also calculated and compared with existing experimental data.

Keywords: Bohr Hamiltonian, Kratzer potential, Critical Point Symmetries, Z(5) Model

Bohr hamiltonian for γ≈0° with Kratzer potential

[1] İBRAHİM YİĞİTOĞLU Gaziosmanpaşa University Physics Department
[2] TUĞBA TURAN Gaziosmanpaşa University Physics Department

An analytical solution of Bohr Hamiltonian for γ≈0° is developed by Nikiforov Uvarov Method using Kratzer potential. This solution will be called X(5)-Kratzer. The energy eigenvalues and wave function are obtained. B (E2) transition rates were calculated. The agreement with experimment is investigated.

Keywords: Bohr Hamiltonian,Critical Point Symmetries,X(5) Model,Kratzer Potentia

l

Thermoluminescence properties of calcite mineral conducted by bacterial calcium carbonate (CaCO3) precipitation in organic soil

HÜSEYİN TOKTAMIŞ, MOHAMMAD KHATEEB

Gaziantep University, Engineering of Physics Dept., Gaziantep, Turkey

Abstract

In the past few years, the use of bacterial calcium carbonate ($CaCO_3$) precipitation (BCCP) has become popular. BCCP has been applied in a variety of civil and geotechnical engineering applications. In this study, the thermoluminescence properties of samples conducted by bacterial calcium carbonate ($CaCO_3$) precipitation (BCCP) in organic soil were investigated. As a result of this work, the calcite mineral conducted by bacterial calcium carbonate ($CaCO_3$) shows Thermoluminescence behavior and a wide linear dose response region between 150Gy and 2.3kGy is observed. In addition, a good reproducibility is seen in the high temperature peaks. The peak temperatures of TL glow curve peaks are not affected by the cycle of experiment.

Keywords: thermoluminescence, dosimeter, bacterial calcium carbonate

Introduction

When the radiation is incident on a material some of its energy may be absorbed and re-emitted as light of a longer wavelength (Stoke's law). This is the process of luminescence. The wavelength of emitted light is characteristic of the luminescent substance and not of the incident radiation. The TL signal is characterised by a so-called "glow curve", with distinct peaks occurring at different temperatures, which relate to the electron traps present in the sample. Thermoluminescence (TL) is a luminescence phenomenon of an insulator or semiconductor which can be observed when the solid is thermally stimulated [1]. The purpose of this thesis is to investigate the thermoluminescence properties of samples conducted by bacterial calcium carbonate ($CaCO_3$) precipitation (BCCP) in organic soil. In the past few years, the use of bacterial calcium carbonate ($CaCO_3$) precipitation (BCCP) has become popular [2-4]. BCCP has been applied in a variety of civil and geotechnical engineering applications The BCCP is located in glass boxes having dimensions 6×6×2 cm are immersed in bacterial medium (Bacillus pasteurii, urea, and $CaCl_2$) for 4 days. During the treatment period, the samples were treated with urea medium and $CaCl_2$ every 6 h. Changes in pH values were monitored at different time intervals. At the end of the treatment period, the amount of $CaCO_3$ was determined with a calcimeter test.

Experiment

The samples conducted by bacterial calcium carbonate ($CaCO_3$) precipitation (BCCP) in organic soil are shown in figure1 .



Fig. 1. The samples conducted by bacterial calcium carbonate (CaCO3) precipitation (BCCP) in organic soil

Figure2 shows the schematic view of biological calcite precipitation in sand matrix [4].

All examples were irradiated at room temperature with a point beta source (^{90}Sr-^{90}Y) which delivers 0.040 Gy/s. The beta source was installed in a 9010 optical dating system which is interfaced to a PC using a serial RS-232 port to control irradiation time. Glow curve measurements were made using a Harshaw TLD System 3500 Manual TLD Reader

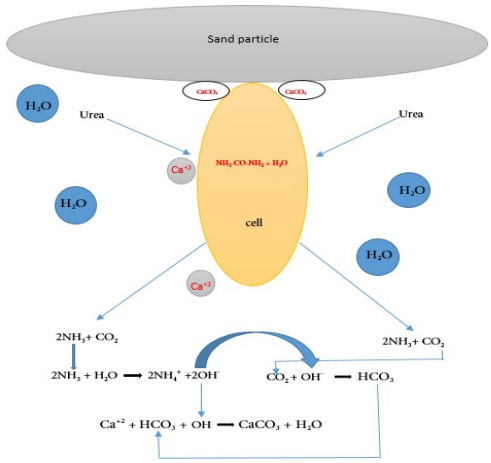

Fig. 2. Schematic view of biological calcite precipitation in sand matrix [4]

Results

In the dose response experiment, all samples were weighted about 15mg and each sample was irradiated by a point source for different dose value. Finaly,they were read out at 1°C/s by the TLD reader. Figure3 shows the variation of the glow curve of the sample as a function of applied dose.

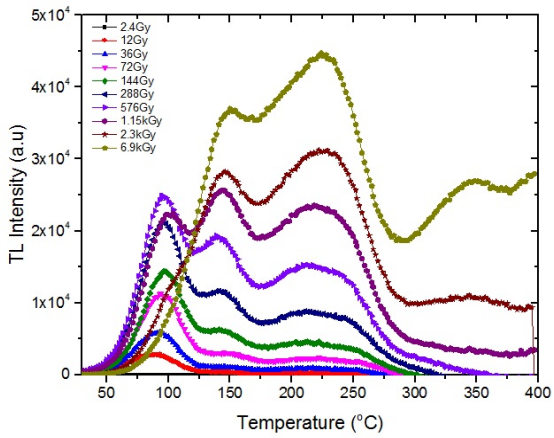

Fig. 3 . Schematic variation of the glow curve of the sample as a function of applied dose

As a result, a good TL glow curve with four distinct peaks at 90, 140, 210°C and 340°C were obtained. At higher dose, 90°C peak disappears and new trap is created around 340°C. The 140°C and 210°C peaks are not affected by variation of applied dose.

In the heating rate experiment, all samples weighted about 15mg were irradiated 36Gy and read out at different heating rate. In the figure4, the glow curve variation as a function of heating rate is seen. No extra distinct peak was produced with variation of heting rate. Increasing heating rate causes a decrease in peak area. Peak temperature shifts to higher temperature region about 27°C for peak 90°C , 26°C for peak 140°C, 33 °C for peak 210 °C and 45 °C for peak 240 °C.

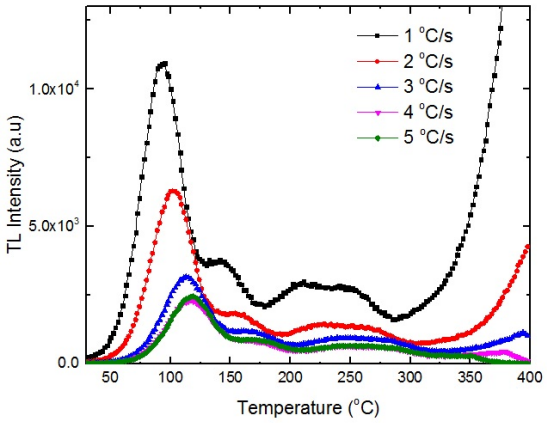

Fig. 4 . The glow curve variation as a function of heating rate.

Figure5 shows the reproducibility (cycle of measurement) of the sample. In this experiment, one sample was irradiated 36 Gy and read out at 1°C/s. This experimet was repeated eight times.

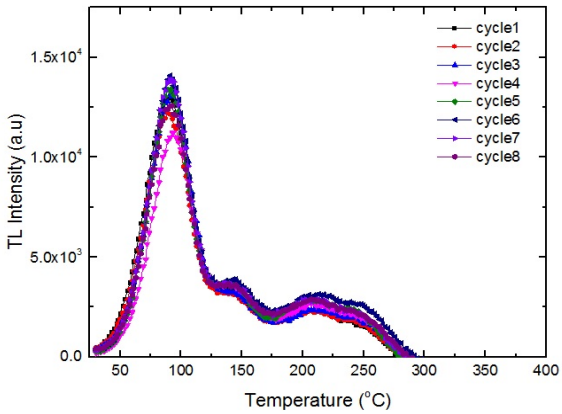

Fig. 5 . TL glow curve variation with respect to cycle of measurement.

No extra distinct peak was produced with repeat of experiment. The nearly same results were observed for the area under the TL glow curve.

It was concluded that the sample of calcite mineral conducted by bacterial calcium carbonate (CaCO3) precipitation in organic soil shows TL properties. The relation between TL intensity and applied dose for the peaks 210°C and 240 °C is linear between 140Gy and 2,4kGy. At higher dose, 90°C peak disappears and new trap is created aroun 340°C.the 140°C and 210°C peaks are not affected by variation of applied dose. A decrease is observed in the TL peak intensity with increasing heating rate. A good reproducibility is observed

Reference

[1] Bos, A.J.J., 2007. Rad. Meas. 41, 45-56.
[2] Ramachandran, S. K., Ramakrishnan, V. & Bang, S. S. (2001). ACI Materials Journal, Vol. 98, pp. 3-9.
[3] Bang, S. S., Galinat, J. K. & Ramakrishnan, V. (2001). Enzyme and Microbial Technology, Vol. 28, pp. 404-409.
[4] Sıddık, W., Canakcı, Kılıc, I.H. (2015). IJST, Transactions of Civil Engineering, Vol. 39, No. C1, pp 201-205.

Excitation functions of nuclear reactions induced by alpha particles up to 50 MeV on ^{46}Ti, ^{45}Sc and ^{51}V

Hatice BİLGİN[1], İsmail H. SARPÜN[2], Abdullah AYDIN[3]

[1]*Afyon Kocatepe University, Physics Dept., Afyonkarahisar, Turkey*
[2]*Akdeniz University, Physics Dept., Antalya, Turkey*
[3]*Kirikkale University, Physics Dept., Kırıkkale, Turkey*

Abstract

Nuclear fuel cycle and particle accelerator facilities require neutron production data of alpha particle induced reactions especially in design and operation steps. Light nuclei have large cross section for (α,n) reactions and therefore have influence on safety design and operation of these facilities. In this study, total cross sections of (α,n) reactions were theoretically calculated on ^{46}Ti, ^{45}Sc, ^{51}V target elements with the TALYS 1.8 nuclear reaction code and compared with available experimental values in the EXFOR Nuclear Data Library.

Keywords: Nuclear physic, Talys 1.8

Introduction

Nuclear Reactions are managed according to the mechanism; compound nuclear reactions, direct reactions and these two can be classified for pre-equilibrium or resonance reactions. Pre-equilibrium reaction models; Reactions with 10-60 MeV energetic proton, neutron and alpha particles are very successful in explaining the high energy location of the energy spectrum. Activation properties can be classified according to: C, Si, Ti, Fe, Cr and V, and the activation elements Al, Ni, Ag, Co and Nb are some of the high activation materials. Choosing only material properties for reactor components is dependent not only on the compatibility with other materials and on the performance of the irradiation but also on the radiological properties.

Today, with the contribution of the theoretical studies to experimental studies, science is progressing rapidly. In addition, the theoretical studies and the experimental studies are engaged in a one-to-one correspondence. It is a temporary short-term life produced in reactors. Therefore, it is not possible to measure the emission cross sections of the nuclei and the emission spectra of the particles precisely. The most important thing to be done in order to save time is to preliminarily calculate the influence sections in a theoretical way. Various computer codes have been developed for these calculations.

In this study, ^{46}Ti, ^{45}Sc, ^{51}V target elements were exposed to α bombardment of Talys 1.8 at 50 MeV. Calculated sections were compared with the data obtained from the EXFOR / CSISRS Library.

Calculation Methods

The calculations of the cross section have been made by TALYS 1.8 nuclear code. The excitation functions of nuclear reactions induced by alpha particles up to 50 MeV at ^{46}Ti, ^{45}Sc and ^{51}V were calculated.TALYS gives an analysis result for all nuclear reaction channels. TALYS is an computer code which runs on Linux and being used for nuclear reactions' analysis and estimation. It can calculate at 1 keV-250 MeV energy range on neutron, proton, deuterium, tritium, ^{3}He, alpha and the gamma entry reactions.

Results

In this study, (α,n) cross sections have been calculated for the reactions which have been generated ^{46}Ti, ^{45}Sc and ^{51}V target nuclei. The graphs of the excitation function, which have been obtained as a response of projectile energy.

The consistence between the data and TALYS 1.8 data at the obtained graphics has been observed. In some places on the graphic TALYS 1.8 data

coincide with experimental values in some high places.

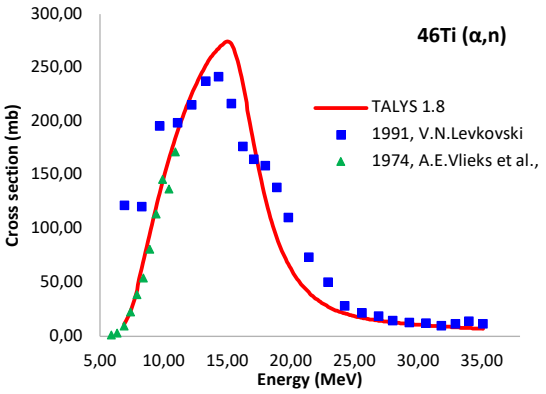

Fig. 1. The comparison of calculated of (α,n) reaction on ^{46}Ti with the experimental data reported in literature. Experimental values were taken from EXFOR.

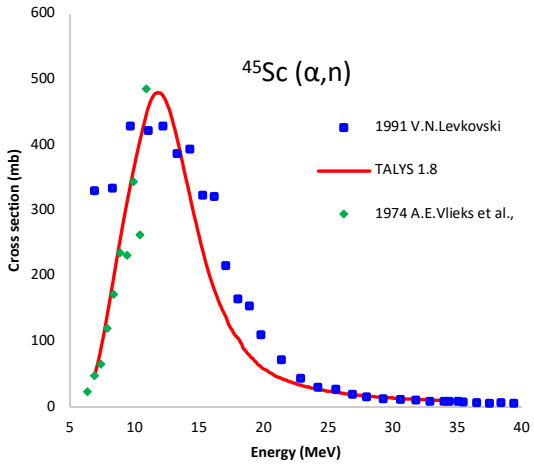

Fig. 2. The comparison of calculated of (α, n) reaction on ^{45}Sc with the experimental data reported in literature. Experimental values were taken from EXFOR.

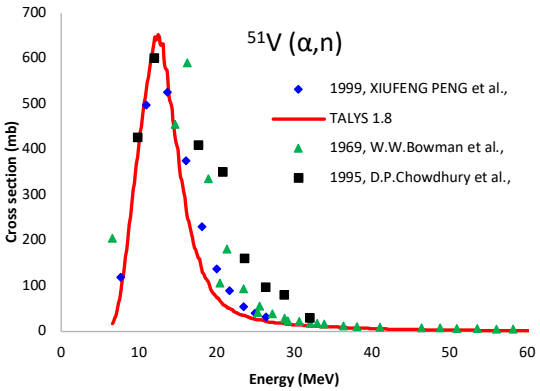

Fig. 3 . The comparison of calculated of (α,n) reaction on ^{51}V with the experimental data reported in literature. Experimental values were taken from EXFOR.

References

1. V.N.Levkovski Act.Cs.By Protons and Alphas,Moscow 1991
2. A.E.Vlieks et al., Nuclear Physics, Section A, Vol.224, p.492 (1974)
3. V.N.Levkovski Levkovskij,Act.Cs.By Protons and Alphas,Moscow(1991)
4. A.E.Vlieks et al., Nuclear Physics, Section A, Vol.224, p.492 (1974)
5. Xiufeng Peng et al., Nucl. Instrum. Methods in Physics Res., Sect.B, Vol.152, p.432 (1999)
6. D.P.Chowdhury et al., Nucl. Instrum. Methods in Physics Res., Sect.B, Vol.103, p.261 (1995)
7. W.W.Bowman et al., Nuclear Physics, Section A, Vol.131, p.513 (1969)
8. EXFOR/CSISRS Experimental Nuclear Reaction Data Center
9. Koning, A., Hilaire, S., Goriely, S., TALYS-1.8 A Nuclear Reaction Program, User Manual (NRG, The Netherlands)
10. ^{197}Au İçin Reaksiyon Tesir Kesiti Hesaplamaları Özdoğan H. Kaplan A.

Theoretically proton emission DDX calculation on Ge isotopes of neutron induced reactions

[1]Gözde DEMİRELLİ, [2]İsmail H. SARPÜN, [3]Abdullah AYDIN

[1]Doğa Private School, Kurtkoy School, Istanbul, Turkey
[2]Akdeniz University, Physics Dept., Antalya, Turkey
[3]Kirikkale University, Physics Dept., Kırıkkale, Turkey

Abstract

In this study, proton emission DDX, necessary in determination of heating and damages in structural fusion material research, of ^{70}Ge and ^{72}Ge target nuclei were theoretically calculated by the TALYS 1.8 code at 200 MeV neutron incident energy and also compared with available experimental data in EXFOR Nuclear Data Library. Furthermore, in theoretical calculations direct, compound and pre-equilibrium reaction contribution have been investigated.

Keywords: DDX, Germanium, TALYS

Introduction

In fusion reactor development, the necessity of double differential cross section (DDX) data of light charged particles emitted due to neutrons impact to reactor devices, especially first-wall and blanket, is discussed in several studies.

In the course of this work, we measured the angular distribution of protons emitted by silicon under bombardment of 200 MeV neutrons. This target was chosen because the proton spectrum from ^{70}Ge and ^{72}Ge(n,p), taken in the forward direction with respect to the neutron beam, has shown a characteristic structure, which seemed to give evidence of the presence of surface direct interaction. The knowledge of the angular distribution of the protons included in these peaks can give us information on the direct effect itself and on the shell-model orbits in which the particles involved are found. Protons can be correlated with the quantum numbers of the shell-model orbits in which the proton is found in the target nucleus, and in which the neutron is captured. These results show the possibility of using the direct n, p reaction to study these shell model orbits.

The deep understanding of nucleon-induced reactions is a crucial step for the further development of nuclear reactions theory in general. In addition, complete information in this field is strongly needed for a large amount of applications, such as the accelerator-driven clean nuclear power System (ADS) has been an interesting focus in nuclear physics. They require accurately nuclear reaction data of common cross sections and especially need the data of neutron and proton-induced energy-angle correlated spectra of secondary light particles (neutron, proton, deuteron, triton, helium and alpha-particle) as well as double differential cross sections. The development of high-quality nuclear data for lead are particularly important due to their role as an important structural and target material in many accelerator-driven system designs.

Results

Double differential cross sections of ^{70}Ge and ^{72}Ge at 1.8°, 2.8°, 5.8°, 9.8° and 14.8° emission angles.

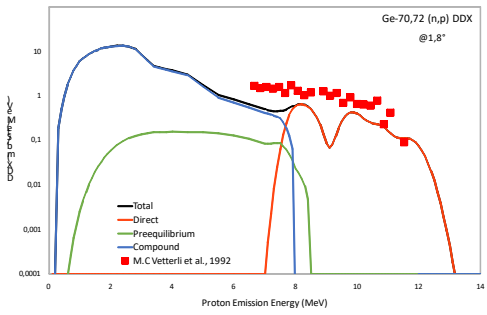

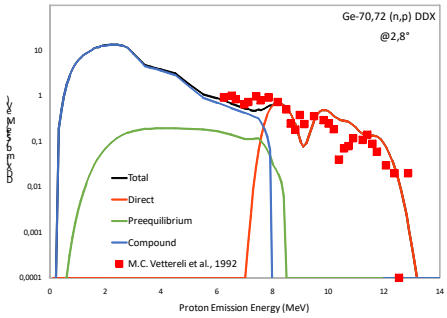

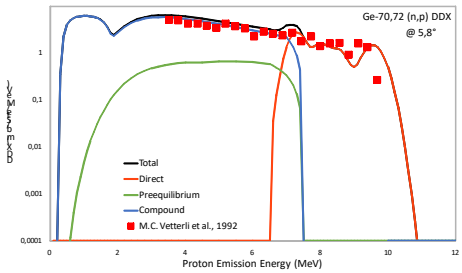

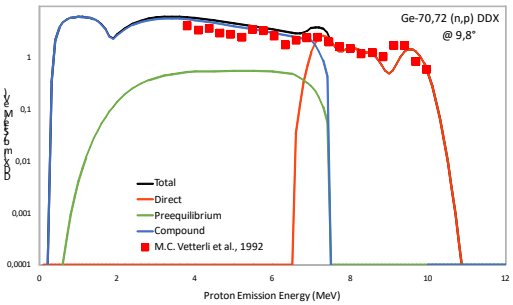

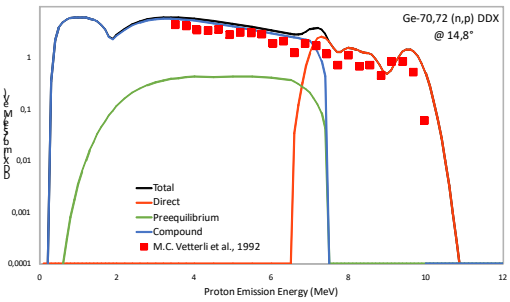

Conclusion

The Double Differential Cross Sections ($d^2\sigma/d\Omega.dE$) for neutron emission for ^{70}Ge and ^{72}Ge (n,p) at 1.8°, 2.8°, 5.8°, 9.8° and 14.8° emission angles have been calculated by the TALYS 1.8 code at 200 MeV incident energy.

The theoretically calculated Double Differential Cross Sections of neutron emissions are compared with the available experimental data in Exfor for ^{70}Ge and ^{72}Ge(n,p) reaction. The pre-equilibrium process is dominant for neutron emission at given energies (200 MeV) whereas the higher energy neutron particles are emitted through the direct reaction.

References

1. M.C.Vetterli - Physical Review, Part C, Nuclear Physics, Vol.45, p.997 (1992), USA
2. L. COLLI - Istituto di Fisica dell' Universit~ - Mila'J~o
3. K. DEBERTIN - J.W.Goethe Univ., Frankfurt/Main, Germany
4. China Institute of Atomic Energy, P.O. Box 275(41), Beijing 102413, People's Republic of China- Yinlu Han
5. Talys 1.8
6. EXFOR/CSISRS, National Nuclear Data Center

Investigation of 131-Cs medical radioisotope production by TALYS

[1] MEHMET BÜYÜKTÜRKMEN Afyon Kocatepe University
[2] BEKİR ORUNCAK Afyon Kocatepe University
[3] BAYRAM DEMİR İstanbul University

Radioisotope production is an expensive and time consuming process. Influence of the cross section of the production path help. The production of radioisotopes is usually based on nuclear reactions. Reaction cross-sectional data are important in understanding nuclear reaction models and in improving the use of radioisotopes produced by these reactions. Since nuclear reactions are not known in more detail as energy dependence, the cross-sections of the effects must be examined for many energies. In this study various manufacturing nuclear reaction cross sections of many unused radioisotopes ^{131}Cs in Turkey calculated with TALYS 1.8 simulation program. The theoretical cross section of each reaction was compared with the experimental cross sections present in the EXFOR library of the International Atomic Energy Agency and the results were discussed.

Keywords: Radioisotope production, Nuclear reaction, Cross Section, TALYS 1.8

Outdoor gamma dose rates in air and assessment of cancer risk for Kocaeli province, Turkey

[1] EROL KAM Yıldız Teknik University
[2] ZEYNEP KARAALİOĞLU Yıldız Teknik University
[3] AREV ARTUN Yıldız Teknik University
[4] M. ERGÜN TURGAY Yalova University

Our study was focused to assessment of inhalation quality for Kocaeli province. In this case, radioactivity analysis in air was realized via air dose rate measurements around this region which is so closed neighbor to big city Istanbul. By measuring of the outdoor gamma dose rates on 35 stations, it was possible to get the average dose rate. Then it was calculated to annual dose in air. Besides, cancer risk was determined for Kocaeli. All these values were compared with the World's references (UNSCEAR) and assumed, finally. It was measured the average dose rate as 19.85 $nGyhr^{-1}$ and annual dose was calculated to 24.34 μSv. This dose is required to excess lifetime cancer risk as $0.7x10^{-4}$. These values could be compared to the similar studies which existed around the world. Finally, the average annual effective dose equivalent and excess lifetime cancer risk for Kocaeli, are less than the world average. This study would be used to a reference for further investigations, besides it will be usefull to compare with different studies for Kocaeli which, will be evaluated in the future, for example after a nuclear pollution, such as based on a reactor leakage, nuclear attacks, etc., too.

Keywords: Dose rate, Air, AEDE, Outdoor Gamma, Cancer Risk, Kocaeli

Sediment chronology and historical evolution of heavy metal contamination in terms of pollution index in Turkish coast, North Aegean Sea

[1] İLKER SERT Ege University

In present study, two cores and fifteen surficial sediment samples were investigated in terms of chronology and pollution levels. Lead-210 (Polonium-210) activity concentrations were measured via alpha spectrometry. Sediment dating was realized by utilizing Lead-210 (CRS, CIC) mathematical models. Residence time of the ^{210}Pb was calculated to improve the precision of the dating in North Aegean Sea. Average residence time of the ^{210}Pb is 2.4 years and average sedimentation rate is 0.237 ± 0.011 cm y-1 in the sea. Sedimentation rates along the cores display irregular increases and decreases in Ayvalik Offshore and Bakircay River Mouth stations. Metal concentrations were evaluated by using pollution indexes (EF, CF, PLI, Igeo) and Lead-isotope ratios (^{206}Pb/^{207}Pb). According the Pollution Load Index, both Ayvalik offshore and Bakircay River Mouth have shown a starting level pollution from past to nowadays but Ayvalik Offshore displayed an acute corruption in 2004. In terms of Geo-accumulation Index, both stations have Ca and Hg pollutions and both stations have had the “unpolluted to moderately polluted” pollution degree since 1995.

Keywords: Sedimentation rate, Residence time of the ^{210}Pb, PLI, Igeo, Lead-isotopes.

Study of gross alpha and gross beta activity concentration in sediments in the Büyükçekmece lake basin (Istanbul, Turkey)

[1] ZEKİ ÜNAL YÜMÜN Namık Kemal University
[2] KÜBRA BAYRAK Yıldız Teknik University
[3] DİLEK KURT Yıldız Teknik University
[4] MÜGE ŞENGÜL Yıldız Teknik University

Environmental pollution, including naturally occurring radiation is one of the most crucial issues of this century. Natural radioactivity depends directly on the regional geology, weather conditions and physic-chemical variability of the water. Industrial processes and other anthropogenic factors may also change the water's nature and raise its activity. The study of gross alpha and gross beta activity concentration in sediment cores was investigated in the Büyükçekmece Lake. The drilling sediment specimens were collected from the Büyükçekmece Lake, where is a brackish lagoon attached to the Marmara Sea, and situated at the western of the Bosphorus. The lake is adversely affected by the increase of settlements, the concentration of industrial activities in the region, the degradation of the streams flowing to it, and the cutting of the sea relation. In this study, a low-background counter (Berthold, LB 770 10 channel α−β low-level counter) counting system was used. The gross alpha activities were higher than the gross beta activities in all locations. The mean gross alpha and beta activity concentrations were 89.2± 24.87 and 431.32± 34.3 Bg kg^{-1}, respectively. The results show the sediment specimens from the Büyükçekmece Lake do not pose a significant radiological risk to the ambient area.

Keywords: Gross alpha, Gross beta, Büyükçekmece Lake, pollution, sediment

Cross-section calculations of gallium and arsenic nuclei for (n,2n) and (n,p) reactions up to 20 MeV

[1] HALİDE ŞAHAN Osmaniye Korkut Ata University
[2] MUHİTTİN ŞAHAN Osmaniye Korkut Ata University
[3] EYYUP TEL Osmaniye Korkut Ata University

In this study, neutron cross sections calculations for ^{69,71}Ga(n,2n), ^{69,7}1Ga(n,p), ^{75}As(n,2n) and ^{75}As(n,p) reactions have been calculated at the neutron energies up to 20 MeV. ALICE/ASH (GDH), TALYS 1.6, and EMPIRE codes have been used for model calculations based on the Weisskopf-Ewing and Hauser-Feshbach theories. Results from three models have been compared with in the JENDL-4.0, TENDL, JEFF-3.3, and ENDF/B-VIII.0 evaluated nuclear data libraries. The (n,2n) and (n,p) reaction cross section calculations for each nuclei have been also estimated at 14.5 MeV using semi empirical formulae developed by Lu and Fink (1971), Konno et al. (1993), Kasugai et al. (1996), Broeders et al. (2006), and Tel et al. (2003, 2008). All results of theoretical calculations were also compared with the experimental data obtained from EXFOR.

Keywords: Nuclear Reactions, cross section, ALICE, TALYS, EMPIRE, EXFOR library

(n,p) reaction cross–section calculations of fission reactor control rod materials ^{107}Ag, ^{111,112,113}Cd, ^{115}In

[1]MERT ŞEKERCİ, [2]HASAN ÖZDOĞAN, [1]ABDULLAH KAPLAN

[1]Süleyman Demirel University, Physics Dept., Isparta, Turkey
[2]Akdeniz University, Biophysics Dept., Antalya, Turkey

Abstract

Since from the industrial revolution, one of the most important and required need has always been energy. There may exists many ways to resolve day by day increasing energy demand but one of the most efficient and sustainable among them is the usage of nuclear energy. Nuclear reactors, which designed to produce energy, work with the chain fission reaction mechanism where a great amount of energy released compared to the same amount of other fuels usage. The chain fission mechanism must be controlled to keep the reactor in a steady and safe situation and this is achieved by using control rods. In this study; (n,p) reaction cross–section calculations have been done for ^{107}Ag, ^{111,112,113}Cd and ^{115}In control rod materials via using computer aided calculation tools whose usage have been tested many times and outcomes have been marked with acceptable accuracy.

Keywords: cross–section, fission reactor materials, reaction models, EXFOR

Introduction

The selection of the right material for control rod production is the first step that has to be completed under high precision and validity with very carefully. To achieve this, it is vital to have the most wide data about the possibly usable material characteristics under different circumstances and reactions. Among many many qualification criteria and variable which may be pointed under the very important topic list, one quantity that has to be noted is the reaction cross–section. The definition of the nuclear reaction cross–section could be done as the probability of a reaction's occurrence and the existence of this data provide many benefits to the researchers like avoiding from unexpected results of a reaction or arranging the amount of sample/product of the reaction. It is possible to obtain this quantity with experimental measurements and also theoretical calculations including high ordered complicated mathematics and many physical assumptions with approache when it may not be able to obtain it experimentally. This quantities experimental measurements and observaitons could also help researchers to understand the mechanism of the reaction itself. Due to many reasons such as experimental difficulties, time/cost efficiencies and/or limitations in scientific and technological situations, experimental data of this quantity may not exist for a reaction. For similar situations, there exist developed theoretical models for nuclear reaction mechanisms and computer based codes to handle the calculation with speed and validity [1]. In this study, by using two of those codes, which are names as TALYS 1.8 [2] and EMPIRE 3.2 [3], reaction cross–section calculations have been performed for ^{107}Ag(n,p)^{109}Pd, ^{111}Cd(n,p)^{111}Ag, ^{112}Cd(n,p)^{112}Ag, ^{113}Cd(n,p)^{113}Ag and ^{115}In(n,p)^{115}Cd reactions.

Theoretical Calculations

Theoretical calculations included in this study have been completed by using TALYS 1.8 and EMPIRE 3.2 codes among many other similar codes since these codes are widely used and have been validated many times for different reactions. It is possible to use both codes in UNIX/LINUX OS where EMPIRE 3.2 has a portable Windows OS version too. Both codes could calculate many properties about a reaction where the incident particle could be neutrons, photons, protons, deuterons, tritons, ^{3}He and alpha–particles. Calculations have been performed with Two Component Exciton [4] and Hauser–Feshbach [5] models from TALYS 1.8 and PCROSS exciton [3] and Hauser–Feshbach models from EMPIRE 3.2. Two Component Exciton and PCROSS exciton models could also be classified as pre–equilibrium models where Hauser–Feshbach model could be pointed as equilibrium model. Achieved results from the theoretical calculations then compared with each other, exist experimental data taken from the EXFOR [6] database and theoretical data taken from the TENDL [7] database to see the models and codes similarity.

Results

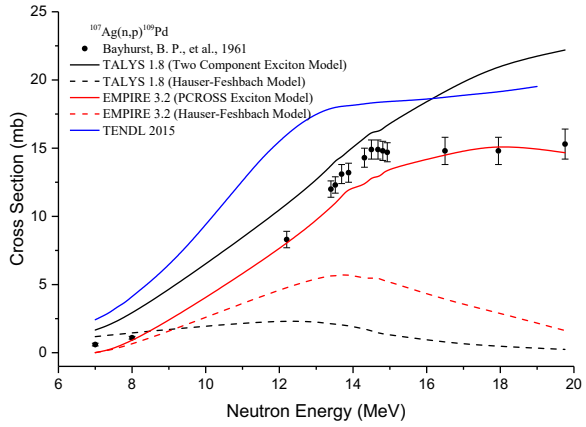

Fig. 1. ^{107}Ag(n,p)^{109}Pd reaction results.

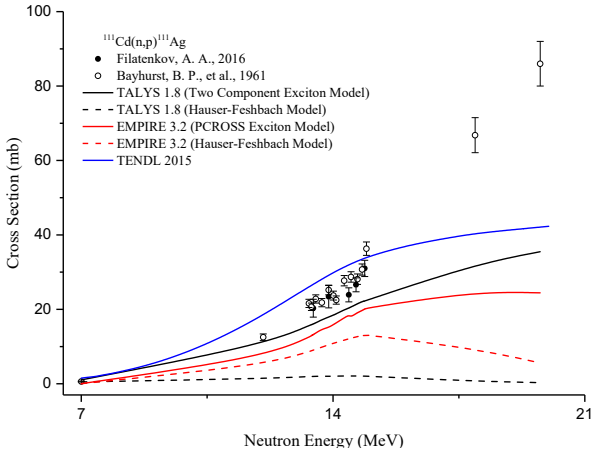

Fig. 2. ^{111}Cd(n,p)^{111}Ag reaction results.

^{107}Ag(n,p)^{109}Pd, ^{111}Cd(n,p)^{111}Ag, ^{112}Cd(n,p)^{112}Ag, ^{113}Cd(n,p)^{113}Ag and ^{115}In(n,p)^{115}Cd reaction cross–section calculations have been done by using Two Component Exciton and Hauser–Feshbach models from TALYS 1.8 and PCROSS exciton and Hauser–Feshbach models from EMPIRE 3.2 within this study and the comparison of obtained results with EXFOR and TENDL 2015 values have been given in Figs. 1-5, respectively.

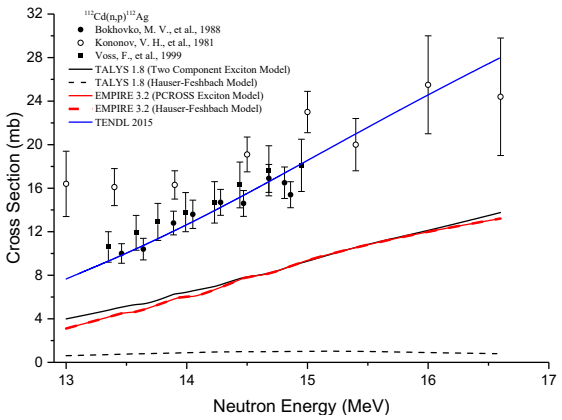

Fig. 3. ^{112}Cd(n,p)^{112}Ag reaction results.

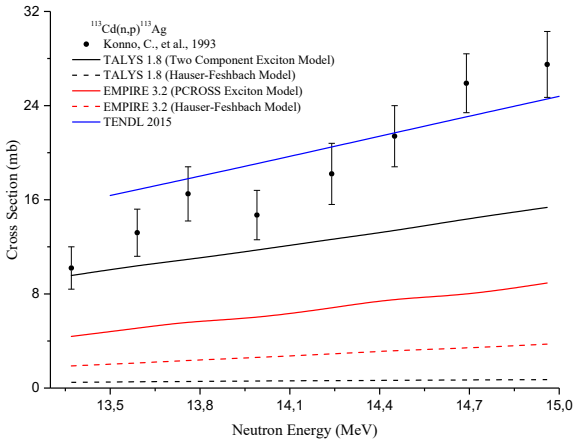

Fig. 4. ^{113}Cd(n,p)^{113}Ag reaction results.

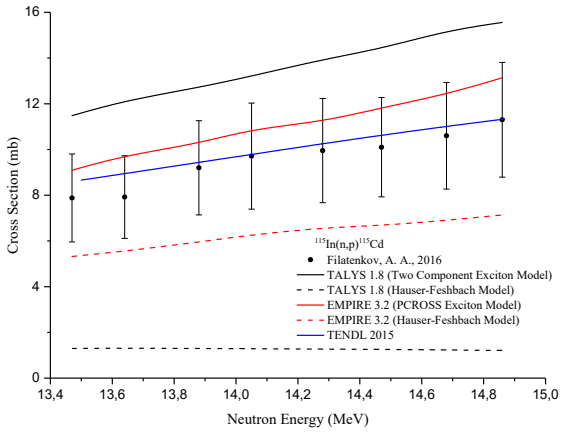

Fig. 5. ^{115}In(n,p)^{115}Cd reaction results.

Comparisons of the obtained calculations with experimental data for each reaction, display that for each investigated reaction the most suitable model is differs from reaction to reaction. For ^{107}Ag(n,p)^{109}Pd reaction, EMPIRE 3.2 PCROSS exciton model has the most harmonious model while TALYS 1.8 Two Component Exciton model has create the most acceptable shape for ^{111}Cd(n,p)^{111}Ag reaction. On the other hand, EMPIRE 3.2 PCROSS exciton and Hauser–Feshbach models almost give the same results for ^{112}Cd(n,p)^{112}Ag reaction with a quite similarity with the TALYS 1.8 Two Component Exciton results. These calculations follow the experimental data from below with the same inclination. A similar situation has also been observed for ^{113}Cd(n,p)^{113}Ag reaction yet there exist a big difference between TALYS and EMPIRE results. For the ^{115}In(n,p)^{115}Cd reaction, EMPIRE 3.2 PCROSS exciton model calculations resulted in the experimental error bars, where EMPIRE 3.2 Hauser–Feshbach and TALYS 1.8 Two Component Exciton model calculations follow the experimental data from above and below,

respectively. It could be said that, for ^{112}Cd(n,p)^{112}Ag, ^{113}Cd(n,p)^{113}Ag and ^{115}In(n,p)^{115}Cd reactions a multiplication / division factor could be investigated to make the calculations more accurate. This and similar studies may very beneficial and useful for material development studies, nuclear structure analysis, theoretical model improvements and etc.

Reference

[1] A Aydın *et al*, *Phys. Atom Nucl.* **77**, 321 (2014).

[2] A Koning, S Hilaire *and* S Goriely, TALYS–1.8 A Nuclear Reaction Program, User Manual, 1st edn. (NRG, The Netherlands, 2016).

[3] M Herman *et al*, EMPIRE-3.2 Malta Modular System for Nuclear Reaction Calculations and Nuclear Data Evaluation, User's Manual (2013).

[4] C Kalbach *Phys. Rev. C.* **33** 818 (1986).

[5] W Hauser *and* H Feshbach, H *Physical Review* **87** 366 (1952).

[6] Brookhaven National Laboratory, National Nuclear Data Center, EXFOR/CSISRS (Experimental Nuclear Reaction Data File). Database Version of 2018-04-11 (2018). (http://www.nndc.bnl.gov/exfor/)

[7] TENDL (Nuclear Data Library), Version 2015, Access: 11.03.2018. https://tendl.web.psi.ch/tendl_2015/tendl2015.html

(n,2n) reaction cross–section calculations of some Cd isotopes

[1]MERT ŞEKERCİ, [2]HASAN ÖZDOĞAN, [1]ABDULLAH KAPLAN

[1]Süleyman Demirel University, Physics Dept., Isparta, Turkey
[2]Akdeniz University, Biophysics Dept., Antalya, Turkey

Abstract

In this study; theoretical reaction cross–section calculations have been completed for (n,2n) reactions on ^{106,108,110,116}Cd isotopes of cadmium in which the material has a great number of known and investigating usage probability in scientific and industrial areas. Calculations have been performed with the TALYS 1.8 code by using Two Component Exciton and Hauser–Feshbach models and EMPIRE 3.2 code by employing PCROSS exciton and Hauser–Feshbach models. To comment about the obtained results from TALYS 1.8 and EMPIRE 3.2, calculations have been compared to the exist experimental and theoretical data from the literature. EXFOR database have been used to access the experimental values while TENDL 2015 database have been used to access the theoretical values.

Keywords: cross–section, cadmium, TALYS, EMPIRE, EXFOR

Introduction

Cadmium; is a silver metal with a bluish metal surface and is a toxic substance. It's melting point is 321,069 °C, atomic number is 48 and the density is 8,69 g/cm^3. Initially, cadmium was used in many industrial fields, mainly in batteries and CRT type televisions, however after proving the negative results of its toxic properties it started to be used in a limited number of areas such as nuclear reactor control rods [1]. The correct material selection for the production and development of critical components like control rods is very important. Knowing all the possible properties of the material in such cases have vital importance since it is only possible to avoid unwanted situations or unexpected results by gathering all possible data about the material itself. Reaction cross–section could be explained as the possibilty of a reaction's occurance probability and gives many useful information and estimation to the researchers. This quantity could be measured by experimentally or could be calculated theoretically by using validated theoretical nuclear reaction models.

There exist different models to clarify the different reaction mechanisms and these models contain highly complex mathematical expressions and steps. To be able to use these models with high accuracy and time efficiently, many computer-based codes have been developed. By this way, it is also possible for researchers to study a reaction where the experimental data are absent since the data obtained from the validated codes may provide an acceptable foresight [2]. In this study, reaction cross–section calculations have been done for ^{106}Cd(n,2n)^{105}Cd, ^{108}Cd(n,2n)^{107}Cd, ^{110}Cd(n,2n)^{109}Cd and ^{116}Cd(n,2n)^{115}Cd reactions by using TALYS 1.8 [3] and EMPIRE 3.2 codes [4].

Theoretical Calculations

Experimental data are inaccessible in situations where experiments can not be performed due to some experimental difficulties, such as time and money efficiency concern or similar obstacles. The existence of acceptable data and estimations of a nuclear reaction, which would like to be investigated in such cases, are of utmost importance. To provide these important data, computer based calculation programs have been developed and these programs can meet different needs by performing many various calculations with high accuracy thanks to their ability to make calculations according to the different nuclear reaction models they contain. In this study, to investigate the (n,2n) reaction cross–section calculations for some Cd isotopes, Two Component Exciton [5] model from TALYS 1.8 and PCROSS exciton [4] model from EMPIRE 3.2 have been employed as pre–equilibrium models where Hauser-Feshbach [6] model from TALYS 1.8 and EMPIRE 3.2 has been selected to perform equilibrium model calculations. It is also possible to investigate the effects of different models, parameters, variations and optimisations on nuclear reactions and reaction mechanism by using TALYS 1.8 and EMPIRE 3.2.

To comment about the obtained results from TALYS 1.8 and EMPIRE 3.2, calculations have been compared to the exist experimental and theoretical data from the literature. EXFOR [7] database have been used to access the experimental values while TENDL [8] database have been used to access the theoretical values.

Results

In this study; it is aimed to obtain the (n,2n) reaction cross–section calculations of some Cd isotopes, where the Cd is very commonly used for the nuclear reactor control rods beside other many industrial and scientific usage areas, and compare the resulting calculations with the existing experimental and theoretical values from the literature.

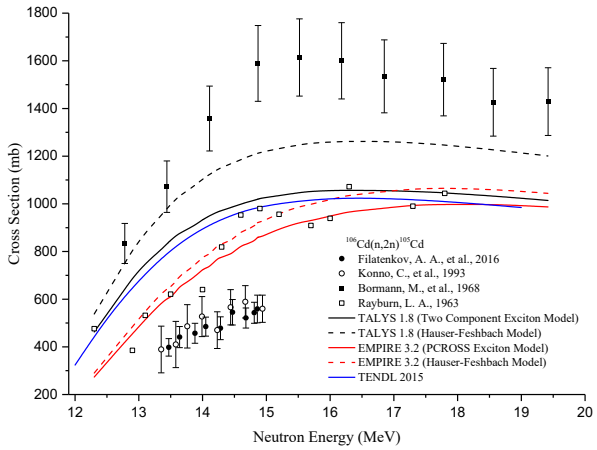

Fig. 1. ^{106}Cd(n,2n)^{105}Cd reaction results.

In order to reach the main aim within this study, the calculations have been done by using Two Component Exciton and Hauser–Feshbach models from TALYS 1.8 and PCROSS exciton and Hauser–Feshbach models from EMPIRE 3.2 where TALYS 1.8 and EMPIRE 3.2 are computer aided calculation tools with a high accuracy and approval rate by the literature. Obtained results of reaction cross–section calculations for ^{106}Cd(n,2n)^{105}Cd, ^{108}Cd(n,2n)^{107}Cd, ^{110}Cd(n,2n)^{109}Cd and ^{116}Cd(n,2n)^{115}Cd reactions have been compared with the experimenal values taken from EXFOR and theoretical values taken from TENDL 2015 databases. All comparisons have been given in Figs. 1-4.

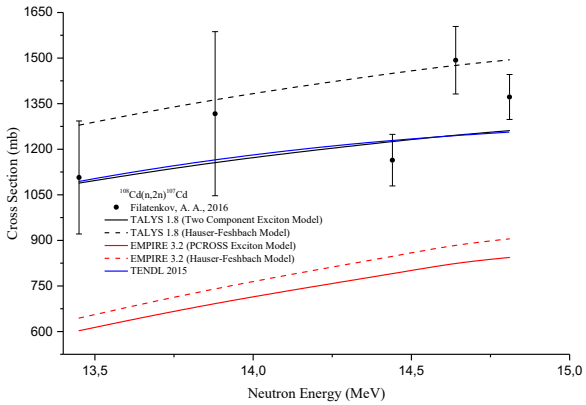

Fig. 2. ^{108}Cd(n,2n)^{107}Cd reaction results.

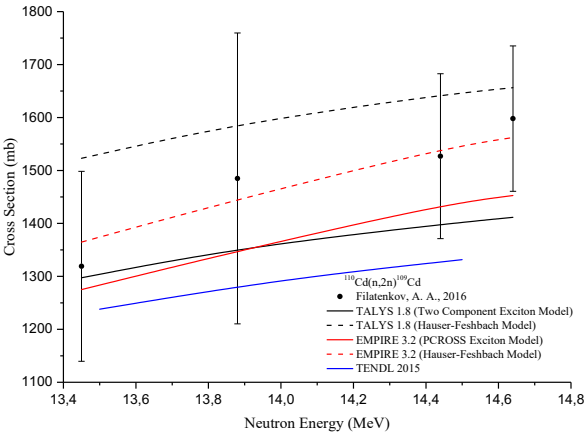

Fig. 3. ^{110}Cd(n,2n)^{109}Cd reaction results.

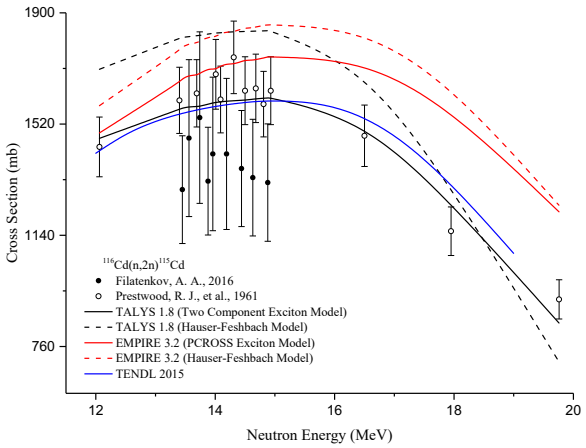

Fig. 4. ^{116}Cd(n,2n)^{115}Cd reaction results.

All model results gave similar geometries with the experimental data for each reaction calculation that are performed separately for itself. For ^{106}Cd(n,2n)^{105}Cd reaction, EMPIRE 3.2 PCROSS exciton model has the best agreement with Rayburn, L. A., 1963 [9] values while TALYS 1.8 Hauser–Feshbach model has the best agreement with Bormann, M., et al., 1968 [10] values. For ^{108}Cd(n,2n)^{107}Cd reaction, TENDL 2015 and TALYS 1.8 Two Component Exciton results have been obtained as almost as the same to each other. In the ^{110}Cd(n,2n)^{109}Cd reaction, EMPIRE 3.2 Hauser–Feshbach calculations have the best agreement with the experimental data. For ^{108}Cd(n,2n)^{107}Cd and ^{110}Cd(n,2n)^{109}Cd reactions, a multiplication/division factor could be suggested. For ^{116}Cd(n,2n)^{115}Cd reaction, in the all investigated energy region all models give similar shapes yet the most compatible shape has been generated by TALYS 1.8 Two Component Exciton Model calculations. From the outcomes of this study, it could be said that these kind of studies have incontrovertible contribution to both the material and the reaction mechanism studies. Moreover, it is also possible to create new databases or strengthen the exist ones by using the obtained data from the calculations.

Reference

[1] Royal Society of Chemistry (RSC), Periodic Table. Access Date: 25.03.2018. http://www.rsc.org/periodic-table

[2] A Kaplan *et al*, *Indian J. Phys.* **85**, 1615 (2011).

[3] A Koning, S Hilaire *and* S Goriely, TALYS–1.8 A Nuclear Reaction Program, User Manual, 1st edn. (NRG, The Netherlands, 2016).

[4] M Herman *et al*, EMPIRE-3.2 Malta Modular System for Nuclear Reaction Calculations and Nuclear Data Evaluation, User's Manual (2013).

[5] C Kalbach *Phys. Rev. C.* **33** 818 (1986).

[6] W Hauser *and* H Feshbach, H *Physical Review* **87** 366 (1952).

[7] Brookhaven National Laboratory, National Nuclear Data Center, EXFOR/CSISRS (Experimental Nuclear Reaction Data File). Database Version of 2018-04-11 (2018). (http://www.nndc.bnl.gov/exfor/)

[8] TENDL (Nuclear Data Library), Version 2015, Access: 11.03.2018. https://tendl.web.psi.ch/tendl_2015/tendl2015.html

[9] L A Rayburn *Bull. Am. Ph. Soc.* **8**, 60 (1963).

[10] M Bormann *et al*, *Nucl. Phys. A* **115**, 309 (1968).

Calculation of the in-air output factors of 6mv photon beam of a medical linear accelerator by means of photon phase spaces attained by the GEANT4/GATE simulation

[1] HEDİYE ACUN BUCHT Harran University, Faculty of Medicine, Department of Biophysics Medical Radiation Physics
[2] DAVID BOERSMA Uppsala University, Medical Radiation Sciences, Institute for Immunology, Genetics and Pathology Medical Radiation Physics
[3] ANDERS AHNESJÖ Uppsala University, Medical Radiation Sciences, Institute for Immunology, Genetics and Pathology Medical Radiation Physics

In-air output factor (S_c), also known as collimator or head scatter factor, is an important quantity in radiotherapy as it indicates the variation of the photon beam fluence relative to the collimator settings. This parameter is measured with ion chambers or diodes with build-up cap in the air at SAD distance. It is challenging to measure S_c for the small field sizes due to the lack of electronic equilibrium and volume averaging effect of the detectors. AAPM TG-74 report formalizes S_c as a ratio of collision water kerma in free-space per MU for a field size of interest to that for reference field. In this study we aim to calculate S_c factors of a 6 MV photon beam for different collimator settings based on the collision kerma formalism, as described in TG-74, using photon phase spaces generated with Geant4/GATE simulations. 6 MV photon beam of Elekta Synergy linac was simulated with Geant4/GATE. Photon phase spaces at SAD distance were generated for four different collimator settings. Collision kerma was calculated by integrating the photon energy fluence with its mass energy absorption coefficient over the phase space. S_c values of the field sizes in question were calculated from the ratios of the collision kerma values and compared with those measured with RK-chamber. S_c values of 5x5, 15x15, 20x20 and 40x40 cm^2 fields were calculated as 0.975, 1.012, 1.016 and 1.020 respectively. Difference between the measured and calculated Sc quantities was found to be less than 1% for all involved fields. There is good consistency between the calculated and measured in-air output factors. The collision kerma formalism based calculation method of S_c can be used for the derivation of the S_c values for small photon beams as a further step of this study.

Keywords: In-air output factor,collision kerma,Monte Carlo, AAPM TG-74

The radiation dose measurements on linear accelarator (linac) unit, produces high energy x-rays

[1]AYSUN İNAL, [2]İSKENDER AKKURT

[1]Antalya Eğitim ve Araştırma Hastanesi, Antalya, Turkey
[2]Süleyman Demirel University, Physics Dept., Isparta, Turkey

Abstract

Linear accelerator is one of the most effective device to be used in radiotherapy. In linac, high energy X-rays (photon) is produced by impinging electrons into high-Z materials. Photon radiotherapy is a treatment method where X-rays produced to destroy cancerous cells by ion creation feature in tissue. Unfortunatelly, none of the tumors are alone, there is certainly a vital organ nearby. While giving the maximum dose to the tumor, it is very important to minimize the dose around the health tissues. For this purpose, the most important development technique in radiatiotherapy is the intensity modulated radiation theraphy (IMRT). This technique requires a special quality control procedure due to the its complexity and challenges. Material and Methods: In this study, the required dose measurement parameters were obtained for 6 and 18 MV photon beam of energy which were used by photon radiotherapy. Various geometric and dosimetric analysis of the device were done using different ion chambers, 2D measurement system(Matrixx) and the X-Omat V films. The measured results were compared with the calculated results by Treatment Planning System (TPS). Gamma evaluation index was used while comparing results. Discussion and Conclusion: The results show the correct quality control tests and limits which should be performed at the starting of IMRT. Radiotherapy clinics should establish quality control procedures in accordance with international protocols, before and during the ongoing IMRT implementation. In the quality control, the appropriate dosimetric measurement method should be determined for each test.

Keywords: IMRT, Quality Control, radiotherapy

Introduction:

The aim of radiotherapy is to protect the healthy tissues while giving the desired dose to the target volume. One of the most important radiotherapy techniques is Intensity Modulated Radiation Therapy (IMRT). IMRT is a complex treatment. Many problems such as small fields, change of photon out-put, irradiation problems in small Monitor Units (MU), design and quality controls of Multi Leaf Collimator (MLC) has to be solved before IMRT applications. IMRT dosimetric and geometric quality controls are classified; Acceptance, commissioning and routine control.

IMRT requires many procedures such as patient selection, immobilization, target and tissue definition, treatment planning, evaluation, and treatment. Accurate and complete implementation of the quality assurance program is essential in implementing a safe IMRT. Some quality control tests are required before starting IMRT. The first one is the geometric and dosimetric controls on the Linear Accelerator (Linac)

In this study, the tests to be performed for the control of open field percent deep dose (PDD), open field profile curves (BP) field flatness (F), field symmetry (S), MLC position accuracy and repeatability of leaf positions are planned. In addition, dosimetric tests such as Linac performance (Linearity) in small MUs, leaf transmission of MLCs, leakage between MLCs, dose control in small fields and appropriate control for clinical cases have been calculated and measured.

Material and Methods

In this study, the percent depth doses (PDD) at different field sizes and the beam profiles (BP) at different depths were measured by water phantom (Scanditronix Wellhöfer Ġba Marka RFA-300) in Elekta SynergyTM Platform model linear accelerator. Measurements were done using 6 and 18 MV photon energies. The measurement results were evaluated and then transferred to the Treatment Planning System (Elekta PrecisePLAN R2.15 model). After the measurements were modeled in TPS, the plans according to the selected setups (Figure 1-4) were prepared and calculated. The calculations were

compared with the measurements taken in the selected setups using the radiographic film (Kodak X-Omat V (XV)) and the 2D array (IBA I'mRT matrix) in the Linac.

The 2D array (Matrixx) used in the study consists of parallel plane 1020 detectors. Above the detector 3.3. mm water equivalent material available. The distance between the centers of the parallel-ion ion chambers is 7.62 mm, the each of the volume is 0.08 cm^3. Film measurements were processed using an Epson 10000XL film scanner. The comparison was performed using the Gamma evaluation method. With this method, a comparison can be made between the two measurement techniques or the measured-calculated results. Comparison was made between ΔDm = %3 ve Δdm = 3 mm acceptance criteria.

In the study, four different sets were established. Calculations and measurements were made in these arrangements. While, the Gantry(G) and collimator angle (C) was '0'; The detectors were placed at 5 cm for SET A (source- surface distance (SSD) 100 cm) and SET B (SSD, 95cm). SETA and SETB are shown in figures 1 and 2, respectively. Also, the detectors were placed at 2 cm at SSD 98 cm for SET C (G=0˚) and SETD (G=90˚). SETC and SETD are shown in figures 3 and 4, respectively.

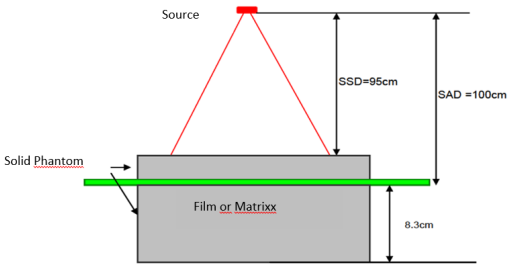

Figure 1: SETA

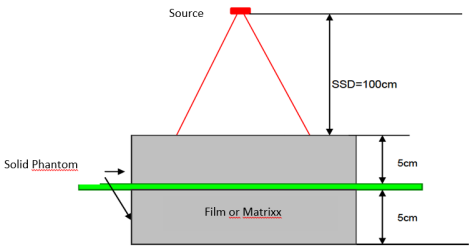

Figure 2: SETB

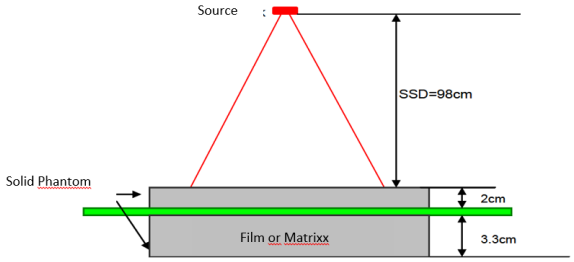

Figure 3: SETC

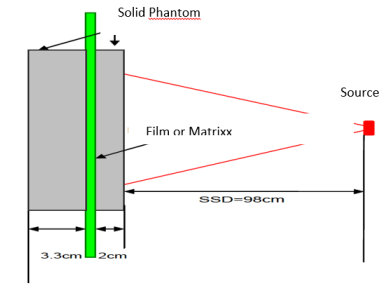

Figure 4: SETD

The transmission and leakage tests for MLC; The 1000 MU irradiation was performed at 10x10 cm^2 field size on SETA. Then, the beam center was completely closed and the irradiation was repeated for the same time.

Position accuracy and reproducibility of MLC position; The adjacent fields (2 cm) to each other were irradiated with 30 MU. Before irradiation, the position of each MLC was checked on the graph paper. For SETC and SETD, the differences due to the collimator angle were examined.

For the MLC reproducibility test; MLCs located at the center (right(CR) and left(CL)), 4 cm above the center (right(ACR) and left(ACL)) and 4 cm below the center (right(BCR) and left(BCL)) were sent to the defined points. Measurements were made according to setA. Each MLC was sent to the same point 20 times.

Whether the MLC went to the same position was checked both on paper and with EPID. Measurements were taken with Matrixx for each step. In addition, a measurement was taken for each position with the film. Figure 5 shows the MLC positions on the right and the EPID image on the center axis.

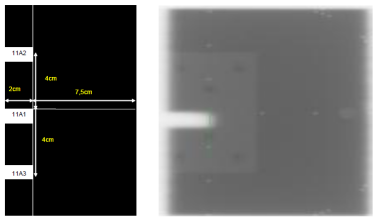

Figure 5: MLC positions on the right and the EPID image on the center axis.

The other test for MLC position accuracy; The stairs was arranged according to SetC and it was aimed to find whether the MLC positions were as planned. The measurement results were compared with calculated ones.

Small Field size test; Measurements were taken for 1x20 and 2x2 cm^2 field sizes according to SetA. Comparisons were made according to measurement techniques.

A field and multiple segments test; According to the SetA, a single field composed of 3 segments was irradiated. Differences between film and matrixx were calculated according to gamma evaluation. In the other test, different MUs were selected for each segment and a field composed of approximately 121 segments was created. Gamma evaluation was performed according to Film-Matrixx measurement results.

Linac performance for small units (Linearity); The dose rate was set at 400 MU / min. Measurements were taken for SSD 100 cm, 10 cm depth and 10x10 cm^2 field size. Provided that the total MU is 200, a plan was created to allow the device to be irradiated with small MUs (1MU ile 200MU). Each measurement was repeated 3 times. The average of three measurements for each MU was found. The 200 MU was taken as reference MU. The linearity of the other output data according to the reference was calculated.

Results

The percent deep doses(PDD) at different field sizes are shown in Figure 6. All measurements were transferred to TPS.

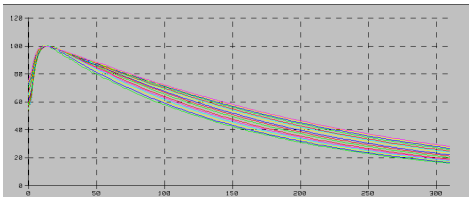

Figure 6: The PDD measurement curves of 1x1 - 40x40 cm^2 square field sizes for 6MV

The films were calibrated for 0, 10, 25, 50, 75, 100, 125, 150, 175 and 200 cGy doses prior to measurements. Figure 7 shows a graph of the dose (cGy) corresponding to the optical density (OD).

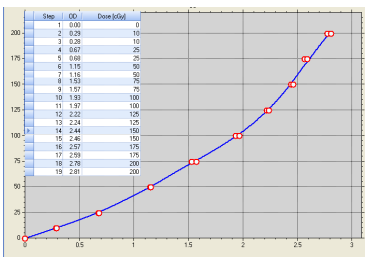

Figure 7: Dose (cGy) graph corresponding to optical density (OD) for X-Omat V film

The measurement result for MLC leakage and transmission test is shown in figure 8. According to the results, the average transmission and leakage of the leaf was found to be 1.9%. and 2.1%, respectively.

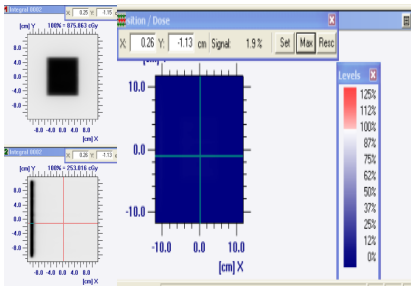

Figure 8: MLC transmission and leakage measurements

According to the film results, the angle-dependent variation of the MLC is shown in Figure 9. The gamma evaluation was found to be within the 99.66%.

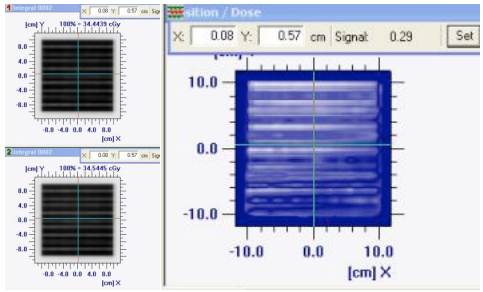

Figure 9: The angle-dependent variation of the MLC for film measurement

The measurements taken at the defined positions and the gamma evaluation for the left center are shown in figure 10. From the calculated - measured comparisons, the gamma evaluation results were found 96%. Calculated and measured percent MLC edge doses are shown in table 1.

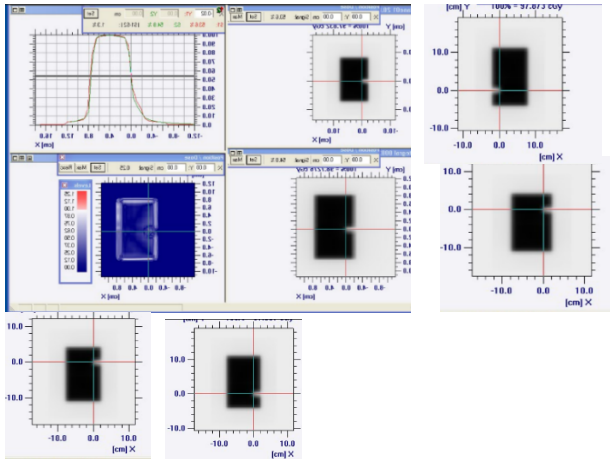

Figure 10: The measurements taken at the defined positions and the gamma evaluation for the left center

Table 1. MLC Edge Dose %

	CR	CL	ACR	ACL	BCR	BCL	Mean
TPS	53.6	52.4	53.1	52.4	51.7	51.2	51.2
Matrixx	54.8	52.1	49.0	51.2	50.2	51.6	51.5
Film	52.4	51.9					52.14

For small field sizes, Film-Matrix comparisons were done. All comparisons were found in 100% according to the results of gamma evaluation. The figure 11 shows film-matrix comparisons of 2x2 cm^2 (a) and 1x20cm^2 (b) field sizes.

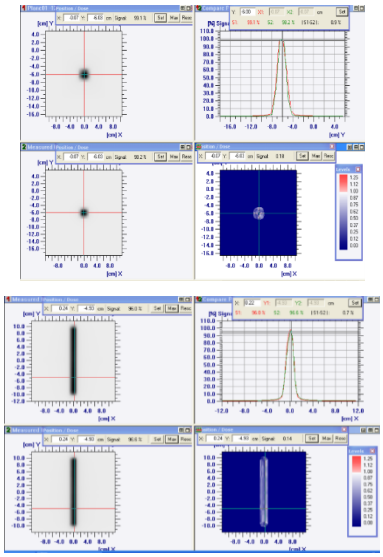

Figure 11: The film-matrix comparisons of 2x2 cm^2 (a) and 1x20cm^2 (b) field sizes

Figure 12 shows the stair test and TPS-film comparison for the accuracy of MLC positions.

It was found in 99.5% according to Gamma evaluation.

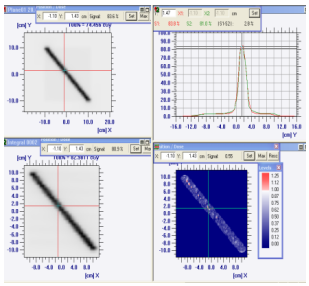

Figure 12: TPS-film comparison for the accuracy of MLC positions.

Figure 13 shows the Film-Matrixx comparison according to the single-field and 3-segment arrangement. The Gamma evaluation was found 99.89%.

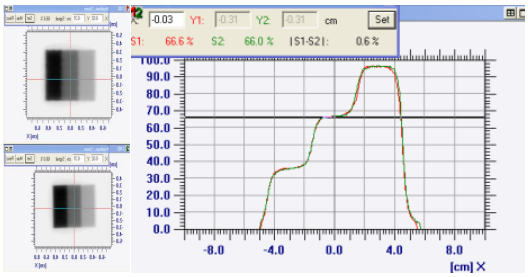

Figure 13: Film-Matrixx comparison according to the single-field and 3-segments

Figure 14 shows the Film-Matrixx comparison according to the single-field and 121-segments arrangement. The Gamma evaluation was found 98.47%.

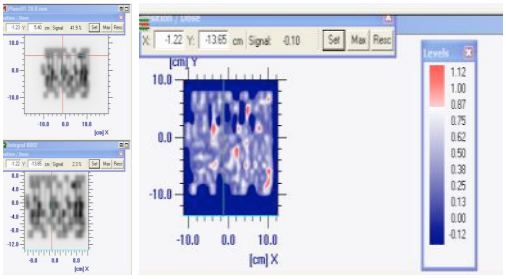

Figure 14: Film-Matrixx comparison according to the single-field and 121-segments

The table of measurements taken for the MU linearity of Linac device is shown below (table 2). According to the results, the device was found to be non-linear for 1 MU (3.8%).

6 MV		X times														
X x Y MU		1	2	3	4	5	6	7	8	10	15	20	30	50	Mean	L
y MU	1 MU	6,76	6,76	6,74	6,77	6,75	6,75	6,74	6,73	6,76	6,72	6,75	6,73	6,74	6,74	3,8
	2 MU	6,69	6,69	6,68	6,68	6,68	6,69	6,67	6,68	6,66	6,65	6,67	6,67	6,68	6,68	2,7
	3 MU	6,65	6,40	6,65	6,62	6,64	6,63	6,63	6,64	6,64	6,64	6,64	6,63	6,64	6,62	1,9
	4 MU	6,63	6,63	6,63	6,62	6,62	6,63	6,63	6,63	6,63	6,62	6,64	6,62	6,63	6,63	2,0
	5 MU	6,63	6,62	6,63	6,63	6,63	6,62	6,62	6,62	6,62	6,62	6,62	6,61	6,60	6,61	1,8
	6 MU	6,62	6,63	6,62	6,63	6,62	6,63	6,60	6,62	6,62	6,62	6,62	6,61		6,62	1,9
	7 MU	6,61	6,60	6,60	6,61	6,61	6,61	6,61	6,60	6,59	6,00	6,60	6,60		6,62	1,9
	8 MU	6,58	6,60	6,58	6,59	6,59	6,60	6,60	6,58	6,59	6,59	6,58	6,58		6,59	1,4
	10 MU	6,54													6,54	0,7
	15 MU	6,53													6,53	0,4
	20 MU	6,52													6,52	0,3
	30 MU	6,52													6,52	0,3
	50 MU	6,51													6,51	0,2
	100 MU	6,50													6,50	0,1
	200 MU	6,50													6,50	0,0

Discussion

Priority tests for MLC are listed as leaf position accuracy and reproducibility, beam stability (output, symmetry, flatness), linearity for low MU, leaf leakage and transmission [1]. The use of ion chambers, film and two-dimensional array is common in tests for IMRT. One of the radiographic films used in radiotherapy is Kodak X-OMAT V (XV) and the other is EDR film [2]. However, the storage of such films, bathing, screening and processing are the processes that require attention [3]. It has been reported that the film and diode array are compatible and give accurate results [4]. The film has high precision, good spatial resolution, small size and easy to use [5].

The transmission of MLCs is very important in IMRT. Because MLC exchange in given MU is much more than three-dimensional treatment. In a study with the Elekta device, MLC leaf transmission and leakage were found

to be 1.8% ± 0.1% and 2.1% ± 0.2% [6-7]. Bayouth et al reported that IMRT requires MLC leaf position accuracy and long-term repeatability [8]. It has been reported that the 0.5 mm change in position may cause a 5% dose difference [9]. This is especially important in terms of gravity. The movement of the MLCs in the irradiated area in IMRT requires a change in the intensity of the beams [11]. Therefore, penumbra validation is critical [12]. The dosimetric accuracy of the plan depends on the accuracy of the penumbra. Acceptance limits in IMRT evaluation were given %5 with ion chamber and 3% with film dosimetry for low-gradient - high-dose region, Whereas, the limits were defined 10% for high-gradient - low dose regions [13]. In such areas, the condition should be evaluated clinically.

Conclusion

The IMRT technique used in radiotherapy is knowledge, care, attention and good team work. This study summarizes the quality assurance tests that medical physicists can perform before the starting of IMRT. Tests can be chosen and applied from simple to complex. First of all, MLC controls should be done precisely and the calibration should be repeated if necessary. Once the small fields and small MU controls are completed. After, it can be continued with a single-segment field beam. Then, single-field multiple segments can be selected. Matrixx and film measurement results, which are used in the study, are generally found to be compatible with both each other and the calculated values. According to these results, it can be said that the use of Matrixx in periodic controls and patient quality control may be sufficient. However, it is recommended that film measurements be used both before starting IMRT and in 6 month periods.

References

1. Moran A., Vijayan K., Aroumougame R,. Alkins R., 2005. Dosimetry Metrology For IMRT. Medical Physics, Vol. 32,(1)
2. Chetty I. J., Charland P.M., 2002. Investigation of Kodak extended dose range (EDR) film for megavoltage photon beam dosimetry. International Journal of Radiation Oncology Biology Physics 47, p. 3629–3641.
3. Childress N. L., Dong L., 2002. Rapid radiographic film calibration for IMRT verification using automated MLC fields. Journal of Medical Physics 29, p. 2384–2390.
4. Papatheodorou S., Rosenwald J.C., Zefkili S., Murillo M., Drouard J., Gaboriaud G., 2000. Dose calculation and verification of intensity modulation generated by dynamic multileaf collimators. Medical Physics, 27(5), P. 960-971.
5. Zhu X.R., Jursinic P.A., Grimm D.F., Lopez F., Rownd J.J., Gillin M.T., 2002. Evaluation of Kodak EDR2 film for dose verification of intensity modulated radiation therapy delivered by a static multileaf collimator. Medical Physics, 29(8).
6. Pasquino M., Borca V., Catuzzo1 P., Ozzello F., Tofani S., 2006. Transmission Penumbra and leaf position accuracy in commisioning and quality assurance program of a multileaf collimator for step and shoot IMRT treatments. Tumori, 92 p.511-516.
7. Venencia C.D., Besa P., 2004. Commissioning and quality assurance for intensity modulated radiotherapy with dynamic multileaf collimator: Experience of the Pontificia Universidad Católica de ChileExperience of the Pontificia Universidad Católica de Chile Journal of Applied Clinical Medical Physics, 5(3), p. 37-54.
8. Bayouth J. E., Wendt D., Morrill S. M., 2003. MLC quality assurance techniques for IMRT applications. Medical Physics 30 (5).
9. Low J., Sohn E., Klein J., Markman S., Dempsey J. F., 2001. Characterization of a commercial multileaf collimator used for intensity modulated radiation therapy. Medical Physics, 28, p. 752–756.
10. Chen Y., Boyer A. L., Ma C. M., 2000. Calculation of x-ray transmission through a multileaf collimator. Med. Phys. 27, p. 1717–1726.
11. Mohan R., Arnfield M., Tong S., Wu Q., Siebers J., 2000. The impact of fluctuations in intensity patterns on the number of monitor units and the quality and accuracy of intensity modulated radiotherapy. Medical Physics, 27, p. 1226–1237.
12. Ezzel G., Galvin J., Low D., Palta J., Rosen I., Sharpe M., Xia P., Xiao P., Xing L., Yu C., 2003. Guidance document on delivery, treatment planning, and clinical implementation of IMRT: Report of the IMRT subcommittee of the AAPM radiation therapy committee. Medical Physics 30(8) p. 2089-2115.
13. Cheng W., Das I. J., 2002. Comparison of beam characteristics in intensity modulated radiation therapy IMRT and those under normal treatment condition. Journal of Medical Physics 29, p. 226–230.

Medical imaging from analog to digital systems: A review

[1] NİNA TUNÇEL Akdeniz University Medical Physics

Along last century, the medical image acquisition highly changes from analog (X-ray screen film) to digital systems (CR, DR and DDR) regarding to growing of digital technology. In the early years the screen-film systems involved manual developing processor and then it changes with automated film processor. Both of them require long working time and special room (dark room). The invention and continuously improving of computed tomography (CT) scanner firstly lead the medical imaging to digital processor in 1970. In 1990, the invention of magnetic resonance imaging (MRI) was established and the requirements of digital processors in the medical imaging strongly arise. Generally, the imaging in diagnostic radiology is rooted in three solutions of diagnostic data acquisition. There are sequentially approaches. The first is analogue systems. The second is computed radiography. The later is direct digital systems (DR) and indirect digital systems (DDR). These detector systems offer excellent image quality and realistic options for dose reduction based on their high dose efficiency. Important tools to describe the physical performance of a detector system that ultimately determines image quality are dynamic range, spatial resolution and dose efficiency. There are many software products that use similar algorithms such as edge enhancement, noise reduction, and contrast enhancement to alter the appearance of the image. It is used to improve image quality by reducing noise, removing technical artefacts, and optimizing contrast for viewing. Spatial resolution is not improved by the processing software because it is dependent on the technical properties of the detector (eg, pixel size). Second revolution in digital imaging has been accompanied by the adoption of picture archiving and communication systems (PACS), which provide electronic storage, retrieval, distribution, and presentation of images from the radiology department.

Keywords: Medical imaging, Analog and digital systems

Recent developments in medical imaging

[1] HÜLYA ÖZDEMİR Akdeniz University
[2] NİNA TUNÇEL Akdeniz University

The main aim of this study is to present the most important recent developments in medical imaging. Technological inventions and developments have created new possibilities in medical diagnostics. Diagnostic imaging is an invaluable tool for medical science today. While medical imaging has been advancing by introduction of new imaging modalities and methodologies as cone-beam/multi-slice scanner, positron-emission tomography, magnetic resonance imaging with diffusion-weighted, current modulation tomography and diffuse optical tomography. So, the new machine-learning algorithms/applications are demanded in the medical imaging field. Algorithms for finding outlines of anatomical structures and other areas of interest are called image segmentation or image segmentation algorithms. Partitioning methods vary depending on a particular application, imaging method, and other factors. Such as, the division of brain and liver tissues needs different methods. In addition, the motion also creates serious effect on the performance of partitioning algorithms. Till now, there are many different partitioning algorithms created for partition medical images to give reasonable results. Some of them are thresholding approaches, region growing approaches, classifiers, and clustering algorithms. The partitioning algorithms restrictedly used in ultrasound imaging. With a development of new imaging based on physiologic function, the requirements for image processing and analysis of acquire images of physiologic function rather than of anatomy is increasing. The recent advances in medical imaging lead to high accuracy in images for better diagnosis of patient. The steady progress on development in multi-modal imaging, dynamic imaging, and diagnostic imaging have been increased not only with ionizing radiation but also with non-ionizing radiation.

Keywords: imaging, medical imaging

Calculation of radiological properties of iodine compounds contrast agents (iodixanol, iohexol, iopamidol, iopromide, ioxagalete)

[1] TAHİR ÇAKIR Yüzüncü Yıl University
[2] BERNA OTO Yüzüncü Yıl University

Ussually contrast agents are used in computed tomography (CT) for tissue imaging in clinical applications. X-ray attenuating contrast media containing atoms of high atomic number are used in clinical applications to obtain images of soft tissues. To generate images with the highest contrast to the surrounding tissue, the energy of the X-ray source can be adjusted to closely match the absorption edge value (k) of the relevant imaging-agent atoms. In this study, the possibility of photon interactions with 5 diffrent iodines (compounds) have been calculated in the wide energy range of 1keV–100GeV using WinXCOM computer program. The variations of mass attenuation coefficient (μ_ρ), effective atomic number (Z_{eff}) and electron density (N_{el}) with photon energy were plotted for total photon interactions. It has been observed that although all compounds have the same type of elements, the variation of the atom numbers in the compound changes the values of μ_ρ, Z_{eff} and N_{el}. The variation of theoretical μ_ρ, Z_{eff} and N_{el} values with energy can be explained by the predominance of different interaction mechanism of photons with compounds. In 0.01MeV-0.1MeV energy range, photoelectric absorption effect, whose cross section depends on Z_{4-5} is dominant process and μ_ρ, Z_{eff} and N_{el} values of the samples are the highest. In this energy range, a few jumps in the calculated values have been observed due to the presence of K, L and M absorption edges of the I element (33.16, 5.18, 4.85, 4.55 and 1.07 keV). In 0.1-3MeV energy range, Compton scattering becomes more dominant. Compton scattering cross section varies with Z and μ_ρ, Z_{eff} and N_{el} values decrease gradually and become the lowest. In 10MeV < E, the pair production becomes dominant. Finally, the values of μ_ρ, Z_{eff} and N_{el} increase and become constant at around 100MeV energy. The μ_ρ, Z_{eff}, N_{el} values of compounds were given comparatively with each other for medical imaging applications.

Keywords: Effective atomic number,mass attenuation coefficient,iodine contrast agent

Node locator: An intraoperative gamma camera

[1] ASUMAN KOLBAŞI Göztepe Training and Research Hospital
[2] ONUR KARAMAN Akdeniz University

The definition of a sentinel lymph node (SLN) is the first lymph node to which cancer cells are most likely to spread from a primary tumour. In some cases, there can be more than one sentinel lymph node. Before the biopsy or surgical removal practices, to know if there is one (or more) sentinel lymph node and the location is important. For this reason, patients are guided to the Nuclear Medicine for preoperative lymphoscintigraphy via peritumoral intradermal injection of Tc-99m radio-pharmaceuticals. In surgery, a mobile gamma probe is used to find the location of SNL and after surgery residual tissue controls also. In this study, a mobile intraoperative gamma ray detector has been designed to define the SNL and the exact location of it in the tissue. Three photomultiplier arrays covering three sides of a cube shaped scintillation material will be used for detection. The XY coordinates of the SNL will given by the array at the bottom of scintillator and the arrays located on sides, will give the Z coordinate (depth). Since the penetration in a material is proportional to the energy of gamma rays, the depth of the source in tissue can be found with this method. The radiation matter interaction calculations is carried out with using Monte Carlo method. A GEANT4 based framework GAMOS is used for the first trials of the simulations to evaluate the mechanism in theoretical aspect.

Keywords: Medical Physics, Radiation Detetor, Gamma Camera, Scintillator, Sentinel Lymph Node, Intraoperative, Monte Carlo, GEANT4, GAMOS, Gamma ray

Application of active-OSL approximation to experimental decay curves from nacl sample exposed to different doses

[1] A. GÜNEŞ TANIR Gazi University
[2] MUSTAFA HİCABİ BÖLÜKDEMİR Gazi University

Active-OSL Approximation (AOSLA) that suggested by Tanır and Bölükdemir was applied to experimental optical stimulated luminescence decay from NaCl sample. The explanation of the AOSLA was based on the radioactive decay law of successive disintegration. It allows obtaining the peak forms of luminescence mechanism. This work shows that detrapping constants that have great importance in dating and dosimeters studies can be rapidly and clearly found using the AOSLA. Also, it can be concluded that the OSL is a process similar to the radioactive decay law of successive disintegration.

Keywords: OSL, radiation, nuclear successive decay

Calculation specific heat capacity of uranium nitride nuclear fuel

[1] ERHAN ESER Gazi University
[2] BURAK DUYURAN Gazi University
[3] HÜSEYİN KOÇ Muş Alparslan University
[4] MUSTAFA HİCABİ BÖLÜKDEMİR Gazi University

Determining thermophysical properties of nuclear fuels is one of the most challenging problems in nuclear physics and material sciences. The safer nuclear fuels to prevent tragic accidents is very important in the design of nuclear reactors. In this context, the Uranium Nitride (UN) fuels have been used as safer fuels in nuclear reactors based on its high uranium density, thermal conductivity and low fission-gas release. For this purpose, we have evaluated the heat capacity, which is one of the most exciting thermal properties of fuels, of UN fuel by the use of Einstein-Debye approach. The obtained results show that our method gives reliable computational efficiency.

Keywords: Uranium Nitride, Specific Heat Capacity, Einstein-Debye Model

A survey distribution of terrestrial radionuclides in surface soil samples in and around Erzin province, Turkey.

[1] FATMA AYSUN UĞUR Osmaniye Korkut Ata University
[2] UĞUR BÜYÜKER Osmaniye Korkut Ata University
[3] MEHMET EMİN KORKMAZ Osmaniye Korkut Ata University

The purpose of this survey is to determine the distribution of terrestrial radionuclides U-238, Th-232, K-40 in surface soil samples collected from different locations in and around Erzin and assess the radiological implication caused from external exposure in out door. Measurements shall be made by gamma spectrometry method. As a result, the results marked on the map will be compared with results obtained in other parts of the turkey.

Keywords: Terrestrial Radionuclides,gamma ray spectrometry,soil

Measurements of gross alpha and gross beta activities in Erzin water

[1] UĞUR BÜYÜKER Osmaniye Korkut Ata University
[2] FATMA AYSUN UĞUR Osmaniye Korkut Ata University
[3] MEHMET EMİN KORKMAZ Karamanoğlu Mehmetbey University

Gross alpha and gross beta activities were determined for seventeen water samples collected from different locations in Erzin city. The instrumentations used to count the gross alpha and gross beta activities were gas proportional counter. Concentrations ranging from 0.083 ± 0.016 Bq/L to 0.886 ± 0.089 Bq/L with average 0.541 ± 0.066 Bq/L and from 0.014 ± 0.004 Bq/L to 0.911 ± 0.044 Bq/l with an average 0.2318 ± 0.023 Bq/L were observed for the gross alpha and gross beta activities, respectively. The results show that the natural activities of alpha and beta emitting radionuclides in water samples did not exceed WHO recommended levels and were conparable with data available in other parts of the world. It suggests that the radioactivity in water for the people residing in Erzin city is not yet a problem. To ensure the safe level of radioactivity in drinking water, however, periodic monitoring of water quality for compliance is necessary.

Keywords: Gross alpha,gross beta,gas proportional counter

Tritium activity levels in drinking water of Adana, Turkey

[1] FATMA AYSUN UĞUR Osmaniye Korkut Ata University
[2] ELİF GÖREN Osmaniye Korkut Ata University

Tritium activity in potable drinking water samples from Adana city were measured using liquid scintillation counting after distillation procedure. The results exposed that the activity concentrations of the tritium measured in one-third of these samples were lower than minimum detectable activity which has a value of 2 Bq/L for counting time of 1,500 min. However, the maximum and mean value of the tritium activity was found to be 9.1 Bq/L (77.3 TU) and 7.0 Bq/l (59.4 TU), respectively. These values were substantially below the 100 Bq/L which is normative limit in Turkey for waters intended for human consumption. The highest values of annual effective dose received by infants, children and adults due to measured tritium activity were estimated as 0.041, 0.057 and 0.120 μSv/y, respectively.

Keywords: Tritium, water, liquid scintilation counter

Investigation of the glow curves of the Ermenek-Sariveliler-Başyayla region soil samples

[1] ERDEM UZUN Karamanoğlu Mehmetbey University

Within this paper, thermoluminescence glow curves of the Ermenek-Sarıveliler-Başyayla region soil samples were investigated. For this purpose, the soil samples were taken from randomly selected 28 points in Karaman province under certain conditions. Samples were dried, sieved and stones in crystal form were separated by using light microscope. Then, they were crushed in a mortar, sieved and treated with 30% HCl to remove calcium carbonate. Treat with 30% H_2O_2 processing to remove organic materials and, washed and dried. Then samples were irradiated with beta radiation for 300s and thermoluminescence glow curve were recorded. Glow curves were also analyzed by using computerized glow curve deconvolution method.

Keywords: otor model, numerical solutions, Runge–Kutta method, Fehlberg coefficients, Şeydişehir alumina

Calculation of diffusion length with Anli-Güngör phase function using un method

[1] AHMET BÜLBÜL Osmaniye Korkut Ata University Osmaniye Vocational High Scholl, Department of Electricity and Energy,
[2] FİKRET ANLI Kahramanmaraş Sütçü İmam University Faculty of Arts and Sciences, Department of Physics

The second kind of Chebyshev polynomial approximation (UN approximation) is applied to neutron transport equation in slab geometry and then diffusion lengths are calculated for positive values of scattering parameters (t) using Anli-Güngör phase function. Numerical results obtained from U1 and P1 approximations are compared with each other for different collision parameters and t parameters.

Keywords: Diffusion length, Anli-Güngör Phase, UN method

The γ-ray strength functions of ^{143,147}Nd isotopes

[1] MUSTAFA ÖZGÜR Eskişehir Osmangazi University
[2] KÜRŞAD OSMAN AY Eskişehir Osmangazi University
[3] MAGNE GUTTORMSEN Oslo University
[4] EMEL ALĞIN Adana Bilim ve Teknoloji University
[5] FRANK LEONEL BELLO GARROTE Oslo University
[6] LUCIA CRESPO CAMPO Oslo University
[7] ANDREAS GORGEN Oslo University
[8] TRINE WIBORG HAGEN Oslo University
[9] ANN CECILIE LARSEN Oslo University
[10] VICTOR MODAMIO Oslo University
[11] FABIO ZEISER Oslo University
[12] SUNNIVA SIEM Oslo University
[13] VETLE WEGNER INGEBERG Oslo University
[14] SUNNIVA ROSE Oslo University
[15] EDA ŞAHİN Oslo University
[16] GRY MERETE TVETEN Oslo University
[17] JORGEN ERIKSSON MIDTBO Oslo University
[18] BONGINKOSI VINCENT KHESWA Oslo University
[19] MALIN KLINTEFJORD Oslo University
[20] THERESE RENSTROM Oslo University

The γ-ray strength function (γ_{SF}) is a measure of the average electromagnetic properties of excited nuclei and was first introduced by Blatt and Weisskopf [1]. The γ_{SF} is one important quantity for calculating neutron-induced reaction cross sections in stellar nucleosynthesis and also in nuclear power reactors. The γ_{SF} has been studied extensively by (γ,γ') and (e,e') reactions and theoretical models [2]. Here, γ-ray strength functions of ^{143,147}Nd in the quasi-continuum have been studied via (d,p) reactions performed on ^{142,146}Nd isotopes at the Oslo Cyclotron Laboratory. The results will be compared with the photo-neutron cross sections of Nd data [3,4] from the neutron separation region up to the 14-MeV energy as well.

[1] J.M. Blatt and V.F. Weisskopf, Theoretical Nuclear Physics, Wiley, New York, 1952.
[2] K. Heyde et al., Rev. Mod. Phys. 82, 2365 (2010).
[3] H.T. Nyhus et al., Phys. Rev. C 91, 015808 (2015).
[4] P. Carlos et al., Nucl. Phys. A 172, 437 (1971).

This study is supported by the Scientific and Technological Research Council of Turkey (TUBITAK) under the Project No: 115F196. mustafaozgr@gmail.com

Keywords: gamma ray strength functions, oslo method,gsf

Investigation of radiation effects on polymer concretes designed with different aggregates

CENGİZ ÖZEL, ALİ NADİ KAPLAN

Süleyman Demirel University, Faculty of Technology, Department of Civil Engineering, Isparta

Abstract

In this study, the effects of different aggregate variations in polymer concrete on stopping power and the penetrating distance of proton and alpha radiations have been investigated. The calculations have been done by using GEANT4 simulation program in the energy range from 1 MeV to 250 MeV with an increase rate of 50 MeV incoming particle energies.

Keywords: polymer, aggregates, shielding, concrete

Introduction

The polymers are widely used for clothing, equipment or construction materials due to its preferable regarding physical, chemical and mechanic properties such as low permeability, ease of synthesizing and light weight etc [1]. Toxic or heavy metals (metallic materials) or concretes (mixtures containing heavy aggregates and cement) are commonly used as radiation shielding materials [2].

A polymer concrete [3], which is a composite material that results from polymerization of a monomer/aggregate mixture, is produced by using the polymer as the binder in concrete.

GEANT4 [4] is a free simulation and calculation code that can be used for investigation of high-energy physics, medical physics, space and radiation physics. GEANT4 is an abundant set of physics models to handle the interactions of particles with matter across a large energy range.

To simulate the effects of induced particles and see the interactions involving penetrating distance of the particles and the stopping power of polymer concrete for each particle, PhysListEmStandard and G4EmStandard-Physics libraries have been selected among many exists inside GEANT4 and the materials have been identified one by one inside the created environment that has the studied sample and geometry inside it.

Materials and Calculations

The investigated samples are generated by using vinylester resin as the binder in polymer concrete where the concrete samples have been generated as 0 % aggregate, 50 % standard CEN sand aggregate and 50 % hematite aggregate of total volume, respectively.

The calculations have been done by using GEANT4 simulation program in the energy range from 1 MeV to 250 MeV with an increase rate of 50 MeV incoming particle energies.

Table. 1. Contents of polymer concrete samples

0 % Aggregate Sample Mixture Contains
▪ 96.015 % Vinylester Resin ▪ 0.691 % Methyl Ethyl Ketone Peroxide (hardener) ▪ 3.024 % Cobalt Octoate (accelerator)
50 % Standard CEN Sand Aggregate Sample Mixture Contains
▪ 48.007 % Vinylester Resin ▪ 0.481 % Methyl Ethyl Ketone Peroxide (hardener) ▪ 1.512 % Cobalt Octoate (accelerator) ▪ 50 % Standart CEN Sand Aggregate
50 % Hematite Aggregate Sample Mixture Contains
▪ 48.007 % Vinylester Resin ▪ 0.481 % Methyl Ethyl Ketone Peroxide (hardener) ▪ 1.512 % Cobalt Octoate (accelerator) ▪ 50 % Hematite Aggregate



Fig. 1. Some kinds of polymer concrete

Results and Discussions

Obtained stopping power and penetrating distance results for the samples have been compared with each other for the possibility of using the polymer concrete as the shielding material. The results for the stopping power values have been obtained in the unit of MeV/cm rather

than MeV.cm^2/g and the penetration distance results have been obtained in the unit of length as millimeter (mm). Stopping power and penetration distance calculations have been compared to each other by concerning the proton and alpha particles where the comparisons have been given as Figure 2 and Figure 3 for proton and alpha particles, respectively. In addition to the visual comparison with the given figures, all obtained calculation results have been given in Table 2.

Table. 2. Stopping power and penetrating distance results for the samples

Energy (MeV)	Proton Stopping Power (MeV/cm)	Proton Penetrating Distance (mm)	Alpha Stopping Power (MeV/cm)	Alpha Penetrating Distance (mm)
0 % Aggregate Sample				
1	271.1590	0.0235	2337.6900	0.0037
50	12.6591	21.8330	154.2890	1.8129
100	7.3994	75.8879	87.8458	6.3091
150	5.5235	155.2900	63.2723	13.1277
200	4.5554	255.7010	50.2640	22.0728
250	3.9649	373.8510	42.1536	32.9981
50 % Standard CEN Sand Aggregate Sample				
1	387.3020	0.0169	3191.4400	0.0029
50	19.6392	14.1786	235.5440	1.2005
100	11.5466	48.8938	135.3730	4.1298
150	8.6425	99.6990	97.9693	8.5421
200	7.1396	163.8150	78.0413	14.3103
250	6.2216	239.1510	65.5784	21.3392
50 % Hematite Aggregate Sample				
1	469.9100	0.0142	3722.2400	0.0026
50	25.7835	10.8687	304.2180	0.9390
100	15.2335	37.2263	176.6360	3.1915
150	11.4376	75.6676	128.3210	6.5657
200	9.4657	124.0670	102.4890	10.9629
250	8.2595	180.8500	86.2818	16.3098

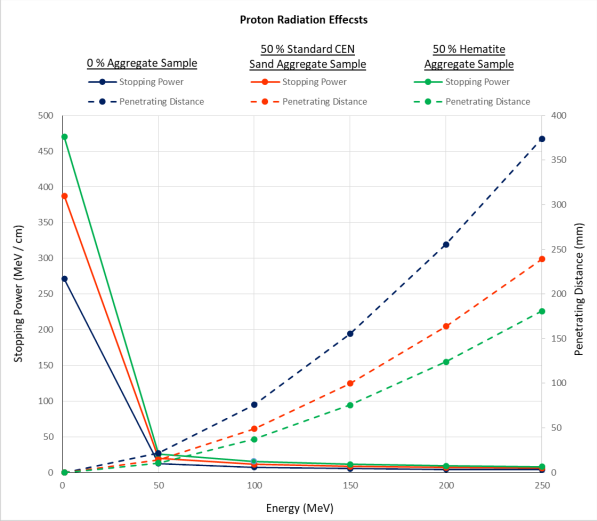

Fig. 2. Stopping power and penetrating distance calculations for the samples under proton radiation

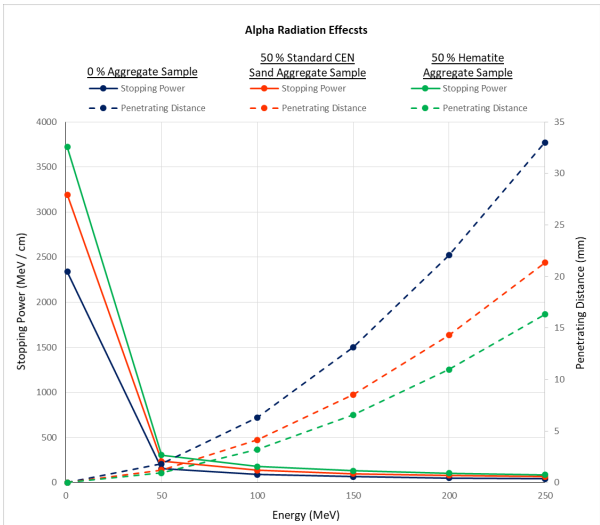

Fig. 3. Stopping power and penetrating distance calculations for the samples under alpha radiation

According to the results of the analysis, the minimum penetration distance is determined in the hematite aggregated sample whereas the maximum penetration distance is found in the non-containing aggregate sample (0% aggregate) for proton and alpha particles.

Similarly, the maximum stopping power is found in the sample containing hematite aggregates while the minimum value is determined in the non-containing aggregate sample for proton and alpha induced particles.

The production of concretes may require different procedures and due to that the production cost and time vary in a very large scale. In the cases where an acceptable foresight could be useful for the further investigations, simulation studies like the one performed within here could be done.

Reference

[1] C Vipulanandan *et al*, *J Matter Civ Eng* **5**, 62 (1993)

[2] S M Malkapur *et al, Appl Radiat Isot* **125**, 86 (2017)

[3] R Bedi *et al*, *Journal of Composites* **2013**, 12 (2013)

[4] S Agostinelli *et al*, *Nucl. Instrum. Methods Phys. Res. A* **506**, 250 (2003)

Proton and alpha radiation effects on hematite aggregated polymer concretes by using GEANT4

[1]ALİ NADİ KAPLAN, [1]CENGİZ ÖZEL,[2]MERT ŞEKERCİ, [3]HASAN ÖZDOĞAN

[1]*Süleyman Demirel University, Faculty of Technology, Department of Civil Engineering, Isparta*
[2]*Süleyman Demirel University, Faculty of Arts and Sciences, Department of Physics, Isparta*
[3]*Akdeniz University, Faculty of Medicine, Department of Biophysics, Antalya*

Abstract

In this study, the effects of different hematite aggregate volume rate in polymer concrete samples have been investigated on the stopping power of alpha and proton radiations. Also, those particles penetration distance calculations have been generated. Samples with different rates of hematite for polymer concrete have been investigated by using GEANT4 simulation program in the energy range from 1 MeV to 250 MeV incoming particle energies.

Keywords: shielding, concrete, GEANT4, hematite

Introduction

Nuclear reactors are one of the pieces of scientific advancement and have many usage areas to serve in many purposes. The most known reason of the nuclear reactor's usage is to produce electricity energy to be used in our daily life. The unexpectedly occurred high energetic particles from the reactions take place in the process of electricity generation may cause various problems.

Radiation shielding has vital to protect against unexpected damage of those particles. One way to avoid from these problems is to use various materials as radiation shielding [1].

Heavyweight concrete is one of the most widely used materials for radiation shielding. As alternative to conventional construction materials, the polymer concrete [2] has been developed by combining the different type of aggregates and the polymers as binders instead of cement and water. Hematite aggregates contain about 88 % of Fe_2O_3 and are called heavy aggregates because of their high density [3].

Materials and Calculations

Four different types of polymer concrete samples have been used for the calculations. The samples are prepared in different concentrations of hematite aggregate (0 %, 33 %, 50 % and 66 % as volume ratios) in the polymer concrete. Vinylester resin is used as the binder material in all polymer concrete.

Samples with different rates of hematite for polymer concrete have been investigated by using GEANT4 [4] simulation program in the energy range from 1 MeV to 250 MeV incoming particle energies.

Table. 1. Contents of polymer concrete samples

0 % Aggregate Sample Mixture Contains
▪ 96.015 % Vinylester Resin ▪ 0.691 % Methyl Ethyl Ketone Peroxide (hardener) ▪ 3.024 % Cobalt Octoate (accelerator)
33 % Hematite Aggregate Sample Mixture Contains
▪ 64.330 % Vinylester Resin ▪ 0.644% Methyl Ethyl Ketone Peroxide (hardener) ▪ 2.026 % Cobalt Octoate (accelerator) ▪ 33 % Hematite Aggregate
50 % Hematite Aggregate Sample Mixture Contains
▪ 48.007 % Vinylester Resin ▪ 0.481 % Methyl Ethyl Ketone Peroxide (hardener) ▪ 1.512 % Cobalt Octoate (accelerator) ▪ 50 % Hematite Aggregate
66 % Hematite Aggregate Sample Mixture Contains
▪ 32.685 % Vinylester Resin ▪ 0.317 % Methyl Ethyl Ketone Peroxide (hardener) ▪ 0.998 % Cobalt Octoate (accelerator) ▪ 66 % Hematite Aggregate



Fig. 1.Hematite aggregate sample

Results and Discussions

Within this study, particle stopping power calculations have been performed for proton and alpha particles with respect to different aggregate rated polymer concretes by using GEANT4 code. To be able to perfom the calculations, all samples have been defined to the GEANT 4 code according to their contents which is also given in Table 1. The definition process contains every piece of ingredient that defines the concrate with the exact rate. Then, two different type of particles have been selected as incoming particles to the samples which are proton and alpha in the range of 1 MeV to 250 MeV with an increase rate of 50 MeV energy. Calculations also contain the particles maximum travelled distance through the material that is also named as penetration distance. There exist two units for the stopping power in the literature which are MeV.cm^2/g and MeV/cm that differs due to the density effect of sample and MeV/cm unit has been accepted in this study. Likewise the stopping power, it is also possible to express the penetration distance value in the terms of g/cm^2 or cm where the lenght based unit has been accepted in this study and the values have been given as millimeter.

Obtained numerical values are tabulated for each sample and both particles where the results are given in Table 2. In addition to the represented numerical values, the obtained results also have been compared according to the incident particle where the comparisons have been given as Figure 2 and Figure 3 for proton and alpha particles, respectively. Given figures have been created with double *y*-axes style where the left *y*-axis represents the stopping power and right *y*-axis represents the penetration distance. Each sample have been given with different colours within the figures.

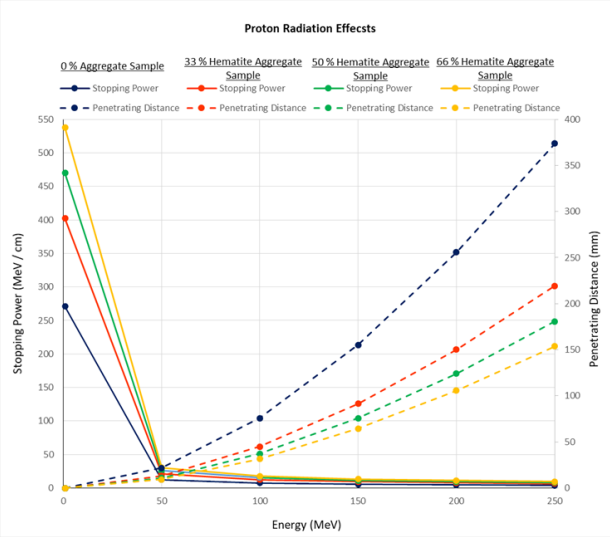

Fig. 2. Stopping power and penetrating distance calculations for the samples under proton radiation

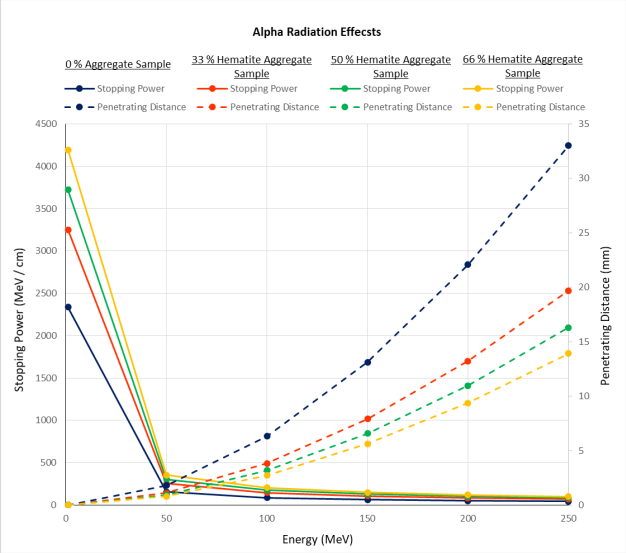

Fig. 3. Stopping power and penetrating distance calculations for the samples under alpha radiation

Table. 2. Stopping power and penetrating distance results for the samples

Energy (MeV)	Proton Stopping Power (MeV/cm)	Proton Penetrating Distance (mm)	Alpha Stopping Power (MeV/cm)	Alpha Penetrating Distance (mm)
0 % Aggregate Sample				
1	271.1590	0.0235	2337.6900	0.0037
50	12.6591	21.8330	154.2890	1.8129
100	7.3994	75.8879	87.8458	6.3091
150	5.5235	155.2900	63.2723	13.1277
200	4.5554	255.7010	50.2640	22.0728
250	3.9649	373.8510	42.1536	32.9981
33 % Hematite Aggregate Sample				
1	402.3390	0.0164	3251.5300	0.0029
50	21.3282	13.0987	253.5210	1.1217
100	12.5735	45.0084	146.5290	3.8325
150	9.4284	91.6157	106.2490	7.9046
200	7.7972	150.3520	84.7612	13.2190
250	6.8000	219.3060	71.2980	19.6874
50 % Hematite Aggregate Sample				
1	469.9100	0.0142	3722.2400	0.0026
50	25.7835	10.8687	304.2180	0.9390
100	15.2335	37.2263	176.6360	3.1915
150	11.4376	75.6676	128.3210	6.5657
200	9.4657	124.0670	102.4890	10.9629
250	8.2595	180.8500	86.2818	16.3098
66 % Hematite Aggregate Sample				
1	537.4970	0.0126	4193.0800	0.0023
50	30.2326	9.2911	354.6240	0.8082
100	17.8904	31.7459	206.6620	2.7359
150	13.4456	64.4602	150.3500	5.6173
200	11.1337	105.6190	120.1900	9.3681
250	9.7187	153.8850	101.2480	13.9258

The numerical results for stopping power and penetrating distance values have been compared for each sample. The results of the analyses illustrate that while the aggregate ratio in the polymer concrete increases, the usability as shielding also increases. In conclusion, similar simulation studies like this one could provide a

prediction to the scientists rather than performing the studies after the material production process which requires relatively long and expensive steps.

Reference

[1] S M Malkapur *et al, Appl Radiat Isot* **125**, 86 (2017)

[2] R Bedi *et al*, *Journal of Composites* **2013**, 12 (2013)

[3] M H Kharita *et al*, *Prog Nucl Energ* **51**, 388 (2009)

[4] S Agostinelli *et al*, *Nucl. Instrum. Methods Phys. Res. A* **506**, 250 (2003)

Comparison of penetrating distance calculations for magnetite and ordinary concrete

[1]HASAN ÖZDOĞAN, [2]ABDULLAH KAPLAN, [2]MERT ŞEKERCİ, [3]ALİ NADİ KAPLAN

[1]Akdeniz University, Biophysics Dept., Antalya, Turkey
[2]Süleyman Demirel Üniversitesi, Physics Dept., Isparta, Turkey
[3]Süleyman Demirel University, Faculty of Technology, Department of Civil Engineering, Isparta

Abstract

The interactions of the charged particles with matter are unique and determine their penetrability through matter and, consequently, the type and amount of shielding needed for radiation protection. To avoid from harmful effects of radiation, different shielding materials can be used. Concrete is one of the most popular and relatively cheap material used for radiation shielding. In this study, we aim to investigate the penetrating distance of charged particles within ordinary and magnetite concrete. Calculations have been performed by using GEANT4 and MCNP codes for the incident proton, deuteron, triton, hellion and alpha particles up to 100 MeV energy by taking into consideration of all possible reactions. The obtained calculation results have been compared with the each other.

Keywords: penetrating distance, concrete, MCNP, GEANT4

Introduction

Particle–matter interactions are one of the investigated topics among scientists. The most simple and basic reason for that is the consequences of these interactions that affect not only the material itself and surrounding but also the human life by direct or indirect ways. These interactions have been studying to understand the fundamentals of the particle–matter relations as well as to see the effects and develop required protection methods from the possible harmful effects of charged particles. The exist knowledge of the penetration distance for different charged particles may also be beneficial for material research and development studies where one of them could be pointed as the studies done for shielding materials.

Radiation shielding ensures that researchers working with radiation do their jobs safely. Construction of radiation building have to meet certain specifications. Concrete is one of the most popular shielding material. It is possible to create a radiation shielding for various types of radiations, such as alpha, beta, gamma, X-rays and neutrons, regarding the indegrants and their qualifications of the concrete in the manner of its high density. Radiation shielding by concrete usage is relatively cheaper, managable and easier with respect to other possibilities where it is also an advantage of the molding flexibility of the concrete into many more desired shapes. It is possible to be used as biological shielding for nuclear power plants, particle accelerators, research reactors, laboratory hot cells and other different radiation sources [1]. In this study, we have used GEANT4 and MCNP codes to investigate penetrating distance calculations of proton, deuteron, trition, helion and alpha particles into the ordinary and magnetite concretes. Compositions of these concretes have been taken from R. G. Williams III et. al. [2].

Material Methods

GEANT4 [3] is a free simulation and calculation code that can be used to investigate the high energy physics, medical physics, space and radiation physics. GEANT4 is an abundant set of physics models to handle the interactions of particles with matter across a large energy range. Data and expertise have been drawn from many sources around the world and in this respect, GEANT4 acts as a repository that incorporates a large part of all that is known about particle interactions. The model which has been employed in this paper is implemented in the TestEM0 package of the GEANT4 toolkit. Detailed description can be found in Ref. 3.

MCNP [4] is a Monte Carlo code that can be used for neutron, photon, electron or coupled neutron/photon/electron transport. Specific areas of application include, but are not limited to, radiation protection and dosimetry, radiation shielding, radiography, medical physics, nuclear criticality safety, detector design and analysis, nuclear oil well logging, accelerator target design, fission and fusion reactor design, decontamination and decommissioning. The code treats an arbitrary three-dimensional configuration of materials in geometric cells bounded by first and second-

degree surfaces and fourth-degree elliptical tori. Detailed description can be found in Ref. 4.

Results and Discussions

In this study, penetrating distance calculations have been carried out up to 100 MeV for proton, deuteron, triton, helion and alpha particles under their interactions with ordinary and magnetite concretes. Calculation results have been given in Figs. 1-5.

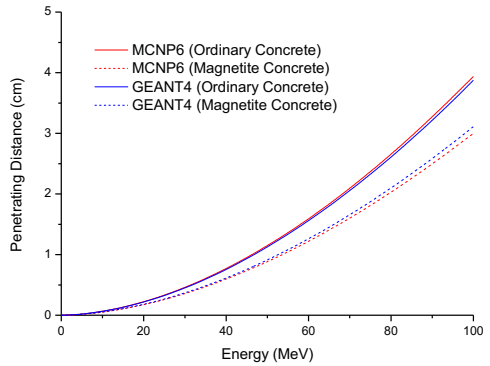

Fig. 1. Penetrating distance calculations for proton.

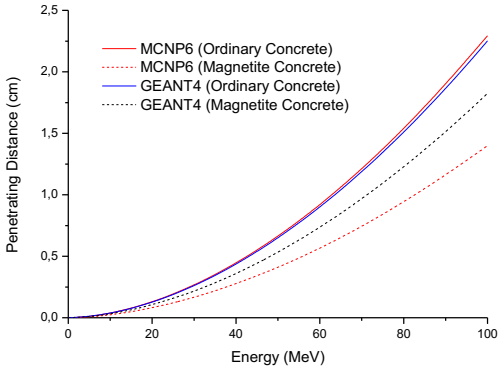

Fig. 2. Penetrating distance calculations for deuteron.

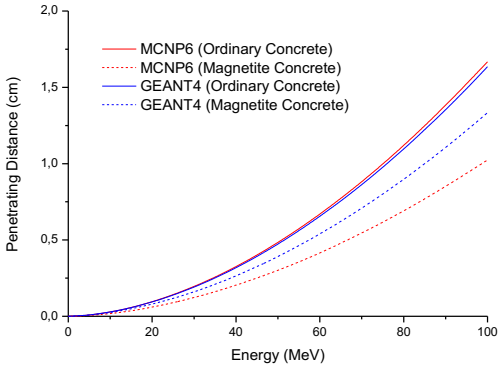

Fig. 3. Penetrating distance calculations for triton.

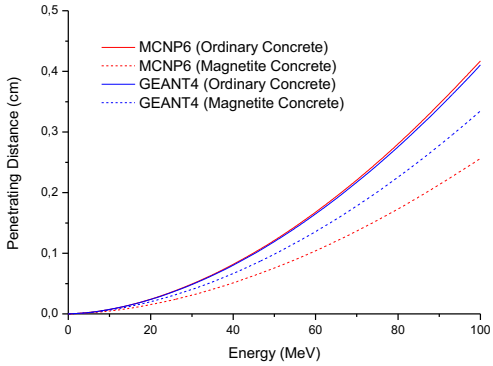

Fig. 4. Penetrating distance calculations for ^{3}He.

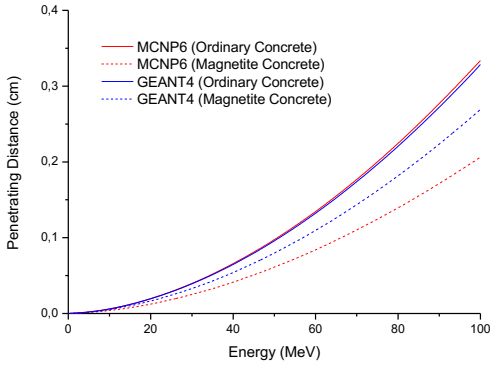

Fig. 5. Penetrating distance calculations for alpha.

In these calculations, GEANT4 and MCNP codes have been used. Penetrating distances of investigated charged particles have been found in the decreasing order of proton, deuteron, triton, ^{3}He and alpha. Discrepancy of penetration distance of ordinary and magnetite concrete have been seen clearly after 30 MeV incident particle energy. According to results magnetite concrete can be used for radiation shielding rather than the ordinary concrete.

Reference

[1] B Han *et al*, Smart and Multifunctional Concrete Toward Sustainable Infrastructures, 329-337, (2017).

[2] R G Williams III *et al*, Compendium of Material Composition Data for Radiation Transport Modeling, 114 p. (2006).

[3] S Agostinelli *et al*, *Nucl. Instrum. Methods Phys. Res. A.* **506**, 250 (2003).

[4] H G Hughes and M R James, MCNP6 Class. Access Date: 17.09.2017. http://permalink.lanl.gov/object/tr?what=info:lanl-repo/lareport/LA-UR-14-21281.

Comparison of stopping power calculations for magnetite and ordinary concrete

[1]HASAN ÖZDOĞAN,[2]ALİ NADİ KAPLAN, [3]MERT ŞEKERCİ, [3]ABDULLAH KAPLAN

[1]Akdeniz University, Biophysics Dept., Antalya, Turkey

[2]Süleyman Demirel University, Faculty of Technology, Department of Civil Engineering, Isparta

[3]Süleyman Demirel Üniversitesi, Physics Dept., Isparta, Turkey

Abstract

There exist many materials for radiation shielding properties yet one of the most prominent is concrete which is comparably unexpensive material used for shielding properties in facilities where different types of radioactive sources and radiation generating equipments may exist. A concrete that contains magnetite ore, cement and water could be pointed as a better shielding product which have better shielding specifacitions rather than ordinary concrete and it possess better strength and ease of handling properties with respect to its derivatives. In this study, stopping power calculations of ordinary and magnetite concrete have been performed for the incident proton, deuteron, triton, hellion and alpha particles up to 100 MeV energy by taking into consideration of all possible reactions such as ionization, scattering, absorption, transmission and charge transfer. In calculations the MCNP and GEANT4 codes, which adopt the Bethe-Bloch approach for charged particle-material interactions, have been employed. To understand the differences of the materials, a graphical comparison has been performed for every particle.

Keywords: Stopping Power, Concrete, MCNP, GEANT4

Introduction

Concrete is used to be protected against harmful effects of ionizing radiation at nuclear reactors, oncology clinics, X-ray rooms, etc. Suitable samples produced for the given purposes are usually generated as the mixture of hydrogen and other light nuclei which own a high atomic number [1, 2]. Concretes whose density are higher than 2.8 g/cm^3 are called heavy concrete. The heavy elements exist in the nature of the aggregate itself, which is an essential ingredient for the shielding concrete, play an indisputable role to the improvement of the shielding properties so samples produced with them have better shielding specifacitions for the neutral and charged particles. The performance requirements of the concrete of containment structures are mainly radiological protection, structural integrity, durability and etc. To compensate this purpose, high performance heavy density concrete is supposed to be used. In the interaction between charged particles and matter, the stopping power or the average energy loss per unit path length plays an important role in many fields. Stopping power consists of two components: collisions and radiative. The first is the most important, resulting from the collision interaction between the incident particles and atomic electrons [3]. Linear stopping power is given by $S=-dE/dx$, where E is charged particle kinetic energy and x is the thickness of the material. The classical (i.e, non-Quantum Mechanical) expression that describes the specific energy loss is known as the Bethe-Bloch formula. A reliable calculation of the stopping power of charged particles is required in Monte Carlo simulation for the precise description of energy loss processes and the correct estimation of their ranges in matter [4].

Material Methods

Simulation codes are oftenly used for many purposes in various fields since they provide a considerably remarkable and acceptable foresights to the researchers for the considered situation. In this study, to examine the particle matter interactions and obtain the particle stopping power of the material, two of the most used and accepted codes have been employed which are GEANT4 [5] and MCNP [6]. Both codes have many detailed operation regulations and benefits in addition to their different and relatively complex procedures.

GEANT4 code, which distrubuted free of charge, is a state of art simulation and calculation code used in may areas where some could be given as high-energy physics, medical physics, space and radiation physics could be

defined as a copious set of previously defined physics models generated to be able to handle many physical phenomenas like the particle-matter interactions across a large energy range. The expertise and the data to improve the code have been gathered from many sources all around the world and as a result GEANT4 has became a repository which integrates a large part of all that is known about particle-matter interactions. The model has been employed in this paper is implemented in the TestEM0 package of the GEANT4 toolkit where the detailed description can be found in Ref. 5.

The other employed code within this study is the MCNP code where the abbreviation refers to the Monte Carlo N-Particle that is used to express the code's ability of simulation many particle-matter interactions. The simulable particles could be given as neutrons, photons, electrons, deutrons, tritons, helions and alpha particles in addition to the coupled variations of these particles. MCNP is distrubuted under a licence that controled by Oak Ridge National Laboratory and it has many usage areas depending on its capabilites where some could be given as radiation protection and dosimetry, radiation shielding, radiography, medical physics, nuclear criticality safety, detector design and analysis, nuclear oil well logging, accelerator target design, fission and fusion reactor design, decontamination and decommissioning. The code treats an arbitrary three-dimensional configuration of materials in geometric cells bounded by first and second-degree surfaces and fourth-degree elliptical tori. Detailed description can be found in Ref. 6.

Results and Discussions

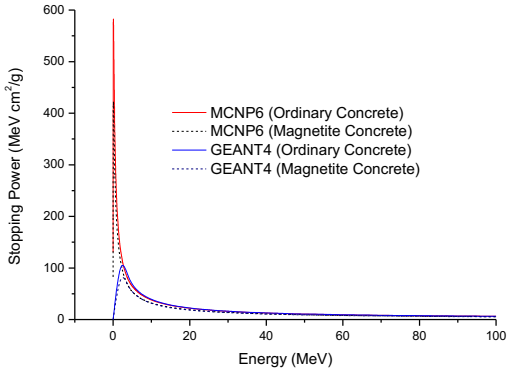

Fig. 1. Stopping power calculations for proton.

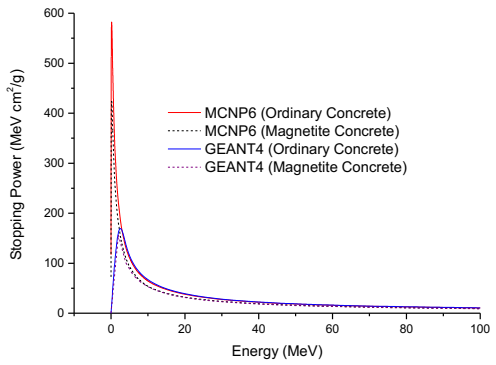

Fig. 2. Stopping power calculations for deuteron.

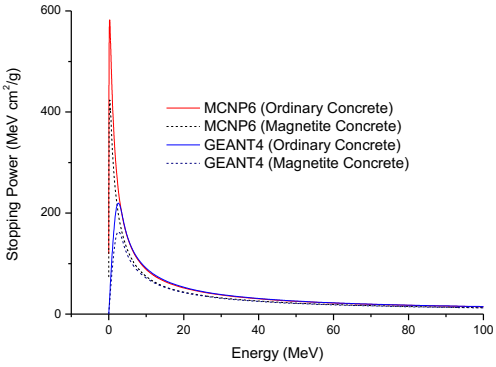

Fig. 3. Penetrating distance calculations for triton.

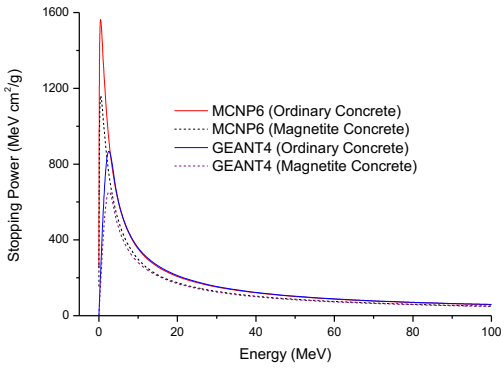

Fig. 4. Penetrating distance calculations for ^{3}He.

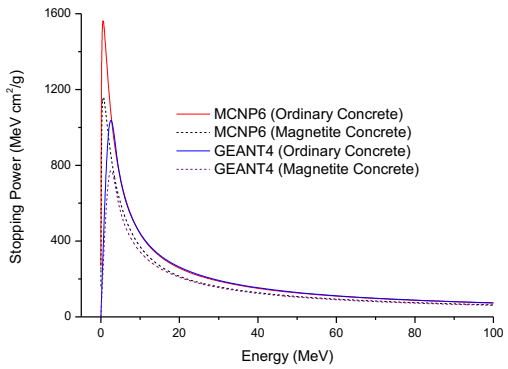

Fig. 5. Penetrating distance calculations for alpha.

In this study, stopping power calculations have been carried out up to 100 MeV for proton, deuteron, triton, helion and alpha particles under their interatcions with ordinary and magnetite concretes. Calculation results have been given in Figs. 1-5. In these calculations, GEANT4 and MCNP codes have been used. Generally, MCNP and GEANT4 calculations give us different results from the each other. However ordinary concrete has bigger stopping power results than magnetite concrete for all incident particles.

Reference

[1] E Creutz *and* K Downes, *J Appl Phys* **20**, 1236 (1949).

[2] M O El-Ghossain, *International Journal of Engineering Technology, Management and Applied Sciences*, **3**, 298 (2015).

[3] A S Ouda, *HBRC Journal*, **11**, 328 (2015)

[4] S Chauvie *et al*, *IEEE Trans Nucl Sci* **54**, 579 (2007).

[5] S Agostinelli *et al*, *Nucl. Instrum. Methods Phys. Res. A.* **506**, 250 (2003).

[6] H G Hughes and M R James, MCNP6 Class. Access Date: 17.09.2017. http://permalink.lanl.gov/object/tr?what=info:lanl-repo/lareport/LA-UR-14-21281.

Deuteron induced reaction cross–section calculations for ^{107,109}Ag, ^{151,153}Eu and ^{160}Gd isotopes

[1] ABDULLAH KAPLAN, [2] HASAN ÖZDOĞAN, [3] MERT ŞEKERCİ

[1]Süleyman Demirel University, Physics Dept., Isparta, Turkey
[2]Akdeniz University, Biophysics Dept., Antalya, Turkey

Abstract

Due to the complexity of the nuclear reaction mechanisms nature, making researches on this topic has always been on the high orders of the researches. The developed models for the nuclear reaction mechanisms make the scientists to understand the processes in a more detailed way and help to resolve nuclear reactions steps. However, the hard and complex mathematical operations which also changes from model to model and reaction type, requires a fast and stabilized way to study on these topics. To overcome this situation, many computer-based codes have been developed by the researches. In this study, two of the most known and used codes among all the exists codes, which are TALYS 1.8 and EMPIRE 3.2, have been selected to calculate the nuclear reaction cross–sections of ^{107,109}Ag, ^{151,153}Eu and ^{160}Gd for deuteron induced reactions. The concept of the nuclear reaction cross–section is also explained in the meaning of a reactions probability to take place. Since the information of a reactions occurrence has many beneficial information about the reaction itself, the data of cross–section has an exclusive importance for the studies. The cross–section calculations have been completed by using two reaction mechanism models within each code which are two component exciton and Hauser-Feshbach models from TALYS 1.8 and PCROSS exciton and Hauser-Feshbach models from EMPIRE 3.2. Obtained results have been compared with the experimental data taken from EXFOR and theoretical computation data library TENDL 2015.

Keywords: cross–section, deuteron induced reactions, TALYS, EMPIRE

Introduction

Due to the complexity of the nuclear reaction mechanisms nature, making researches on this topic has always been on the high priority of the researches. The developed models for the nuclear reaction mechanisms make the scientists to understand the processes in a more detailed way and help to resolve a nuclear reaction's steps. However the hard and complex mathematical operations, which also change from model to model and reaction type, require a fast and stabilized way to study on these topic. To overcome this situation, many computer based codes have been developed by the researches. The concept of the nuclear reaction cross–section is also explained in the meaning of a reaction's probability to take place. Since the information of a reaction's occurrence has many beneficial information about the reaction itself, the data of cross–section has an exclusive importance for the studies [1].

Theoretical Calculations

The concept of the nuclear reaction cross–section can be explained as the meaning of a reaction's probability to take place. This quantity provides many beneficial and useful information about the reaction itself and due to that the data of cross–section has an exclusive importance for the studies. Materials that contain Ag, Eu and Gd have many industrial and applicational usage fields that is known and also expanding such as nuclear reactors, medical diagnostic and treatment devices etc. Due to the high demand on these elements, ^{107,109}Ag, ^{151,153}Eu and ^{160}Gd isotopes have been selected for investigation under the effect of deuteron induced reactions. Many nuclear reaction models have been developed for different types of reactions to understand and resolve a nuclear reaction's steps. However, the hard and complex mathematical operations, which also differ from model to model and reaction type, requires a fast and stabilized way to study on these topic. To overcome this situation, many computer based codes have been developed by the researches. Theoretical calculations within this study have been completed by employing two most used computer codes which are also well known and validated codes as TALYS 1.8 [2] and EMPIRE 3.2 [3]. Fortran is the main programming language used to code EMPIRE core (physics modules) and utility codes and the current version, which is EMPIRE-3.2, Malta version, released in 2011. This version of the code can treat multiple

emissions of the neutrons, protons, alphas, deuterons, tritons, helions and light ions. Likewise EMPIRE, TALYS is a nuclear reaction program that created at NRG Petten, the Netherlands and CEA Bruyères-le-Châtel, France. The idea to make TALYS was born in 1998. On December 21, 2007 the first official version of the code, TALYS-1.0, was released. With the employed version of TALYS in this study, which is TALYS 1.8, it is possible to simulate the nuclear reactions that involve neutrons, photons, protons, deuterons, tritons, ^{3}He- and alpha-particles, in the 1 keV – 1 GeV energy range and for target nuclides of mass 12 and heavier. Among many possible models exist in the codes for theoretical calculations, Two Component Exciton [4] and Hauser–Feshbach [5] models from TALYS 1.8 and PCROSS exciton [3] and Hauser–Feshbach models from EMPIRE 3.2 have been used. Obtained results have been compared with the experimental data taken from EXFOR [6] and TENDL [7] databases.

Results

Reaction cross–section calculations have been performed for ^{107}Ag(d,2n)^{107}Cd, ^{109}Ag(d,2n)^{109}Cd, ^{151}Eu(d,2n)^{151}Gd, ^{153}Eu(d,2n)^{153}Gd and ^{160}Gd(d,2n)^{160}Tb reactions in this study by using Two Component Exciton and Hauser–Feshbach models from TALYS 1.8 and PCROSS exciton and Hauser–Feshbach models from EMPIRE 3.2. Obtained results have been compared with the experimental data taken from EXFOR and theoretical computation data library TENDL 2015 where all the comparisons have been given in the Figures 1–5, respectively.

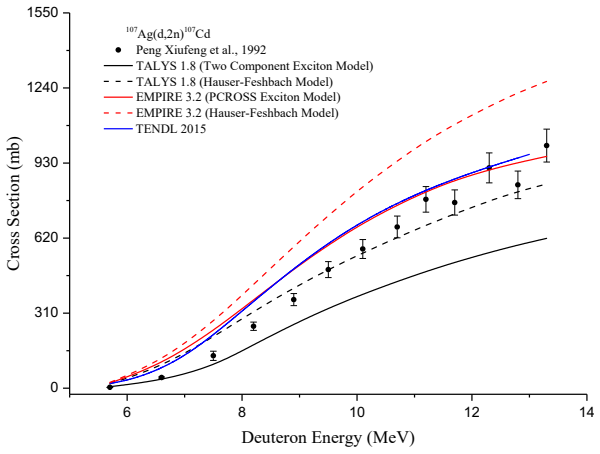

Fig. 1. ^{107}Ag(d,2n)^{107}Cd reaction results.

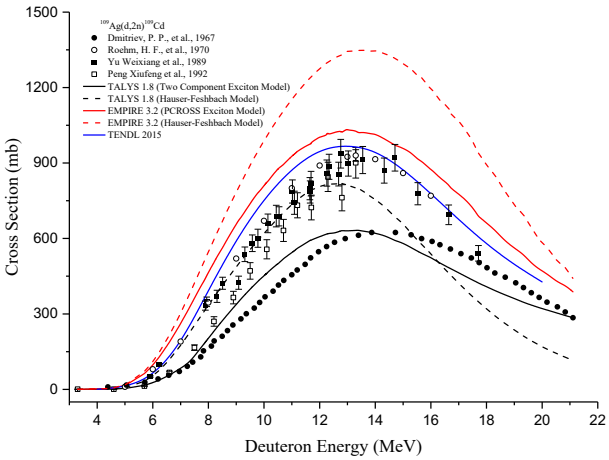

Fig. 2. ^{109}Ag(d,2n)^{109}Cd reaction results.

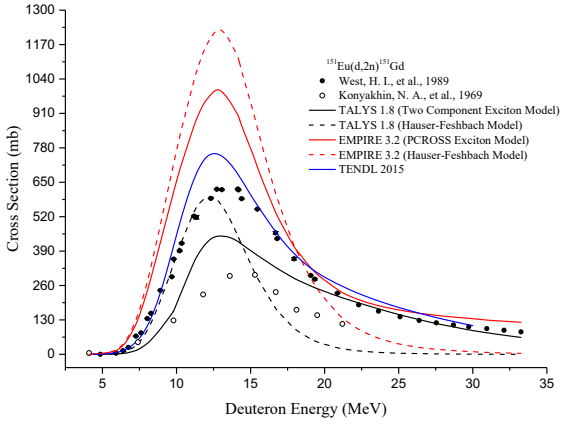

Fig. 3. ^{151}Eu(d,2n)^{151}Gd reaction results.

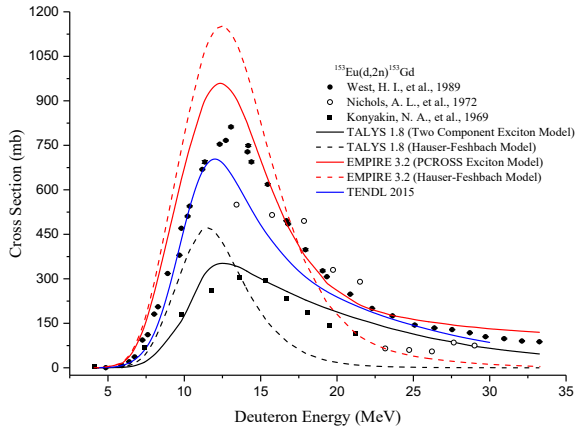

Fig. 4. ^{153}Eu(d,2n)^{153}Gd reaction results.

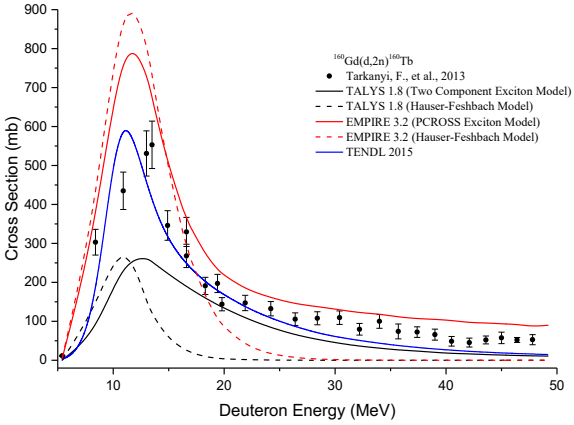

Fig. 5. ^{160}Gd(d,2n)^{160}Tb reaction results.

The calculations with different models of both TALYS 1.8 and EMPIRE 3.2 codes give similar shapes with the experimental data. TENDL 2015 values are also in agreement with the experimental values in each figure. Even the calculation results are obtained with similar shapes, different models give more significant similarity with the experimental data for every reaction. For ^{107}Ag(d,2n)^{107}Cd and ^{109}Ag(d,2n)^{109}Cd reactions, TALYS 1.8 Hauser–Feshbach model has the best agreement with the experimental data. On the other hand, for over all energy region, it could be said that for ^{151}Eu(d,2n)^{151}Gd, ^{153}Eu(d,2n)^{153}Gd and ^{160}Gd(d,2n)^{160}Tb reactions TALYS 1.8 Two Component Exciton model has the best agreement with the experimental data. In every calculation, EMPIRE 3.2 model results give higher cross–section values rather than TALYS 1.8 model calculations. These kind of studies provide high level contribution to not only the reaction mechanism studies but also the material studies. Furthermore, the obtained data from the calculations could be used to create new theoretical cross–section databases or strengthen the exist ones.

Reference

[1] A Kaplan *et al*, *J. Fusion Energ.* **32**, 97 (2013).

[2] A Koning, S Hilaire *and* S Goriely, TALYS–1.8 A Nuclear Reaction Program, User Manual, 1st edn. (NRG, The Netherlands, 2016).

[3] M Herman *et al*, EMPIRE-3.2 Malta Modular System for Nuclear Reaction Calculations and Nuclear Data Evaluation, User's Manual (2013).

[4] C Kalbach *Phys. Rev. C.* **33** 818 (1986).

[5] W Hauser *and* H Feshbach, H *Physical Review* **87** 366 (1952).

[6] Brookhaven National Laboratory, National Nuclear Data Center, EXFOR/CSISRS (Experimental Nuclear Reaction Data File). Database Version of 2018-04-11 (2018). (http://www.nndc.bnl.gov/exfor/)

[7] TENDL (Nuclear Data Library), Version 2015, Access: 11.03.2018. https://tendl.web.psi.ch/tendl_2015/tendl2015.html

Neutron production cross–section calculations of ^{111}Cd for (p,xn) reactions

[1]ABDULLAH KAPLAN, [2]MERT ŞEKERCİ, [3]HASAN ÖZDOĞAN

[1]Süleyman Demirel University, Physics Dept., Isparta, Turkey
[2]Akdeniz University, Biophysics Dept., Antalya, Turkey

Abstract

There exist many parameters used in the investigations of nuclear reactions. Some of these parameters could only be observed with the experiments while some of them could also be calculated by using validated models. One of these parameters is the reaction cross–section value which indicates the probability of a reactions formation. The importance of the cross–section data may vital for many cases since this knowledge helps researchers to understand the outcomes of the reaction and also help to be prevented from not desired outcomes. For this reason, there exists many tools for reaction cross–section calculations by using the theoretical models. The main idea of using computer based tools instead of self-calculations is due to the great time and effort gain especially because of the complex and upper level mathematical processes that the models contains. In this study, TALYS 1.8 and EMPIRE 3.2 computer codes have been used among all exists computer based calculation programs to complete the neutron production cross–section calculations for ^{111}Cd(p,n), ^{111}Cd(p,2n), ^{111}Cd(p,3n) and ^{111}Cd(p,4n) reactions. While both codes provide many theoretical models for

calculations, two component exciton and Hauser-Feshbach models from TALYS 1.8 and PCROSS exciton and Hauser-Feshbach models from EMPIRE 3.2 have been selected. Experimental data for the investigated reactions have been taken from EXFOR library and used for comparisons of the obtained calculation results. Also, theoretical calculation results from TENDL 2015 library have been included to these comparisons.

Keywords: cross–section, cadmium, TALYS, EMPIRE

Introduction

There exist many parameters used in the investigations of nuclear reactions. Some of these parameters could only be observed with the experiments while some of them could also be calculated by using validated models. One of these parameters is the reaction cross–section value which indicates the probability of a reaction's formation. The importance of the cross–section data may vital for many cases since this knowledge helps researchers to understand the outcomes of the reaction and also help to be prevented from not desired outcomes. For this reason, there exist many tools for reaction cross–section calculations by using the theoretical models [1]. The main idea of using computer based tools instead of self-calculations is due to the great time and effort gain especially because of the complex and upper level mathematical processes that the models contain. Due to the given circumstances, the theoretical neutron production cross–section calculations of ^{111}Cd for (p,xn) reactions have been completed in this study.

Theoretical Calculations

There exist many tools for reaction cross–section calculations by using the theoretical models. Computational tools may provide an acceptable suggestion to the researchers while it is not possible to reach the experimental data for some reactions. Due to that and many more features of theoretical calculations, the results from validated programs are highly respected. In this study, reaction cross–section values have been calculated with such two programs that also accepted in the literature which are TALYS 1.8 [2] and EMPIRE 3.2 [3]. The main features of these codes are to calculate the different reaction properties of a certain reaction that is defined by the user and these properties could be total and partial cross sections, energy spectra, elastic and inelastic angular distributions etc. and many more. Both codes need an input where specifications of the desired reaction, calculation requirements and other definitions have given. One of the most important parameter among all is the theoretical model selection. Employed codes are able to run with a number of options of theoretical models exist in their core codes. In this study, Two Component Exciton [4] and Hauser–Feshbach [5] models from TALYS 1.8 and PCROSS exciton [3] and Hauser–Feshbach models from EMPIRE 3.2 have been used. By this way, the calculations have been performed via both pre–equilibrium and equilibrium models where Two Component Exciton and PCROSS exciton models have been used for pre–equilibrium model calculations while Hauser–Feshbach model has been used for equilibrium model calculations. The outcomes of the calculations have been compared to each other for every reaction and also the available experimental data taken from EXFOR [6] and theoretical data taken from TENDL [7].

Results

In this study, reaction cross–section values have been calculated with two programs that also accepted in the literature which are TALYS 1.8 and EMPIRE 3.2. One of the most important part while using these codes is the theoretical model selection. Employed codes are able to run with a number of options of theoretical models exist in their core codes. Among them, Two Component Exciton and Hauser–Feshbach models from TALYS 1.8 and PCROSS exciton and Hauser–Feshbach models from EMPIRE 3.2 have been used. Obtained results of reaction cross–section calculations for ^{111}Cd(p,n)^{111}In, ^{111}Cd(p,2n)^{110}In, ^{111}Cd(p,3n)^{109}In and ^{111}Cd(p,4n)^{108}In have been compared with the experimental values taken from EXFOR and theoretical values taken from TENDL 2015 databases where Figures 1–4 have been given to represent the comporisons, respectively.

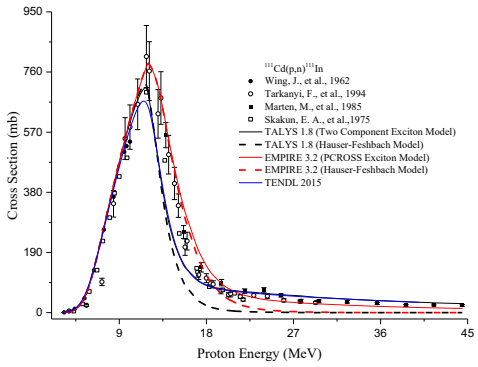

Fig. 1. ^{111}Cd(p,n)^{111}In reaction results.

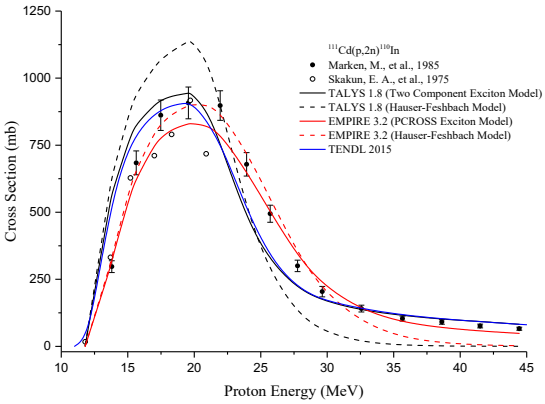

Fig. 2. $^{111}Cd(p,2n)^{110}In$ reaction results.

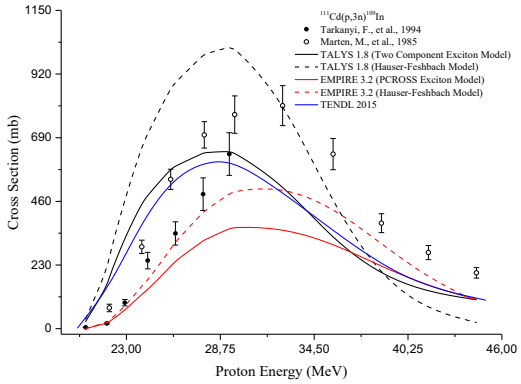

Fig. 3. $^{111}Cd(p,3n)^{109}In$ reaction results.

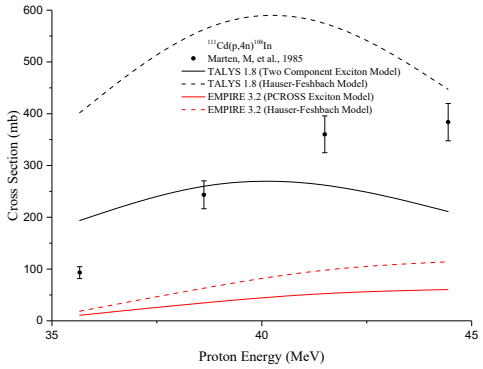

Fig. 4. $^{111}Cd(p,4n)^{108}In$ reaction results.

The comparisons of the obtained results from calculations and experimental values that have been taken from EXFOR show that, as the number of neutrons in the output channel increases, the harmonization of the results become more incongruent. Correspondingly, more similar geometries have been observed in the $^{111}Cd(p,n)^{111}In$ and $^{111}Cd(p,2n)^{110}In$ reactions while less similarity has been seen for $^{111}Cd(p,3n)^{109}In$ reaction and no similarity has been seen for $^{111}Cd(p,4n)^{108}In$ reaction. In the all studied energy ranges of $^{111}Cd(p,n)^{111}In$ and $^{111}Cd(p,2n)^{110}In$ reactions, the most compatible results have been obtained by EMPIRE 3.2 PCROSS Exciton model. For $^{111}Cd(p,3n)^{109}In$ reaction, the EMPIRE Hauser–Feshbach model could be pointed in this manner. TENDL 2015 data create similar geometries with the experimental values for those reactions, however the data are absent for $^{111}Cd(p,4n)^{108}In$ reaction where only one experimental value was catched by TALYS 1.8 Two Component Exciton model.

Reference

[1] A Aydin *et al*, *J. Fusion Energ.* **34**, 1105 (2015).

[2] A Koning, S Hilaire *and* S Goriely, TALYS–1.8 A Nuclear Reaction Program, User Manual, 1st edn. (NRG, The Netherlands, 2016).

[3] M Herman *et al*, EMPIRE-3.2 Malta Modular System for Nuclear Reaction Calculations and Nuclear Data Evaluation, User's Manual (2013).

[4] C Kalbach *Phys. Rev. C.* **33** 818 (1986).

[5] W Hauser *and* H Feshbach, H *Physical Review* **87** 366 (1952).

[6] Brookhaven National Laboratory, National Nuclear Data Center, EXFOR/CSISRS (Experimental Nuclear Reaction Data File). Database Version of 2018-04-11 (2018). (http://www.nndc.bnl.gov/exfor/)

[7] TENDL (Nuclear Data Library), Version 2015, Access: 11.03.2018. https://tendl.web.psi.ch/tendl_2015/tendl2015.html,

ESR investigation of radiation effect on CoQ10 drug

[1] M. ÖZGÜR SEZER Selçuk University
[2] EMEL ECE Karamanoğlu Mehmetbey University
[3] AYHAN ÖZMEN Selçuk University
[4] RECEP BIYIK Türkiye Atom Enerjisi Kurumu
[5] ÜLKÜ SAYIN Selçuk University

Electron Spin Resonance (ESR) is a special technique that allows direct radical determination of paramagnetic centers containing unpaired electrons and allows repeated measurements without damaging the examined sample. Radiation is nowadays, widely used for the treatment of certain diseases, sterilization of medicinal products as well as medicines. Due to the irradiation process, radiation-induced radicals can form in the structure of drugs. Since medicines have an important role in our life, it is very important to identify these radiation-induced radicals and determine their sensitivity to radiation, their stability, their behavior in different physical conditions, and even their usefulness as an accident dosimeter. CoQ10 is an enzyme found naturally in the human body and responsible for the conversion of food into energy. There are many studies about the usage of this enzyme, which is very popular recently, in the treatment of diabetes, cholesterol, Parkinson's disease and migraine. It is claimed that antioxidants and anti-aging properties are also present. It may be added in the content of some vitamins and food supplements, and even can be used as a CoQ10 tablet alone. In this study, the effects of radiation on the CoQ10 enzyme were investigated through ESR technique, taking into account its important role in terms of health. For this purpose, the spectra of natural and irradiated samples were recorded under different spectrometer conditions. The behavior of the radiation-induced radicals in terms of absorbed dose, microwave power and different temperature conditions was investigated. Using the obtained data, the characteristic features of the radical are revealed.

Keywords: Electron Spin Resonance (ESR), radiation, CoQ10, radical

Thermoluminescence heating rate behaviour of $Zn(BO_2)2:0.05Dy3+$

[1] SÜMEYRA BALCI-YEĞEN Çukurova University, Department of Physics, Adana, Turkey
[2] MEHMET YÜKSEL Çukurova University, Department of Physics, Adana, Turkey
[3] NİL KÜÇÜK Uludağ University, Department of Physics, Bursa, Turkey
[4] YÜKSEL KARABULUT Manisa Celal Bayar University, Department of Physics, Muradiye, Manisa, Turkey
[5] MEHMET AYVACIKLI Manisa Celal Bayar University, Department of Physics, Muradiye, Manisa, Turkey
[6] NURDOĞAN CAN Jazan University, Saudi Arabia
[7] MUSTAFA TOPAKSU Çukurova University, Department of Physics, Adana, Turkey

$Zn(BO_2)_2:0.05Dy3+$ phosphor prepared by using the nitric acid method was examined via thermoluminescence (TL) technic. The TL glow curves of the sample exposed to beta ray in the dose range of 1-80 Gy show a TL maximum at c.a. 180°C (preheated at 140°C and measured at a constant heating rate (HR) value: 2°C s^{-1}, by using Lexsyg Smart TL reader). The linearity was noted and TL signal saturation has not been observed up to 80 Gy. Furthermore TL glow curves of $Zn(BO_2)_2:0.05Dy3+$ phosphor exposed to 20 Gy beta dose were studied using different HRs in the range of 0.5–10°C s^{-1}. While HR value increases: (i) the temperature value at maximum TL intensity (Tm) shifts to higher temperature values, (ii) maximum TL intensity value of the glow peak decreases, (iii) the integrated peak area of the glow curve decreases, and (iv) full width at half maximum (FWHM) increases, as presence evidences of temperature lag effect and thermal quenching phenomenon.

Keywords: Thermoluminescence, Zinc borate, dosimetry, heating rate

Variation of the kinetic parameters of traps found in the fluorapatite mineral ($Ca_5F(PO_4)_3$) in tooth enamel under the different annealing temperatures

DİLEK TOKTAMIŞ, HÜSEYİN TOKTAMIŞ, A. NECMEDDİN YAZICI

Gaziantep University, Engineering of Physics Dept., Gaziantep, Turkey

Abstract

Fluorapatite, $Ca_5F(PO_4)_3$, is a kind of important thermoluminescence dosimeter (TLD) material, because the effective atomic number of fluorapatite is close to that of human bones and teeth. In this study, the kinetic parameters of the traps found in the fluorapatite mineral ($Ca_5F(PO_4)_3$) in tooth enamel were obtained at different annealing temperatures (from 500°C to 1100°C) by using a computer glow curve deconvulation program and analysed how the kinetic parameters vary at different annealing temperatures. All samples were irradiated about 35 Gy by the beta source and read out by the TLD reader at 1°C/s after each annealing process.

Keywords: Thermoluminescence, kinetic parameters, fluorapatite, annealing

Introduction

Tooth enamel is the hardest part of tooth and protects the dentine. In terms of its weight, it consists of 95% inorganic minerals, 1% organic minerals, and 3% water [1–3]. It is a complex biomaterial, a composite of elongated mineral crystallites in the form of biological apatite bonded by polymeric proteins and peptide chains saturated with water [4]. It has a hierarchical structure with crystals of hexagonal cross-section tightly packed into rods (prisms) (width 5 mm) [5] and enclosed by polymeric sheaths (width 0.1 mm) [4]. In 1964 about twenty inorganic elements except oxygen, hydrogen and carbon were found in tooth enamel. Hydroxyapatite [$Ca_{10}(PO_4)_6(OH)_2$] and fluorapatite [$Ca_5F(PO_4)_3$] are two major inorganic apatite minerals in tooth enamel. Apatites are a family of compounds characterized by a similar structure, albeit with different compositions.

A trap found in the sample is characterized by kinetic parameters such as activation energy (E_a), frequency factor (s), kinetic order (b) and carrier concentration (n_o). Activation energy is the required energy to release carrier in the trap. Kinetic order gives the relation between the rate of retraping and recombination. Frequency factor is the number of attempt of carrier to escape from the trap. The carrier concentration gives the number of trapped carrier and peak integral generally gives it.

Experiment

The tooth enamel samples were taken from a dentist who separated enamel from dentine. The samples were crushed in the agate mortar to get powder form. The powdered tooth enamel sample was etched for 5 min in a 20% acetic acid water solution followed by drying [6]. It is sieved using fine sieves which have different dimensions and the samples whose grain sizes are between 100 mm and 120 mm were used in all TL measurements. Each experiment was performed with 10 mg aliquot samples.

During performing experiment, a microprocessor controlled furnace was used to anneal the sample at different annealing temperatures (from 600 to 1100 °C). All examples were irradiated about 36 Gy at room temperature with a point beta source (^{90}Sr-^{90}Y) which delivers 0.040 Gy/s. Its activity is about 3.7 GBq (100 mCi). Glow curve measurements were made using a Harshaw TLD System 3500 Manual TLD Reader at 1 °C/s heating rate experiment. Each experiment was repeated three times for different aliquots. The kinetic parameters of the traps found in the annealed sample at different temperature were obtained by a computerised glow curve deconvulation method developed by Afouxenidis et al [7].

Results

Figure 1 shows the fitted glow curves of annealed sample at 600, 700, 800, 900, 1000 and 1100°C with eight individual peaks. The black glow curve is the experimental data and red one is fitted glow curve. The figure of merit (F.O.M) was calculated as 0.92, 0.99, 0.57, 1.15, 0.34 and 0.88%, respectively. Generally, four of individual peaks are lying in the low temperature peaks and others in the high temperature peaks.

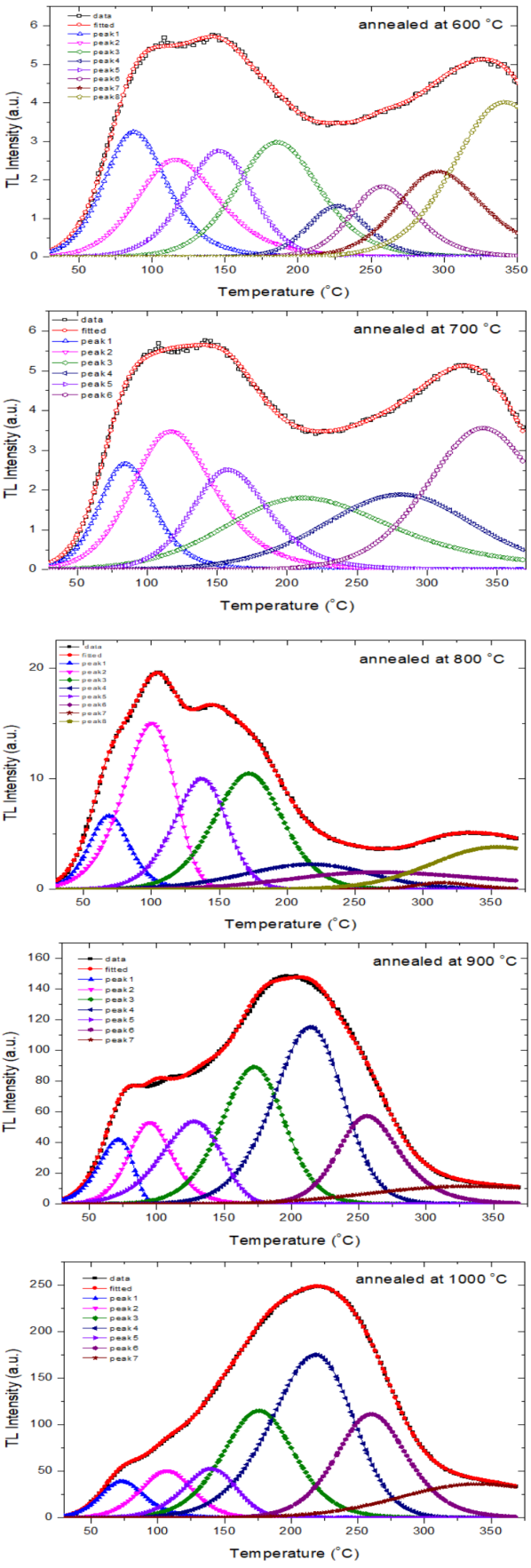

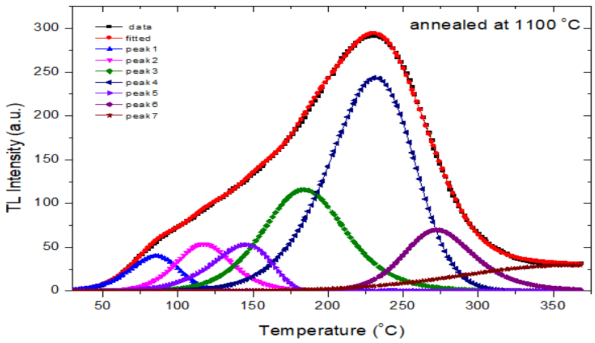

Fig. 1. Fitted glow curves of annealed sample at 600 °C, 700 °C, 800 °C, 900 °C, 1000 °C and 1100 °C with eight individual peaks with 8 peaks.

In the figure 2, the variation of trap depths (activation energy) of low and high temperature peaks lying ~100 °C and ~300 °C as a function of annealing temperature are given. The trap depth of low temperature peak increases with increasing annealing temperature. However, the trap depth of high temperature peak decreases until 800 °C of annealing temperature then starts to increase.

Figure 3 shows the variation of kinetic order of low and high temperature peaks as a function of annealing temperature. The kinetic orders of low and high temperature peaks fluctuate between 1.6 and 2 by increasing annealing temperature.

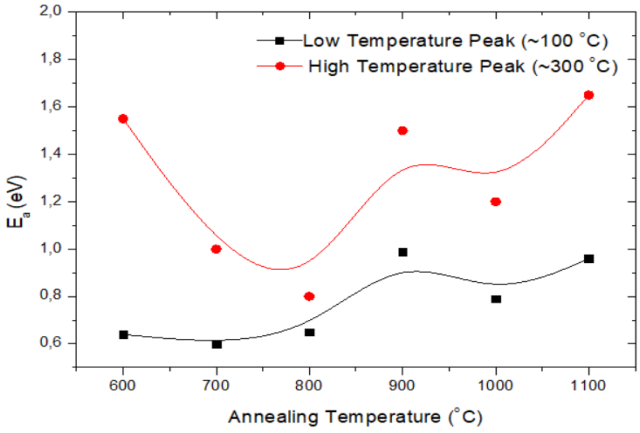

Fig. 2. The variation of trap depths of low and high temperature peaks as a function of annealing temperature

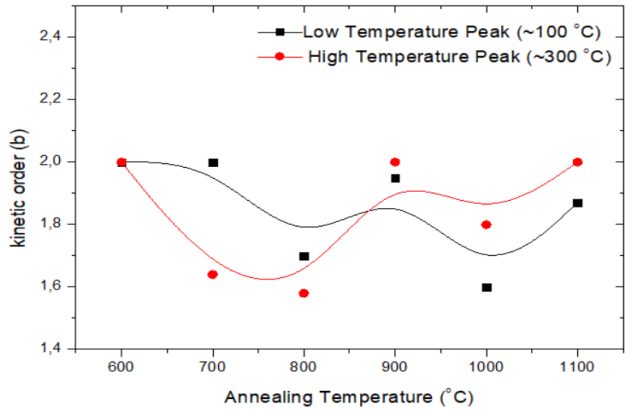

Fig. 3. The variation of kinetic order of low and high temperature peaks as a function of annealing temperature

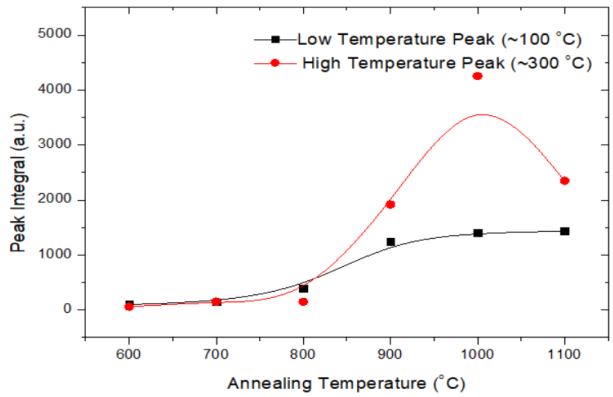

Fig. 4. The variation of peak integral of low and high temperature peaks as a function of annealing temperature

The Figure 4 shows how the peak integrals of low and high temperature peaks vary with increasing annealing temperature. There is no important change in the peak integral for both of low and high temperature peaks up to 800 °C annealing temperature but a huge increase in the peak integral (especially high temperature peaks) was observedabove the 800 °C annealing temperature.

In brief, annealing at different temperatures affects the TL glow curve. A computerised glow curve deconvulation method (CGCD) developed by Afouxenidis et al [7] was used. Generally, TL glow curves are fitted to seven satalite peaks with good FOM values. The activation energy of main peak of low temperature peak varies between 0.6eV and 1 eV for the different annealing temperatures. The activation energy of main peak of high temperature peak varies between 1.1eV and 1.7 eV for the different annealing temperatures. Carrier concentration (n_o, peak integral) does not affected by variation of annealing temperature up to 800 °C, beyond this temperature value it increases.

Reference

[1] J.L. Bernier, J.G. Muhler, Improving Dental Practice Through Preventive Measures, The C.V. Mosby Company, Saint Louis, 1970, pp. 139-145.

[2] J.C. Hess, Endodontiel, II, Librairie Malonine, S.A Paris, 1970.

[3] H. Sicher, E.L. Dubrul, Oral Anatomy, The C.V. Mosby Company, 1970.

[4] A.G. Fincham, J. Moradian-Oldak, J.P. Simmer, J. Struct. Biol. 126 (1999) 270-299.

[5] G.A. Macho, Y. Jiang, I.R. Spears, J. Hum. Evol. 45 (2003) 81-90.

[6] C.E. Secu, M. Cherestes, V. Paraschiva, C. Barca, Radiat. Meas. 46 (2011) 1109-1112.

[7] T. Matsumoto, M. Okazaki, M. Inoue, S. Yamaguchi, T. Kusunose, T. Toyonaga, Y. Hamada, J. Takahashi, Biomaterials 25 (2004) 3807-3812

Investigation of the lambda hypernuclei in nuclear reactions

[1] NİHAL BÜYÜKÇİZMECİ Selçuk University
[2] RIZA OĞUL Selçuk University

Recently, hypernuclei coming from fragmentation and multifragmentation of spectator residues obtained in relativistic heavy ion collisions were investigated in Ref. [1]. We have compared two different mass formula [1-4] for the production of hypernuclei and their properties. The effect of addition of a single Lambda in a non-strange normal nucleus is investigated through the one-neutron and one-proton separation energies. In this way, one can distinguish between different mass formulae of hypernuclei. These kind of investigations give us the opportunity to understand the properties of exotic hypernuclei in the future.

[1] Buyukcizmeci N., Botvina A.S., Pochodzalla, J., Bleicher, M., Phys. Rev. C 88, 014611 (2013).
[2] Botvina A.S and Pochodzalla, J., Phys. Rev. C 76, 024909 (2007).
[3] Samanta C, Roy Chowdhury P and Basu D N., J. Phys. G: Nucl. Part. Phys. 32 363(2006).
[4] Samanta, C., Roy Chowdhury, P., BasuD.N., J. Phys. G: Nucl. Part. Phys. 35 065101(2008).

the work has been performed in the framework of COST 114F328 project and COST Action THOR-CA15213

Keywords: Lambda hyperon, hypernuclei, nuclear reactions

Excitation function of (p,xn) reactions for ^{113}Cd nucleous

[1] BEKİR ORUNCAK Afyon Kocatepe University

The excitation function of (p,n), (p,2n) and (p,3n) reactions for ^{113}Cd target nucleus has been measured up to 400 MeV excitation energy. Reaction cross sections were calculated using Talys 1.8 Nuclear reaction code and compared with the experimental data available in EXFOR nuclear data library. Experimental and calculated cross sections are in good agreement.

Keywords: Nuclear reaction, Talys, Excitation function

Evaluation of the dosimetric results of 3 mm geometric error in linear accelerator (linac) beam data measurements

[1] AYSUN İNAL Antalya Eğitim ve Araştırma Hastanesi Radyasyon Onkolojisi Bölümü

Introduction: It is aimed to find the dosimetric results of 3mm geometric error which can be made in beam data(BD) measurements taken for Treatment Planning System(TPS) modeling. Material and Methods: BD measurements were obtained for 6MV photon energy by the LINAC. Measurements were made for two different sets. At first, the ionisation chambers were positioned at the central axis (T6MVX) and the other was positioned with a 3mm error (F6MVX). The data was loaded into the TPS for modeling. Absorbed doses(AD) corresponding to 100 monitor unit were calculated at points created in the TPS. The dose calculations were made different field sizes. The total dose of cancer patient's Intensity Modulated Radiation Therapy (IMRT) plan was calculated. Also, dose maps were obtained for the same fields and the IMRT plan on a 2-D ion chamber array (I'mRTMatrixx). Measurements were taken on the Linac under the same conditions for all sets. Differences between the calculated-measured values were assessed by performing an AD and gamma evaluation (GE). The differences between the two sets were compared in terms of critical organ (OAR) doses of the IMRT plan. Results: The largest difference between calculated-measured of AD was 0.7%. The percentage difference between the calculated-measured AD, T6MVX and F6MVX was 0.6% and 2.7%, respectively for IMRT. As a result of I'mRTMatriXX, the greatest difference for calculated-measured GE was found 0.5%. When OAR's was compared between T6MVX-F6MVX plans for IMRT, the maximum difference was for the spinal cord (3.1%). Discussion and Conclusion: At TPS quality control, both point-dose and 2-D dose maps (2DDM) should be used in symmetric and AF. Also, central axis, off-axis absorbed dose and 2DDM should be checked. It was observed that the 3 mm geometric error was not recognized in GE for 2 mm, 2% criteria. However, an error was noticed when evaluated for the criterion of 1mm,1%.

Keywords: Beam data, absorbed dose, dose map

Calculation of mass attenuation coefficients of hormirad and galena materials for radiation shielding by Monte Carlo method

[1]NURİ YORULMAZ, [2]MEHMET MURAT YAŞAR, [3]AHMET BOZKURT

[1]Harran University, Department of Physics, Sanliurfa, Turkey
[2]Harran University, Health Vocational School, Sanliurfa, Turkey
[3] Akdeniz University, Department of Biomedical Engineering, Antalya, Turkey

Abstract

When utilizing the benefits of radiation in different applications such as health and energy production, it is necessary to minimize the possible hazards on public, workers and the environment. Therefore, shielding plays an important role among the radiation protection measures, especially for external radiation sources. The composition and thickness of a material to be chosen for a specific shielding design can be determined either through laboratory measurements or computer simulations. The aim of this study is to obtain mass attenuation coefficients of hormirad and galena, a shielding material using the Monte Carlo technique. The simulation results produced with MCNP5 were compared with those from XCOM database and literature data based on GEANT4 simulations and good agreement was observed.

Keywords: Hormirad, Galena, Mass Attenuation Coefficient, Monte Carlo, MCNP5

Introduction

Ionizing radiation is the term used for the energy emitted from an atom which can travel in space and penetrate through materials. It can be obtained either from radioactive sources or radiation devices such as x-ray tubes. It is called ionizing because it has the ability to interact with the atoms of the material it traverses. As a result of the energy deposition in matter, electrons and charged particles (positive ions) are produced which in turn is the reason for such a name. This phenomenon may induce some adverse effects in living species and therefore protection from ionizing radiation is an essential part of the practice in facilities where ionizing radiation sources are present.

As its name implies, radiation protection aims to protect people and the environment from the detrimental effects of ionizing radiation. Protection from an external radiation source is usually expressed as three basic principles; namely reducing the exposure time, increasing the distance to the source and putting shielding across the source [1]. In most situations, limiting the time of exposure along with keeping a large distance from the source may suffice. However, there are many applications using ionizing radiation that necessitate implementing some form of shielding to keep the exposure below acceptable limits so that people can work or live around the source without encountering any harmful effects.

The choice of shielding material depends on the type and energy of the radiation. In recent years, the Monte Carlo (MC) method has found extensive uses in various radiation applications ranging from instrument and detector design to radiation shielding optimization, as well as analysis of biological effects [2]. There are software programs such as FLUKA, GEANT4 and MCNP5 that allow carrying out simulations to find the properties of shielding materials for certain applications [3]. This study investigates two candidate materials, namely galena and hormirad, that can be used to shield photon sources.

Material and Methods

Photon interactions in matter are commonly characterized using mass attenuation coefficients, denoted by $\frac{\mu}{\rho}$. This parameter describes the rate of energy loss by a photon beam as it traverses a medium. Because it is independent of the density of the absorbing medium, the amount of attenuation the material provides becomes exclusively dependent on its atomic structure and the energy of the photons in the beam.

A narrow beam of mono-energetic photons with an incident intensity I_0, penetrating a layer of material with thickness x and density ρ, emerges with intensity I given by the exponential attenuation law [4]

$$\frac{I}{I_0} = \exp\left[-\left(\frac{\mu}{\rho}\right)x\right] \quad (1)$$

This equation can be employed to calculate attenuation coefficient for any material either from results of experimental measurements or computations. An experimental setup to determine values of $\frac{\mu}{\rho}$ for a material is shown in Figure 1. This geometry was created in MCNP5 Monte Carlo simulation program as shown in Figure 2. The values in Table 1 were used for the weight composition of the elements forming the materials studied here [5].

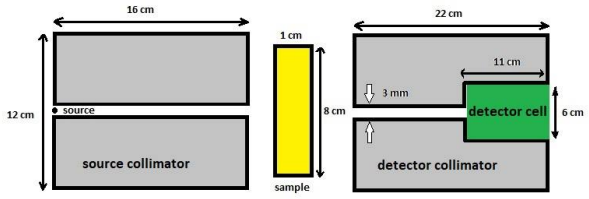

Figure 1. Experimental setup for determination of mass attenuation coefficient.

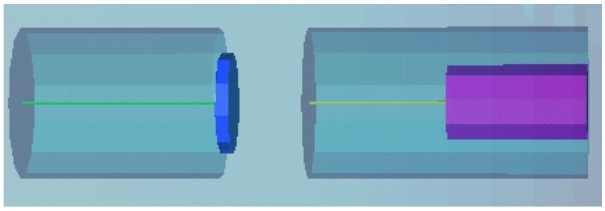

Figure 2. Simulation setup for determination of mass attenuation coefficient by MCNP5.

Table 1. Elemental composition of the materials studied.

Material	Density (g/m^3)	Composition (%)
Hormirad	3.44-4.10	Fe (60.8), O (31.26), Ca (4.36), Si (1.87), H (0.44), Mg (0.39), P (0.29), Ti (0.19), Al (0.17), K (0.06), Mn (0.06), V (0.05), C (0.04), S (0.01), N (0.003)
Galena	7.00-7.50	Pb (86.59),S (13.40)

Results

In this study, mass attenuation coefficients of galena and hormirad were calculated by MCNP5 simulation program using the geometry shown in Figure 2. In Table 2, the obtained values were compared with those provided by XCOM database [5]. It was seen that the results were consistent. When the values in Table 2 and Table 3 are examined, the values obtained with MCNP5 are noticeably in agreement with the values obtained from GEANT4 and XCOM computations.

Table 2. The results and error rates between MCNP5 and XCOM results.

Energy (MeV)	MCNP5	GEANT4	XCOM	Diff. (%)
0.276	0.4362	0.4313	0.431	1.21
0.303	0.3598	0.3566	0.357	0.79
0.356	0.2587	0.2624	0.262	1.27
0.383	0.2316	0.2305	0.231	0.24
0.663	0.1030	0.1056	0.106	2.80
1.25	0.0566	0.0585	0.0585	3.26
2	0.0444	0.0459	0.0459	3.38
6	0.0399	0.0419	0.0419	4.77

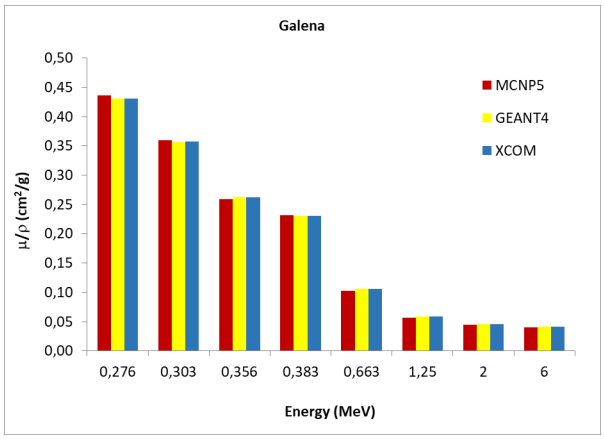

Figure 3. Graphical comparison of MCNP5, GEANT4 and XCOM values for Galena.

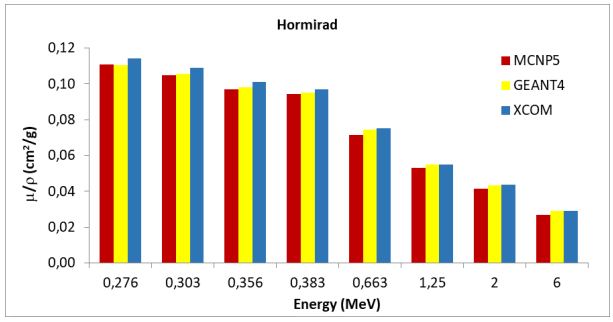

Figure 4. Graphical comparison of MCNP5, GEANT4 and XCOM values for Hormirad.

Table 3. The error rate shows the difference between MCNP5 and XCOM.

Energy (MeV)	MCNP5	GEANT4	XCOM	Diff. (%)
0.276	0.1110	0.1104	0.114	2.66
0.303	0.1050	0.1056	0.109	3.70
0.356	0.0969	0.0982	0.101	4.02
0.383	0.0945	0.0951	0.0971	2.71
0.663	0.0715	0.0745	0.0752	4.91
1.25	0.0532	0.0549	0.0551	3.47
2	0.0415	0.0435	0.0436	4.82
6	0.0270	0.029	0.029	6.90

References

[1] H. Cember, T. E. Johnson, Introduction to Health Physics: 4th Ed., McGraw Hill, 2008.

[2] P. Andreo, Monte Carlo techniques in medical radiation physics, Phys. Med. Biol. **36**:7, 1991.

[3] MCNP - A General N-Particle Transport Code, Version 5, LA-UR-03-1987 (2003).

[4] J.H. Hubbell, Photon Mass Attenuation and Energy-Absorption Coefficients from 1 keV to 20 MeV, 1982.

[5] V. P. Singh, N. M. Badiger. Novel High Strength Economical Shielding Materials, Sinop Uni J Nat Sci **2**(1): 1-12 (2017).

Dosimetric comparison of three different VMAT techniques in head and neck cancer radiotherapy

[1] OĞUZ AYDIN Uludağ University
[2] DUYGU BOLAT Uludağ University
[3] SEMA GÖZCÜ TUNÇ Uludağ University
[4] CANDAN DEMİRÖZ ABAKAY Uludağ University
[5] SİBEL KAHRAMAN ÇETİNTAŞ Uludağ University
[6] MERAL KURT Uludağ University
[7] ALİ ALTAY Uludağ University

In head and neck cancer radiotherapy, at three different radiotherapy plans prepared by Volumetric Modulated Arc Therapy (VMAT) technique, target volume, dose and critical organ doses were examined. In this study, 8 head and neck cancer cases were evaluated. In radiotherapy plans; (sVMAT) as a one bean-double arc and two beam as double rotation (dVMAT)and double arc as 150-3450 collimator angular (cVMAT) plans were prepared. For each patient, three VMAT plans were generated to meet the same objectives of the PTV.And the results were compared dosimetrically. PTV doses, Homogeneity index (HI), Conformity index (CI) and monitor unit (MU) were compared and analyzed with the IBM SPSS Statistics 20 program. The target volume doses, HI, CI and MU was examined and there was no statistically significant difference between methods. The sVMAT technique gave a lower dose value when there was no significant difference in right parotid D_{mean} ($p = 0.412$) and V30% ($p = 0.412$). In the left parotid D_{mean} ($p = 0.939$) and V30% ($p = 0.714$), three techniques gave similar results. There was no significant difference in oral cavity D_{mean} ($p = 0.616$), but lower dose values were observed in the sVMAT technique The statistical result of the mandibular data was found to be $p = 0.957$ for the D_{max} value and no significant difference was observed between the methods; but maximum dose was little bit higher in plans using collimator angles. Result of this study, we are considering that the three techniques are suitable for use in patient treatment because they provide the desired tumor dose and critical organ doses in limitations, but also, we believe that in sVMAT technique can minimize side effects that may occur at patients, because of providing lower dose to the critical organs.

Keywords: Colimator Angle, Head and Neck Cancer, Monaco, VMAT

Triple differential cross sections for the single ionization of water molecule (H_2O) by electron impact

[1] BOUMEDIENE LASRI University Tahar Mouly of Saïda, Algeria.
[2] MOHAMED SAHLAOUI Science and Technology Preparatory School, Tlemcen, Algeria
[3] FATIMA BOUASRIA University Tahar Moulay of Saïda, Algeria
[4] MAMMAR BOUAMOUD University Center of Naama, Algeria
[5] MEVLÜT DOĞAN Turkey

The single ionization of atomic and molecular targets by electron impact called (e,2e) is one of the complex and fundamental processes in collision theory. An accurate description of this reaction is very important for several fields, such as plasma physics, astrophysics, laser physics, and radiobiology as the macroscopic effects of radiations on biological tissues. However, dealing with the ionization of a molecular target is a challenge. So, several approximations are necessary to construct an accurate formalism. In this work, we present our analytical formalism developed to calculate triple differential cross section (TDCS) for the ionization by electron impact of simple molecules with the chemical form XHn. This formalism is used in this case to predict the triple differential cross sections for the single ionization of a water molecule by electron impact. Our theoretical calculations (First Born, second Born and Schwinger approximations) stay in good agreement with experimental data.

Keywords: TDCS, Born Approximation, cross section, ionization process

Theoretical calculation of neutron induced fission cross section on some actinides

[1] ASİYE GÜROL,[2] İSMAİL HAKKI SARPÜN,[3]AHMET BOZKURT

[1]Afyon Kocatepe University, Institute of Sciences, Dept. of Physics, Afyonkarahisar
[2]Akdeniz University, Science Faculty, Dept. of Physics, Antalya
[3]Akdeniz University, Biomedical Engineering Dept., Antalya

Abstract

Actinide element, any of a series of 15 consecutive chemical elements in the periodic table from actinium to lawrencium (atomic numbers 89–103). As a group, they are significant largely because of their radioactivity. Although several members of the group, including uranium (the most familiar), occur naturally, most are man-made. Both uranium and plutonium have been used in atomic weapons for their explosive power and currently are being employed in nuclear plants for the production of electrical power. In this study, fission cross section (n,f) of neutron induced reaction were theoretically calculated by Talys 1.8 nuclear reaction code and compared with experimental data in the EXFOR Nuclear Data Library.

Keywords: Fisssion, Actinides, TALYS

Introduction

Theoretical calculations of nuclear reaction cross section of light charged particles using theoretical models due to limited experimental data are very important. In addition, nuclear cross section data is necessary for the correction of nuclear theories. Especially, if the experimental data is not likely to be produced due to experimental difficulties, excitation functions of nuclear reaction are needed to ensure that the nuclear reaction model.

TALYS is a nuclear reaction code created at NRG Petten, the Netherlands and CEA Bruye`res-le- Chatel, France. The objective is to provide a complete and accurate simulation of nuclear reactions in the 1 keV-200 MeV energy range, through an optimal combination of reliable nuclear models, flexibility and user-friendliness. TALYS can be used for the analysis of basic scientific experiments or to generate nuclear data for applications [1]. This code is commonly used to analyze and predict the nuclear reactions involving n, γ, p, d, t, ^{3}He, and α particles in the 1 keV–1 GeV energy range for target nuclei heavier than Li.

Results

The fission cross sections of neutron induced fission reactions for ^{249}Bk, ^{249}Cf, and ^{248}Cm were theoretically calculated with Talys 1.8 nuclear reaction code and compared with available experimental data in EXFOR library [2].

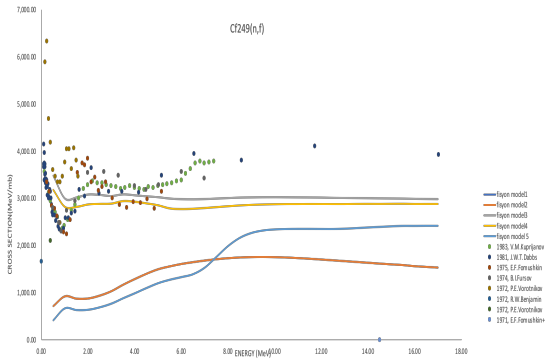

Fig. 1. ^{249}Cf (n,f) reaction

When the fission models are examined from the Fig. 1 for ^{249}Cf(n,f) reaction, the Model 3 and 4 are in good agreement with experimental values. It is same for Fig 2 and Fig 3 for ^{248}Cm(n,f) and ^{249}Bk(n,f) reactions, respectively.

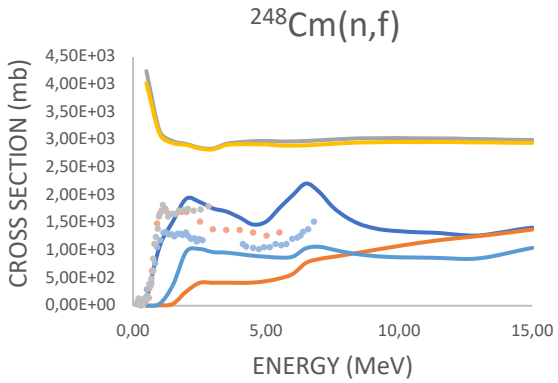

Fig. 2. ^{248}Cm (n,f) reaction

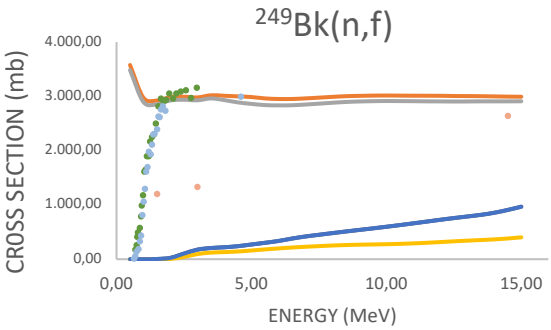

Fig. 3: ^{249}Bk (n,f) reaction

References

[1] A Koning, S Hilaire *and* S Goriely, TALYS–1.8 A Nuclear Reaction Program, User Manual, 1st edn. (NRG, The Netherlands, 2016).

[2] Brookhaven National Laboratory, National Nuclear Data Center, EXFOR/CSISRS (Experimental Nuclear Reaction Data File). Database Version of 2018-04-11 (2018). (http://www.nndc.bnl.gov/exfor/)

Theoretical calculation of gamma induced fission cross section on some actinides

[1]ASİYE GÜROL,[2]İSMAİL HAKKI SARPÜN, [3]RIDVAN ÜNAL

[1]Afyon Kocatepe University, Institute of Sciences, Dept. of Physics, Afyonkarahisar
[2]Akdeniz University, Science Faculty, Dept. of Physics, Antalya
[3]Usak University, Medical Imaging Dept., Usak

Abstract

The Actinide series contains elements with atomic numbers 89 to 103 and is the third group in the periodic table. These elements all have a high diversity in oxidation numbers and all are radioactive. The most common and known element is Uranium, which is used as nuclear fuel when its converted into plutonium, through a nuclear reaction. In this study, fission cross sections of some actinides were calculated by Talys 1.8 nuclear reaction code for gamma induced reactions. Theoretical calculated results were compared with experimental data available in the EXFOR Nuclear Data Library.

Keywords: Fission, Actinide, Talys

Introduction

Theoretical calculations of light charged particles induced nuclear reaction cross section using theoretical models due to some difficulties in experiments are very important. Furthermore, cross section data is necessary for the nuclear theory corrections. Especially, if there is no experimental data for a particular reaction, excitation functions of nuclear reaction are needed to develope the nuclear reaction model.

TALYS is a nuclear reaction code created at NRG Petten, the Netherlands and CEA Bruye`res-le- Chatel, France. The objective is to provide a complete and accurate simulation of nuclear reactions in the 1 keV-200 MeV energy range, through an optimal combination of reliable nuclear models, flexibility and user-friendliness. TALYS can be used for the analysis of basic scientific experiments or to generate nuclear data for applications [1]. This code is commonly used to analyze and predict the nuclear reactions involving n, γ, p, d, t, ^{3}He, and α particles in the 1 keV–1 GeV energy range for target nuclei heavier than Li.

Results

The fission cross sections of gamma induced fission reactions for ^{249}Bk(g,f), ^{243}Cm(g,f), ^{245}Cm(g,f), and ^{249}Cf(g,f) were theoretically calculated with Talys 1.8 nuclear reaction code and compared with available experimental data in EXFOR library [2].

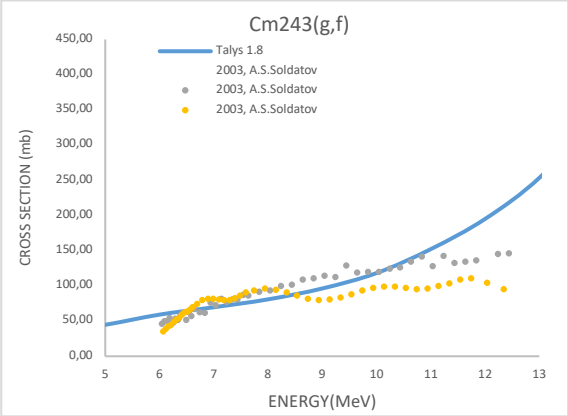

Figure 1. ^{243}Cm(g,f) reaction cross section

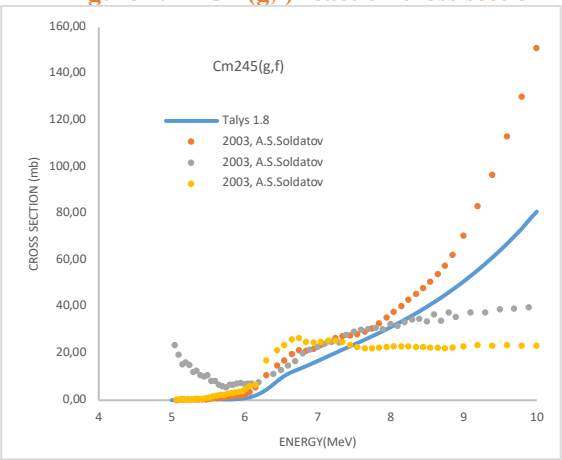

Figure 2. 245Cm (g,f) reaction cross section

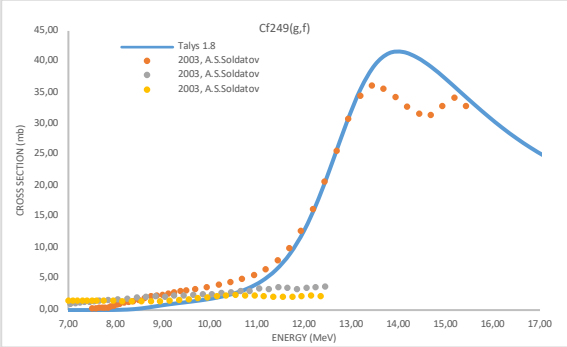

Figure 3. ^{249}Cf (g,f) reaction cross section

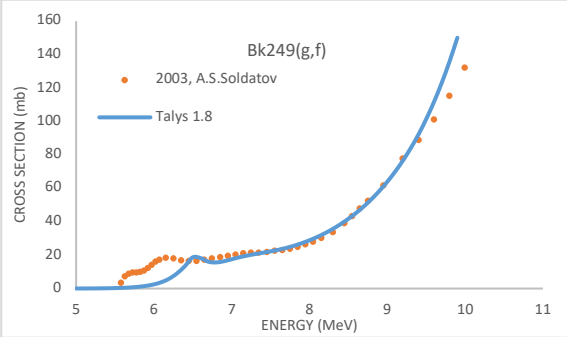

Figure 4. ^{249}Bk(g,f) reaction cross section

References

[1] A Koning, S Hilaire *and* S Goriely, TALYS–1.8 A Nuclear Reaction Program, User Manual, 1st edn. (NRG, The Netherlands, 2016).

[2] Brookhaven National Laboratory, National Nuclear Data Center, EXFOR/CSISRS (Experimental Nuclear Reaction Data File). Database Version of 2018-04-11 (2018). (http://www.nndc.bnl.gov/exfor/)

High performance graphene-based photodetectors

[1] CEREN KARAMAN Pamukkale University Faculty of Engineering,Department of Chemical Engineering
[2] A. GÜNEŞ TANIR Gazi University
[3] İSMAİL HAKKI SARPÜN Akdeniz University
[4] ONUR KARAMAN Akdeniz University
[5] EDİP BAYRAM Akdeniz University Department of Chemistry
[6] ASUMAN KOLBAŞI Göztepe Training and Research Hospital

Graphene promise many outstanding physicochemical properties such as high carrier mobility, good light transmittance within wide wavelength range, great mechanical strength and flexibility, excellent electrical and thermal conductivity which indicate several potentials in electronics and optoelectronic device applications. The versatility of graphene enables its application in several areas such as ultrafast and ultrasensitive detection of light in the ultraviolet, visible, infrared and terahertz frequency ranges. These detectors can be integrated with other photonic components based on the same material, as well as with silicon photonic and electronic technologies. A variety of graphene-based optoelectronic devices including transparent electrodes in displays and photovoltaic modules, optical modulators, plasmonic devices and ultrafast lasers have already been investigated. Among these, developing photodetectors, based on a graphene and related materials, have gained importance. Distinct characteristics and unique properties of graphene based photodetection systems have been studied over the past few years. Here, it is provided an overview of state-of-the-art photodetectors based on graphene, and hybrid systems based on the combination of different crystals and other nanomaterials. It is concluded that photodetectors based on graphene are being developed, with great promise for a wide variety of application fields. It can be said that in order to enhance the graphene-based detector performance, it is need to produce large-scale, high quality graphene at low cost, and to establish large-scale integration with existing photonic and electronic platforms.

Keywords: Graphene, physicochemical properties, photodetectors

Photo-neutron cross section calculations of ^{84,86,87,88}Sr

[1]İSMAİL HAKKI SARPÜN, [2]HASAN ÖZDOĞAN, [3]MERT ŞEKERCİ, [3]ABDULLAH KAPLAN

[1]Akdeniz University, Physics Dept., Antalya, Turkey
[2] Akdeniz University, Biophysics Dept., Antalya, Turkey
[3]Süleyman Demirel Üniversitesi, Physics Dept., Isparta, Turkey

Abstract

The data from photonuclear reactions are very essential to understand the arrangements and behaviors of the atomic nucleus. The investigation of photon induced reactions are crucial for many exist and emerging fields, such as radiation transport, shielding studies, design of fusion-fission reactors etc. The one of the most important input in the computation of cross section of photonuclear reactions is gamma strength function. In this study, the purpose is to investigate gamma strength function effect on photo-neutron cross sections using TALYS 1.8 code through the five different gamma strength function models. The reaction cross sections of ^{84,86,87,88}Sr(γ,n) have been calculated using Kopecky-Uhl generalized Lorentzian Model (KLM), Brink-Axel Lorentzian Model (BLM), Hartree-Fock BCS tables (HBCS), Hartree-Fock-Bogolyubov tables (HBT) and Goriely's Hybrid Model (GHM). To select the best gamma strength function model, a relative variance calculation is used. Experimental data for the investigated reactions have been taken from EXFOR library and used for comparisons of the obtained calculation results.

Keywords: Photoneutron, Talys, Gama-Strength function

Introduction

For many purposes like obtaining and detecting neutrons and charged particles of different energies, measuring the cross–section values and etc. various experimental techniques and procedures have been generated to cover different particle–induced reactions [1]. With the advencements and improvements in the computer technologies, it has become possible to carry out the nuclear reaction calculations in virtual environments. For this purpose and overcome the difficulties like the absence of the experimental data and experimental problems or costs, scientists have been developed many calculation codes related to the nuclear reactions. It is possible to use these codes in the reaction cross-section calculations, spectrum of outgoing particles etc. for a long time [2]. The examples for some of the known and used codes could be given as CEM95, ALICE/ASH, PCROSS, FLUKA, GEANT, TALYS and EMPIRE. Due to above mentioned diffuculties; computer aided codes, which utilize the nuclear reactions theories, are required. With the developments in scientific and industrial areas, the experimental studies in nuclear fields have been extended where photonuclear reaction studies could be pointed as one of them. Over the past fifty years, these studies have been carried out for lots of nuclei since photon matter interactions give us crucial information about structure of atomiv nuclei, energy levels, half life etc. Our purpose within this study is to investigate the gamma strength function effects on photonuclear reactions.

Material Methods

Photo-neutron cross section calculatins of ^{84,86,87,88}Sr isotopes have been done up to 25 MeV photon energy. For calculations TALYS 1.8 [3] code has been used. Constant Temperature Fermi Gas Model [4] has been chosen as level density option. The photo-neutron cross-section calculations of ^{84,86,87,88}Sr isotopes have been carried out by using different gamma strength function models from TALYS 1.8 computation code. KLM, BLM, HBCS, HBT and GHM have been employed for calculations. Detailed description of the models that are employed within this study can be found in Ref 3. The best gamma strength function model has been selected according to relative variance, D, analysis [5]. The best theoretical models with respect to the experimental data have been chosen by considering the smallest value of D. Calculations result through the different gamma strength functions have been compared with the experimental data taken from EXFOR [6] database.

Results and Discussions

In the present study, photo-neutron cross–sections of ^{84,86,87,88}Sr isotopes have been calculated by using TALYS 1.8 computer code. The comparison of reaction cross–sections with experimental data taken from EXFOR have been given in Figs. 1–4. In addition, statistical analysis results have been given in Table 1.

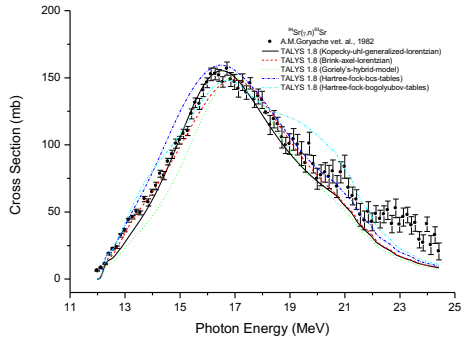

Fig. 1. $^{84}Sr(\gamma,n)^{83}Sr$ reaction cross-sections

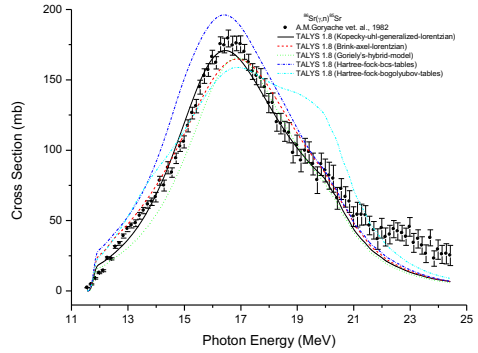

Fig. 2. $^{86}Sr(\gamma,n)^{85}Sr$ reaction cross-sections

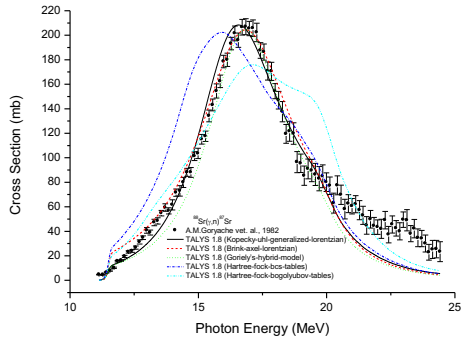

Fig. 3. $^{87}Sr(\gamma,n)^{86}Sr$ reaction cross-sections.

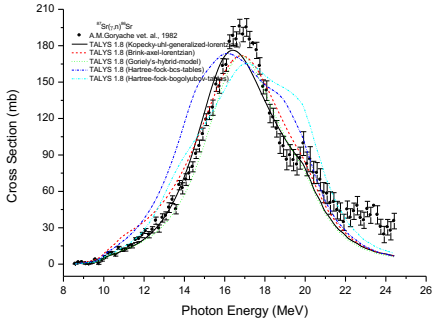

Fig. 4. $^{88}Sr(\gamma,n)^{87}Sr$ reaction cross-sections.

Table 1. Statistical analysis of photo-neutron reactions

Target	KLM	BLM	HBCS	HBT	GHM
^{84}Sr	5.231	4.5435	5.6124	4.7895	5.8211
^{86}Sr	3.6276	5.6132	8.0327	5.945	4.13
^{87}Sr	0.3113	0.5441	0.5393	0.5393	0.3333
^{88}Sr	4.4206	6.5606	11.6041	6.7526	5.0044

As summarized:

1) Generally all model calculation results are in good conformity with the EXFOR data.
2) KLM is the best gamma strength function model except from $^{84}Sr(\gamma,n)^{83}Sr$ reaction.
3) For $^{84}Sr(\gamma,n)^{83}Sr$ reaction BLM calculations have better accordance with experimental data rather than the other models.

Reference

[1] A Forrest, J Kopecky, J-Ch., The European Activation File: EAF-2005 Cross Section Library, UKAEA FUS 515 (2005)

[2] P.M. Raole et al., Trans. IIM 62, 2 (2009)

[3] A. Koning, S. Hilaire, S. Goriely, TALYS–1.8 A Nuclear Reaction Program, User Manual, 1st edn. (NRG, The Netherlands, 2015.

[4] Ignatyuk, A.V., Istekov, K.K., Smirenkin, G.N., 1979. The role of collective effects in the systematics of nuclear level densities. Yad. Fiz. 29, 875–883.

[5] Kurenkovb, N.V., Luneva, V.P., Shubina, Yu.N., 1999. Evaluation of calculation methods for excitation functions for production of radioisotopes of iodine, thallium and other elements. Appl. Radiat. Isot. 50, 541–549.

[6] Brookhaven National Laboratory, 2018. National Nuclear Data Center, EXFOR/CSISRS (Experimental Nuclear Reaction Data File). Database Version of July 17, 2018. ⟨http://www.nndc.bnl.gov/exfor/⟩.

Proton, deuteron and alpha emission of TiN composites

[1]İSMAİL HAKKI SARPÜN, [2]AHMET BOZKURT, [3]ABDULLAH AYDIN,[4]SUAT PAT, [5]MOHAMED BELGAID

[1]Akdeniz University, Physics Dept., Antalya, Turkey
[2]Akdeniz University, Biomedical Engineering Dept., Antalya, Turkey
[3]Kırıkkale University, Physics Dept., Kırıkkale, Turkey
[4]Eskişehir Osmangazi University, Physics Dept., Eskişehir, Turkey
[5]USTHB, Physics Faculty, Algiers, Algeria

Abstract

Titanium nitride composites (TiN) are industrially available materials that are considered to be promising for applications in nuclear technology, especially, as fusion reactor structural material. They are known to be particularly resistant to very high neutron irradiation environments due to low activation characteristics. In this study, TiN composites, which were produced in Eskisehir Osmangazi University by plasma RF sputtering method, have been investigated as a target material using Monte Carlo simulations to obtain proton, deuteron and alpha emission spectra under neutron irradiation.

Keywords: MCNP, Composite, TiN

Introduction

In a fusion reactor, one of the possible reactions that can be used to generate energy is the deuterium-tritium reaction. One of the advantages of D-T reaction is that it produces 14 MeV neutrons. These produced neutrons impact to the reactor devices and lose their energy. Light charged particles, i.e. protons, deuterons and alpha particles, are produced in these nuclear reactions. The amount of energy lost by these particles is important for determining the mean free path in reactor elements that neutrons hit, that is, the thickness of this element [1,2].

Titanium nitride (TiN) (sometimes known as tinite) is an extremely hard ceramic material, often used as a coating on titanium alloys, steel, carbide, and Al components to improve the substrate's surface properties. Applied as a thin coating, TiN is used to harden and protect cutting and sliding surfaces, for decorative purposes (due to its golden appearance), and as a non-toxic exterior for medical implants. In most applications a coating of less than 5 micrometres (0.00020 in) is applied.

In this study, one of the candidate materials, TiN composites, which were produced by plasma RF sputtering method in Turkey, Eskişehir Osmangazi University, have been bombardment by neutrons to obtain light charged particle (proton, deuteron and alpha) emission spectra using MCNP code.

Calculation Methods

Monte Carlo N - Particle Transport (MCNP) is a code developed by the Los Alamos National Laboratory (LANL) to simulate radiation interactions using the Monte Carlo method. Each card in the input file that needs to be entered into the MCNP code provides information about the geometric properties of the problem, the information identifying the material in question, the properties of the source, and the type of results desired using the three bases. card sets: cell, surface, and data cards. The MCNP code obtains the physical rules of the interactions in the form of cross-sectional data files that are evaluated to transport each particle through the target materials between the source and the detector [5]. Electron microscopy image of samples is shown in Fig. 1.

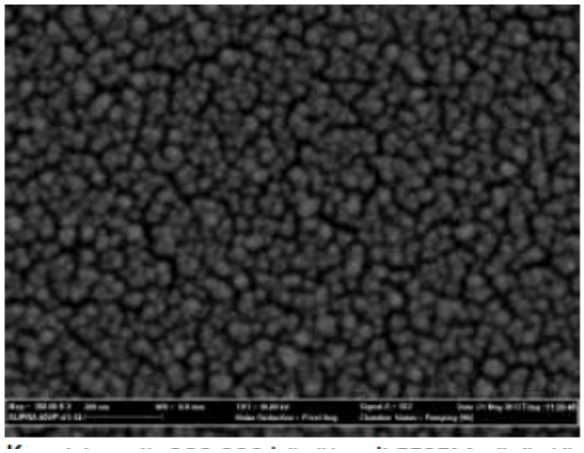

Fig. 1. Electron microscope image of TiN composite

In this work, a neutron beam of 14 MeV is directed to TiN composite specimens used as the target material in the MCNP simulation. In simulations, it has been shown that the energy and flux values of protons, deutrons and alpha particles are monitored as a result of interaction with the target using specific types of drills acting as detectors. The spectrum of these secondary particles produced from neutron interactions is shown in Fig. 2.

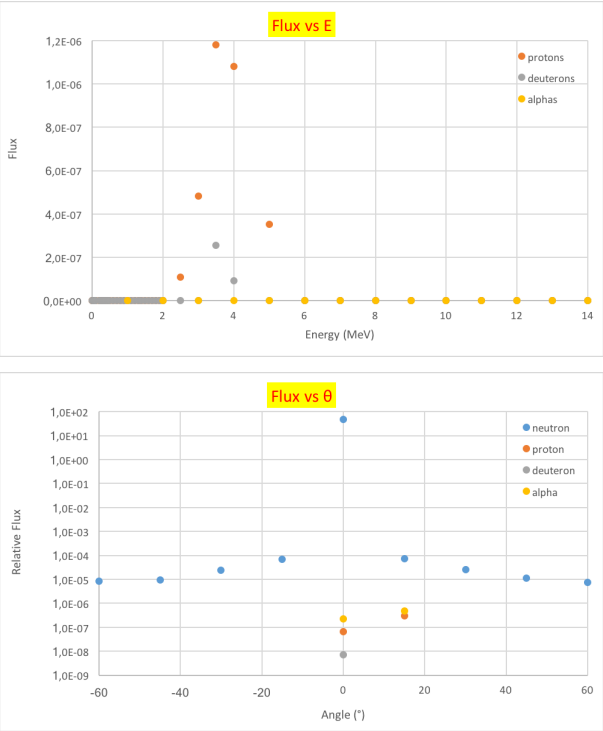

Fig. 2. The spectrum of charged particles

Different sample thickness have used in calculations and Table 1 shows the effect of thickness to charged particle emission.

Table 1. The effect of sample thickness to charged particle emission

Thickness	neutron	proton	deuteron	alpha
mm	ptcl/cm2	ptcl/cm2	ptcl/cm2	ptcl/cm2
1	47.1207	6.71628E-08	7.30674E-09	2.,26077E-07
10	47.1207	6.71628E-08	7.30674E-09	2.26077E-07
100	47.1197	6.7200E-08	7.30673E-09	2.26152E-07
1000	47.1094	6.7560E-08	7.30671E-09	2.2691E-07

Conclusion

The main outcome of the study was to establish the fact that TiN composites are potential candidate structural materials for reactor applications. The next step of the project will be in Algeria via USTHB. Samples will be bombarded with neutrons.

References

1. Demir B., Sarpün İ.H., Kaplan A., Çapalı V., Aydın A., Tel E., 2015. Double differential cross section and stopping power calculations of light charged particle emission for the structural fusion materials ^{50,52}Cr, J. Fusion Energy, 34, 808-816.
2. Sarpün İ.H., Aydın A., Kaplan A., Demir B., Tel E., Çapalı V., 2015. Double differential charged particle emission cross sections and stopping power calculations for structural fusion materials ^{58,60}Ni, J. Fusion Energy, 34, 1306-1315.
3. Höglund C., Birch J., Andersen K., Bigault T., Buffet J.-C., Correa J., Esch P., Guerard B., Hall-Wilton R., Jensen J., Khaplanov A., Piscitelli F., Vettier C., Vollenberg W., Hultman L., 2012. B_4C thin films for neutron detection, J. Applied Physics 111, 104908.
4. Briesmeister, J.F., Editor, 2000. MCNP- A General Monte Carlo N-Particle Transport Code System. LA-12625-M, Version C

Calculation of linear attenuation coefficient of amethyst material for radiation shielding by Monte Carlo method

[1]MEHMET MURAT YAŞAR,[2]NURİ YORULMAZ, [3]AHMET BOZKURT

[1]Harran University, Health Vocational School, Sanliurfa, Turkey
[2]Harran University, Department of Physics, Sanliurfa, Turkey
[3]Akdeniz University, Department of Biomedical Engineering, Antalya, Turkey

Abstract

When utilizing the benefits of radiation in different applications such as health and energy production, it is necessary to minimize the possible hazards on public, workers and the environment. Therefore, shielding plays an important role among the radiation protection measures, especially for external radiation sources. The composition and thickness of a material to be chosen for a specific shielding design can be determined either through laboratory measurements or computer simulations. The aim of this study is to obtain linear attenuation coefficients of amethyst, a natural shielding material using the Monte Carlo technique. The simulation results produced with MCNP5 were compared with those from XCOM database and literature data based on FLUKA simulations and good agreement was observed.

Keywords: Amethyst, Linear Attenuation Coefficient, Monte Carlo, MCNP5

Introduction

In facilities employing radiation devices or radioactive sources that emit radiation, radiation protection is an important part of the practice which aims to protect people and the environment from the detrimental effects of ionizing radiation. Protection from an external radiation source is usually expressed as three basic principles; namely reducing the exposure time, increasing the distance to the source and putting some form of shielding across the source [1]. Shielding is used in nuclear power plants, industrial facilities and medical clinics in the form of lead, concrete or water, the choice being dependent on the type and energy of the radiation in question. There are continuos efforts for finding the most suitable shielding materials that protect better and cost less.

Amethyst is a natural material that contains many elements in different proportions and is a natural resource found in various regions of the world. Whether it can be an alternative shielding mateial can be understood either using laboratory experiments or computer simulations. In recent years, the use of Monte Carlo (MC) simulations has rapidly increased with applications ranging from instrument design to radiation shielding and analysis of biological effects [2]. Programs such as FLUKA, GEANT4 and MCNP5 allow modeling of shielding materials such as amethyst. In this study, MCNP5 Monte Carlo Simulation program was used to determine the shielding properties of amethyst material [3].

Material and Methods

The decision on a material to be used as a suitable radiation shielding material is usually based on the attenuation coefficient which, is usually expressed as linear or mass attenuation coefficient, is a measure of shielding capability of a material against radiation. Linear attenuation coefficients of elements, compounds, mixtures and materials are widely used in applications with radiation sources such as space physics, dosimetry, plasma physics, etc. [4].

As can be seen from Figure 1, radiation incident on a material of thickness x passes through the material with a decreased intensity. This behavior is summarized by Beer- Lambert Law, which states that a radiation beam exhibits an exponential decrease by the thickness of the target material and by the effect of the linear attenuation coefficient.

$$I = I_0 e^{-\mu x} \qquad (1)$$

Here; I_0 is defined as the initial intensity from the source, x is the thickness of the target material, μ is the linear attenuation coefficient of the material, and I is the intensity of the radiation passing through the material.

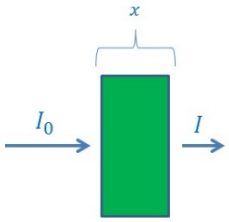

Figure 1. Reduction in the intensity of radiation passing through a material of thickness x.

In this study, Monte Carlo modeling was performed using MCNP5 package and Beer- Lambert Law. The data used as geometry modeling are: density of amethyst material is 2.65 g/cm^3; the beam path was a cylinder with 0.15 cm radius; the target thickness is 5 cm and 4 cm radius; collimator for beam path is 16 cm thick and 6 cm radius; collimator for detector is 22 cm thick and 6 cm radius (Figure 2). The values in Table 1 were used for the weight composition of the elements forming the amethyst material [5]. After the geometry was created,

eight different source energy were studied. These are: 0.276 MeV, 0.303 MeV, 0.356 MeV, 0.383 MeV, 0.663 MeV, 1.25 MeV, 2.0 MeV ve 6.0 MeV [6]. The obtained results were compared with the values in XCOM and literature.

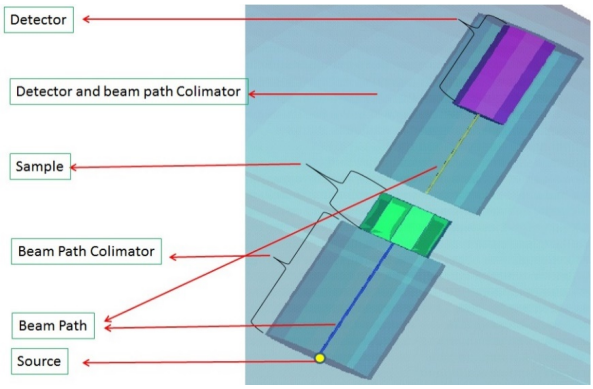

Figure 2. Geometry generated by MCNP5 modeling of the linear attenuation coefficient.

Table 1. Elemental composition of amethyst (density 2.65 g/m³).

Composition (%)					
B: 6.1003	F: 0.3541	Cr: 0.0213	Mn: 0.2220	Na: 0.2141	Mg: 0.2187
Al: 1.384	Si: 89.8957	P: 0.0486	S: 0.0647	Cl: 0.0706	K: 0.3889
Fe: 0.7050	Ca: 0.2008	Ti: 0.0434	Ni: 0.0101	Zn: 0.0053	Br: 0.0007
Sr: 0.0026	Yt: 0.0027	As: 0.0119	U: 0.0053	Ga: 0.0071	

Results

In this study, the results obtained from the output file of the linear attenuation coefficient of amethyst material computed with MCNP5 are given in Table 2. When the values for modeling in this study are examined, the error rate is usually less than 5% as seen in the results obtained with MCNP5 (Table 2). This suggests that the modeling is appropriate.

Table 3 compares the values obtained with FLUKA and XCOM from previous studies. It is seen that the values obtained with MCNP5 are close to those obtained with the mentioned methods. As seen from the graphical comparison in Figure 3, the first five energy values in XCOM were not found in the literature and the other eight energies are compatible with both FLUKA and XCOM values.

Table 2. Flux values obtained with MCNP5.

Energy (MeV)	F4 Flux (1/cm²)	% Error
0.276	4.02E-08	4.20%
0.303	4.26E-08	4.08%
0.356	4.64E-08	3.90%
0.383	4.82E-08	3.83%
0.663	6.46E-08	3.31%
1.25	8.25E-08	2.93%
2	9.73E-08	2.70%
6	1.23E-07	2.40%

Table 3. Comparison of the data obtained with MCNP5 and the literature.

	Literature		Literature diff (%)	
MCNP5	FLUKA	XCOM	FLUKA	XCOM
0.2930	0.291	-	0.69%	-
0.2814	0.2792	-	0.78%	-
0.2642	0.2613	-	1.11%	-
0.2564	0.2553	-	0.44%	-
0.1981	0.2018	-	1.85%	-
0.1490	0.1494	0.1503	0.28%	0.88%
0.1160	0.1169	0.1184	0.74%	2.00%
0.0691	0.0734	0.0732	5.87%	5.61%

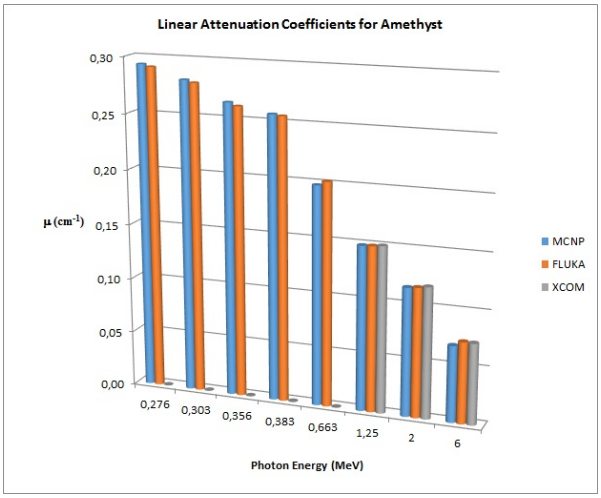

Figure 3. Graphical comparison of the values computed by MCNP5, FLUKA and XCOM.

References

[1] *H. Cember, T. E. Johnson, Introduction to Health Physics: 4th Ed., McGraw Hill, 2008.*

[2] *P. Andreo, Monte Carlo techniques in medical radiation physics, Phys. Med. Biol.* ***36****:7, 1991.*

[3] *MCNP - A General N-Particle Transport Code, Version 5, LA-UR-03-1987 (2003).*

[4] *M.T. Teli, R. Nathuram, C.S. Mahajan, Radiation Measurements,* ***32****, 329-333, (2000).*

[5] *T. Korkut, H. Korkut, A. Karabulut, G. Budak, Ann. of Nucl. En.* ***38****, 56–59, (2011).*

[6] *http://www.gemselect.com/otherinfo/amethyst-deposits.php.*

Leukemia incidence in the Russian cohort of Chernobyl emergency workers: estimates of radiation risks in the follow-up period 1986–2014

SERGEY KARPENKO A. Tsyb Medical Radiological Research Center – branch of the National Medical Research Radiological Center of the Ministry of Health of the Russian Federation (A. Tsyb MRRC)

Leukemia incidence was studied in the Russian cohort of male emergency workers of 78,110 persons over the follow-up period 1986–2014. The mean age of emergency workers at the time of entry to the Chernobyl zone was 34 years. Radiation risk of leukemia (chronic lymphocytic leukemia excluded) was analyzed for emergency workers having official data about individual external whole-body gamma radiation dose accrued over the recovery works period. A total of 157 cases of leukemia were detected (excluding chronic lymphocytic leukemia). The mean dose for emergency workers was 108 mGy. For the period 1986–1997, a linear dose response of leukemia is found to be statistically significant ($p<0.05$), with the excess relative risk per Gy (ERR Gy^{-1}) = 4.17 [90% confidence internal (CI): 0.18; 13.24]. From 1998 to the end of the follow-up period, as well as for the whole follow-up period (from 1986 to 2014), no statistically significant excess relative risks were found. A statistically significant excess incidence of leukemia that may be due to external gamma radiation exposure for the Russian cohort of emergency workers is seen in the period 0-11 years after exposure, based on our estimates.

Keywords: Radiation risk, Leukemia incidence, Excess relative risk, Relative risk, Chernobyl accident, Liquidators

Influence of backscattering on fission rate of excited nuclei

[1] MARIA CHUSHNYAKOVA Omsk State Transport University, Omsk, Russia (Present) Akdeniz University, Antalya, Turkey
[2] IGOR GONTCHAR Omsk State Transport University, Omsk, Russia

The nuclear fission of excited nuclei is an example of the thermal decay of a metastable state [1-3]. We model this process numerically using the Langevin equations [2,4]. Within such modeling, this process is described as a Brownian particle motion which is affected by conservative, dissipative, and fluctuating forces. When this particle overcomes fission barrier, it still has a chance to be scattered back to the potential well due to fluctuations [4,5]. We study the effect of this backscattering for the wide range of the friction coefficient. Usually, to model numerically thermal decay of a metastable state one uses different approaches for different ranges of friction [1,2,6]. We perform numerical modeling of this process within the framework of the very same approach for all values of friction coefficient. First, we compare two approximate analytical Kramers rates with the numerical quasistationary fission rates: one of the analytical formulas is for the case of middle and large friction (spatial diffusion regime) [1] and the other is for the case of relatively small friction (energy diffusion regime) [1,7]. Second, we analyze the influence of descent of the Brownian particle from the barrier on the quasistationary fission rate: as the friction coefficient decreases, this influence gradually disappears. It is found, in the energy diffusion regime, backscattering absents and therefore the descent stage does not influence the fission rate. As the value of friction increases, the descent stage alters the rate by more than 50%.

[1] Kramers// Physica 7 (1940) 284-304
[2] Fröbrich, Gontchar// Phys. Rep. 292 (1998) 131-237
[3] Gontchar, Chushnyakova// Pramana J. Phys. 88 (2017) 90
[4] Chushnyakova, Gontchar// PRE 97 (2018) 032107
[5] Boilley, Marchix, Jurado, Schmidt// EP JA 33 (2007) 47-52
[6] Gontchar, Chushnyakova, Aktaev, Litnevsky, Pavlova// PRC 82 (2010) 064606
[7] Buttiker, Harris, Landauer// PRB 28 (1983) 1268

Keywords: Fissi

on rate, Langevin dynamics

Measurement of natural radioactivity in quartz stone

[1] AYDAN ALTIKULAÇ Muğla Sıtkı Koçman University, Ula Ali Koçman MYO

Granite is a natural stone in the structure of quartz and alkali feldspar. These are 35% Quartz, 45% Potassium feldspar and mica (biotite) minerals in the structure. Some granites are known to contain radioactivity due to radionuclides present in their mineralogica compositions. Quartz is a crystal group mineral that is very common in nature. In this study, natural radioactivity analysis was performed from quartz stones. The mean radioactivity values of ^{226}Ra, ^{232}Th and ^{40}K were found to be 9.1, 22.5 and 615.8 Bq/kg respectively.

Keywords: Natural radioactivity, granite, quatrz

Determination of radioactivity levels in feldspar samples in Turkey

[1] AYDAN ALTIKULAÇ Muğla Sıtkı Koçman University, Ula Ali Koçman MYO

Feldspar is one of the most important mineral group that the make up rocks on earth and make up 60% of the earth's crust and is the most commonly found mineral group on earth. It is also used as raw material in the glass and ceramics industry. In this study, natural radioactivity measurements were made in different feldspar samples (K-Feldspar, Na Feldspar) from the southern Aegean region in Turkey. The mean radioactivity concentrations of ^{226}Ra, ^{232}Th and ^{40}K in K-Feldspar samples determined to be 60.65, 62.3 and 1821.85 Bq/kg, respectively. The measurements result of Na-Feldspar samples were 57.9, 70.63 and 785.80 Bq/kg, respectively.

Keywords: Gamma spectrometry, radioactivity, feldspar

The effects on radiation damage of some nuclear libraries in a hybrid reactor

MEHTAP DÜZ, GÖKMEN ŞEKER

İnönü University, Science and Art Faculty, Physics Dept., Malatya, Turkey

Abstract

In this study, salt-heavy metal mixture consisting of 79.9% $Li_{17}Pb_{83}$ + 20% ThF_4 + 0.1% AmO_2 was used as fluid. The fluid was used in the liquid first-wall, blanket and shield zones of the designed hybrid reactor system. A beryllium (Be) zone with a width of 3 cm was used for neutron multiplicity between the liquid first wall and the blanket. V_4Cr_4Ti ferritic steel with the width of 4 cm was used as the structural material. Proton, deuterium, tritium, He-3 and He-4 gas production rates are the parameters of radiation damage. In this study, the effect on the radiation damage of the selected fluid and libraries were investigated for 30 full power years (FPYs) in the structural material. Three-dimensional analyses were performed using the most recent MCNPX-2.7.0 Monte Carlo radiation transport code, NJOY and the some nuclear data libraries.

Keywords: Hybrid Reactor, Monte Carlo, MCNPX, liquid first-wall

Introduction

Generating energy from traditional nuclear reactors, waste management as a result of fuel burning is one of the most important problems today. Transformation of waste to stable and shortlived isotopes with nuclear reactions is a radical solution. With this aim, a hybrid reactor system was developed where fusion and fission occur at the same time. The fuel used in hybrid reactors is generally D–T fuel. When D–T fuel enters into fusion reaction, 14.1 MeV fusion neutrons and 3.5 MeV alpha particles are liberated. In hybrid reactors fissile fuel breeding is just as important as energy production. The plasma is surrounded by a wall of fertile material. Thus, the high-energy 14.1 MeV fusion neutrons that are emitted from the plasma react with the fertile materials ^{238}U or ^{232}Th resulting in fissile materials ^{239}Pu or ^{233}U [1-6].

In this study, we calculated proton, deuterium, tritium, He-3 and He-4 gas production rates because the high-energy neutrons liberated from the plasma and from the other nuclear reactions will produce radiation damage such as proton, deuterium, tritium, He-3 and He-4 gas production via nuclear reactions within the structural material. The main objective of this study is to investigate the effect of evaluated nuclear data libraries on proton, deuterium, tritium, He-3 and He-4 gas production rates in the structural material of the designed the hybrid reactor system.

Method

Numerical Calculations

In Table 1 is shown the radial structure of designed the hybrid reactor system. Hybrid reactor system used in the study is in the shape of a torus. In this study was used $Li_{17}Pb_{83}$ molten salt, Beryllium (Be) neutron multiplier, V_4Cr_4Ti ferritic steel. In this study, we calculated nuclear parameters in liquid first wall, blanket and shield zones with three nuclear data libraries currently the most recent: ENDF/B-VIII.0 T = 300 K, JEFF-3.2 T = 300 K and CENDL-3.1 T = 300 K with the help of Monte Carlo method the MCNPX-2.7.0 in three-dimensional. The NJOY was used for processing of ENDF/B-VIII.0, JEFF-3.2, and CENDL-3.1 libraries. The NJOY code is a modular nuclear data processing system for producing libraries of nuclear data for reactor physics calculations from evaluated data. Analysis was performed for neutron wall loading 10 MW/m^2 and fusion power 4000 MW.

Radiation Damage

Structural materials are exposed to high neutron flux, which continuously kicks atoms out of their lattice sites. This leads to various types of damage in the material, such as hardening, swelling and embrittlement, which directly influence its function. Radiation damage refers to the localized disruption of the crystal lattice of a solid by high-energy radiation passing through it. Proton, deuterium, tritium, He-3 and He-4 gas production amounts are the parameters of radiation damage. Gas production in the metallic lattice, resulting from nuclear reactions, is one of the important damage mechanisms. While the hydrogen atom and its isotopes can diffuse out of the first wall material with high temperatures, the helium atoms will cumulate in the first wall of the hybrid reactor. All this damage will affect the strain of the first wall and restrict the operation lifetime of the reactor. [7-12]. In structural material one desires a minimum production of radiation damage parameters.

Table 1. The radial build of the hybrid reactor system design.

Inboard side		Outboard side	
Zone	**r (cm)**	**Zone**	**r (cm)**
SS316LN	276	Plasma	667
Vacuum vessel[a]	278	SOL	695
SS316LN	294	Liquid First Wall[d]	697
GAP	296	Be[e]	700
Shield[b]	301	Blanket[d]	750
Ferritic Steel[c]	350	Ferritic Steel[c]	754
Blanket[d]	354	Shield[b]	804
Be[e]	404	GAP	838
Liquid First Wall[d]	407	SS316LN	840
SOL	409	Vacuum vessel[a]	866
Plasma	437	SS316LN	868

[a] 80% SS316LN, 20% H_2O

[b] 60% V_4Cr_4Ti, 40% (79,9% $Li_{17}Pb_{83}$ + 20% ThF_4 + 0,1% AmO_2)

[c] 100% V_4Cr_4Ti

[d] 79,9% $Li_{17}Pb_{83}$ + 20% ThF_4 + 0,1% AmO_2

[e] 100% Be

Numerical Results

In this study were investigated the effect of the some nuclear data libraries on the radiation damage parameters in the structural material, such as proton, deuterium, tritium, He-3 and He-4 gas production rates, measured in atomic parts per million (appm). In this study was used 79,9% $Li_{17}Pb_{83}$ + 20% ThF_4 + 0,1% AmO_2 as fluid in liquid first wall, blanket and shield zones, ENDF/B-VIII.0, JEFF-3.2 and CENDL-3.1 as evaluated nuclear data library from 10^{-11} to 20 MeV and V_4Cr_4Ti as structural material.

Table 2 shows the radiation damage parameters (appm/30 FPY), including proton, deuterium, tritium, He-3 and He-4 gas production rates, in the structural material for the three different nuclear data libraries.

To reduce the effect of the radiation damage on the structure materials, neutrons in the liquid second wall (blanket) should be slowed down and absorbed through nuclear reactions. $Li_{17}Pb_{83}$ is powerful material in attenuating high energy neutrons due to inelastic scattering-absorption in lithium and (n,2n) reactions in lead. Lithium, on the other hand, is a good moderator for both high-energy and low-energy neutrons through inelastic scattering in ^7Li and absorption in ^6Li. The presence of fissionable material ^{232}Th in ThF_4 increase the number of neutrons. Therefore, this process will increase radiation damage on the first wall material. On the other hand, it softens the neutron spectrum at the same time and, thus, increases neutron absorption so these adverse effects compensate each other with respect to radiation damage.

Table 2. The change of the radiation damage parameters according to the selected nuclear data libraries in the structural material.

(appm/30 FPY)	ENDF/B-VIII.0	JEFF-3.2	CENDL-3.1
Proton Production	37.3	26.1	26.5
Deuterium Production	2.1	10.8	2.21
Tritium Production	$5.07.10^{-2}$	4.15	$2.83.10^{-2}$
He-3 Production	$3.42.10^{-6}$	$3.47.10^{-5}$	$3.15.10^{-5}$
He-4 Production	7.05	8.03	7.46

In Table 2 was observed supply from ENDF/B-VIII.0 in general of the biggest contribution and from JEFF-3.2 of the smallest contribution between selected libraries at the proton production in the structural material. Furtherfore, it was observed supply from JEFF-3.2 in general of the biggest contribution at the deuterium, tritium, He-3 and He-4 production in the structural material. These differences between some evaluated nuclear data files may be due to uncertainties in the reaction cross sections.

Results and Discussion

In the study was investigated the effect on the radiation damage of the some nuclear data libraries in the structural material of the designed hybrid system.

The radiation damage parameters was investigated for some nuclear data libraries in the structural material with a decrease in the radial neutron flux distribution due to elastic or inelastic collisions and other nuclear reactions.

In structural material one desires a minimum production of radiation damage parameters. Therefore, the radiation damage parameters obtained according to the selected nuclear data libraries in the structural material with JEFF-3.2 for proton production, ENDF/B-VIII.0 for deuterium, He-3 and He-4 production, CENDL-3.1 for tritium production showed the best performance.

Acknowledgements

This work was supported by İnönü University Research fund with the project number 2015/68.

Reference

[1] S Şahin, M Übeyli *Energy Convers. Manage*. 46 3185 (2005).

[2] H M Şahin *Ann. of Nucl. Energy* 34 861 (2007).

[3] B Şarer, et al., *Fusion Sci. Technol*. 52 107 (2007).

[4] M Günay, et al., *Ann. of Nucl. Energy* 38(12) 2757 (2011).

[5] M Günay, et al., *Ann. of Nucl. Energy* 55 292 (2013).

[6] M Günay, et al., *Ann. of Nucl. Energy* 63 157 (2013).

[7] M A Abdou *Appl. Electromag. Mech*. 151 (2001).

[8] J Blink, et al., Lawrence Livermore National Laboratory, UCRL-53559 (1985).

[9] J J Duderstadt, G A Moses *Inertial Confinement Fusion* (1982).

[10] M Perlado, et al., International Atomic Energy (1995).

[11] S. Ünalan *Fusion Eng. Des*. 38 393 (1998).

[12] M Z Youssef, et al., Paper presented at the 13th Topical Meeting on the Technology of Fusion Power (1998).

The calculation of neutron flux for some nuclear libraries using Monte Carlo method

MEHTAP DÜZ, HİLAL BARDAKÇI

İnönü University, Science and Art Faculty, Physics Dept., Malatya, Turkey

Abstract

In this study, a hybrid reactor system was designed by using 79,9% $Li_{17}Pb_{83}$ + 20% ThF_4 + 0,1% AmO_2 fluid, some evaluated nuclear data libraries and V_4Cr_4Ti ferritic steel structural material. The fluid was used in the liquid first wall, liquid second wall (blanket) and shield zones of a fusion–fission hybrid reactor system. The neutron flux was calculated according to total, radial and energy spectrum in the designed hybrid reactor system for the selected fluid, some nuclear libraries and structural material. Three-dimensional nucleonic calculations were performed using the most recent version MCNPX-2.7.0 the Monte Carlo and NJOY code.

Keywords: MCNPX-2.7.0, Nuclear Libraries, Thorium, Hybrid Reactor

Introduction

The fuels used in hybrid reactor systems are generally deuterium–tritium (D-T) or deuterium–deuterium (D-D) fuels. When D-T fuel enters the fusion reaction, 14.1 MeV fusion neutrons and 3.5 MeV alpha particles are released. The plasma is surrounded by a wall made of fertile material, which cannot undergo the fusion reaction with thermal neutrons, but can undergo conversion with high energy neutrons, such as the 14.1 MeV neutrons produced by the fusion reaction. Thus, the high energy fusion neutrons convert fertile materials to fissile fuel, fission neutrons, and produce energy. The hybrid reactor produces 30 times more nuclear fuel per nuclear energy quantity than fast reactors [1-6].

In this study, a hybrid reactor system was designed. The hybrid reactor system can generate secure energy in large quantities with D-T fuel usage and subcritical study. Furthermore, it enables the production of a self-sufficient fuel for the reactor through the reaction of the neutrons released by the plasma. The main objective of this study is to investigate the neutron flux according to total, radial, energy spectrum in the designed hybrid reactor system for the selected fluid, library and structural material.

Method

Numerical Calculations and Neutron Flux

The radial structure of the hybrid reactor system is shown in Table 1. Calculation of all the parameters of the fission and fusion reactors, accelerator-driven systems, and other areas of nuclear technology depend on the cross-section data. The experimental data are limited for neutron-produced reactions in certain energy ranges [7-12]. In this study, we calculated nuclear parameters in liquid first wall, blanket and shield zones with four nuclear data libraries currently the most recent: ENDF/B-VIII.0 T = 300 K, JENDL-4.0 T = 300 K, JEFF-3.2 T = 300 K and CENDL-3.1 T = 300 K with the help of Monte Carlo method the MCNPX-2.7.0 in three-dimensional. The NJOY was used for processing of ENDF/B-VIII.0, JENDL-4.0, JEFF-3.2, and CENDL-3.1 libraries. The NJOY code is a modular nuclear data processing system for producing libraries of nuclear data for reactor physics calculations from evaluated data. This study was performed with neutron wall loadings of 10 MW/m^2 and fusion power of 4000 MW.

It is important for neutronic calculations to know the flux distrubution of the neutrons in a nuclear fission reactor, fusion reactor, and hybrid reactor. The neutron flux is defined as the total path of thermal neutrons in a unit volume around point r in a second. The neutron flux expresses a scalar value of dimensions $m^{-2}s^{-1}$. In the nuclear reactors, fast neutrons are nearly exclusively produced in the fission reactions.

Table 1. The radial build of the hybrid reactor system design.

Inboard side		Outboard side	
Zone	**r (cm)**	**Zone**	**r (cm)**
SS316LN	276	Plasma	667
Vacuum vessel[a]	278	SOL	695
SS316LN	294	Liquid First Wall[d]	697
GAP	296	Be[e]	700
Shield[b]	301	Blanket[d]	750
Ferritic Steel[c]	350	Ferritic Steel[c]	754
Blanket[d]	354	Shield[b]	804
Be[e]	404	GAP	838
Liquid First Wall[d]	407	SS316LN	840

SOL	409	Vacuum vessel[a]	866
Plasma	437	SS316LN	868

[a] 80% SS316LN, 20% H_2O

[b] 60% V_4Cr_4Ti, 40% (79,9% $Li_{17}Pb_{83}$ + 20% ThF_4 + 0,1% AmO_2)

[c] 100% V_4Cr_4Ti

[d] 79,9% $Li_{17}Pb_{83}$ + 20% ThF_4 + 0,1% AmO_2

[e] 100% Be

In the nuclear reactors, the fast neutrons gradually slow due to collisions with the atoms of the moderator and the various nuclear processes taking place in the reactor [13]. As these formations are the functions of neutron energy, the neutron flux distribution should also be expressed as a function of neutron energy. The Boltzmann equation is a common way to calculate neutron flux in a reactor, which is given in below:

$$\frac{1}{v}\frac{\partial}{\partial t}\phi(r,\Omega,E,t) + \Omega.\nabla\phi(r,\Omega,E,t) + \sum_t(r,E,t)\phi(r,\Omega,E,t) = q(r,\Omega,E,t) \quad (1)$$

$\frac{1}{v}\frac{\partial}{\partial t}\phi(r,\Omega,E,t)$= Change of neutron flux in unit time,

$\Omega.\nabla\phi(r,\Omega,E,t)$ = Neutron loss because of convection,

$\sum_t(r,E,t)\phi(r,\Omega,E,t)$ = Neutron loss because of nuclear reactions.

Terms in equation (1) for $q(r,\Omega,E,t)$ can be defined as follow:

$$q(r,\Omega,E,t) = \int_0^\infty dE' \int_{4\pi} d\Omega \sum(r,E' \longrightarrow E,\Omega' \longrightarrow \Omega)\phi(r,\Omega',E',t) + S(r,\Omega,E,t) \quad (2)$$

$\int_0^\infty dE' \int_{4\pi} d\Omega \sum(r,E' \longrightarrow E,\Omega' \longrightarrow \Omega)\,\phi(r,\Omega',E',t)$= Contribution of neutrons on neutron flux due to scattering,

$S(r,\Omega,E,t)$= Contribution of neutron source independent on the neutron flux.

The transport equation is currently handled by the Monte Carlo method. The Monte Carlo method provides an instrument to solve the equations by simulating the neutron activities. In this study, neutron transport calculations of the neutron flux distrubutions were investigated using MCNPX-2.7.0 to solve the Boltzmann transport equation (1), (2) with Monte Carlo code.

Numerical Results

In this study was used 79,9% $Li_{17}Pb_{83}$ + 20% ThF_4 + 0,1% AmO_2 as fluid, ENDF/B-VIII.0, JENDL-4.0, JEFF-3.2 and CENDL-3.1 evaluated nuclear data library.

Table 2 shows variation of the total neutron fluxes in the reactor system versus the selected some nuclear data libraries of 79,9% $Li_{17}Pb_{83}$ + 20% ThF_4 + 0,1% AmO_2 in the liquid first wall, blanket and shield zones.

Table 2. The variation of the total neutron fluxes in the hybrid reactor system according to nuclear data libraries.

	ENDF/B-VIII.0	JENDL-4.0	JEFF-3.2	CENDL-3.1
Total Neutron Flux n/cm²·s	$1.485.10^{15}$	$1.423.10^{15}$	$1.273.10^{15}$	$1.404.10^{15}$

Fig. 1 shows the radial neutron flux distribution in the designed system for the some nuclear data libraries of the selected fluid. The variation of the neutron flux distribution in the inboard and outboard of the reactor system decreases nearly exponentially with distance from the reactor center (plasma) for selected the some nuclear data libraries.

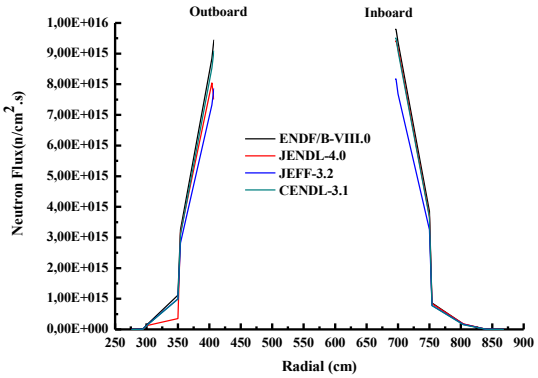

Fig. 1. The variation of the radial neutron flux distribution in the inboard and outboard of the reactor system for the selected some nuclear libraries.

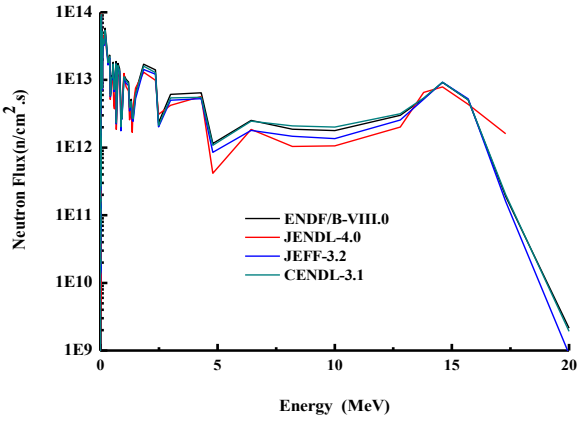

Fig. 2. The variation of the neutron flux distribution according to neutron energy spectrum in the reactor system for the selected some nuclear libraries.

Fig. 2 shows the average neutron flux distribution according to neutron energy spectrum (0-20 MeV) in the reactor system for the selected some nuclear data

libraries. In Fig. 2, it was seen that the average neutron flux distribution decreases between 0-14 MeV, a peak around 15 MeV and decrease later in the designed system.

Results and Discussion

In this study were investigated the effect on the neutron flux distribution of the selected some nuclear data libraries. The neutron flux increases due to the fission reaction of thorium isotope, inelastic scattering of ^{7}Li and the exothermic $^{6}Li(n,\alpha)T$ reaction of ^{6}Li in the $Li_{17}Pb_{83}$ molten salt, (n,2n) reaction of lead, elastic and other nuclear reactions of atoms in the fuel zone. Therefore, in the calculation was observed that the radial neutron flux distribution decreases nearly exponentially with distance from the plasma for selected the some nuclear data libraries in the inboard and outboard of the reactor system. In this study, the average neutron flux distribution were investigated according to the neutron energy spectrum (0-20 MeV) in the system for the selected some nuclear data libraries. The neutron spectrum produces high energy γ-rays in the range of 5-10 MeV by (n,γ) reactions, 2 MeV fission neutrons and 14.6 MeV fusion neutrons. In the calculation was seen that the average neutron flux distribution due to fission, fusion and other nuclear reactions, and had a peak approximately 14-16 MeV, decreasing thereafter. The values between the 0-20 MeV energy gap were approximately the same values of the neutron flux distribution according to the energy in the system for different four nuclear data libraries.

Acknowledgements

This work was supported by İnönü University Research fund with the project number 2015/68.

Reference

[1] S Şahin, M Übeyli *Energy Convers. Manage*. 46 3185 (2005).

[2] H M Şahin *Ann. of Nucl. Energy* 34 861 (2007).

[3] B Şarer, et al., *Fusion Sci. Technol*. 52 107 (2007).

[4] M Günay, et al., *Ann. of Nucl. Energy* 38(12) 2757 (2011).

[5] M Günay, et al., *Ann. of Nucl. Energy* 55 292 (2013).

[6] IAEA, International Atomic Energy Agency, IAEA-TECDOC-1349 (2003).

[7] M Piera, et al., *Energy Convers. Manage*. 51 1758, (2010).

[8] A Ying, et al., *APEX Interim Report* (1999).

[9] B Şarer, et al., *Ann. of Nucl. Energy* 36 417 (2009).

[10] M Günay, et al., *Ann. of Nucl. Energy* 53 59 (2013).

[11] M B Chadwick, et al., *Nucl. Data Sheets* 107 2931 (2006).

[12] D B Pelowitz *MCNPX User's Manual*, Version 2.7.0, LA-CP-11-00438 (2011).

[13] J J Duderstadt, G A Moses *New York: John Wiley&Sons* (1982).

Three-dimensional Monte Carlo calculation of the nuclear parameters for some nuclear libraries

MEHTAP DÜZ, HİLAL BARDAKÇI

İnönü University, Science and Art Faculty, Physics Dept., Malatya, Turkey

Abstract

In this study, a fusion–fission hybrid reactor system was designed by using V_4Cr_4Ti Ferritic steel structural material and the molten salt-heavy metal mixture 79,9% $Li_{17}Pb_{83}$ + 20% ThF_4 + 0,1% AmO_2, as fluid. The fluid was used in the liquid first wall, blanket and shield zones of a fusion–fission hybrid reactor system. Beryllium (Be) zone with the width of 3 cm was used for the neutron multiplication between the liquid first wall and blanket. In this study was investigated the nuclear parameters such as tritium breeding ratio (*TBR*), energy multiplication factor (*M*), heat deposition rate, fission reaction rate in liquid first wall, blanket and shield zones. Three-dimensional analyses were performed by using the Monte Carlo code MCNPX-2.7.0, NJOY and some nuclear data libraries.

Keywords: fusion-fission hybrid reactor system, Three-Dimensional Monte Carlo Calculation, Nuclear Libraries

Introduction

The waste management required as a result of fuel burning to generate energy from traditional nuclear reactors is one of the most important problems today. For this reason, hybrid reactor system has been developed where fusion and fission occur at the same time. Hybrid reactor is a system developed to obtain more energy and nuclear fuel, decrease the waste amounts in storage areas, recover transuranic elements in used fuels through reprocessing, and render fission products harmless [1-6].

In this study, $Li_{17}Pb_{83}$ molten salt was used, which has low melting temperatures and low vapor pressure, to acquire sufficient tritium breeding. Beryllium (Be) is used as a neutron multiplier [7]. In this study, a Be zone with a thickness of 3 cm was used between the liquid first-wall and the blanket. In this study, V_4Cr_4Ti ferritic steel was chosen as a structural material because it has low activation, which can help to extend the lifetime of the reactor system. The main objective of this study is to investigate tritium breeding ratio (*TBR*), energy multiplication factor (*M*), heat deposition rate, fission reaction rate in the designed hybrid reactor system for the selected fluids, library and structural material.

Method

Numerical Calculations

Hybrid reactor system used in the study is in the shape of a torus. The radial structure of designed the hybrid reactor system is shown in Table 1. Calculation of all the parameters of the fission and fusion reactors and other areas of nuclear technology depend on the cross-section data [8-10]. In this study, we calculated nuclear parameters in liquid first wall, blanket and shield zones with four nuclear data libraries currently the most recent: ENDF/B-VIII.0 T = 300 K, JENDL-4.0 T = 300 K, JEFF-3.2 T = 300 K and CENDL-3.1 T = 300 K with the help of Monte Carlo method the MCNPX-2.7.0 in three-dimensional. The NJOY was used for processing of ENDF/B-VIII.0, JENDL-4.0, JEFF-3.2, and CENDL-3.1 libraries. The NJOY code is a modular nuclear data processing system for producing libraries of nuclear data for reactor physics calculations from evaluated data. Analysis was performed for neutron wall loading 10 MW/m^2 and fusion power 4000 MW.

Tritium Breeding

The tritium breeding ratio (*TBR*) is defined as the ratio of the rate of tritium production in the system to the rate of tritium burning in the plasma. The hybrid reactor has to breed the tritium it requires [11,12]. Tritium is bred through the reaction of lithium with neutrons. The $^6Li(n,\alpha)T$ reaction is produced with thermal neutrons, and the $^7Li(n,\alpha n')T$ reaction with fast neutrons. In the hybrid reactor system, the working liquid must be a lithium-containing medium to provide adequate tritium. The required *TBR* for a fission reactor conceptual design must be 1.1 [11-15]. *TBR* can be given as follows:

$TBR = T_6 + T_7$ (1)

$T_6 = \iint \Phi \cdot \Sigma_{(n,\alpha)T}\, dE\, dV$, for ^6Li (2)

$T_7 = \iint \Phi \cdot \Sigma_{(n,n'\alpha)T}\, dE\, dV$, for ^7Li. (3)

In this study $Li_{17}Pb_{83}$ molten salt was used, which has low melting temperatures and low vapor pressure, to acquire sufficient tritium breeding.

Table 1. The radial build of the hybrid reactor system design.

Inboard side		Outboard side	
Zone	**r (cm)**	**Zone**	**r (cm)**
SS316LN	276	Plasma	667
Vacuum vessel[a]	278	SOL	695
SS316LN	294	Liquid First Wall[d]	697
GAP	296	Be[e]	700
Shield[b]	301	Blanket[d]	750
Ferritic Steel[c]	350	Ferritic Steel[c]	754
Blanket[d]	354	Shield[b]	804
Be[e]	404	GAP	838
Liquid First Wall[d]	407	SS316LN	840
SOL	409	Vacuum vessel[a]	866
Plasma	437	SS316LN	868

[a] 80% SS316LN, 20% H_2O

[b] 60% V_4Cr_4Ti, 40% (79,9% $Li_{17}Pb_{83}$ + 20% ThF_4 + 0,1% AmO_2)

[c] 100% V_4Cr_4Ti

[d] 79,9% $Li_{17}Pb_{83}$ + 20% ThF_4 + 0,1% AmO_2

[e] 100% Be

Energy Multiplication Factor, Heat Deposition Rate and Fission Reaction Rate

The energy multiplication factor *M* is the ratio of nuclear heating and source neutron energy incident on the first wall [16]. The energy produced must exceed the energy produced by the plasma. To obtain high thermal power, the *M* value should be as large as possible. It is desirable that *M* is greater than 1.2 in a D-T fueled reactor [17]. *M* can be defined as follows:

$M = [(200x(\Phi \cdot \Sigma_f) + 4.784xT_6 - 2.467xT_7)/14.1] + 1$ (4)

$(\Phi \cdot \Sigma_f) = \iint \Phi \cdot \Sigma_f\, dE\, dV$, total fission rate. (5)

The contributions of the neutron flux, fission, and other reactions to the integrated *M* and heat deposition rate are very important. The main contributions to the integrated *M* and heat deposition rate are from the neutron flux, the fission reaction of thorium isotope in ThF_4 and the exothermic $^6Li(n,\alpha)T$ reaction of $Li_{17}Pb_{83}$ molten salt.

Numerical Results

In this study, hybrid reactor system have designed by using 79,9% $Li_{17}Pb_{83}$ + 20% ThF_4 + 0,1% AmO_2 fluid in liquid first wall, blanket and shield zones, ENDF/B-VIII.0, JENDL-4.0, JEFF-3.2 and CENDL-3.1 evaluated nuclear data library from 10^{-11} to 20 MeV and V_4Cr_4Ti structural material.

Table 2 shows the *TBR*, *M*, heat deposition rate and fission reaction rate in the liquid first wall, blanket and shield regions per fusion source neutron for the some nuclear data libraries.

Integrated TBR values calculated in the liquid first wall, blanket and shield regions for the libraries used in the study are, from large to small, respectively, 1.799 for JENDL-4.0, 1.796 for ENDF/B-VIII.0, 1.473 for JEFF-3.2, and 0.873 for CENDL-3.1. It was found that *TBR* values calculated for some nuclear data libraries (except CENDL-3.1) higher than 1.1 the limit value. The *M* value was obtained to be between 1.2 and 1.56 values. This values is greater than 1.2 value desirable of *M*. In the pertinent zones of the reactor, integrated heat deposition rate values for all four libraries selected are, from large to small, respectively, 107.863 W/cm^3 for JENDL-4.0, 105.42 W/cm^3 for ENDF/B-VIII.0, 103.972 W/cm^3 for CENDL-3.1, 91.782 W/cm^3 for JEFF-3.2. This unexpected finding differences between the libraries was attributed to a bug in the version of the NJOY code used to process the data.

Table 2. The variation of the *TBR*, *M*, heat deposition rate and fission reaction rate for the some nuclear data libraries in the liquid first wall, blanket and shield zones.

	ENDF/B-VIII.0	**JENDL-4.0**	**JEFF-3.2**	**CENDL-3.1**
TBR	1.796	1.799	1.473	0.873
M	1.55	1.56	1.49	1.2
Heat Deposition Rate (W/cm^3)	105.42	107.863	91.782	103.972
Fission Reaction Rate	$1.3.10^{-2}$	$1.14.10^{-2}$	$1.29.10^{-3}$	$1.28.10^{-2}$

Results and Discussion

In the study the effect of the some nuclear data libraries in the designed system on three-dimensional neutronic measurements, such as *TBR*, *M*, heat deposition rate and fission reaction rate, was investigated.

It was found that *TBR* values calculated for some nuclear data libraries (except CENDL-3.1) higher than 1.1 the limit value. It was found that the greatest contribution to *TBR* comes from JENDL-4.0 nuclear data library.

All *M* values found from selected nuclear data libraries are close to each other. The increase between the minimum and maximum of heat deposition rates, *M* and fission reaction rate values for the different nuclear data libraries was approximately the same. It was found that the greatest contribution to *M* and the heat deposition rate comes from JENDL-4.0 nuclear data library and the greatest contribution to fission reaction rate comes from ENDF/B-VIII.0 nuclear data library.

Acknowledgements

This work was supported by İnönü University Research

fund with the project number 2015/68.

Reference

[1] S Şahin, M Übeyli *Energy Convers. Manage*. 46 3185 (2005).

[2] H M Şahin *Ann. of Nucl. Energy* 34 861 (2007).

[3] B Şarer, et al., *Fusion Sci. Technol*. 52 107 (2007).

[4] M Günay, et al., *Ann. of Nucl. Energy* 38 (12) 2757 (2011).

[5] M Günay, et al., *Ann. of Nucl. Energy* 55, 292 (2013).

[6] M Günay, et al., *Ann. of Nucl. Energy* 63, 157 (2013).

[7] IAEA, International Atomic Energy Agency, IAEA-TECDOC-1349 (2003).

[8] B Şarer, et al., *Ann. of Nucl. Energy* 36, 417 (2009).

[9] M Günay, et al., *Ann. of Nucl. Energy* 53, 59 (2013).

[10] M Günay, et al., *Ann. of Nucl. Energy* 63, 432 (2014).

[11] M E Sawan, et al., *Fusion Engineering and Design*, 81 1131 (2006).

[12] J Jung, et al., *Nuclear Technol./Fusion*, 4 361 (1983).

[13] M A Abdou, et al., *Fusion Technol*., 9 250 (1986).

[14] W Kuan, et al., *Fusion Technol*., 35 309 (1999).

[15] M Z Youssef, et al., *Fusion Technol*., 9 286 (1986).

[16] S Şahin, et al., *Energy Convers. Manage*., 45 1497 (2004).

[17] A H Dhaba'an, et al., *Progress in Nuclear Energy* 29 1 (1995).

The investigation of convert $^{232}Th(n,\gamma)^{233}U$ for some nuclear libraries in a hybrid reactor

MEHTAP DÜZ, GÖKMEN ŞEKER

İnönü University, Science and Art Faculty, Physics Dept., Malatya, Turkey

Abstract

In this study, the fluid was composed mixture the molten salt-the heavy metals 79.9% $Li_{17}Pb_{83}$ + 20% ThF_4 + 0.1% AmO_2. In study, the effect of some nuclear libraries on convert to $^{232}Th(n,\gamma)^{233}U$ was investigated in designed the hybrid reactor system. Beryllium (Be) is neutron multiplicity by (n,2n) reactions. Thence, Be zone in thick 3 cm was used in order to contribute on ^{233}U between liquid first wall and blanket. V_4Cr_4Ti ferritic steel is used as a structural material.

The convert to $^{232}Th(n,\gamma)^{233}U$ was calculated in liquid first wall, blanket and shield zones, which thorium content. Three-dimensional nucleonic calculations were performed by using the most recent version MCNPX-2.7.0 Monte Carlo code and some nuclear data libraries.

Keywords: Hybrid Reactor, Monte Carlo, MCNPX, liquid first wall

Introduction

Hybrid reactor has an enormous potential to provide a clean, cheap and unlimited energy source. Hybrid reactor in which nucleus fusion and fission events can be operated together is a system developed to obtain more energy and nuclear fuel, decrease the waste amounts in storage areas, recover transuranic elements in used fuels through reprocessing, and render fission products harmless. Important advantage of hybrid reactor system is that it has a subcritical reactor system in which reactor can operate securely.

In hybrid reactor system are used generally D-T or D-D fuels. In hybrid reactors, the energy 14.1 MeV of the fusion power (D,T) is carried with neutrons that penetrate the first wall and blanket and dissipate energy through exothermic nuclear reactions. The energy produced in a hybrid reactor should be as high as possible than energy produced by plasma. In addition to, the fissile fuel breeding capability in hybrid reactor is as important as the energy production capability. Hybrid reactor produces 30 times more nuclear fuel per nuclear energy amount it unleashes compared with fast reactors.

The fissile material added to the produced energy by the use of fuel material in the hybrid reactor chamber causes inexpensive energy production because it increases the total revenues from the investment in the fusion reactor. Fissile isotopes can be produced by the (n,γ) reactions of fertile isotopes. The high-energy 14.1 MeV fusion neutrons that are emitted from the plasma react with the fertile material resulting in fissile materials as ^{239}Pu, ^{233}U. Breeding reactions of mother and doughter nuclei can be defined as equation (1) and (2), respectively:

$$dN_1 = -\lambda_1 N_1 dt \quad (1)$$

$$dN_2 = \lambda_1 N_1 dt - \lambda_2 N_2 dt \quad (2)$$

where, dN = number nuclei decaying, λ = decay constant, N = nuclei, dt = unit time.

In the hybrid reactor is used to energy production in the reactor a very small fraction of the fissile material produced. The rest of the fissile material is retrieved from the reactor via appropriate methods and used as fuel in fission reactors [1-6].

Method

Numerical Calculations

The radial build of designed the hybrid reactor system in this study is shown in Table 1. Hybrid reactor system used in the study is in the shape of torus. In this study was used $Li_{17}Pb_{83}$ molten salt, Beryllium (Be) neutron multiplier, V_4Cr_4Ti ferritic steel [7-10]. In this study, we calculated nuclear parameters in liquid first wall, blanket and shield zones with three nuclear data libraries currently the most recent: ENDF/B-VIII.0 T = 300 K, JEFF-3.2 T = 300 K and CENDL-3.1 T = 300 K with the help of Monte Carlo method the MCNPX-2.7.0 in three-dimensional. The NJOY was used for processing of ENDF/B-VIII.0, JEFF-3.2, and CENDL-3.1 libraries. The NJOY code is a modular nuclear data processing

system for producing libraries of nuclear data for reactor physics calculations from evaluated data. Analysis was performed for neutron wall loading 10 MW/m^2 and fusion power 4000 MW.

Table 1. The radial build of the hybrid reactor system design.

Inboard side		Outboard side	
Zone	**r (cm)**	**Zone**	**r (cm)**
SS316LN	276	Plasma	667
Vacuum vessel[a]	278	SOL	695
SS316LN	294	Liquid First Wall[d]	697
GAP	296	Be[e]	700
Shield[b]	301	Blanket[d]	750
Ferritic Steel[c]	350	Ferritic Steel[c]	754
Blanket[d]	354	Shield[b]	804
Be[e]	404	GAP	838
Liquid First Wall[d]	407	SS316LN	840
SOL	409	Vacuum vessel[a]	866
Plasma	437	SS316LN	868

[a] 80% SS316LN, 20% H_2O

[b] 60% V_4Cr_4Ti, 40% (79,9% $Li_{17}Pb_{83}$ + 20% ThF_4 + 0,1% AmO_2)

[c] 100% V_4Cr_4Ti

[d] 79,9% $Li_{17}Pb_{83}$ + 20% ThF_4 + 0,1% AmO_2

[e] 100% Be

Numerical Results

In study, the effect of some nuclear libraries on convert to $^{232}Th(n,\gamma)^{233}U$ was investigated in designed the hybrid reactor system. The convert to $^{232}Th(n,\gamma)^{233}U$ was calculated in liquid first wall, blanket and shield zones, which thorium content. In this study was used 79.9% $Li_{17}Pb_{83}$ + 20% ThF_4 + 0.1% AmO_2 as fluid in liquid first wall, blanket and shield zones, ENDF/B-VIII.0, JENDL-4.0, JEFF-3.2 and CENDL-3.1 as evaluated nuclear data library from 10^{-11} to 20 MeV and V_4Cr_4Ti as structural material. In this study, neutron transport calculations that ^{233}U fissile fuel production was investigated by using MCNPX-2.7.0 Monte Carlo code and NJOY for the some nuclear data libraries.

A substantial amount of fissile fuel would be produced by using heavy metal. ^{232}Th isotope in ThF_4 heavy metals used in the liquid first wall, blanket and shield zones can be converted by the (n,γ) reactions to precious nuclear fuel as ^{233}U.

Table 2 shows $^{232}Th(n,\gamma)^{233}U$ production in the liquid first wall, blanket and shield regions for the some nuclear data libraries.

Table 2. The variation of the fissile fuel breeding ^{233}U versus the some nuclear data libraries in the liquid first wall, blanket and shield zones.

	ENDF/B-VIII.0	JENDL-4.0	JEFF-3.2	CENDL-3.1
Fissile Fuel Production (kg/year)	$1.48.10^4$	$1.51.10^4$	$1.29.10^4$	$1.36.10^4$

Results and Discussion

In this study was used four different nuclear data libraries with molten salt 79,9% $Li_{17}Pb_{83}$ + 20% ThF_4 + 0,1% AmO_2. In this study was investigated the effect on ^{233}U by (n,γ) reaction of the some nuclear data libraries in designed the system.

In the calculation, ^{232}Th used with (n,γ) reactions in heavy metals contents of the system was converted to ^{233}U. It was observed that ^{233}U fissile fuel production increases in selected the some nuclear data libraies due to the fission reaction of thorium isotope and the exothermic $^6Li(n,\alpha)T$ reaction of $Li_{17}Pb_{83}$ molten salt. In conclusion, it was found that JENDL-4.0 library causes a significant increase of ^{233}U fissile fuel production in the reactor system.

Acknowledgements

This work was supported by İnönü University Research fund with the project number 2015/68.

Reference

[1] S Şahin, M Übeyli *Energy Convers. Manage*. 46 3185 (2005).

[2] H M Şahin *Ann. of Nucl. Energy* 34 861 (2007).

[3] B Şarer, et al., *Fusion Sci. Technol*. 52 107 (2007).

[4] M Günay, et al., *Ann. of Nucl. Energy* 38(12) 2757 (2011).

[5] M Günay, et al., *Ann. of Nucl. Energy* 55 292 (2013).

[6] M Günay, et al., *Ann. of Nucl. Energy* 63 157 (2013).

[7] M Piera, et al., *Energy Convers. Manage*. 51 1758, (2010).

[8] A Ying, et al., *APEX Interim Report* (1999).

[9] B Şarer, et al., *Ann. of Nucl. Energy* 36 417 (2009).

[10] M Günay, et al., *Ann. of Nucl. Energy* 53 59 (2013).

The effect of varying constant source over albedo problem for quadratically anisotropic scattering

[1] ALİ ZAFER BOZKIR Kırıkkale University
[2] R. GÖKHAN TÜRECİ Kırıkkale University

One speed, time independent neutron transport equation with quadratically anisotropic scattering is solved with a constant neutron source. The general solution is written and half-space albedo problem is thought for proper boundary conditions. The tabulated values are calculated for the varying scattering coefficients, secondary neutron numbers and varying source terms.

Keywords: Neutron transport theory, Quadratically anisotropic scattering, Constant source, Albedo, Modified FN method

Tritium activity levels in bottled water and mineral water sold in Azerbaijan

[1] ORKHAN MUKHTARLI Recep Tayyip Erdoğan University
[2] SERDAR DİZMAN Recep Tayyip Erdoğan University
[3] RECEP KESER Recep Tayyip Erdoğan University
[4] FİLİZ KORKMAZ GÖRÜR Abant İzzet Baysal University

Water constitutes about three quarters of our planet and human body. Considering the daily consumption level of drinking water, the purity and cleanliness of the consumed water is very important. The cleanliness of the water also depends on the tolerable levels of radionuclide materials in water. One of the radionuclides in water is tritium. Tritium is a radioactive isotope of hydrogen that emits low-energy beta particles, with a maximum energy of 18.6 keV, and with a half live of 12.3 years. In present study, tritium activity concentrations in 8 different bottled mineral water and 7 different bottled water brands sold in Azerbaijan were measured by liquid scintillation counter (LSC). Liquid scintillation counting is the most commonly used technique for determining tritium in low-level environmental samples. The MDA for this method was 1.69 Bq/L. The tritium concentrations of 1 bottled water samples (14.3 %) and 4 bottled mineral water samples (50 %) were below of the MDA. The average tritium activity levels of collected water samples are found as 2.69±0.91 Bq/L for bottled water samples and 2.43±0.89 Bq/L for bottled mineral water samples, respectively. These results are much lower than the upper levels determined by WHO, USEPA, TSI and MOH. Also, the annual effective doses for studied water samples were evaluated and compared with the limit values determined by international organizations.

Keywords: Tritium, Water, Mineral Water, Azerbaijan

Investigation of using neutron generator source in thorium fuel efficiency at new generation nuclear reactor types

[1]EYYUP TEL, [2] YUSUF KAVUN, [1]SULTAN KILIÇ, [1]AFİFE BÖLÜKBAŞI

[1]Osmaniye Korkut Ata University, Faculty of Arts and Science, Department of Physics, Osmaniye, TURKEY

[2]Kahramanmaras Sutcu Imam University, Vocational School of Health Services, Department of Medical Imaging Techniques, Kahramanmaras, Turkey

Abstract

Today, electricity can be generated from conventional fission reactors and the next-generation reactors based on accelerators continue to be investigated in many developed countries, especially in China, Canada and the USA. But it is not yet commercialized due to economic problems. In this study, thorium-fueled reactor types using neutron generators, a new type of nuclear reactor planned to be used in energy generation of the future, were investigated. In addition, the cross sections of reactions occurring through neutron generators were calculated using newly developed formulas.

Keywords: neutron generator, nuclear reactors, cross-section

Introduction

Nuclear reactors now play an important role in energy production worldwide. The main purpose of the nuclear reactor in this process is to initiate and control a sustained nuclear chain reaction [1]. The most of the nuclear reactor types built to date are reactor types that use enriched uranium fuel. It has been provided about 90% of nuclear power production capacity with these reactor types so far. Since the Gen.III nuclear reactors are not sufficiently developed and can not respond to the needs of today's energy needs, the Gen.IV nuclear reactor designs have been speeded up since the beginning of the 21st century. When compared with Gen.III reactor types, one of the fundamental advantages for Gen.IV nuclear energy systems is that they will have a clear life-cycle cost advantage over other energy sources. But the Gen.IV reactor is still in its early stages of development and requires at least two or three decades to be used for commercial purposes.

Molten Salt Reactors (MSRs) are one of the most well known Gen. IV nuclear reactors which use a fluid fuel as salt form instead of the solid fuel used in most reactors. Also, MSRs Works under high temperature and low pressure. There are many type of MSRs but Liquid Fluoride Thorium Reactor (LFTR) is most popular one. LFTR use Thorium and Uranium dissolved in a fluoride salt as fuel. Fission generates much more times more energy than the best liquid hydrocarbon fuels. Thorium MSRs can burn its fuels 100 times more efficiently than traditional nuclear reactors and thus, it is reducing the number of years the final waste has to be stored.

The fast neutron reactors do not have moderators and also fast neutrons in these reactors cause the fission [1]. This is a more effective method than slow neutron to activate uranium. it may be necessary to produce a neutron in order to use thorium as fuel in the nuclear reactor because normal thorium contains ver low fissile material to start chain reactions unlike uranium [2]. For this reason it is necessary to use neutron generators in such reactors to initiate the fuel cycle. ^{232}Th absorbs neutrons to produce ^{233}U in a thorium-fueled reactor.

In this study, thorium-fueled reactor types using neutron generators, a new type of nuclear reactor planned to be used in energy generation of the future, were investigated. In addition, the cross sections of reactions occurring through neutron generators were calculated using newly developed formulas.

Method

In this study, the neutron density $\rho_n(r_l)$, of the nuclei will be used instead of the constant asymmetry parameter, the varying asymmetry parameter depending on the radius in which the values of proton density $\rho_p(r_l)$ in the cross section formulas. In the literature, this method is frequently used in the calculation of neutron skin effect $t = r_n - r_p = \rho_n(r_l) - \rho_p(r_l)$, which is the difference between neutron and proton mean density radiations[3]. The neutron of the target nuclei, the proton density values will be obtained using the Skyrme Hartree-Fock Potential method with nucleon-nucleon interaction. Here, instead of N, Z, A fixed numbers in the asymmetry parameter S=(N-Z)/A, neutron density $N = \rho_n(r_l)$, target density, proton density $Z = \rho_p(r_l)$ and mass density $A = \rho_n(r_l) + \rho_p(r_l)$ values will be used. For the first purpose, the type of the appropriate Skyrme potential (SKM*,SLY4,SLY6 vb.) [4-9] for the target nuclei will be investigated and the selection of the appropriate potential for the nuclei structure will be made. Secondly,

the asymmetry parameter will be recalculated with the neutron and proton density values obtained using the selected potential and these values will be added to the Tel et al.[10] (n,p) cross section formula. Tel et al. formula defined at 14 -15 MeV for 17 ≤A ≤239 mass range as follows;

$$14.56\,(A^{1/3}+1)^2\,exp[-26.58s] \qquad (1)$$

Finally, the appropriate interaction radius will be obtained by comparing the theoretical cross sections obtained according to the radius with the experimental values.

Results

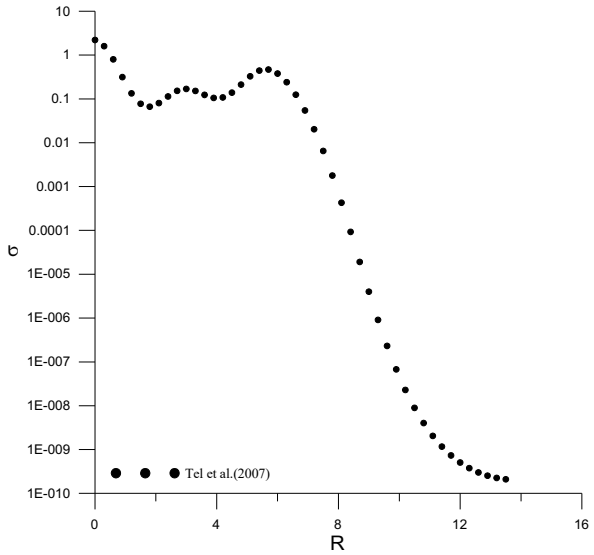

Fig.1 Calculated parameter neutron and proton densities of ^{232}Th element by using the SKM* parameter [10].

In this study, for the ^{232}Th initial neutron and proton exciton numbers have been calculated from the neutron and proton densities by using new calculation method. Since the experimental data for ^{232}Th can not be found in the literature, the theoretical data calculated using the Tel et al. [10] formula are shown in fig. 1. As can be seen from Fig.1, The theoretical calculations by using the initial exciton numbers with SKM* parameters have been peaked at R = 5 fm. The new calculation method is successfully for the GDH calculations and this method has given more information for nuclear reaction mechanisms researchers such as basic nucleon-nucleon potential interaction (such as Woods-Saxon, Harmonic Oscillator. etc.) for nucleon induced pre-equilibrium. The GDH model calculates the density distribution of the nucleus and it describes the nuclear density and potential by a two parameter Fermi function. In addition, diffuse surface effects resulting from higher impact parameters are included in model calculations [11-13].

Reference

[1] *Krane, K., S., Introductory Nuclear Physics, Wiley, New York, (2002).*

[2] *Xianjun Zheng, Baiquan Deng, Wei Ou, et al., 4, 222-227, (2014).*

[3] *E. Tel, S¸. Okuducu, M.H. Bolukdemir, G. Tanır, Inter. J. Mod. Phys. E 17, 1–17 (2008).*

[4] *Tel E.,Şarer B., OkuducuŞ.,AydınA.,Tanır G., Journal Of Physics G: Nuclear And Particle Physics, 29, 2169–2177, (2003).*

[5] E. Tel, A. Aydın, E.G. Aydın, A. Kaplan, O. Yavas, I.A. Reyhancan, PRAMANA Indian Academy of Sciences 74, 6, 931, (2010).

[6] M. Sahan, E. Tel, H. Sahan, et al., J Fusion Energ, 34 ,493, (2015).

[7] E. Tel, A. A. Gok, M. Sahan, I˙. H. Sarpun, Y. Kavun, A. Aydin, J. Fusion Energ, 36 (4-5), (2017).

[8] *E. Tel, H.M. Sahin, A. Kaplan, A. Aydin, T. Altinok, Ann. Nucl.Energy 35(2), 220 (2007).*

[9] Skyrme T H R., the Nuclear Surface. Phil. Mag. 1: 1043-1054, (1956).F Iachello *Phys.Rev.Lett* **91** 132502 (2003).

[10] *E. Tel et al., J Fusion Energ 30:421–427, (2011).*

[11] M. Blann, Ann. Rev. Nucl. Sci. 25, 123 (1975)

[12] A. Aydin, E. Tel, M. S¸ahan, J. Fusion. Eng. 30(1), 34–38 (2011)

[13] E. Beta´k, R. Mikołajczak, J. Staniszewska, S. Mikołajewski, E. Rurarzet, Radiochim. Acta. 93(6), 311 (2005)

Determination of the dead layer thickness for hpge detector: Measurements vs Monte Carlo methods

[1] ABDELLATİF ELANIQUE University Ibn Zohr, Morocco

The activity concentration of radionuclides in the environment is routinely measured using high-purity germanium (HPGe) detectors. A very important characteristic of a gamma-ray detector is its intrinsic efficiency which is usually measured by calibration sources or calculated by Monte Carlo simulations. The intrinsic efficiency depends on many factors among which are the detector to sample geometry, photon transmission of the entrance window of the cryostat and the crystal dead layer (DL). The in vivo laboratory (IVM) at Karlsruhe Institute of Technology (KIT), Germany, is running HPGe

detectors having very thin DL< 0.5 μm. An initial HPGe detector model was recently developed using scanning measurements with collimated radiation sources. However, no information about DL thickness, which is essential at low photon energy range, was derived. In the work reported here we developed a method to determine DL thickness using one of the HPGe detectors. Its intrinsic efficiency curve was measured using an Americium-241 radioactive source in 10-60 keV energy range. A comparison between experimental efficiency and Monte Carlo results (MCNPX) showed that the DL value of 0.4 μm, initially quoted by the manufacturer, has to be changed to 7.5 μm to reproduce measurements. The validated detector model will permit an accurate Monte Carlo calibration of the in vivo counting system.

Keywords: Dead layer, HPGe detector, Monte Carlo, MCNP, Radioactive source.

Validation of a NaI(Tl) and $LaBr_3$(Ce) detector's models: Experiment and Monte Carlo simulations

[1] MOHAMED YOUSSEF MESSOUS National Center for Energy, Sciences and Nuclear Techniques CNESTEN, Rabat, Morocco
[2] ISSAM MOUHTI Laboratory of Condensed Matter and Nanomaterials for Renewable Energy, Faculty of Sciences, University Ibn Zohr Agadir, Morocco
[3] ABDELLATİF ELANIQUE Laboratory of Condensed Matter and Nanomaterials for Renewable Energy, Faculty of Sciences, University Ibn Zohr Agadir, Morocco

Lanthanum Bromide $LaBr_3$(Ce) inorganic scintillator is a new type of nuclear detector used in gamma spectrometric systems. It is becoming an attractive alternative to the conventional NaI(Tl) detector because of its promising intrinsic performances: Compared to NaI(Tl) detector, the $LaBr_3$(Ce) scintillator has many useful characteristics: improved energy resolution (3% at 662 keV), fast time response (decay constant of circa 26 ns) enabling high count rate applications, high gamma detection efficiency, operation at room temperature and promising technology for manufacturing crystal at larger sizes. This work relates to the study and characterization of the response function of two cylindrical scintillation detectors with similar size: 2"x2" NaI(Tl) and 2"x2" $LaBr_3$(Ce). The photon detection efficiency and energy resolution curve were measured for the NaI(Tl) detector in the gamma energy range from 60 keV to 1408 keV. A precise mathematical model of the two scintillators was developed using the Monte Carlo simulation code MCNP. Comparison of the efficiency data with MCNP simulations showed good agreement enabling the validation of the computational models for both NaI(Tl) and $LaBr_3$(Ce) detectors. The energy resolution function was determined experimentally and used to improve the simulated spectra.

Keywords: Monte Carlo, scintillation detector, NaI, $LaBr_3$

Determination of direct capture reaction rate for $^{26}Si(p,\gamma)^{27}P$

[1] MURAT DAĞ Ahi Evran University

^{26}Al is a radioisotope produced in a variety of stellar sites such as novae, supernovae, Wolf Rayet (WR) stars, and Asymptotic Giant Branch (AGB) stars. The possible reaction sequence for production of ^{26}Al is $^{24}Mg(p,\gamma)^{25}Al(\beta+,\nu)$ $^{25}Mg(p, \gamma)^{26}Al$, and its ground state $\beta+$ decays to the first excited state of ^{26}Mg which then deexcites to its ground state, emitting a characteristic γ-ray line at E γ = 1.809 MeV. This γ-ray emission at 1.809 MeV were first observed by HEAO3 satellite, and later measured by the COMPTEL telescope installed on the CGRO (Compton Gamma Ray Observatory) satellite and INTEGRAL. Since the half-life ($T_{1/2}$ = $7.2x10^5$ yrs) of the radioisotope ^{26}Al is very short compared to the time scale of galactic chemical evolutions out in an all-sky distribution of 1.809MeV γ-rays over the galaxy, which provided a confirmation that ongoing nucleosynthetic processes are active. However, due to the proton capture on ^{25}Al being faster than its β-decay in the sites which have high stellar density and temperature, the possible dominant chain of the production of ^{26}Al can be by-passed through $Si(p,\gamma)^{27}P$ reaction is therefore of interest in connection with its role in the destruction of the important astrophysical observable ^{26}Al, and determination of reaction rate for the radioactive proton capture $^{26}Si(p,\gamma)^{27}P$ at stellar energies is of great importance for determining the quantity of the ground state of ^{26}Al produced through thermal equilibrium.

This work was supported by Ahi Evran University Scientific Research Projects Coordinations Unit. Project Number: FEF.A4.18.005

Keywords: Reaction Rate, thermal equilibrium, proton capture reaction

Optimization of the electrophoretic deposition parameters (hydroxyapatite concentration, collagen concentration, and deposition temperature speed) for biocomposite hydroxyapatite/chitosan/collagen/h-BN coatings via response surface methodology

[1] İSMAİL HAKKI KARAHAN Mustafa Kemal University
[2] ALİ TOZAR Mustafa Kemal University
[3] YASİN YÜCEL Mustafa Kemal University

Titanium and its alloys are very good alternatives for orthopedic operations and commonly utilized as bone substitute materials due to their excellent mechanical and corrosion properties and their decent biocompatibility. Due to its excellent bone bonding properties, HA becomes widely used metal coatings in biomedical applications. HA coatings constitute an osteoconductive surface for new bone growth. Thereby stabilizing the metal implant and transferring the load to the skeleton, HA coatings help to deal with bone atrophy problem. Electrophoretic deposition draws interest due to its low cost, ease of use, room temperature application, controllable parameters and various alternatives for both precursors (dissolved salts, suspensions, sols) and substrates. Nevertheless, electrophoretically deposited pure HA coatings need further high-temperature sintering causing decomposition of HA to tricalcium phosphate. To overcome this issue and further enhancement of biocompatibility moreover functionalize HA, composite coatings of HA with organic and/or inorganic materials has become a hot research topic. Response Surface Methodology (RSM) which is a technique for modeling and analyzing the relationship between independent variables. This technique is a beneficial chemometric practice for determining the mutual effects of empirical parameters and moreover for optimizing primary parameters with the fewest count of experiments. In this study, Ti_6Al_4V alloy biomedical implant materials have been coated with a biocomposite hydroxyapatite/chitosan/collagen/h-BN layer using electrophoretic deposition method at room temperature. RSM and Central Composite Design (CCD) have been employed for modeling and optimizing the electrophoretic deposition parameters of HA concentration, collagen concentration, and deposition temperature.

Keywords: optimization, response surface methodology, electrophoretic deposition, corrosion, biomedical, h-BN

The effect of chitosan concentration on the corrosion characteristics of the biomedical grade Ti_6Al_4V implants electrophretically coated with hydroxyapatite/chitosan biocomposites

[1] İSMAİL HAKKI KARAHAN Mustafa Kemal University
[2] ALİ TOZAR Mustafa Kemal University

Using Ti_6Al_4V alloy as implant material draws much interest because of its great corrosion resistance and appropriate mechanical strength. However, the biocompatibilities of these type of biomaterials are the major concern for the biomedical field researchers. In order to improve the biocompatibility, the coating of the implant surface with hydroxyapatite (HA) has been greatly studied and is still being studied due to the mineral component of bone is composed of HA. Various methods are being used for HA coating on metallic implant surfaces such as pulsed laser deposition, micro-arc oxidation, plasma spraying, RF magnetron sputtering, ion beam assisted deposition, and electrophoretic deposition (EPD). Unfortunately, these techniques require during and post-production high temperatures procedures that cause decomposition of HA into far less biocompatible tricalcium phosphate (TCP) form. In order to avoid the during and post-production high-temperature procedures, EPD of HA/chitosan (HA/CTS) composite coatings on Ti_6Al_4V implants is becoming a very encouraging technique due to its versatility, low-cost and not requiring of high-temperature procedures. In this study, HA/CTS biocomposite coatings have been produced on biomedical grade Ti_6Al_4V implants by EPD. The effect of concentration of chitosan in the EPD suspension on the corrosion protection performance of the coatings has been investigated. Our results showed that the corrosion protection performance of the HA/CTS coating increases with the increase of chitosan concentration up to 2.5 g/L and than slightly decreases.

Keywords: biomedical, hydroxyapatite, chitosan, electrophoretic deposition, corrosion

A study of mean free path on the radiation shielding properties of normal concrete

[1]EYYUP TEL, [2]YUSUF KAVUN, [1]ALİ ARMAĞAN GÖK, [1]MESUT DEPEDELEN

[1]Osmaniye Korkut Ata University, Faculty of Arts and Science, Department of Physics, Osmaniye, TURKEY
[2] Kahramanmaras Sutcu Imam University, Department of Medical Imaging Techniques, Kahramanmaras, TURKEY

Abstract

Today along with developing technology and rapid population growth, energy needs have been increasing in the worldwide. In order to supply rising energy demands, the countries have been tending to nuclear power plants which have high productivity. In nuclear power plants established by using high technology, required precautions are adopted by assessing all negative effects that can harm environmental health. For this reason, it is important to investigate the radiation shielding and efficiency of traditional concretes. In this study, it was studied efficiency of shielding at different energies and also calculated macroscopic cross-sections and mean free path of normal concrete material. So, the consequences of using normal concrete material in nuclear power plants have been investigated.

Keywords: nuclear energy, normal concrete material, macroscopic cross-section, mean free path

Introduction

The microscopic cross-section and macroscopic cross-section is usually a mixed concept due to used in to represent atomic diameter and calculation of cross section. The microscopic cross section represents the effective target area of a single target nucleus for an incident particle and its units are barns or cm^2. But, macroscopic cross-section represents the effective target area of all of the nuclei contained in the volume of the material and its unit is cm^{-1}. These terms are commonly used in cross section calculations and are important for the efficiency of shielding.

Shielding is very important in nuclear power plants in order to make energy production processes more efficient and not harming nature. Therefore, the resistance of the reactor materials to radiation and the radiation absorption are very important. A wide variety of concrete is used in the construction of power plants and these concretes must have high radiation absorption properties [1]. The various materials can be added into concrete mixtures and absorption properties can be increased[2].

In this study, in order to achieve high quality shielding in the nuclear power plant concrete materials, ^{12}C and ^{39}K is investigated that exist in the structure of normal concrete.

Macroscopic Cross Section Calculation

In the production of artificial radioisotopes, in absorption, in scattering or the incoming particles from any nuclear reaction , needs to know what can happen when they hit target cores. Also, this effects depend on target type, reaction type, incoming particle type and energy. For a better understanding of these processes, Tel et al. suggested an new experimental the cross-sections of the (n,p) reactions which are dependent on the asymmetry parameter [3] $s = (N-Z)/A$. The formula of Tel et al for the (n,p) reaction cross-sections at the energy of 14 MeV can be given as follows

Author – Energy (MeV)	Mass number	σ (n,p) Formulas
Tel et al. I [3]		
14 -15	17 <A<239	$14.56\,(A^{1/3}+1)^2\,exp[-26.58s]$
Tel et al. II [4]		
14-15	Even-Z, Even -N	$16.33\,(A^{1/3}+1)^2\,exp[-26.17s]$
14-15	Even -Z, Odd-N	$9.71\,(A^{1/3}+1)^2\,exp[-21.87s]$
14-15	Odd -Z, Even -N	$7.31\,(A^{1/3}+1)^2\,exp[-20.21s]$
Levkovskii [5]		
14	$40 \leq A \leq 202$	$45.2(A^{1/3}+1)^2\exp[-33s]$

Atomic density: $N_0 = \frac{\rho . N_A}{A}$

N_0: Atomic Density$(molecule/cm^3)$, ρ: Density (g/cm^3), N_A:Avagadro Number $(0{,}6022x10^{24})$, A: Atomic Mass. Probability of being affected per path length taken in neutrons:

$$\sum\nolimits_{(n,p)} = \sigma_{(n,p)} . N$$

Average free path: $\lambda = \frac{1}{\Sigma_{(n,p)}}$

Results and Calculation

For ^{12}C Tel et al. II (n, p) reaction cross section (mb)

calculations,

$$N = \frac{\rho N_A}{A} = \frac{2,267 g 0,6022 \times 10^{24}}{12} = 0,1138 \times 10^{24} \text{ molecule}/cm^3$$

The atomic density is calculated. In Table 1, Tel et al. II If Even-Z, Even-N formula is used;

$$\sigma_{(n,p)} = 16.33 \times (A^{(1/3)} + 1)^2 g exp[-26.17s]$$

$$\sigma_{(n,p)} = 16.33 \times (A^{(1/3)} + 1)^2 g exp[-26.17 \times (N - Z/A)]$$

$$\sigma_{(n,p)} = 176,76mb = 0,1767barn$$

$$\sum_{(n,p)} = \sigma_{(n,p)}.N$$

$$\sum_{(n,p)} = 0,1767 \times 10^{-24} g 0,1138 \times 10^{24} = 0,020108 \text{ molecule}/cm^3$$

$$\lambda = \frac{1}{\Sigma(n,p)} = \frac{1}{0,020108} = 49,79cm^{-1}$$

For ^{12}C Levkovski (n, p) reaction cross section (mb) calculations,

$$N = \frac{\rho N_A}{A} = \frac{2,267 g 0,6022 \times 10^{24}}{12} = 0,1138 \times 10^{24} \text{ molecule}/cm^3$$

The atomic density is calculated. In Table 1, Levkovski $\sigma_{(n,p)}$ is used;

$$\sigma_{(n,p)} = 45.2(A^{1/3} + 1)^2 \exp[-33s]$$

$$\sigma_{(n,p)} = 45.2(A^{1/3} + 1)^2 g exp[-33 \times (N - Z/A)]$$

$$\sigma_{(n,p)} = 489,25mb = 0,48926barn$$

$$\sum_{(n,p)} = \sigma_{(n,p)}.N$$

$$\sum_{(n,p)} = 0,48926 \times 10^{-24} g 0,1138 \times 10^{24} = 0,05567 \text{ molecule}/cm^3$$

$$\lambda = \frac{1}{\Sigma(n,p)} = \frac{1}{0,05567} = 17,963cm^{-1}$$

For ^{39}K Tel ve ark. I (n, p) reaction cross section (mb) calculations,

$$N = \frac{\rho N_A}{A} = \frac{0,89 g 0,6022 \times 10^{24}}{39} = 0,0138 \times 10^{24} \text{ molecule}/cm^3$$

The atomic density is calculated. In Table 1, Tel ve ark. I $\sigma_{(n,p)}$ is used;

$$\sigma_{(n,p)} = 14,56 \times (A^{(1/3)} + 1)^2 g exp[-26.58s]$$

$$\sigma_{(n,p)} = 14,56 \times (A^{(1/3)} + 1)^2 g exp[-26.58 \times (N - Z/A)]$$

$$\sigma_{(n,p)} = 281,89 \times 0,5065$$

$$\sigma_{(n,p)} = 142,80mb = 0,1428barn$$

$$\sum_{(n,p)} = \sigma_{(n,p)}.N$$

$$\sum_{(n,p)} = 0,0138 \times 10^{-24} g 0,1428 \times 10^{24} = 0,001971 \text{ molecule}/cm^3$$

$$\lambda = \frac{1}{\Sigma(n,p)} = \frac{1}{0,001971} = 507,45cm^{-1}$$

For ^{39}K Levkovski (n, p) reaction cross section (mb) calculations,

$$N = \frac{\rho N_A}{A} = \frac{0,89 g 0,6022 \times 10^{24}}{39} = 0,0138 \times 10^{24} \text{ molecule}/cm^3$$

The atomic density is calculated. In Table 1, Levkovski $\sigma_{(n,p)}$ is used;

$$\sigma_{(n,p)} = 45.2(A^{1/3} + 1)^2 \exp[-33s]$$

$$\sigma_{(n,p)} = 45.2(A^{1/3} + 1)^2 g exp[-33 \times (N - Z/A)]$$

$$\sigma_{(n,p)} = 45,2 \times 19,36 g 0,43$$

$$\sigma_{(n,p)} = 375,96mb = 0,376barn$$

$$\sum_{(n,p)} = \sigma_{(n,p)}.N$$

$$\sum_{(n,p)} = 0,0138 \times 10^{-24} g 0,376 \times 10^{24} = 0,00518 \text{ molecule}/cm^3$$

$$\lambda = \frac{1}{\Sigma(n,p)} = \frac{1}{0,00518} = 193,05cm^{-1}$$

Conclusion

Due to the there is no experimental values for (n,p) reactions in literature, we can not compare these results. Obtained theoritical results are important for shielding at nuclear reactors and radiation and our purpose is to get new datas to literature.

Reference

[1] Akarslan, F., Üncü, I., S., Kılınçarslan, S., Akkurt, I. and Molla, T., 1653, 020007, (2015).

[2] Witte, L., P. and Backstrom, J., E., 51,6,65-88, (1954).

[3] Tel, E., Şarer, B., Okuducu, Ş, Aydın. A. and Tanır, G., Journal of Physics G: Nuclear and Par-ticle Physics29, 2169-2177, (2003).

[4] Aydın, A., Tel, E., Şarer, B., Phys. Scr.,75,299-306, (2007).

[5] V.N. Levkovskii, Sov. Phys. JETP 18, 213–217 (1964).

Necessity of nuclear energy in Turkey

[1]YUSUF ALPER KAPLAN, [1]MERVE KARAGÖZ, [2]EYYUP TEL,

[1]Osmaniye Korkut Ata University, Engineering Faculty, Energy Systems Department, Osmaniye, Turkey
[2]Osmaniye Korkut Ata University, Faculty of Arts and Sciences, Physics Department, Osmaniye, Turkey

Abstract

Concerning the basic needs of the world we live in 21st century (AC), energy has a huge priority. For energy wise, any country wishes to progress or develop requires itself to find different solutions for generating that energy, which will help them to be self dependent. For this occasion, Turkey must have interest in nuclear energy along with renewable energy. Nuclear power plants, which are built to generate nuclear energy, are known to have negative sides such as high building costs and raditation risks, but apart from that it also takes attention for supplying non-stop(uninterrupted) energy resource especially for industrial complexes. In this study, the subjects concerning the ways for Turkey to have less external dependence along with the ways to reduce the energy deficiency in the country has been examined.

Keywords: Energy, Nuclear energy, Energy policy

Introduction

The steady increase in energy needs nowadays leads the states to provide energy diversity and to use new and alternative energy sources. The countries have started to work on renewable energy sources as well as nuclear energy due to energy shortage problems. Nuclear power is active in many countries, such as electricity generation, medicine, and space technology. One of the most important uses of nuclear technology is to generate electricity through nuclear power plants. When you look at the world scale; there is a large increase in demand for electricity, especially in developing countries [1]. In order to meet this demand, renewable energy sources and nuclear energy are also used. Around 11% of the world's electricity is generated by about 450 nuclear power reactors. About 60 more reactors are under construction, equivalent to 16% of existing capacity, while an additional 150-160 are planned, equivalent to nearly half of existing capacity [2].

Turkey's Energy View

Located between developing countries in Turkey; with industrialization, investments are being made for new technologies, increasing population and living standards the demand for energy is increasing day by day [3]. Turkey's electric energy consumption in 2016 was realized as 278.4 billion kWh. Electricity consumption increased by 4.7% compared to the end of July of the previous year as of July, 2017 and 167,1 billion kWh of electricity production was realized as 167.3 billion kWh by increasing by 6.7% compared to the end of July of the previous year. By the end of July, 34% of our electricity production was from natural gas, 31% from coal, 24% from hydraulic power, 6% from wind, 2% from geothermal energy and 3% from other sources [4]. Electricity consumption is expected to reach 385 TWh in 2023 with an average annual increase of 4.8% according to the baseline scenario. At the end of November, 2017, the total electricity board power reached 83138.9 MW. Since the rate of demand and supply of energy in our country is increasing day by day, the increase in electricity generation from all sources of energy has become a matter of course. When the change over the years have electricity installed capacity in Turkey, especially in recent years examined in Table 1, we see that increased solar power and wind power installed.

Table 1 . Change of the power of the electricity power in our country according to years

Years	Thermal	Hydraulic	Geothermal	Wind	Solar	Total
2006	27420.2	13062.7	81.9			40564.8
2007	27271.6	13394.9	169.2			40835.7
2008	27595.0	13828.7	29.8	363.7		41817.2
2009	29339.1	14553.3	77.2	791.6		44761.2
2010	32278.5	15831.2	94.2	1320.2		49524.1
2011	33931.1	17137.1	114.2	1728.7		52911.1
2012	35027.2	19609.4	162.2	2260.6		57059.4
2013	38648.0	22289.0	310.8	2759.7		64007.5
2014	41801.8	23643.2	404.9	3629.7	40.2	69519.8
2015	41903.0	25867.8	623.9	4503.2	248.8	73146.7
2016	43494.769	26681.1	820.9	5751.3	832.5	78497.4
2017	44311.7	27043.6	860.8	6161.3	1362.6	79740

2.1 Solar Energy

By the end of 2016 in our country, 34 solar power plants with 402 MW installed capacity were licensed to 2 solar power plants with preliminary license and 12.9 MW installed capacity. By the end of 2016, with the establishment of unlicensed power generation plants, the number of solar power plants is seen as 1043, while the installed power of these power plants is 819.6 MW and total installed power together with 2 licensed solar energy power plants reached 832.5 MW[4]. However, the infrastructure works for increasing the share of solar energy in electricity generation is gaining momentum. Analysis of the total installed solar capacity by 2030 in Turkey envisages exceed 17 GW. For 2040 years, solar energy capacity is expected to climb to more than 40 GW and constitute almost 30% of the total installed capacity [6]. As can be seen in Table 2, solar power generation by 2014 is only 40 MW and electricity production is 2060 MW by the end of 2017.

2.2 Wind Energy

Turkey, which is among the countries in the world conducive to the use of wind energy. It is located. Turkey's current electricity generating dams 36 to 10 times as wind energy is claimed to have. In parallel with the development in the world in 2020 be consumed in Turkey is expected to meet 10% of electricity from wind energy It is aimed[7].

It is estimated by the General Directorate of Renewable Energy (YEGM) that 5 MW power plants per square meter can be installed in areas with wind speeds above 50 m and 7.5 m / s. The total installed capacity corresponds to 1.3% of the total area of the country and the total installed capacity is 48 GW. In the evaluation of the wind power, the parameters such as the capacity utilization rates and the return period of the investment gain importance. The results obtained by YEGM are summarized in Table 3 [8].

Table 2: Solar Energy Development (MW) Between 2012-2017

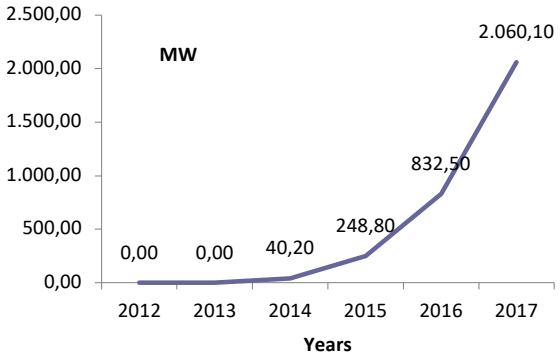

Table 3: Investment Grade Wind Power Potential in Turkey

Wind Power	50 m Height Wind Power [W/m²]	50 m Height Wind Velocity [m/s]	Total Area [m²]	Total Capacity [MW]
Well	400-500	7.5-8.1	5851.87	29259.36
Excellent	500-600	8.1-8.6	2598.86	12994.32
Excellent	600-800	8.6-9.5	1079.98	5399.92
Excellent	>800	>9.5	39.17	195.84
TOTAL			**9569.88**	**47849.44**

Electricity generation from wind energy in the world, which was 17.4 MW in 2000, was 432.9 GW in 2015. By 2030, this figure is expected to reach 1749.8 GW. In Turkey, which is in operation by the end of 2016 licensed wind power installed capacity of 5738 MW, while the figure was realized at the end of October 6353 MW (Table 4) [8].

2.3 Hydroelectric Energy

Hydroelectric power plants with a share of 34% in electricity generation; It is important because it is environment friendly, clean, renewable, high efficiency, fuel-free, long-lasting, very low operating costs and not dependent on foreign sources. Turkey's hydroelectric potential is 1% of the total constitutes 16% of total world Europe[4].

Tablo 4: Between 2012-2017 Wind Energy Development(MW)

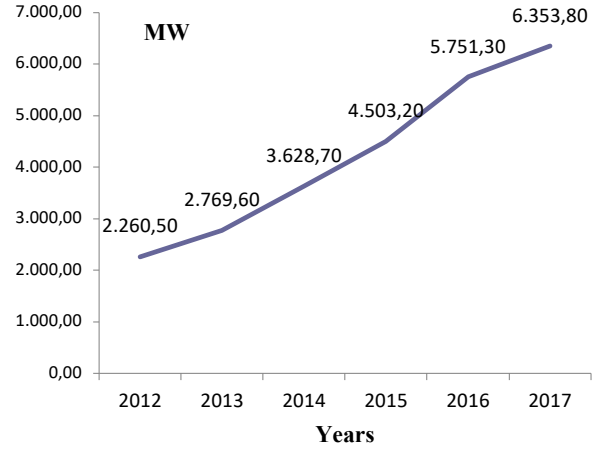

Hydroelectric power plants are a production method depending on meteorological conditions, which causes problems over time. The share of total hydroelectric power from light and dam power plants in electricity generation is 34% in 2016 and 33% in October 2017 [8].

Table 5.Hydroelectric Power Development between 2012-2017(MW)

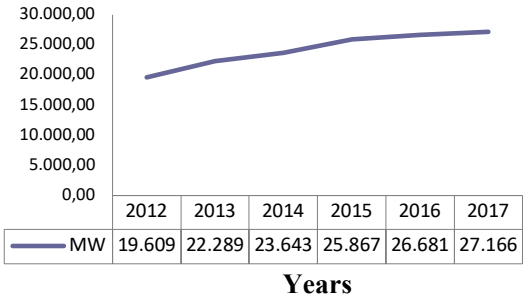

2.4 Nuclear Energy

Nuclear energy is linked to the atomic nucleus, and it occurs in different situations. These are fusions with the formation of two small nuclei, and the second is the fragmentation of a large nucleus. In these cases, the energy from the reaction can be converted into heat and electric energy can be generated. Nuclear power has a significant share in world electricity generation[10]. The available capacity of nuclear power plants is higher than the capacity of the plants operating with renewable energy sources. 30.000 MW wind power or 38.000 MW solar power plant is required to be installed in order to correspond to 10.000 MW nuclear power plant. In addition, a nuclear reactor at a power of 1,000 MWe produces approximately 27 tons of spent fuel per year. In terms of Turkey, Akkuyu and Sinop nuclear power plants are expected to be 80 billion kWh of electricity production annually, thanks. In addition, it is necessary to import about 16 billion m3 of natural gas to obtain an electricity from natural gas plants in this amount. "In the 3rd year, 4 units of nuclear power plant can be established in Mersin-Akkuyu with the money to be paid for natural gas import[11].

3 Nuclear Power Plants Are Being In Turkey

Inadequacy attempts made in Turkey in the field of wind and solar energy, make nuclear energy issue require more importance[12]. Turkey's nuclear energy between the energy source located resulting in inadequacy of resource diversity. Until 2023 it is planned to establish two nuclear power plant in Turkey[3]. Figure 2 shows the plants planned to be installed in Turkey.



Figure 2: Nuclear power plants are being planned in Turkey[2]

3.1 Akkuyu NPP

Akkuyu NPP Project consists of 4 units. The power of each unit will be 1200 MWe. The operational life of Akkuyu Nuclear Power Plant will be 60 years. The first reactor of the plant will be completed in 2020, consisting of 4 reactors. Turkey Electricity Trading and Contracting Company (TETAS) will buy a fixed proportion of the power at a fixed price of US$ 12.35 cents/kWh for 15 years. The proportion will be 70% of the output of the first two units and 30% of that from units 3&4 over 15 years from commercial operation of each. The remainder of the power will be sold by the project company on the open market. After 15 years, when the plant is expected to be paid off, the project company will pay 20% of the profits to the Turkish government. (These sovereign guarantees are not on offer for the Sinop plant. Turkey Atomic Energy Agency (TAEK) granted a construction licence for the project at the beginning of April 2018, and start of construction was announced on 3 April 2018 [2].

3.2 Sinop NPP

The Sinop nuclear project is planned to establish a French-Japanese joint venture ATMEA-1 type nuclear reactor with 4,805 MW of power, each with four units of 1,120 MW. The EIA application file for the Sinop Nuclear Power Plant Project was submitted to the Ministry of Environment and Urbanism on January 2018 and the public participation meeting on the project was held in Sinop on 6 February 2018. The feasibility studies of the project are being continued with the EIA studies.

3.3 Igneada

There are plans to build further nuclear capacity at another site, as part of 100 GWe required by 2030. TAEK has identified Igneada in Kirklareli province on the Black Sea, 12 km from the Bulgarian border, and this was confirmed in October 2015. Akcakoca between it and Sinop was also considered. Ankara – with low seismic risk – and Tekirdag on the northwest coast of the Sea of Marmara had also been mentioned as possible sites. When agreement for the development of the Sinop plant was to have been finalised, the energy ministry was to announce the site for the third plant with an invitation for expressions of interest to be issued by the end of 2013. This didn't happen and in October 2014 the prime minister said that the project would be substantially indigenous, with construction start about 2019 [2] .

4 Conclusion

Turkey is a country dependent on foreign supplies of energy to meet the demand. Nuclear energy should be seen as alternative energy to reduce this external dependency. The need for energy is increasing every day because it is a developing country. Especially industial applications necessary non-stop(uninterrupted) energy power so nuclear energy must be an alternative source in Turkey. It must diversify its energy sources and utilize nuclear energy so that it can meet its growing energy needs and reduce its dependency on the outside. Energy sources such as wind, sun, hydropower are dependent on meteorological and climate events. Located between developing countries in Turkey; with industrialization,

investments are being made for new technologies, increasing population and living standards the demand for energy is increasing day by day. In this context, we have to make use of nuclear energy, which is the non-stop(uninterrupted) source of energy for industial applications.

Acknowledge

The study is supported by Osmaniye Korkut Ata University through the projects OKUBAP-2017-PT5-010.

References

[1] http://www.21yuzyildergisi.com/assets/ uploads/ files/107.pdf

[2] http://www.world-nuclear.org/

[3] F KAYA, and E GÖRAL. "TÜRKİYENİN NÜKLEER ENERJİ POLİTİKASI." *Akademik Bakış Uluslararası Hakemli Sosyal Bilimler Dergisi* 57 (2016): 421-438.

[4] http://www.enerji.gov.tr

[5] "Türkiye Elektrik Sistemi Kuruluş ve Yakıt Cinslerine Göre Kurulu Güç", TEİAŞ, www.teias.gov.tr/yukdagitim/kuruluguc.xls,

[6] http://www.solarbaba.com

[7] İLKILIÇ, Z . "Türkiye'de Rüzgar Enerjisi ve Rüzgar Enerji Sistemlerinin Gelişimi". Batman Üniversitesi Yaşam Bilimleri Dergisi 6 (2016): 1-13 <http://dergipark.gov.tr/buyasambid/issue/ 29826/320977

[8] Türkiye Rüzgâr Enerjisi Birliği, Rüzgâr Enerjisi ve Etkileşim Raporu, Kasım, 2016

[9] https://assets.kpmg.com/content/dam/kpmg /tr/pdf/ 2018/02/sektorel-bakis-2018-enerji.pdf

[10] FURUNCU, Y. "Türkiye'nin Enerji Bağımlılığı ve Akkuyu Nükleer Enerji Santralı." *Cumhuriyet Science Journal* 37 (2016): S198-S207.

[11] UÇKUN, A. "Arz Güvenliği ve İklim Değişikliği Açısından Nükleer Enerji Bir Zorunluluk Mudur?." *Enerji ve Diplomasi Dergisi* (2015): 4.

[12] KARA, E. "AB'ye Uyum Sürecinde Türkiye İçin Nükleer Enerji.

The role of nuclear energy for generating electric in Turkey

[1] MERVE KARAGÖZ Osmaniye Korkut Ata University
[2] YUSUF ALPER KAPLAN Osmaniye Korkut Ata University

As being continuosly developing country, Turkey's necessity for energy resources increases as a result of having constant economic growth that happens every year. Having limited domestic production which fairly does not cover for meeting the ever growing energy demand, substantial amount of energy is met by importation. Having high rate imports have negative effects for Turkey in areas such financial stability, sustainable growth, energy demand safety. Looking at recent developments, the state primarily put nuclear energy option in the effect as an alternative to solve this problem. In this study, we examined the differences or alteration on electric production subject as Turkey leans to nuclear energy. Akkuyu power plant project, having 1200MW each, consist of 4 units. Sinop power plant project consist of 4 units and has a established power of 4480MW.

Keywords: Energy, Nuclear Energy, Energy generating

Hydrogen recombination in REKO-4 facility and analysis of recombination

MAHMUT CÜNEYT KAHRAMAN

Yalova University, Energy Systems Engineering Dept., Yalova, Turkey

Abstract

Previous accidents happened in LWR have proved that safety device installation to the reactors is necessary to remove the hydrogen gases inside the vessel in case of an accident. The aim of the study was to investigate a PAR with catalyst sheets as a safety device to calculate the hydrogen consumption, determine the temperature distribution and inlet velocity in the test facility, REKO-4, Jülich Forschungszentrum (Research Center) Germany.Test series were carried out under atmospheric pressure and natural flow conditions. For the test purposes, hydrogen between 2.0 and 6.0 vol. % was injected to the vessel with volumetric flow, 1.9 m^3/h. The first rise in the temperature of the PAR inlet was found after 100 seconds of first hydrogen injection, this result demonstrated that reaction started and hydrogen was consumed. Additionally, in order to investigate the buoyancy-driven flows, particles velocity was measured by PIV and particles motion was examined. The experiment results show that the PAR is an ideal device for removing of hydrogen from vessel and creating the buoyancy-driven flow, it conforms the purpose of installing PAR to the system.

Keywords: Hydrogen, REKO-4, Recombination, Reactor, Safety

Introduction

In case of a severe accident in a Light Water Reactor (LWR) such as loss of coolant accident, large amounts of hot steam and hydrogen may be released from the primary circuit into the containment.

For LWR, due to inadequate make-up water or delayed action of the emergency core cooling system, the coolant flow rate is insufficient, and the reduced cooling of the core can lead to Zircaloy oxidation. Hydrogen is generated as a result of oxidation. Releasing hydrogen to containment area may be resulted to ignition. Some accidents happened in the past due to this reason.

There are some studies in Europe and United States about how the hydrogen detonation can be prevented. First point, hydrogen concentration in containments needs to be controlled and managed. In order to reduce the accumulation of hydrogen and thus to mitigate the risk of a combustion, PARs have been installed within LWR containments in several European countries such as Germany, France or Hungary [1]. However, The PWRs in USA have not installed any special devices for hydrogen control. Their containment volume is supposed to be large enough not to create high (>10%) concentration hydrogen mixture.

Experiments performed on PARs to analyse device behaviour and provide the data for model validation. Based on these data, the computer code REKO-DIREKT was developed at Jülich with the cooperation of RWTH Aachen and FZJ. First experiments were performed in the REKO-3 facility under well-defined forced-flow conditions that were focused on the processes inside the catalyst section of a PAR. The next step is that REKO-4 has been developed to focus more hydrogen recombination investigation, the PAR design and its interaction with the surrounding conditions [2].

This paper describes investigation of hydrogen recombination in REKO-4 and PARs designs with measurement of the flow velocity and direction by using PIV method. On this project at IEK-6, the research was performed in REKO-4 to clarify hydrogen inlet and outlet concentration. The reason of it is to illustrate recombiner reaction capability. Secondly, flow direction and velocity of gases at the inlet of PAR is calculated by PIV technique in order to ensure that recombiner can establish the internal upward chimney flow. Moreover, the different points' temperatures with different heights of catalysts were measured by thermocouples to have a better understanding of the reaction rate. During the experiments, PIV technique and other measurements such as temperature, pressure and concentration of hydrogen by using measurement devices such as thermocouples, pressure gauges, thermal conductivity gauges (katharometers) were used. Different analyses are done and final data is discussed and evaluated to have a better understanding of PARs working principle and catalyst sheets

Hydrogen Recombination- PARS

Hydrogen recombination is one method in order to prevent hydrogen explosion or destroying of reactor in LWR in case of coolant leakage in reactor. The release rate and the total amount of hydrogen depend on the particular severe accident scenario and also on the reactor type.

In case of coolant leakage, high heat is observed in the reactor. Zirconium oxidation which occurs by reaction of zirconium with steam, adds extra thermal load due to exothermic reaction. Hydrogen is generated at temperatures above 1200◦C by a runaway exothermic reaction between steam and Zircaloy fuel cladding. The stoichiometric equation for oxidation of the Zircaloy cladding with steam is:

$$Zr + 2H_20 \rightarrow ZrO_2 + 2H_2 + Q \quad (1)$$

where Q = −586 kJ mol−1 is the exothermic heat release per unit mol of zirconium oxidized [3].

PARs are used to prevent accidents mentioned above and consume of hydrogen. Hydrogen and oxygen react exothermically on the catalytic surfaces inside a PAR generating steam and heat. The reaction heat creates a buoyancy-driven flow which makes a PAR a completely passive operating device. Therefore, PARs do not consume energy.

$$H_2 + 1/2O_2 \rightarrow H_2O + \Delta Q \quad (2)$$

The steam and hydrogen, generated by oxidation reaction and released from primary circuit, will flow through up due to density differences. After cooling at the dome ceiling and on the containment walls, a downward-directed flow close to the walls is expected to occur. For a high efficiency hydrogen recombination, flow direction and flow velocity takes important role. PARs are expected to establish the internal upward chimney flow against the downward local containment flow. During my study, some tests were performed to analyse flow direction and flow velocity using by PIV technique. Results will be discussed in results section. A PAR picture from a LWR and recombination steps are shown in the Fig.1.

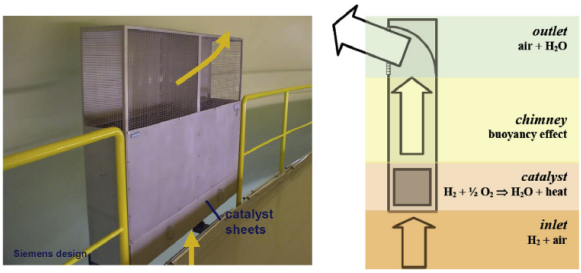

Fig. 1. Recombination in PARs. (Simulation of the efficiency of hydrogen; Ernst-Arndt Reinecke, StephanKelm, WilfriedJahn, ChristianJakel, Hans-Josef Allelein)

In Fig. 1, Recombination process and PARs principle are shown shortly. In the leading part of PAR, catalyst sheets are located. The catalyst sheets are surfaces where recombination reaction occurs. The catalyst sheets are shown in Fig. 2. They form a set of parallel vertical flow channels. Hydrogen entering to the PAR is converted with oxygen to steam. Since heat is generated during the reaction, the buoyancy-driven flow is created. The buoyancy-driven flow is induced inside the chimney part which ensures a continuous gaseous flow through the PAR. It is vital for hydrogen consuming continuously in recombination process. In order to assess the efficiency of PAR applications, substantial efforts have been spent on developing model strategies by some companies such as AREVA, AECL, and NIS. Issues for modelling of PARs can be given in four main titles:

- As a result of catalytic surface reaction, buoyancy-driven flow and hydrogen consuming.
- The interaction of PARs outflow with atmosphere of containment and effects on mixed process.
- Protection of the catalyst against poisoning and related deactivation effects.
- Possible ignitions at the hot parts as a result of exothermic reactions.

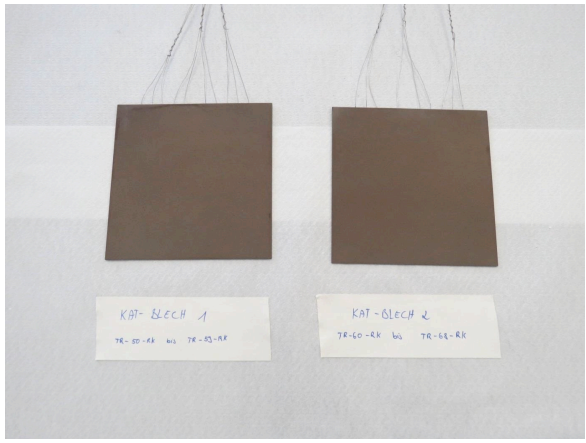

Fig. 2. Catalyst sheets

Results

Prior work has documented in the REKO-3 facility which were focused on the processes inside the catalyst section of the PAR. Those tests were performed under well-defined forced flow conditions.

In this experiment, we tested the PAR in REKO-4 facility. The main aims of these test series were to investigate detailed hydrogen recombination under natural convection conditions, examine the PAR design and REKO-4 facility. Tests were performed under atmospheric pressure with hydrogen injection concentration between 2-6 vol. percent. During the tests, we applied to PIV technique to indicate the particle movement and velocity with details.

We found the first temperature rise after 100 seconds first hydrogen was injected. It tells us that hydrogen recombination started on the trailing part of the catalyst sheets after this time. However; it required more time, at least 200 seconds for start-up of operation on the leading part of the PAR. After start-up of the operation, we observed sharply decrease in the hydrogen concentration. 80% of hydrogen concentration was consumed in 30 minutes. This data provides that the PAR is an ideal device for removing of hydrogen from vessel, it conforms the purpose of installing PAR to the system.

Additionally, this study indicates that the PAR is a passive device and can work without supplying any energy. PIV results provide compelling evidence that

buoyancy driven flows occurred 300 seconds later after first hydrogen injection. Particle movement through the PAR inlet and particle velocity around 0.5 m/s were observed as expected.

Moreover, another important correlation was seen between hydrogen concentration and catalyst sheet temperature after catalyst sheet reached the working temperature. The data, which was read from measurement devices, showed that increasing of hydrogen concentration provide a rise in the catalyst temperature.

Finally, this study has revealed that this test facility, REKO-4, succeeds in recombining of hydrogen under natural conditions and has showed that it is suitable for these test series. Test results and analyses supported the idea that PAR device enable to consume hydrogen gases released to vessel and avoid the hydrogen explosion. PIV technique was used effectively and offered the understanding or particle behaviour inside the vessel.

However, some limitations are worth. These test series were performed only under atmospheric pressure conditions. Low pressure tests are still being performed in Jülich, Forschungszentrum. Therefore, this study results should be compared with low pressure tests to verify the performance of the PAR. Secondly, the number of measurement devices should be increased in REKO-4 facility to get more accurate results.

Reference

[1] Simon, B. et al., Start-up behaviour of a passive auto-catalytic recombiner under counter flowconditions: Results of a first orienting experimental study. Nuclear Engineering and Design, 278,pp.317–322. (2014)

[2] F Simon, B. et al.,Investigation of PAR Behavior in the REKO-4 Test Facility. Volume 2: PlantSystems, Structures, and Components; Safety and Security; Next Generation Systems; Heat Exchangers and Cooling Systems, 2(1), p.345. (2012)

[3] Cand. oec. Ing. Benjamin Häfele. Realisierung und Vermessung einer abwärts gerichteten,wandnahen Gasströmung innerhalb des Versuchsstandes REKO-4. (2012)

[4] Reinecke, E.A. et al.,. Simulation of the efficiency of hydrogen recombiners as safety devices.International Journal of Hydrogen Energy, 38(19), pp.8117–8124.(2013)

Determination of morphological characteristics and mineralogical structure of the Kulakcayiri sediments by SEM and XRD

[1] GÜLDEREN AÇIKGÖZ Yıldız Teknik University
[2] ZEKİ ÜNAL YÜMÜN Namik Kemal University
[3] EROL KAM Yıldız Teknik University
[4] KÜBRA BAYRAK Yıldız Teknik University

The Kulakcayiri Lake is located in the town of Arnavutkoy in the province of Istanbul. It is a shallow lake formed on the ore deposits which have been closed in the past. This study was carried out to investigate the morphological and mineralogical attributes of the sediments of Kulakcayiri Lake. For this purpose, 3 core sediments were extracted from the depths of 5, 10 and 15 meters of the lake. First, SEM images were taken by JEOL JSM-6390LV and then mineralogy of sediment samples was determined by XRD. SEM analysis is an imaging technique in which the topographic and morphological properties of materials can be examined. During SEM analysis, the accelerating voltage for each sample was set to 20 kV. The SEM images of the samples were examined in μm dimension (up to X3500 magnification). The complex structure of SEM images is noteworthy because the sediments are composed of various organic and inorganic compounds. XRD is an analytical technique based on the fact that X-rays form different diffraction profiles due to the unique atomic structure and arrangement of crystals. As a result of XRD analysis, a large number of peaks were obtained and various minerals were detected from the obtained peaks. Crystal structure of the minerals such as Hematite (Fe_2O_3), Quartz (SiO_2), Calcite ($CaCO_3$) and Corundum (Al_2O_3) were investigated and evaluated. In conclusion, the physical and chemical properties of the sediments of Kulakcayiri Lake are reflected by this study. The mineralogical structure of the different depths of the lake was evaluated and compared with each other.

Keywords: Kulakcayiri Lake, sediment, SEM, XRD

Evaluation outdoor gamma dose rates in air and cancer risk determination for nevsehir, turkey

[1] MERVE YAPRAK Yildiz Technical University
[2] M. ERGÜN TURGAY Yalova University
[3] EROL KAM Yildiz Technical University

Assessment of inhalation quality for Nevşehir which well-known touristic destination, is important for local population nearby also for visitors. In this case, spread map was prepared in order to take a lot of output around this province as well distinguished cities as Kapadokya, Avanos, Göreme, Ihlara and Ürgüp especially. Radioactivity analysis in air was realized by using air dose rate measurements around the province. Via counting of 46 stations, it was possible to get the average dose rate. Then it was calculated to annual dose in air. Besides, cancer risk was determined for Nevşehir. All these values were compared with the World's references (UNSCEAR) and assumed, finally. It was measured the average dose rate as 87.39 $nGyhr^{-1}$ and annual dose was calculated to 107.18 μSv. This dose is required to excess lifetime cancer risk as $3.75x10^{-4}$. These values could be compared to the similar studies which existed around the world. Finally, the average annual effective dose equivalent and excess lifetime cancer risk for Nevşehir, are more than the world average but less than Artvin and Çanakkale. This study would be used to a reference for further investigations, besides it will be useful to compare with different studies which, will be evaluated in the future, for example after a nuclear pollution, or to compare the seasonal results, or such as based on a reactor leakage, nuclear attacks, etc., too.

Keywords: Nevsehir, ADRA, AEDE, Radioactivitiy, Cancer Risk

Estimate of individualized radiation risk coefficients under internal exposure for the cohort of Russian emergency workers

SERGEY LOVACHEV A. Tsyb Medical Radiological Research Center – branch of the National Medical Research Radiological Center of the Ministry of Health of the Russian Federation (A. Tsyb MRRC)

International basic radiation safety standards 2011 of the International International Atomic Energy Agency require to inform the exposed persons about possible effects of radiation on their health. This information applies to all types of exposure situations (planned, emergency and existing). In accordance with the Recommendations of the ICRP in 2007 (Publication 103), the nominal risk coefficients and the effective doses can not be used for assessment of the individual radiological exposure consequences and harm to health. This is relevant for the radiation risk estimation of internal exposure, when the exposure of different organs and tissues is uneven. The purpose of the study is to determine the dependence of lifetime radiation risk (LAR) on sex and age at exposure (inhalation intake for internal exposure) for Russian exposed cohorts. The ICRP radiation risk models (Publication 103), Russian age-sex cancer incidence and mortality rates and death rates from all causes were used for risk calculations. The LAR calculation for a single inhalation intake can be generalized to the case of repeated or prolonged exposure, provided that the excess absolute risk (EAR) are additive. We used the standard conditions the aerosol U234 intermediate type of solubility (P) with AMAD=1μm. The dynamics of equivalent doses in tissues and organs can be found in the ICRP database. The value of LAR/Sv for lungs may be approximated by a polynomial of the fifth degree. The risk coefficient for Russian exposed cohorts exceeds the nominal risk coefficient from Radiation Safety Standards 99/2009 for adults (0.041/Sv) in next cases: -internal exposure: men younger than 54, women younger than 69.

Keywords: ICRP radiation risk models, internal exposure, radionuclides, ICRP dose coefficients

A Monte Carlo calculation of the x-ray attenuation of tungsten functional papers (TFP)

ASUMAN KOLBAŞI Göztepe Training and Research Hospital

In radiology units of Hospitals, the Lead aprons are widely used for protection from the radiation which produced in imaging devices using the ionizing X- and gamma rays. However, the regular usage of these aprons may cause back pain and disk diseases. Other disadvantages of the lead aprons are inflexibility and toxicity. Because of the negative health effects of Lead, a strong demand for lead-free product development in health-care and industrial applications.
There are several studies of alternative x-ray protection materials. Usage of Tungsten Functional Papers (TFP) is one of the alternative materials. Since they are lead-free, easy to cut and fold; the TFPs are less harmful to the body.
In this study, GEANT4 based GAMOS framework is used to calculate the shielding effect of TFP sheets with different thicknesses and the results are compared with the Lead as reference.

Participant list

1. **ABDELLATIF ELANIQUE (Algeria)**
2. ABDULLAH AYDIN
3. ABDULLAH KAPLAN
4. ADEM PEHLİVANLI
5. AFİFE BÖLÜKBAŞI
6. AHMET BİÇER
7. AHMET BOZKURT
8. AHMET BÜLBÜL
9. ALİ ARMAĞAN GÖK
10. ALİ İHSAN KILIÇ
11. ALİ NADİ KAPLAN
12. ALİ ZAFER BOZKIR
13. **ASGAR HOSSEINNEZHAD (Iran)**
14. ASİYE GÜROL
15. ASLIHAN ÇAĞLAR
16. ASUMAN KOLBAŞI
17. AYDAN ALTIKULAÇ
18. **AIDIN GHALEHASADI (Iran)**
19. AYLA GÜMÜŞ
20. AYSUN İNAL
21. BEKİR ORUNCAK
22. **BOUMEDINE LASRI (Algeria)**
23. BURCU UÇAR
24. CEREN KAHRAMAN
25. DİLEK TOKTAMIŞ
26. DOĞAN YAŞAR
27. DUYGU BOLAT
28. ELİF EBRU ERMİŞ
29. ELİF GÖREN
30. ENİS KAPDAN
31. ERCAN YILDIZ
32. ERDEM UZUN
33. ERHAN ESER
34. EROL KAM
35. ERSİN ÇİÇEK
36. ESRA UYAR
37. EYYUP TEL
38. F. AYSUN UĞUR
39. FATİH EKİNCİ
40. FATMA YAKUT
41. FURKAN OK
42. **GHAZI ALSBEIH (Saudi Arabia)**
43. GÖKMEN ŞEKER
44. GÖZDE DEMİRELLİ
45. GÜLPER AKSOY
46. A. GÜNEŞ TANIR
47. HANDE KAYACIK
48. HANDE ÜNAL
49. HASAN BİRCAN
50. HASAN ÖZDOĞAN
51. HATİCE BİLGİN
52. HATİCE KÜBRA BELEN
53. HEDİYE ACUN BUCHT
54. HİLAL BARDAKÇI
55. HÜLYA ÖZDEMİR
56. HÜSEYİN ALİ YALIM
57. HÜSEYİN TOKTAMIŞ
58. İBRAHİM HALİL MUTLU
59. İLKAY TÜRK ÇAKIR
60. İLKER SERT
61. İSMAİL HAKKI KARAHAN
62. İSMAİL HAKKI SARPÜN
63. **JAMEEL-UN NABI (Pakistan)**
64. KAAN MANİSA
65. KEMAL TAŞDÖVEN
66. KENAN ÖZKAYA
67. KÜRŞAD OSMAN AY
68. KÜBRA BAYRAK
69. M. ERTAN KÜRKÇÜOĞLU
70. M. MURAT YAŞAR
71. M. ÖZGÜR SEZER
72. MAHMUT BÖYÜKATA
73. M. CÜNEYT KAHRAMAN
74. **MARİA CHUSHNYAKOVA (Russia)**
75. MEHMET BÜYÜKTÜRKMEN
76. MEHMET EMİN KORKMAZ
77. MEHMET ERDOĞAN
78. MEHMET KOŞAL
79. MERT ŞEKERCİ
80. MERVE AYDOĞAN
81. MERVE KARAGÖZ
82. **MOHAMED BELGAID (Algeria)**
83. **MUHAMMED SYAHIR SARKAWI (Malaysia)**
84. MUHİTTİN ŞAHAN
85. MURAT DAĞ
86. MUSTAFA HİCABİ BÖLÜKDEMİR
87. MUSTAFA ÖZGÜR
88. NAZMİ T. OKUMUŞOĞLU
89. NİHAL BÜYÜKÇİZMECİ
90. NİNA TUNÇEL
91. NURİ YORULMAZ
92. OĞUZ AYDIN
93. ONUR KARAMAN
94. ORKHAN MUKHTARLI
95. OZAN TOKER
96. ÖNDER SÖNMEZ
97. ÖZGÜR CULFA
98. ÖZLEM DAĞLI
99. ÖZLEM TOYKAN
100. PINAR KAAN
101. PINAR KARACAN
102. R. GÖKHAN TÜRECİ
103. R. ÖMER TURHAN
104. RIDVAN ÜNAL
105. **SABIN STOICA (Romania)**
106. SALEH SULTANSOY
107. SALİH MUSTAFA KARABIDAK
108. SEFER BALCI
109. **SERGEY KARPENKO (Russia)**
110. **SERGEY LOVACHEV (Russia)**
111. **SEYED KHALIL MOBAREKH (Iran)**
112. SULTAN KILIÇ
113. SÜMEYRA BALCI-YEĞEN
114. TAHİR ÇAKIR

115. TARIK SAĞEL
116. **THOMAS CALLIGARO (France)**
117. TOLGA AYDIN
118. TUĞBA ÇEPNİ
119. TUĞBA DEMİRBAY
120. TUĞBA TURAN
121. TUĞÇE GÜLÜMSER
122. UĞUR BÜYÜKER
123. ÜNER ÇOLAK
124. VİLDAN ÖZKAN BİLİCİ
125. VOLKAN SERT
126. YAREN ERGİN
127. **YOUSRY ABUSHADY (Egypt)**
128. YUNUS EMRE DOĞAN
129. YUSUF KAVUN
130. YUSUF ALPER KAPLAN

Index

A. GÜNEŞ TANIR 159, 199
A. NECMEDDİN YAZICI 185
ABDELLATİF ELANIQUE 224, 226
ABDULLAH AYDIN 24, 85, 101, 124, 202
ABDULLAH KAPLAN114, 117, 144, 146, 173, 175, 178, 180, 200
ABDÜLKADİR SIRIT 98
ADEM PEHLİVANLI 113
AFİFE BÖLÜKBAŞI 223
AHMET BİÇER 12, 13
AHMET BOZKURT 24, 191, 195, 202, 204
AHMET BÜLBÜL 165
AIDIN GHALEHASADI 11
ALEX BROWN 20
ALİ ALAÇAKIR 77
ALİ ALTAY 193
ALİ ARMAĞAN GÖK 230
ALİ İHSAN KILIÇ 20
ALİ KAYA 102
ALİ NADİ KAPLAN 167, 170, 173, 175
ALİ TOZAR 72, 228, 229
ALİ ZAFER BOZKIR 221
ALPEREN YÜNCÜ 78
ANDERS AHNESJÖ 149
ANDREAS GORGEN 27, 166
ANN CECILIE LARSEN 27, 166
AREV ARTUN 140
ARİFE SEDA BÖLÜKDEMİR 77
ASGAR HOSSEINNEZHAD 11
ASİYE GÜROL 195, 197
ASLIHAN ÇAĞLAR 78
ASUMAN KOLBAŞI 158, 199, 244
AYDAN ALTIKULAÇ 208, 209
AYDIN ÖZBEY 78
AYHAN ÖZMEN 182
AYLA GÜMÜŞ 47
AYNUR ÖZCAN 126
AYSUN İNAL 150, 190
AYŞEN BARUT 54
BARRY DAVIDS 20
BAYRAM DEMİR 73, 74, 97, 139
BEKİR ORUNCAK 139, 189
BERNA OTO 157
BETÜL YASATEKİN 77
BİLAL KOVAN 74
BONGINKOSI VINCENT KHESWA 27, 166
BOUMEDIENE LASRI 15, 194
BURAK DUYURAN 160
BURCU DİRLİK SEVİM 73, 74
BURCU UÇAR 88, 130
CAN ERTUGAY 68
CANDAN DEMİRÖZ ABAKAY 193
CENGİZ ÖZEL 167, 170
CEREN KARAMAN 30, 32, 34, 67, 199
CİHAN ÇİÇEK 78
CÜNEYT ÇELİKTAŞ 104, 108
DAVID BOERSMA 149
DİLEK KURT 142
DİLEK TOKTAMIŞ 185
DOĞAN YAŞAR 26
DUYGU BOLAT 76, 193
EDA ŞAHİN 27, 166
EDİP BAYRAM 34, 67, 199
ELİF EBRU ERMİŞ 104, 108
ELİF GÖREN 55, 163
EMEL ALĞIN 27, 166
EMEL ECE 182
EMİN YELTEPE 52, 54
EMRE VATAN 51
ENİS KAPDAN 26, 95
ERCAN YILDIZ 21
ERDEM UZUN 46, 164
ERHAN ESER 39, 160
ERKAN BOSTANCI 28, 29
ERKAN HALAY 98
EROL KAM 86, 87, 121, 140, 241, 242
ERSİN ÇİÇEK 77
ERSOY ÖZ 99, 100
ESRA UYAR 39
ESRA YÜKSEL 16
EYYUP TEL 43, 90, 143, 223, 230, 233
EZGİ SUNAR 78
FABIO ZEISER 27, 166
FADİME KILIÇ 20
FARIDAH MOHAMAD IDRIS 35
FATIMA BOUASRIA 15, 194
FATİH EKİNCİ 28, 29, 64, 66
FATİH YAMAN 78
FATMA AYSUN UĞUR 40, 41, 55, 96, 161, 162, 163
FATMA YAKUT 40, 41
FİKRET ANLI 165
FİLİZ KORKMAZ GÖRÜR 222
FRANK LEONEL BELLO GARROTE 27, 166
FURKAN OK 16
GENCEBAY KARAKAYA 68
GHAZI ALSBEIH 45
GÖKHAN KURT 29
GÖKHAN ÜNEL 78
GÖKMEN ŞEKER 210, 219
GÖRKEM TÜREMEN 78
GRY MERETE TVETEN 27, 166
GÜLDEREN AÇIKGÖZ 241
GÜLNUR ERASLAN 125
HADI SABRI 11, 42
HAKAN ÇETİNKAYA 78
HAKAN EMMEZ 28
HALİDE ŞAHAN 143
HALUK YÜCEL 52, 54
HANDE BOYDAŞ 85, 124
HANDE KAYACIK 69
HASAN BİRCAN 12, 13, 51
HASAN ÖZDOĞAN 144, 146, 170, 173, 175, 178, 180, 200
HAŞİM ZAHİD GÜVEN 16
HATİCE KOVAN 73
HATİCE KÜBRA BELEN 101
HEDİYE ACUN BUCHT 149
HİLAL BARDAKÇI 213, 216
HÜLYA ÖZDEMİR 156
HÜSEYİN ALİ YALIM 47, 56, 82, 127
HÜSEYİN KOÇ 160
HÜSEYİN OZAN TEKİN 68
HÜSEYİN TOKTAMIŞ 132, 185
HÜSEYİN YILDIZ 78
IGOR GONTCHAR 207
ISSAM MOUHTI 226
İBRAHİM HALİL MUTLU 7
İBRAHİM YİĞİTOĞLU 88, 89, 130, 131
İHSAN KILIÇ 77
İLKAY TÜRK ÇAKIR 6
İLKER SERT 120, 141
İSMAİL HAKKI KARAHAN 72, 228, 229
İSMAİL HAKKI SARPÜN20, 24, 34, 56, 67, 97, 195, 197, 199, 200, 202
JAMEEL-UN NABI 19
JASMAN ZAINAL 35
JORGEN ERIKSSON MIDTBO 27, 166
KAAN MANİSA 12, 13, 51
KEMAL TAŞDÖVEN 56
KUTSAL BOZKURT 16
KÜBRA BAYRAK 121, 142, 241
KÜRŞAD OSMAN AY 27, 166

LUCIA CRESPO CAMPO 27, 166
M. ERGÜN TURGAY 86, 87, 140, 242
M. ÖZGÜR SEZER 182
MAGNE GUTTORMSEN 27, 166
MAHMUT BÖYÜKATA 23, 123, 124
MAHMUT CÜNEYT KAHRAMAN 238
MAHMUT ÖZGEN 90
MALIN KLINTEFJORD 27, 166
MAMMAR BOUAMOUD 15, 194
MARIA CHUSHNYAKOVA 207
MATEM ERDOĞAN 98
MEHMET AYVACIKLI 184
MEHMET BÜYÜKTÜRKMEN 139
MEHMET EMİN KORKMAZ 14, 68, 80, 81, 161, 162
MEHMET ERDOĞAN 12, 13, 51
MEHMET ERTAN KÜRKÇÜOĞLU 38
MEHMET KILIÇ 69, 70, 71
MEHMET MURAT YAŞAR 191, 204
MEHMET YÜKSEL 184
MEHTAP DÜZ 210, 213, 216, 219
MERAL KURT 193
MERT ŞEKERCİ114, 117, 144, 146, 170, 173, 175, 178, 180, 200
MERVE AYDOĞAN 23
MERVE KARAGÖZ 233, 237
MERVE YAPRAK 242
MESUT DEPEDELEN 230
MEVLÜT DOĞAN 194
MOHAMAD HAIRIE RABIR 35
MOHAMED BELGAID 24, 65, 202
MOHAMED SAHLAOUI 194
MOHAMED YOUSSEF MESSOUS 226
MOHAMMAD KHATEEB 132
MOHAMMED SAHLAOUI 15
MUHAMMAD MAJID 19
MUHAMMAD RAWI MOHAMED ZAIN 35
MUHAMMAD RIAZ 19
MUHAMMAD SYAHIR SARKAWI 35
MUHARREM KORKMAZ 26
MUHİTTİN ŞAHAN 90, 143
MURAT BEKEN 99, 100
MURAT DAĞ 53, 227
MUSTAFA HİCABİ BÖLÜKDEMİR39, 64, 66, 77, 113, 159, 160
MUSTAFA ÖZGÜR 27, 166
MUSTAFA TOPAKSU 184
MÜGE ŞENGÜL 142
NAZMİ TURAN OKUMUŞOĞLU 9
NESLİ BİNGÖLDAĞ 51
NESLİHAN CEREN KAPLAN 54
NESRİN ALTINSOY 95
NİHAL BÜYÜKÇİZMECİ 79, 188
NİL KÜÇÜK 184
NİNA TUNÇEL 155, 156
NURÇİN KARADENİZ 82, 127
NURDOĞAN CAN 184
NURİ YORULMAZ 191, 204
OĞUZ AYDIN 76, 193
ONUR KARAMAN 34, 67, 158, 199
ORHAN İÇELLİ 69, 70, 71, 99, 100
ORKHAN MUKHTARLI 222
OSMAN AĞAR 68, 80
OZAN TOKER 99, 100
ÖMER TOPDAĞI 99, 100
ÖNDER EYECİOĞLU 99, 100
ÖNDER SÖNMEZ 126
ÖZGÜR CULFA 14, 68, 75, 80, 81
ÖZKAN BİNGÖL 103
ÖZLEM DAĞLI 28, 29
PINAR KAAN 37
R. GÖKHAN TÜRECİ 36, 37, 221
RECEP BIYIK 51, 182
RECEP BORA NARTTÜRK 52, 54
RECEP KESER 222
RIDVAN ÜNAL 17, 98, 125, 197
RIFAT ÇAPAN 98
RIZA OĞUL 79, 188
SABIN STOICA 18
SALEH SULTANSOY 5
SALİH MUSTAFA KARABIDAK 102, 103
SAMRA KAİM 123
SEFER BALCI 52, 54
SELAHATTİN BOZKURT 98
SELÇUK ALP 99, 100
SELİM KAYA 103
SELİN SAATCI 54
SEMA GÖZCÜ TUNÇ 76, 193
SERDAR DİZMAN 222
SERGEY KARPENKO 206
SERGEY LOVACHEV 243
SEYED KHALIL MOUSAVI MOBARAKEH 42
SİBEL KAHRAMAN ÇETİNTAŞ 193
SUAT PAT 24, 202
SULTAN KILIÇ 223
SUNNIVA ROSE 27, 166
SUNNIVA SIEM 27, 166
SÜMEYRA BALCI-YEĞEN 184
SÜREYYA SARIHAN 76
TAHİR ÇAKIR 157
THERESE RENSTROM 27, 166
THOMAS CALLIGARO 8
TRINE WIBORG HAGEN 27, 166
TUĞBA ÇEPNİ 73, 74
TUĞBA DEMİRBAY 71
TUĞBA TURAN 89, 131
TUĞÇE GÜLÜMSER 114, 117
TUNCAY ERDOĞAN 17
UĞUR BÜYÜKER 161, 162
ÜLKÜ SAYIN 182
ÜNER ÇOLAK 2
VEDAT SANSOY 73, 74
VETLE WEGNER INGEBERG 27, 166
VEYSİ ERKCAN ÖZCAN 78
VICTOR MODAMIO 27, 166
VİLDAN ÖZKAN BİLİCİ 30, 32
VOLKAN SERT 80, 81
YAREN ERGİN 70
YASER AÇIKBAŞ 98
YASİN YÜCEL 228
YAŞAR KARABUL 69, 70, 71
YEŞİM OLGAÇ 77
YUNUS EMRE DOĞAN 97
YUSUF ALPER KAPLAN 233, 237
YUSUF KAVUN 43, 90, 223, 230
YÜKSEL KARABULUT 184
ZEHRA NUR ÖZER 82, 127
ZEKİ ÜNAL YÜMÜN 121, 142, 241
ZENCİYE KIRAY 76
ZERRİN YİĞİT 73, 74
ZEYNEP GÜVEN ÖZDEMİR 69, 70, 71
ZEYNEP KARAALİOĞLU 140
ZEYNEP ŞİLAN TURHAN IRAK 30, 32